# TWO APPROACHES TO GREEN CHEMISTRY IN INDUSTRIALLY DRIVEN PROCESSES:

# ALUMINUM TERT-BUTOXIDE AS A RATE ENHANCING MEERWEIN-PONNDORF-VERLEY REDUCTION CATALYST APPLIED TO THE TECHNOLOGICAL TRANSFER FROM BATCH TO CONTINUOUS FLOW

# AND

# STRUCTURAL MODIFICATIONS OF FUNCTIONALIZED TRIALKYLSILYLAMINES AS ENERGY EFFICIENT CARBON DIOXIDE CAPTURE SOLVENTS

A Thesis
Presented to
The Academic Faculty

By

Kyle Flack

In Partial Fulfillment
Of the Requirements for the Degree
Doctor of Philosophy in Chemistry

Georgia Institute of Technology

August 2012

**TWO APPROACHES TO GREEN CHEMISTRY IN INDUSTRIALLY DRIVEN PROCESSES:**

**ALUMINUM TERT-BUTOXIDE AS A RATE ENHANCING MEERWEIN-PONNDORF-VERLEY REDUCTION CATALYST APPLIED TO THE TECHNOLOGICAL TRANSFER FROM BATCH TO CONTINUOUS FLOW**

**AND**

**STRUCTURAL MODIFICATIONS OF FUNCTIONALIZED TRIALKYLSILYLAMINES AS ENERGY EFFICIENT CARBON DIOXIDE CAPTURE SOLVENTS**

Approved By:

Dr. Charles Liotta, Co-Advisor
School of Chemistry and Biochemistry
*Georgia Institute of Techonology*

Dr. Angelo Bongiorno
School of Chemistry and Biochemistry
Georgia Institute of Technology

Dr. Charles Eckert, Co-Advisor
School of Chemical and Biomolecular Engineering
*Georgia Institute of Techonology*

Dr. Christopher Jones
School of Chemical and Biomolecular Engineering
Georgia Institute of Technology

Dr. Stefan France
School of Chemistry and Biochemistry
*Georgia Institute of Technology*

Date Approved: May 25, 2012

*This thesis is dedicated to David O. Halvorson, who was a loving grandfather and superb chemist*

## ACKNOWLEDGMENTS

I would first like to begin by thanking my advisors Dr. Charles Liotta and Dr. Charles Eckert for their unparalleled assistance and guidance through my thesis work. Dr. Liotta has helped me realized that keeping a chin-up approach to graduate school and staying positive is vital in success. Both advisors encouragement and collaborative approach to problem solving have really helped me see the importance of fundamental science and understanding and how it plays into a much larger overall picture. I would like to also thank my committee members for their support through each of the obstacles in my graduate career. Your questions and helpful insight have been important in continuing my research.

I would next like to thank all of my colleagues, former and current, that have helped each of the projects move forward. Specifically, I would like to give appreciation to Dr. Pamela Pollet's scholarly vision and answers to even the simplest questions that have led to my personal progress. Specifically, I'd also like to thank Kristen Kitagawa (Fisher) for her mentorship when I joined the group as well as her continual involvement in seeing my career progress. I'd be remiss if I didn't thank all of the members of the Eckert-Liotta group between 2008 and 2012. I've had the pleasure in working with you all in some form whether it was every day in the lab or just a chat in the office. The DOE and ConocoPhillips research teams have been instrumental in the progression of this thesis work that has helped lead to interesting insights in $CO_2$ capture.

My colleagues Michael Bayless, Evan Davey, Jackson Switzer, Amy Rohan, Emily Nixon, and Will Heaner have become great friends outside of work, and I thank you for keeping my life interesting for sure!

I'd lastly like to thank my fiancé Meghan Young for being my best friend (in Atlanta). You have kept me grounded and focused and I can't wait for all of our adventures to come. To my family and friends in North Carolina, including the Avett Brothers, I could not have done this without your love and support!

## TABLE OF CONTENTS

## LIST OF TABLES

## LIST OF FIGURES

## LIST OF ABBREVIATIONS

| | |
|---|---|
| (*R,S*)-CMA | *N*-(tert-butyloxycarbonyl)-(3*S*)-3-amino-1-chloro-4-phenyl-(2*R*)-butanol |
| (*S*)-CMK | *N*-(tert-butyloxycarbonyl)-(3*S*)-3-amino-1-chloro-4-phenyl-2-butanone |
| (*S,S*)-CMA | *N*-(tert-butyloxycarbonyl)-(3*S*)-3-amino-1-chloro-4-phenyl-(2*S*)-butanol |
| α,αDM-TEtSA | 2-methyl-4-(triethylsilyl)butan-2-amine |
| $Al(OEt)_3$ | aluminum triethoxide |
| $Al(OiPr)_3$ | aluminum tri-isopropoxide |
| $Al(OtBu)_3$ | aluminum tri-*tert*-butoxide |
| AMP | 1-amino-2-methyl propanol |
| AMPAC | American Pacific Chemical Co. |
| αM-TEtSA | 3-(aminobutyl)triethylsilane |
| AO | atomic orbital |
| $B(OEt)_3$ | triethoxyborane |
| βE-TEtSA | 2-((triethylsilyl)methyl)butan-1-amine |
| BINOL | 1,1'-Bi-2-naphthol |
| βM-TEtSA | 2-methyl-3-(triethylsilyl)propan-1-amine |
| BOC | *tert*-butoxycarbonyl |
| CDMSA | 3-(aminopropyl)cyclohexyldimethylsilane |
| $CO_2$ | carbon dioxide |
| DCM | dichloromethane |
| DEA | diethanolamine |

| | |
|---|---|
| DESDA | bis-3-(aminopropyl)diethylsilane |
| DFT | density functional theory |
| DH | reaction enthalpy |
| DMESA | 3-(aminopropyl)dimethylethylsilane |
| DOE | Department of Energy |
| *dr* | diasteremoeric ratio |
| DSC | differential scanning calorimetry |
| EA | elemental analysis |
| EPA | Environmental Protection Agency |
| FSA | 3-((aminopropyl)(1H,1H,2H,2H-perfluoropentyl)diisopropyl)silane |
| GE | General Electric |
| HIV | Human Immunodeficiency Virus |
| HPLC | high performance liquid chromatography |
| IL | ionic liquid |
| iPrOH | isopropanol |
| LUMO | lowest unoccupied molecular orbital |
| MEA | monoethanolamine |
| ML | molecular liquid |
| mL | milliliter |
| MPV | Meerwein-Ponndorf-Verley |
| MTBE | methyl *tert*-butylether |
| NMR | nuclear magnetic resonance |
| PDMSA | 3-(aminopropyl)phenyldimethylsilane |
| Pt-DVDS | platinum-divinyltetramethyldisiloxane |
| RB | round-bottomed |

| | |
|---|---|
| RevIL | reversible ionic liquid |
| RT | room temperature |
| SDMESA | 3-(dimethylethylsilyl)-N-methylpropan-1-amine |
| STEtSA | *N*-methyl-3-(triethylsilyl)propan-1-amine |
| TEMSA | (aminomethyl)triethylsilane |
| TESBA | 4-(aminobutyl)triethylsilane |
| TESEA | 2-(aminoethyl)triethylsilane |
| TEtSA | 3-(aminopropyl)triethylsilane |
| TFA | trifluoroacetic acid |
| TGA | thermal gravimetric analysis |
| THF | tetrahydrofuran |
| THSA | 3-(aminopropyl)trihexylsilane |
| TIPSA | 3-(aminopropyl)triisopropylsilane |
| TPSA | 3-(aminopropyl)tripropylsilane |

## SUMMARY

The Meerwein-Ponndorf-Verley (MPV) reduction of three model compounds benzaldehyde, acetophenone, and (*S*)-CMK, a pharmaceutical intermediate, were shown to be enhanced through the use of an improved catalyst, $Al(OtBu)_3$. The conventional catalyst, $Al(OiPr)_3$ is effective at reducing aldehydes and ketones to their respective alcohols but the tetrameric aggregation state of the catalyst limits the rate of reductions as compared to the dimeric state of $Al(OtBu)_3$. Because of the increased rate of reduction with $Al(OtBu)_3$ in both neat iPrOH as well as mixed toluene:iPrOH systems, lower catalyst loading was achievable. The first successful MPV reduction in continuous flow was demonstrated on benzaldehyde. The reduction of benzaldehyde was optimized to continuously run at full conversion in only 11 minutes with less half of the conventional catalyst loading.

A new $CO_2$ capture system was investigated using non-aqeuous amines, as opposed to conventional aqueous amine solvents, to reduce the amount of energy required for capture. This is extremely important as $CO_2$ emissions continue to increase. Trialkylsilylamines were reacted with $CO_2$ to form ionic liquids that are thermally reversible. It was found that small structural modifications around the silicon atom, the amine reactive site, and along the backbone linking the two, greatly altered the physical and thermodynamic properties of the formed ionic liquids. $CO_2$ capture capacities higher than predicted were achieved through a dual capture mechanism (chemical and physical absorption) as well as through incomplete equilibrium to form carbamic acids. Synthesis of a library of trialkylsilylamines was achieved, lending valuable information towards the

optimization of improved $CO_2$ capture solvents that meet the requirements of high capacity and low energy.

# CHAPTER 1: INTRODUCTION

## 1.1 Green Chemistry Principles

Organic chemistry has continuously evolved to respond to dynamic challenges in all aspects of modern life. As growth continues, evaluation of established reactions and procedures with more stringent standards, especially from environmental and economic standpoints, has become prominent. Regulations and an increasingly open, global market have created an incentive to establishing environmentally friendly and economically superior alternative organic reactions. The 12 guiding principles of green chemistry are milestones that highlight the importance of reducing chemical waste from reactions, improving atom economy, using more economically and sustainable chemical alternatives, and eliminating or reducing toxic and dangerous reagents, among others.[1] Green engineering also has articulated 12 guiding principles which directly tie into the chemistry initiatives because in the real world one cannot progress without the other.[2] Multidisciplinary approaches to real problems are keys when considering processes and reactions on industrial scales.[3]

My thesis work comprises two main projects within the area of green organic chemistry. Because of the Eckert/Liotta group multidisciplinary setting, organic chemistry and chemical engineering are intertwined, which allows for a fundamental and applied approach to solving real-world problems. The two main projects that will be discussed within my thesis work are (1) the enhancement of Meerwein-Ponndorf-Verley (MPV) reductions with $Al(OtBu)_3$ and their conversion to continuous flow and (2) trialkylsilylamines for improved $CO_2$ capture. Both projects are focused on the implementation of green chemistry principles and enabling sustainable solutions to

current industrial challenges. The term sustainability has widely used to describe solely green chemistry in the past decade, but my vision is that green chemistry must be economically efficient and competitive than current technologies.[4] In order to fully understand the context of my work, I will first present a background and motivation for both projects.

### 1.2 Alcohols and their formation through carbonyl reduction

Alcohols are extremely valuable in that they are found in pharmaceutical precursors, intermediates, and drugs, in biodiesel, in alcoholic beverages, sugars, and many other products. The formation of alcohols is possible from many other functional groups, including ketones and aldehydes via reduction. Many reagents and methods have been described to carry out reductions of ketones and aldehydes including borohydrides,[5] aluminum hydrides,[6] hydrogenation with transition metal catalysts,[7] and aluminum alkoxides.[8] The latter is known as the Meerwein-Ponndorf-Verley reduction or MPV reduction.[9] It is a widely used synthetic approach as it is relatively inexpensive, chemoselective and requires mild reaction conditions for the reduction of ketones and aldehydes. Although in principle the aluminum alkoxide can be used in catalytic quantities, it is generally used in stoichiometric amounts.[10] The impractical high catalyst loading is the major limitation of the MPV reduction. In some cases, elevated temperatures are desirable to push the equilibrium towards the alcohol products.

I approached these limitations by investigating the reduction of three model compounds: a pharmaceutically relevant compound *N*-(tert-butyloxycarbonyl)-(3*S*)-3-amino-1-chloro-4-phenyl-2-butanone or (*S*)-CMK, benzaldehyde and acetophenone with different aluminum alkoxides. The goal was to enhance the rate of reduction in order to achieve fast reactions with lower catalyst loadings. It was found that $Al(OtBu)_3$ was

effective in doing this in both the conventional isopropanol solvent as well as a mixed alcohol solvent system. By lowering the catalyst loading, amounts of aluminum alkoxide required are reduced and therefore the amount of aluminum waste generated from the reduction is also reduced, both favorable from a sustainability point of view. Furthermore, $Al(OtBu)_3$ is also inexpensive and commercially available making this entire MPV system competitive. This work led to the transfer of batch reactions to continuous flow technology.

### 1.3 Continuous flow technology

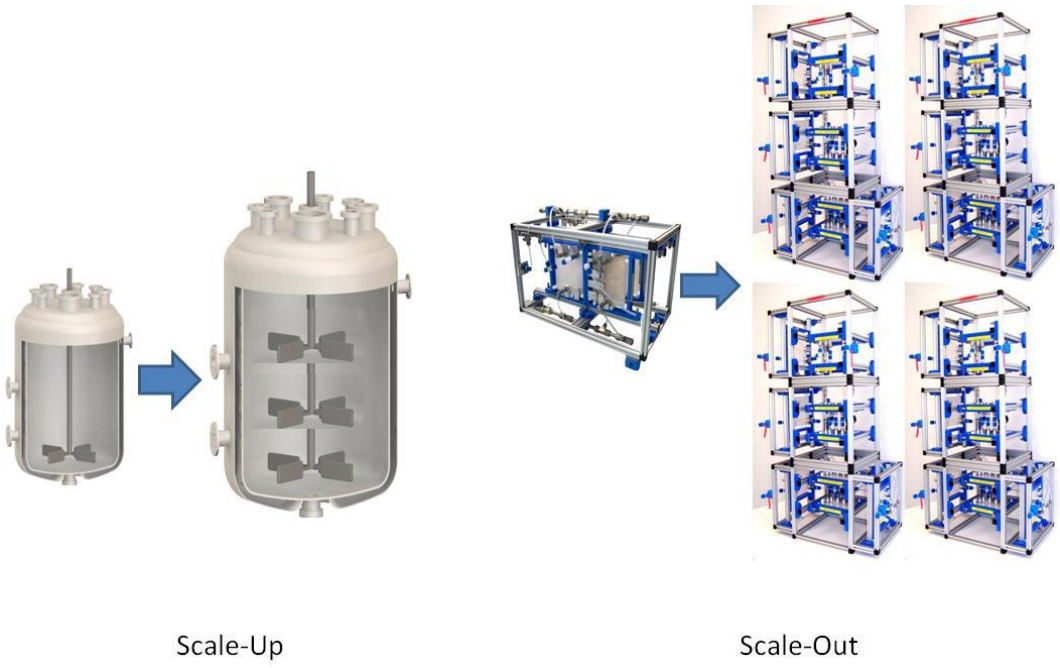


**Figure 1.1.** Scale out in continuous flow versus scale up in batch

Batch processing is a flexible approach for industry and research labs to achieve desired chemistries but requires optimization at every level of **scale-up** from the bench to industrial production. This can be problematic in industries like the pharmaceutical industry where time to market from patent filing is extremely important. Current patent life is 20 years from file date.[11] To add to that, multistep syntheses require separate batch reactions and separations between them. An alternative approach that has been used in other chemical sectors such as refining is continuous flow technology. The pharmaceutical industry could benefit greatly from the conversion of current batch reactions to continuous flow systems, including continuous multistep syntheses. Specifically, the Pharmaceutical Green Chemistry Roundtable made up of representatives from top chemical synthesis and pharmaceutical companies have highlighted continuous flow research as the top priority moving forward.[12] Continuous flow technologies have been developed to address the limitations with batch reactions. Particularly, more efficient heating through using small channels, packed mixing columns, and continuous flow with less amount of reagents needed have all been realized.[13] Continuous flow uses a **scale-out** approach to production, placing continuously running flow reactors in parallel, eliminating the time constraint to technology transfer to production as well as hazards with scale-up (Figure 1.1). This is beneficial with respect to atom economy and higher product quality and reproducibility. Because of scale-out, conditions used on a lab scale can then be implemented directly to production and by multiplying the number of reactors, one can increase the amount of chemical produced. This is very important in implementation of patented technology with respect to time to market and man power required.

There are commercial examples of continuous flow technologies which are important for the pharmaceutical and chemical industry which are adaptable to many

different reactions or conditions. One pertinent example is the Corning® Glass Continuous Flow Reactor.[14] This system was specifically designed for high throughput, fast transitions from lab to production, and is modular for multi-step synthesis. The Eckert/Liotta group received a Corning® Glass Continuous Flow reactor as a gift and I had envisioned the introduction of the MPV reduction in continuous flow. Chapter 2 focuses on the improvement of the MPV reduction and Chapter 3 describes the improvements as they relate to the facile transition to continuous flow. The MPV is a pharmaceutically relevant reaction and its implementation was felt to be very important and advantageous for the industry. My other project also focused on the improvement of a continuous system. As mentioned previously, one area of industry that has used continuous flow systems is the petroleum and energy industry. Particularly, recyclable processes that are constantly operating such as $CO_2$ capture processes are of interest. The second project embodies the work that I have done on the development of more sustainable technologies for $CO_2$ capture.

### 1.4 Carbon capture with amine based solvents

It is necessary to put into context the pressing need for efficient $CO_2$ capture processes from the coal fired power plants. Carbon dioxide has been cited as a greenhouse gas because it becomes trapped within the earth's atmosphere and allows for UV penetration without efficient escape, contributing to global warming.[15] As global warming becomes a major concern, the identification and contribution of the primary (man-caused) sources of $CO_2$ were reported. In fact, the burning of coal is one of the largest producers of $CO_2$ in the United States, as released in a study by the EPA.[16] From Figure 1.2, it can be seen that energy related industries produced 83.6% of the U.S. $CO_2$ emissions in 2010. The industrial sector generating the largest amount of $CO_2$ is the

energy sector, and within that, the burning of coal and other fossil fuels is by far the highest, generating 5,388 Tg (million metric tons) per year.

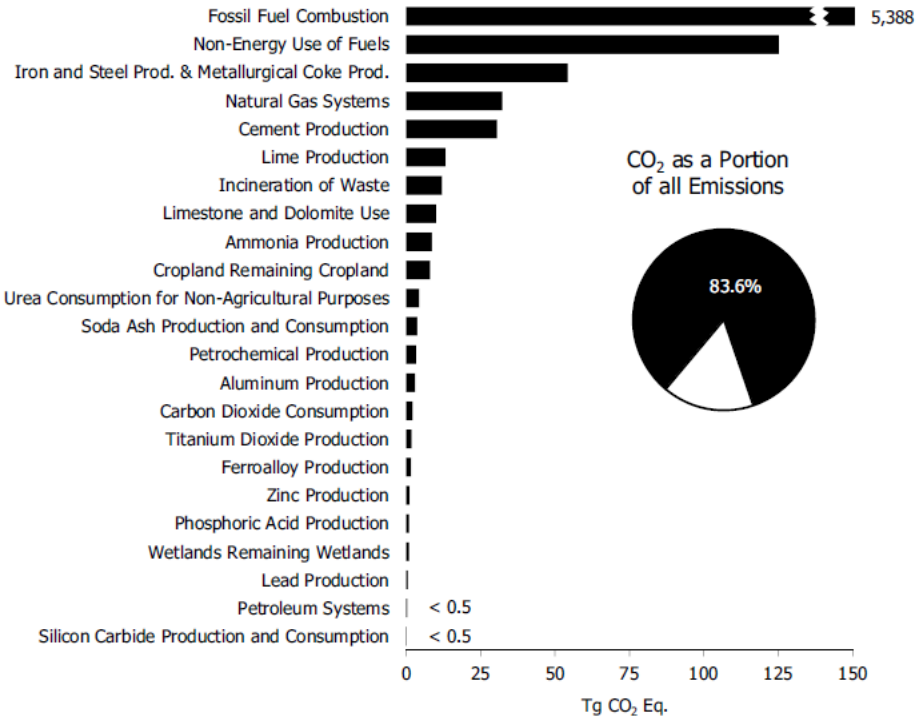


**Figure 1.2.** $CO_2$ emissions in the U.S. per sector in 2010[16]

Predictions have shown that as population continues to grow and energy demands increase, the burning of coal will also continue to grow. The EPA and DOE have implemented a program to develop technology that will meet the following requirements, 90% capture of emitted $CO_2$ without increasing more than 35% of the utility costs per user.[17] This is an ambitious task for researchers to develop $CO_2$ capture technologies that are extremely cost and energy efficient. Flue gas remains one of the highest targeted $CO_2$ streams because it is responsible for the majority of $CO_2$ emitted. A sample flue gas stream is shown in Table 1.1.[18] $CO_2$ makes up 11.8% of the total stream along with water, nitrogen, and oxygen accounting for the majority of the

composition. Because the percentage of $CO_2$ is relatively low in a flue gas stream, capture methodology must be selective and efficient.

**Table 1.1.** Flue gas composition (Wyodak Power Plant)

| Flue Gas Component | Percentage (by weight) |
|---|---|
| Nitrogen ($N_2$) | 67 |
| Carbon Dioxide ($CO_2$) | 11.8 |
| Water ($H_2O$) | 8 |
| Oxygen ($O_2$) | 12 |
| Nitrous Oxides ($NO_x$) | 150 ppm |
| Sulfurous Oxides ($SO_x$) | 180 ppm |

It has been well documented that amines are effective at capturing $CO_2$ through chemical reaction.[19] The nitrogen atom has an available lone pair which is at low enough energy to react with the lowest unoccupied molecular orbital (LUMO) of the $CO_2$. In the LUMO of $CO_2$, the carbon atom has the largest atomic orbital (AO) coefficient. Reaction takes place by reaction of the amine with the carbon of the carbon dioxide. Because of this favorable reaction, amines have been widely used for the capture of $CO_2$.[20] These reactions have also been shown to be thermally reversible, regenerating the reactive amine and $CO_2$ separately upon heating. The benchmark in amine driven $CO_2$ capture technology is monoethanolamine, or MEA. It is cheap, widely available and reacts chemically to form an ammonium and carbamate ion pair (Figure 1.3).

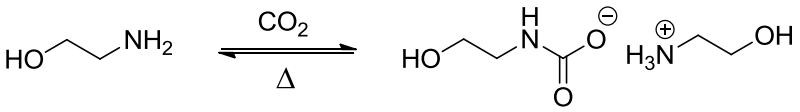


**Figure 1.3.** Reversible reaction of monoethanolamine with $CO_2$

The viscosity of the resulting ion pair and the corrosivity of the molecular liquid prevent its implementation under neat conditions. However, a 30% solution of MEA in water reduces both the viscosity and corrosion issues. The 30% MEA aqueous solutions are effective at capturing $CO_2$ from low pressure $CO_2$ streams and are thermally reversible. Typically temperatures of reversal are around 120°C. This is required to vaporize the water in the capture solution for recycle. Despite recyclability, the high boiling point and high heat capacity of water makes the reversal and recycle process very energy intensive. Another problem with MEA recycling is the inherent degradation (thermally and oxidatively) involving both the alcohol and amine sites.[21] Though MEA is the reference for comparison in regards to $CO_2$ capture, many other aqueous amine blends have been developed and investigated and examples are shown in Figure 1.4.[22]

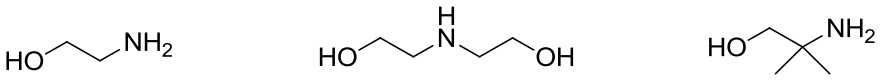


**Figure 1.4.** Examples of amines studied in aqueous solutions

Aqueous amine solutions for $CO_2$ capture have really progressed in their effectiveness for $CO_2$ capture. In fact primary amines like MEA are not the only aqueous amine systems that have been studied. The drive to increase the $CO_2$ capacity of

aqueous amine systems led to the study of branched amine systems, secondary, and tertiary amines to increase the basicity of the amine.[23] By increasing the basicity and lowering the nucleophilicity, the equilibrium then lies towards protonation of the amine as opposed to the reaction of the amine with $CO_2$.

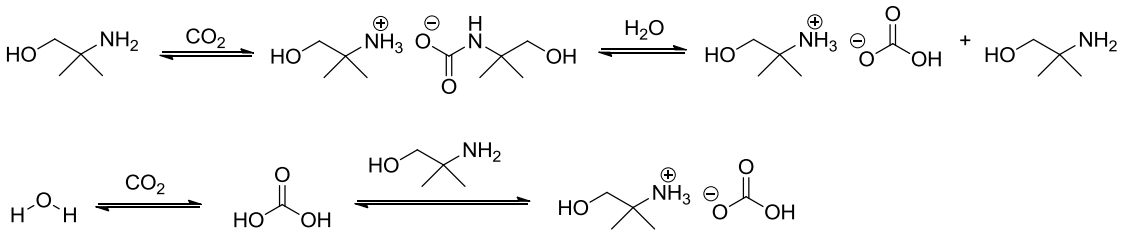


**Figure 1.5.** Equilibrium reaction of aqueous hindered amines with $CO_2$ for increased capacities

The water used to control viscosity and corrosion is also reactive with $CO_2$, having the ability to form carbonic acid. In the presence of an amine, such as MEA, the carbonic acid is deprotonated and an ion pair is formed, bicarbonate anion and an ammonium cation (Figure 1.5). Through this reaction, $CO_2$ capacity in terms of mol $CO_2$/mol amine is 1:1 rather than 1:2 when the amine is reacted without water. Tertiary amines do not actually react with $CO_2$ but in aqueous conditions can be protonated to form an ammonium/bicarbonate ion pair. This has been studied and applied for improvements in chemical capacity of aqueous amines through reaction with $CO_2$ or through acid/base reactions with bicarbonate. Although aqueous amines have remained the forefront of $CO_2$ capture studies, many other methods for $CO_2$ capture have been developed. Examples of these are gas filtration membranes,[24] solid absorbents,[25] reactive solid absorbents,[26] algae and biological captors,[27] and ionic liquids.[28] Many of

these methods are the focus of other research groups here at Georgia Tech. Our goal was to investigate alternative solvents for $CO_2$ capture based on the reaction of amines with $CO_2$ with the caviat that the systems did not need water to operate due to the parasitic energy required with aqueous solutions during reversal.

The systems that we have designed that meet this requirement of lower reversal energy and high capacity are trialkylsilylamines that form reversible ionic liquids (RevILs) upon reaction with $CO_2$. These systems have both a silicon and a nitrogen atom; the silicon to contribute to reducing viscosity and nitrogen to react with $CO_2$. Because the properties of ionic liquids change with substitution and structural changes, I worked to develop a structure-property relationship with respect to the silylamine structure and the reversible ionic liquid properties from reaction with $CO_2$. The modifications investigated were changing the alkyl groups on the silicon atom, varying the distance between the silicon atom and the reactive amine, studying both primary and secondary amine derivatives, and hindering the amine reactive site through inclusion of alkyl groups along the propylamine backbone. Each of these derivations are described in their own chapters, 4-6, respectively. Properties that were studied were $CO_2$ capacity or the amount of $CO_2$ that could be captured with respect to structure, viscosities of the ionic species formed through reaction with $CO_2$, reversal temperatures to regenerate the silylamine and $CO_2$ and the enthalpy required for reversal. All of these considerations are important because our goal is to use existing technologies, for example, conventional absorber and stripper columns[29] (Figure 1.6).

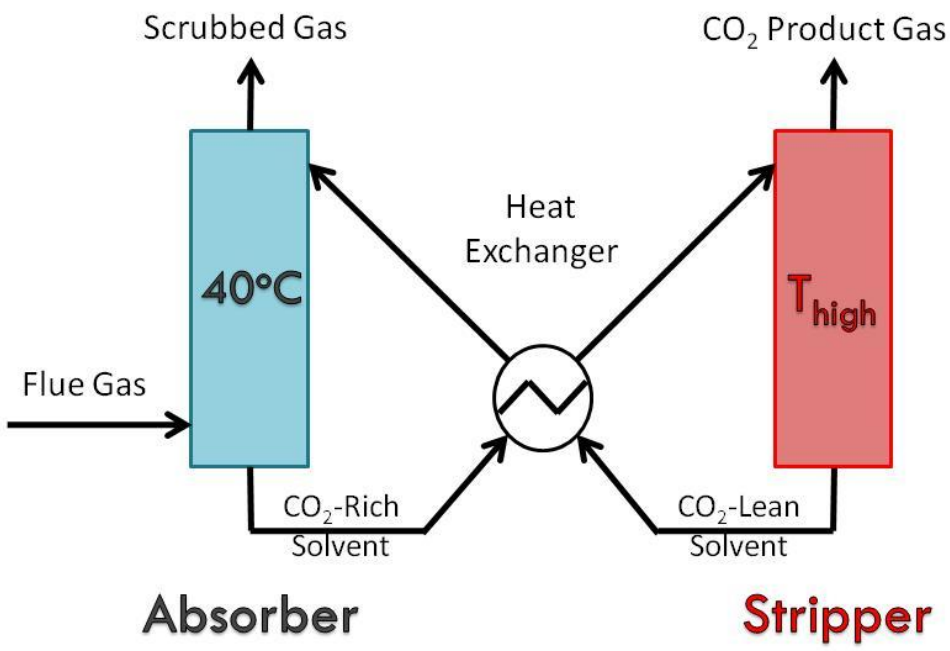


**Figure 1.6.** Absorber/Stripper capture schematic for liquid amine $CO_2$ capture

In order for this type of system to work, low viscosity liquids are required, and capacities must be high. To lower the energy required for capture and reversal, reversal temperature needed to be lower than 120°C, the temperature to reverse aqueous amine solutions, and the enthalpy needed to be lower, if possible than the MEA technology. Structure-property relationships were developed through the structural modifications on silylamines to uncover appropriate directions towards meeting the aforementioned goals.

## 1.5 References


(1) *Green chemistry: theory and practice*; Anastas, P. T.; Warner, J. C., Eds.; Oxford University Press: Oxford, England, 1998.

(2) Anastas, P. T.; Zimmerman, J. B. *Environmental Science & Technology* **2003**, *37*, 94.

(3) Mulvihill, M. J.; Beach, E. S.; Zimmerman, J. B.; Anastas, P. T. In *Annual Review of Environment and Resources, Vol 36*; Gadgil, A., Liverman, D. M., Eds.; Annual Reviews: Palo Alto, 2011; Vol. 36. Anastas, P. T. *Chemsuschem* **2009**, *2*, 391.

(4) Manley, J. B.; Anastas, P. T.; Cue, B. W. *Journal of Cleaner Production* **2008**, *16*, 743.

(5) Chaikin, S. W.; Brown, W. G. *Journal of the American Chemical Society* **1949**, *71*, 122.

(6) Nystrom, R. F.; Brown, W. G. *Journal of the American Chemical Society* **1947**, *69*, 1197.

(7) Noyori, R.; Hashiguchi, S. *Accounts of Chemical Research* **1997**, *30*, 97.

(8) Cha, J. S. *Bulletin of the Korean Chemical Society* **2007**, *28*, 2162.

(9) Wilds, A. *Organic Reactions* **1944**, *2*, 178.

(10) Degraauw, C. F.; Peters, J. A.; Vanbekkum, H.; Huskens, J. *Synthesis-Stuttgart* **1994**, 1007.

(11) U.S. Patent and Trademark Office. Laws, Regulations, Policies, and Procedures. http://www.uspto.gov/patents/law/index.jsp (accessed May 4, 2012).

(12) Jimenez-Gonzalez, C.; Poechlauer, P.; Broxterman, Q. B.; Yang, B. S.; Ende, D. A.; Baird, J.; Bertsch, C.; Hannah, R. E.; Dell'Orco, P.; Noorrnan, H.; Yee, S.; Reintjens, R.; Wells, A.; Massonneau, V.; Manley, J. *Organic Process Research & Development* **2011**, *15*, 900.

(13) Jas, G.; Kirschning, A. *Chemistry-A European Journal* **2003**, *9*, 5708.

(14) Barthe, P.; Guermeur, C.; Lobet, O.; Moreno, M.; Woehl, P.; Roberge, D. M.; Bieler, N.; Zimmermann, B. *Chemical Engineering & Technology* **2008**, *31*, 1146.; Roberge, D. M.; Zimmermann, B.; Rainone, F.; Gottsponer, M.; Eyholzer, M.; Kockmann, N. *Organic Process Research & Development* **2008**, *12*, 905.

(15) Cox, P. M.; Betts, R. A.; Jones, C. D.; Spall, S. A.; Totterdell, I. J. *Nature* **2000**, *408*, 184.

(16) EPA. *Inventory of Greenhouse Gas Emissions and Sinks: 1990-2010.* Environmental Protection Agency, Washington, D.C.: 2010.

(17) Ciferno, J.; Litynski, J. National Energy Technology Laboratory, 2011.

(18) Robertson, E. P. *International Journal of Coal Geology* **2009**, *77*, 234.

(19) Wright, H. B.; Moore, M. B. *Journal of the American Chemical Society* **1948**, *70*, 3865.; Hirst, L. L.; Pinkel, II *Industrial and Engineering Chemistry* **1936**, *28*, 1313.

(20) Kohl, A.; Neilsen, R. *Gas Purification*; Gulf Publishing Company: Houston, TX, 1997.

(21) Strazisar, B. R.; Anderson, R. R.; White, C. M. *Energy & Fuels* **2003**, *17*, 1034.; Bello, A.; Idem, R. O. *Industrial & Engineering Chemistry Research* **2005**, *45*, 2569.

(22) Littel, R. J.; Versteeg, G. F.; Vanswaaij, W. P. M. *Chemical Engineering Science* **1992**, *47*, 2027.; Dubois, L.; Mbasha, P. K.; Thomas, D. *Chemical Engineering & Technology* **2010**, *33*, 461.; Sander, M. T.; Mariz, C. L. *Energy Conversion and Management* **1992**, *33*, 341.

(23) Sartori, G.; Savage, D. W. *Industrial & Engineering Chemistry Fundamentals* **1983**, *22*, 239.

(24) Favre, E.; Roizard, D.; Bounaceur, R.; Koros, W. J. *Industrial & Engineering Chemistry Research* **2009**, *48*, 3700.

(25) Samanta, A.; Zhao, A.; Shimizu, G. K. H.; Sarkar, P.; Gupta, R. *Industrial & Engineering Chemistry Research* **2012**, *51*, 1438.

(26) Choi, S.; Gray, M. L.; Jones, C. W. *Chemsuschem* **2011**, *4*, 628.

(27) Ho, S.-H.; Chen, C.-Y.; Lee, D.-J.; Chang, J.-S. *Biotechnology Advances* **2011**, *29*, 189.

(28) Scovazzo, P.; Camper, D.; Kieft, J.; Poshusta, J.; Koval, C.; Noble, R. *Industrial & Engineering Chemistry Research* **2004**, *43*, 6855.; Bara, J. E.; Camper, D. E.; Gin, D. L.; Noble, R. D. *Accounts of Chemical Research* **2010**, *43*, 152.

(29) Jassim, M. S.; Rochelle, G. T. *Industrial & Engineering Chemistry Research* **2006**, *45*, 2465.

# CHAPTER 2: ENHANCED MEERWEIN-PONNDORF-VERLEY (MPV) REDUCTIONS WITH $Al(OtBu)_3$

## 2.1 Introduction

The formation of alcohol functionalities is extremely important. Alcohol functional groups are widely found in active pharmaceutical ingredients, as starting materials for commercial polymers like polyester, and in the beverage industry. Alcohols can also be used in reaction with other functional groups to create esters, ethers, amines, carboxylic acids, aldehydes, ketones, epoxides, and many others.[1] Since formation of alcohols are of great interest, many methods have been developed to produce them through reduction of carbonyl groups, specifically from aldehydes and ketones.

### 2.1.1 The MPV Reduction

Many methods have been developed for the synthesis of primary and secondary alcohols from ketones and aldehydes including borohydride reductions,[2] asymmetric hydrogen transfer reactions with transition metals,[3] lanthanide catalysts,[4] and aluminum alkoxides to name a few. The latter is known as the Meerwein-Ponndorf-Verley (MPV) reduction shown in Figure 2.1.[5]

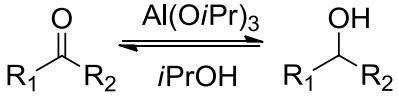


**Figure 2.1.** Meerwein-Ponndorf-Verley reduction

MPV is an established strategy in academia and industry alike because it is (1) chemoselective, (2) inexpensive, (3) operates under mild conditions, and (4) is easily scalable.[6] The accepted mechanism for the reduction of ketones and aldehydes with an aluminum alkoxide catalyst, most commonly $Al(OiPr)_3$, is shown in Figure 2.2.[7] The reaction proceeds by coordination of the carbonyl oxygen to the aluminum, followed by a hydride transfer from the alkoxide ligand on the aluminum to the carbonyl substrate through a 6-membered transition state. In the presence of excess alcohol, generally 2-propanol or iPrOH, the alkoxide exchange is facile and results in the regeneration of the active aluminum catalyst and the desired alcohol product.

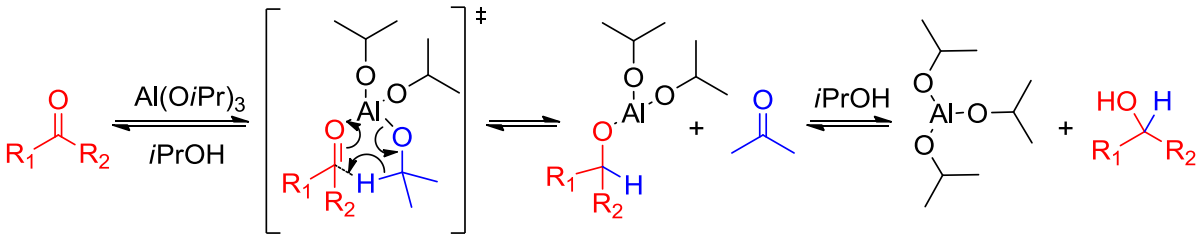


**Figure 2.2.** MPV reduction mechanism through a six-membered transition state

As seen in Figure 2.2, the MPV reduction is an equilibrium reaction, the reverse reaction is known as the Oppenauer oxidation.[8] As a result, stoichiometric amounts of aluminum alkoxide catalyst, large excess of α-hydride donating alcohol (often solvent & reactant), and elevated temperatures are used to drive the reaction to completion.

To provide a baseline for comparison of catalyst modification for improved MPV reductions, it is first important to look at the conventional MPV reduction. The MPV reduction uses aluminum isopropoxide ($Al(OiPr)_3$) in the presence of iPrOH. The catalyst

has one coordination site, the aluminum center to promote the reaction. Alkoxides are used as ligands because they can participate in exchange with the alcohol solvent, an imperative step in the progress of the reaction. Alkoxide ligands also introduce electron density onto the aluminum center which can make Lewis type coordination slow. Because the MPV reduction is such a commonly used method for the formation of alcohols, even in industry, improving the reaction rate and efficiency is important.

Many catalysts and conditions have been developed to enhance the MPV reduction with respect to rate and yield for the reductions of aldehydes and ketones.[9] Examples include bidentate aluminum reagents,[10,11] alkoxyboranes,[12,13] and lanthanide based systems.[14] Alkoxy boranes have been investigated as analogs of aluminum alkoxides. Specifically, $B(OEt)_3$ at 30 mol% was not effective in reducing aromatic ketones at room temperature but enabled the reduction of aliphatic ketones.[12] Examples in Figure 2.3 show a bidentate aluminum species that has been successfully used to improve the reduction rate of benzaldehyde by incorporating two aluminum centers on one catalyst.[10] This made the coordination of benzaldehyde to a reactive aluminum center much more facile, promoting the reduction. BINOL-alkoxides have also been shown to be effective in reducing prochiral ketones enantioselectively.[11] 1,1'-Bi-2-naphthol or BINOL is a chiral ligand due to the naphthyl rings being twisted away from each other. Because these are chiral, reduction of the carbonyl is preferred on one face over the other. Lanthanide based BINOL derivatives have shown to be effective in performing the reduction of acetophenone with 10 mol% at room temperature but the reaction required 41 hrs to reach completion and although the conversion was 100%, the yield was only 64%.[14]

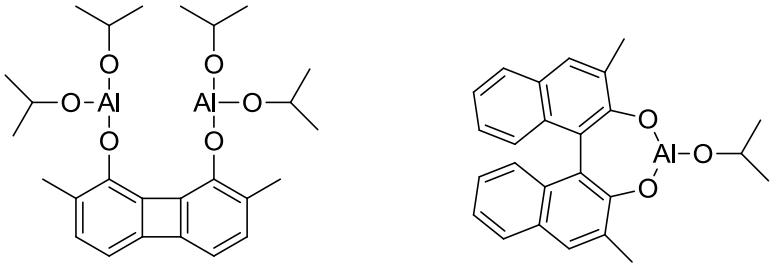

**Figure 2.3.** Examples of bidentate and BINOL-Al catalyst complexes

Even though bidentate ligands show superior reduction capabilities compared to the conventional $Al(OiPr)_3$ catalyst, the formation of the bidentate ligands and BINOL-Al complexes requires *in-situ* synthesis from reactive, highly air-sensitive trimethylaluminum. Although uncontested improvements were made to the reaction performances, practical, industrial applications remain limited by the reactive nature of alkylaluminum species such as pyrophoricity.

Alternatively, simple aluminum alkoxide catalysts that are commercially available such as $Al(O\textit{t}Bu)_3$ have not been extensively studied. $Al(O\textit{t}Bu)_3$ for instance does not have an α-hydrogen available to perform the reduction, making it intuitively a poor choice for MPV reduction but in the presence of a secondary alcohol reaction is possible through alkoxide-alcohol exchange. Few reports nonetheless have documented $Al(O\textit{t}Bu)_3$ catalyzed MPV reduction of steroids in an effort to enhance stereoselectivity (via preferential catalyst approach on the less sterically hindered face).[15] TFA-$Al(O\textit{t}Bu)_3$ adducts have been shown to reduce benzaldehyde at an enhanced rate because the alkoxides are protonated which draws electron density from the aluminum center making it more Lewis acidic and improving carbonyl coordination.[16] Although improved over the conventional catalyst, this MPV reduction suffers from competition of the product alcohols reacting with the carbonyl groups in solution, catalyzed by TFA.

Though many methods have been researched for improved MPV reductions, limitations in cost, toxicity and health hazards, and time for catalyst preparation have led $Al(OiPr)_3$ to be the mainstay in industrial MPV processes. One example in particular is the reduction of *N*-(tert-butyloxycarbonyl)-(3*S*)-3-amino-1-chloro-4-phenyl-2-butanone or (*S*)-CMK. Our initial work focused on the improvement of diastereoselectivity in the reduction of (*S*)-CMK.

### 2.1.2 The MPV reduction of (S)-CMK

(*S*)-CMK is reduced industrially to form the product alcohols, *N*-(*tert*-butyloxycarbonyl)-(3*S*)-3-amino-1-chloro-4-phenyl-(2*R*)-butanol (or (*R,S*)-CMA) and *N*-(*tert*-butyloxycarbonyl)-(3*S*)-3-amino-1-chloro-4-phenyl-(2*S*)-butanol (or (*S,S*)-CMA), which are intermediates in the synthesis of commercial HIV-protease inhibitors Atazanavir®, Saquinavir® and Amprenavir® (Figure 2.4).[17]

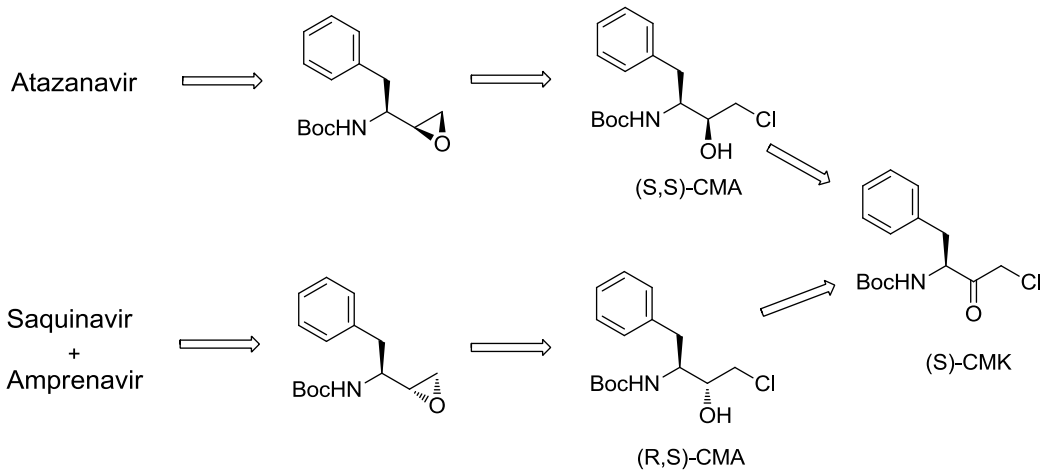


**Figure 2.4.** Retrosynthesis in the formation of HIV-Protease inhibitors from (*S*)-CMK

At industrial scale, (*S*)-CMK is reduced via a classic MPV protocol utilizing $Al(OiPr)_3$ loadings of 50 mol% at 50°C in iPrOH for two hours (Figure 2.5).[18]

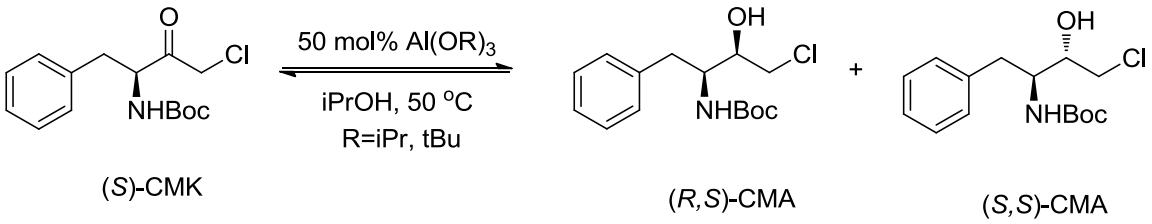


**Figure 2.5.** Industrial conditions in the MPV reduction of (*S*)-CMK

Notably, (*S*)-CMK is a relatively complex molecule. It is an α-chloro ketone, thus is susceptible to dehalogenation and has an acid-sensitive Boc-protected amine. An MPV reduction protocol is particularly pertinent to enable selective reduction of the carbonyl to an alcohol while maintaining the integrity of (*S*)-CMKs functional groups. We sought to investigate the role of the aluminum alkoxide structure on the reduction of (*S*)-CMK to its two diastereomeric alcohols, (*R,S*)-CMA and (*S,S*)-CMA in an attempt to change the diastereoselectivity of the preferred alcohol product.

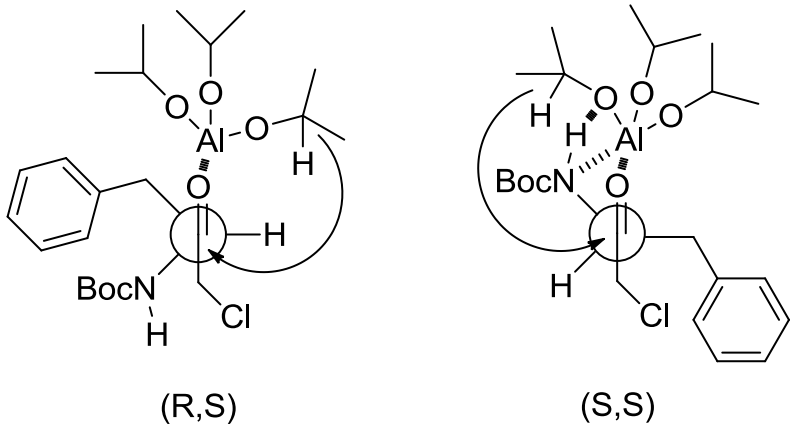


**Figure 2.6.** Newman projection of the transition states in the selective reduction of (*S*)-CMK

The current industrial MPV reduction method with $Al(OiPr)_3$ is highly diastereoselective for the (*S,S*)-CMA over the (*R,S*)-CMA diastereoisomer.[19] The preference for the formation of the (*S,S*)-CMA was attributed to the favorable hydrogen bonding of the amine with the alkoxide oxygen as well as coordination to the aluminum center of the amine lone pair in the transition state, shown in Figure 2.6. This is a chelation-control model based on the interaction of the nitrogen lone pair with the aluminum alkoxide center. In both models, the steric hindrance of the benzyl group favors reduction through addition of the hydride on the least hindered face. The chelation aids in the selectivity for the (*S,S*)-CMA diastereomer. Developing efficient synthetic routes to the (*R,S*) stereoisomer is important because both the (*S,S*) and (*R,S*) diastereomers are intermediates in the synthesis of the commercial drugs Atazanavir® and Amprenavir®, respectively. We have investigated new approaches to favor the formation of the (*R,S*)-CMA over the (*S,S*)-CMA using various reduction techniques including chiral borane reductions, asymmetric hydrogenations with ruthenium catalysts,

and MPV reductions with variables including solvent, aluminum alkoxide catalyst, and amine protecting groups on the (*S*)-CMK.

### 2.1.3 Prior work

Dr. Kristen Kitagawa from our group, reported a significant increase in the diastereomeric ratio of (*R,S*)-CMA to (*S,S*)-CMA by limiting hydrogen bonding ability of the amine on the (*S*)-CMK starting material. Specifically, by replacing the amine protecting group from BOC to phthalimide , the diastereomeric ratio was increased from 0.06:1 to 1.1:1. She also investigated MPV reductions of (*S*)-CMK in different organic solvents with a wide range of polarities and solvent properties from toluene to DMSO. The highest *R,S* to *S,S* ratio (0.39:1) was achieved with acetonitrile as solvent, which was, the most hydrogen bond accepting solvent.[20] Herein, I report our investigation of aluminum alkoxide catalysts toward an enhanced MPV protocol for a more efficient reduction of carbonyls in terms of environmental impact as well a cost-competitiveness. Our study focused on three-substrates: the two model compounds benzaldehyde and acetophenone, and the pharmaceutically relevant (*S*)-CMK.

## 2.2 Results and Discussion

### 2.2.1 Changes in aluminum alkoxide structure

The effect of the structure of the aluminum alkoxide structures in the MPV reduction of (*S*)-CMK was further investigated. Specifically we chose $Al(OEt)_3$, $Al(OiPr)_3$, and $Al(OtBu)_3$ as they exhibit increased steric hindrance around the aluminum, coordination center. Otherwise, the conditions of the reaction remained identical to the one reported in industry including 50 mol% of the catalyst, a temperature of 50°C, and iPrOH as the solvent and reagent. It was hypothesized that the steric hindrance

surrounding the aluminum center may limit the hydrogen bonding ability between alkoxide oxygen and the amine of the (*S*)-CMK and therefore alter the diastereoselectivity of the reaction, seen in Figure 2.7.

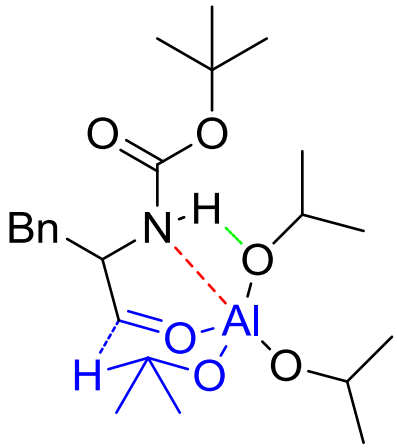


**Figure 2.7.** Six-membered transition state for the formation of (*S,S*)-CMA through interaction of the amine with the aluminum alkoxide

Shown in Table 2.1 below are the HPLC results of varying aluminum alkoxide used in the reduction of (*S*)-CMK at 50$^{o}$C for 2 hours. HPLC was used to monitor the reaction progress because the separation of the (*S*)-CMK, (*S,S*)-CMA, and (*R,S*)-CMA was achieved and could be quantified from calibration curves. The conversion was measured based on the amount of starting material disappearance and the yield based on the amount of products formed. The diastereomeric ratio (*dr*) was calculated based on the area of the (*R,S*)-CMA to (*S,S*)-CMA formed. The reduction with $Al(OtBu)_3$ suprisingly had the highest conversion and yield at 99% conversion and 86% yield. The $Al(OiPr)_3$ and $Al(OEt)_3$ had similar conversions of about 90% and yields in the range of 75%. The difference between yield and conversion was expected to be from the acid workup of the reaction deprotecting the BOC group and small amounts of de-

chlorination. The measured *dr* are about 0.06 indicating that the steric hindrance on the catalyst does not significantly affect the stereoselectivity of the reduction. Although no change was observed in the *dr*, a critical experimental observation was made. When $Al(OtBu)_3$ was used as the catalyst, the precipitation of the alcohol products was observed after only 10 minutes of reaction. This was unexpected and triggered further studies.

**Table 2.1.** Results from the reduction of (*S*)-CMK with different aluminum alkoxides

| | ***dr*** | **% Conversion** | **% Yield** |
|---|---|---|---|
| **$Al(OtBu)_3$** | 0.05 ± 0.01 | 99.0 ± 0.2 | 86 ± 1.3 |
| **$Al(OiPr)_3$** | 0.06 ± 0.00 | 89.0 ± 5.4 | 71 ± 5.2 |
| **$Al(OEt)_3$** | 0.06 ± 0.00 | 90.0 ± 2.1 | 76 ± 0.7 |

It must be highlighted that this observation was even more surprising from the standpoint that $Al(OtBu)_3$ has no α-hydrogens available for reduction to proceed (see mechanism-Figure 2.2). In the presence of iPrOH as solvent, the reaction not only proceeds but proceeds faster. Alkoxide transfer has been widely documented and is known to be rapid.[21] iPrOH can exchange with tert-butoxide ligands on the aluminum center and form aluminum isopropoxide bonds, resulting in an active catalyst. Although the reaction was expected to take place, it was not clear why the rate of the reduction was drastically enhanced. To understand this rate enhancement, kinetic studies were performed between the $Al(OiPr)_3$ and $Al(OtBu)_3$ catalysts in the reduction of (*S*)-CMK.

### 2.2.2 MPV reduction rates comparing $Al(OiPr)_3$ and $Al(OtBu)_3$ in iPrOH

#### 2.2.2.1 MPV reduction of (*S*)-CMK in iPrOH

The direct comparison in the reduction of (*S*)-CMK with $Al(OiPr)_3$ and $Al(OtBu)_3$ is reported below. The reductions were conducted with the industrially used reaction conditions, 50 mol% representative aluminum alkoxide at 50°C in a carousel. Reactions were quenched with 2M HCl and diluted with MeOH at defined time intervals to derive the kinetic data shown below in Figure 2.8. The conversion and yield were derived from HPLC calibration curves. The conversion was calculated from the loss of starting material and the yield from the formation of products.

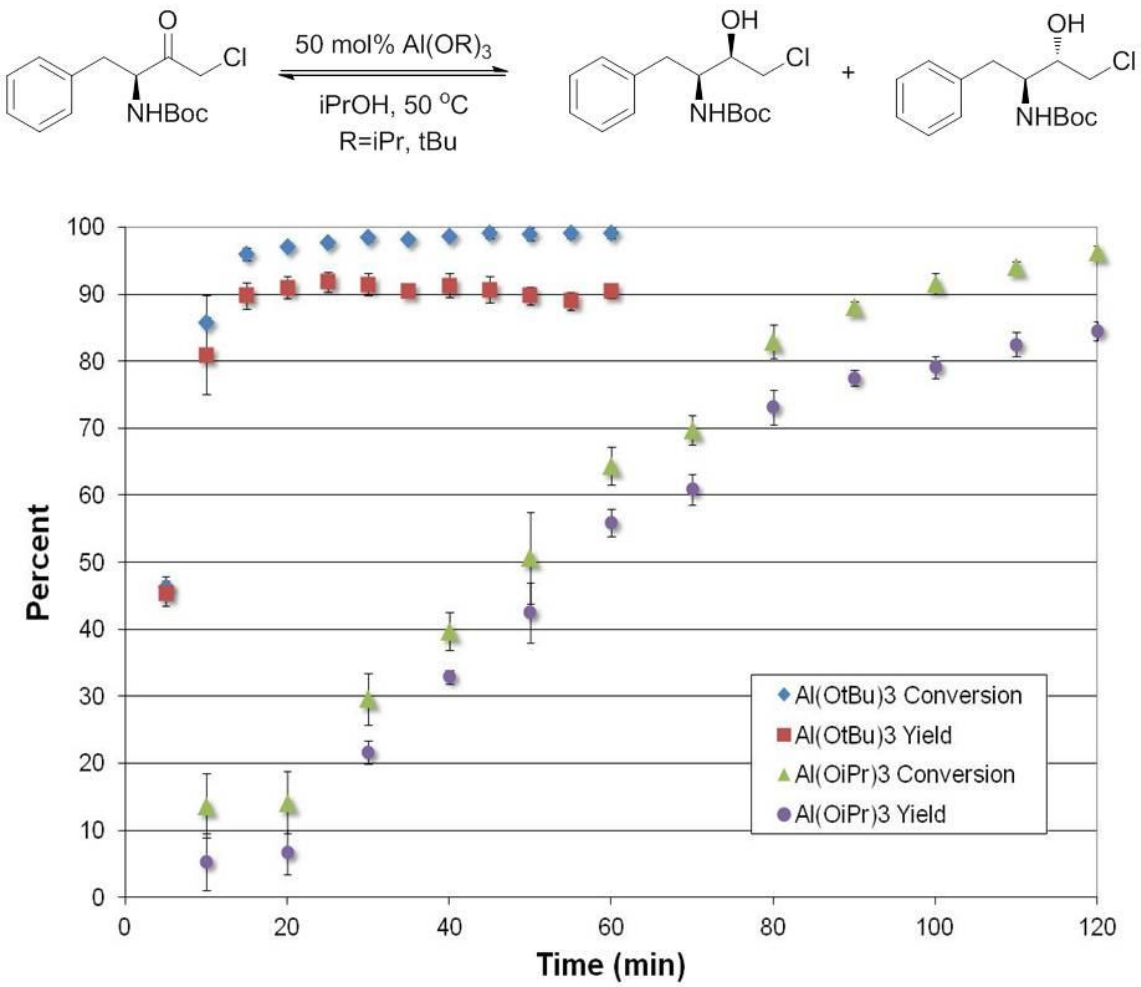


**Figure 2.8.** Reduction of (*S*)-CMK in iPrOH with 50 mol% $Al(OtBu)_3$ and $Al(OiPr)_3$ at 50°C

Figure 2.8 shows the reaction progress as a function of time for the reduction of (*S*)-CMK with two different aluminum alkoxide catalysts. With $Al(OtBu)_3$ as the catalyst, the (*S*)-CMK starting material was completely converted after only 20 minutes to CMA products. In contrast, reductions at the same conditions with $Al(OiPr)_3$ as the catalyst resulted in complete conversion after 120 minutes—6 times longer than the *tert*-butoxide analog. It is also important to note that the product alcohols precipitate from the iPrOH

solution, possibly acting as a driving force to push the equilibrium forward meaning faster reaction.

An initial rate constant was calculated for the $Al(OtBu)_3$ and $Al(OiPr)_3$ catalyzed reductions. The $k_{app}$ or apparent rate constants assuming pseudo-first order rate expressions, are shown in Table 2.2. The method of calculation can be found in the experimental section at the end of the chapter. One can see that the initial rate is almost 9 times as fast in the reduction with $Al(OtBu)_3$ versus $Al(OiPr)_3$ with $k_{app}$ calculated as 0.0856 and 0.0101, respectively.

**Table 2.2.** Apparent rate constants for the reduction of (*S*)-CMK at 50°C

| Starting material | Catalyst | $k_{app}$ ($min^{-1}$) |
|---|---|---|
| (*S*)-CMK | $Al(OtBu)_3$ | 0.0856 |
| | $Al(OiPr)_3$ | 0.0101 |

This rate study was extended to two model compounds, benzaldehyde and acetophenone, representative aldehyde and ketone species to broaden the scope of the MPV enhancements.

2.2.2.2. MPV reduction of benzaldehyde in iPrOH

At 50°C, the reduction of benzaldehyde with 50 mol% $Al(OtBu)_3$ reached completion after about 3 minutes. As a consequence, the kinetic experiments were conducted in triplicate at 40°C. Analysis followed quenching the reactions with 2M HCl and diluting with MeOH. The samples were run with HPLC and quantified based on established calibration curves for benzaldehyde and benzyl alcohol.

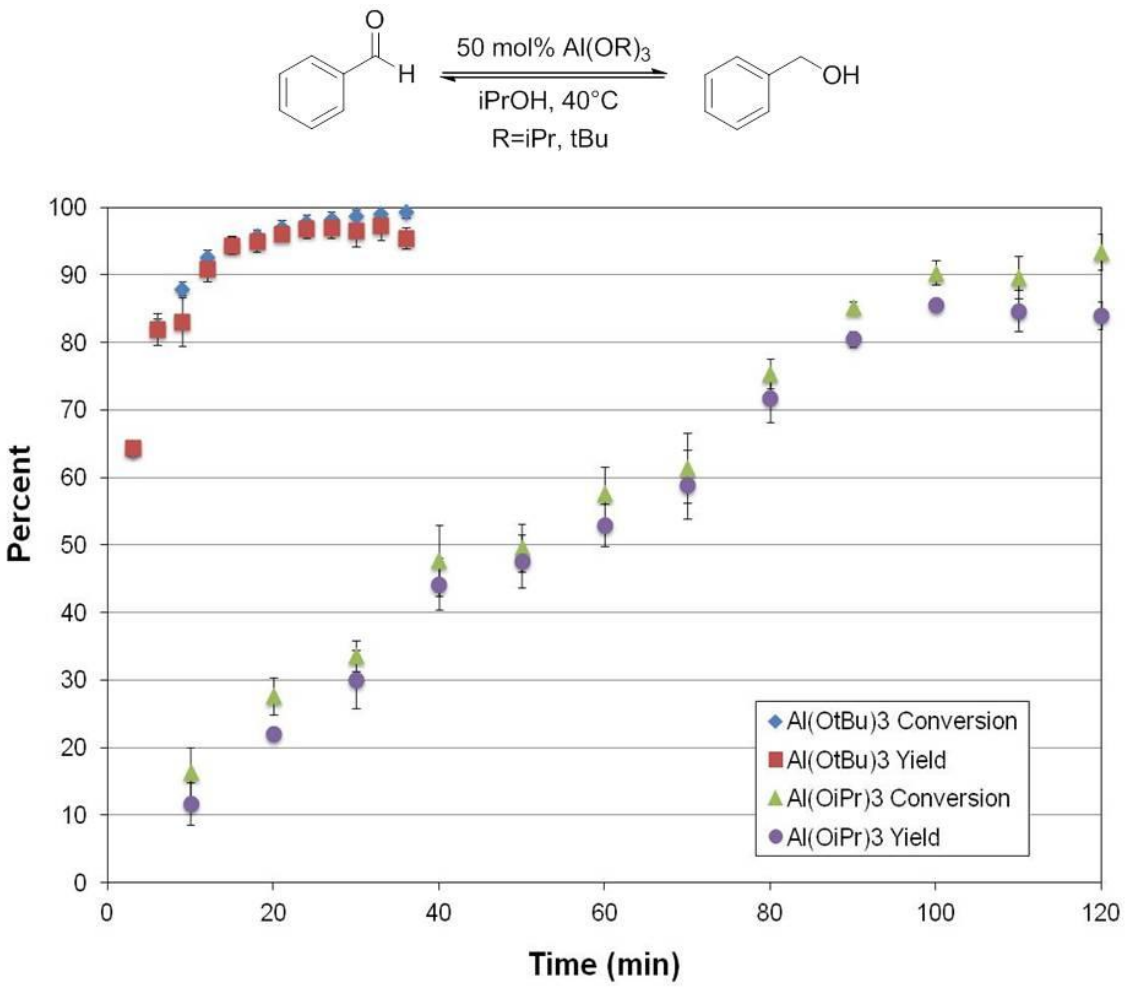


**Figure 2.9.** Reduction of benzaldehyde with 50 mol% $Al(OtBu)_3$ and $Al(OiPr)_3$ in iPrOH at 40°C

From Figure 2.9 above, it is apparent that the $Al(OtBu)_3$ is indeed a more active catalyst in the reduction of benzaldehyde. The reduction reaches completion after about 30 minutes at 40°C. With $Al(OiPr)_3$ under the same conditions, the reduction requires close to 120 minutes to reach completion. Initial rate calculations from Table 2.3 show that the $Al(OtBu)_3$ is actually 20 times faster than the $Al(OiPr)_3$ catalyzed system!

**Table 2.3.** Apparent rate constants in the reduction of benzaldehyde at 40°C

| Starting Material | Catalyst | $k_{app}$ ($min^{-1}$) |
|---|---|---|
| Benzaldehyde | $Al(OtBu)_3$ | 0.2141 |
| | $Al(OiPr)_3$ | 0.0116 |

2.2.2.3. MPV Reduction of acetophenone in iPrOH

Acetophenone was also reduced with both catalysts. Again, the $Al(OtBu)_3$ outperformed the $Al(OiPr)_3$ with respect to reaction rate and after 120 minutes the reaction was about 65% complete. In order to reach 65% completion with $Al(OiPr)_3$, the reaction time was on the order of 350 minutes. This data is shown in Figure 2.10.

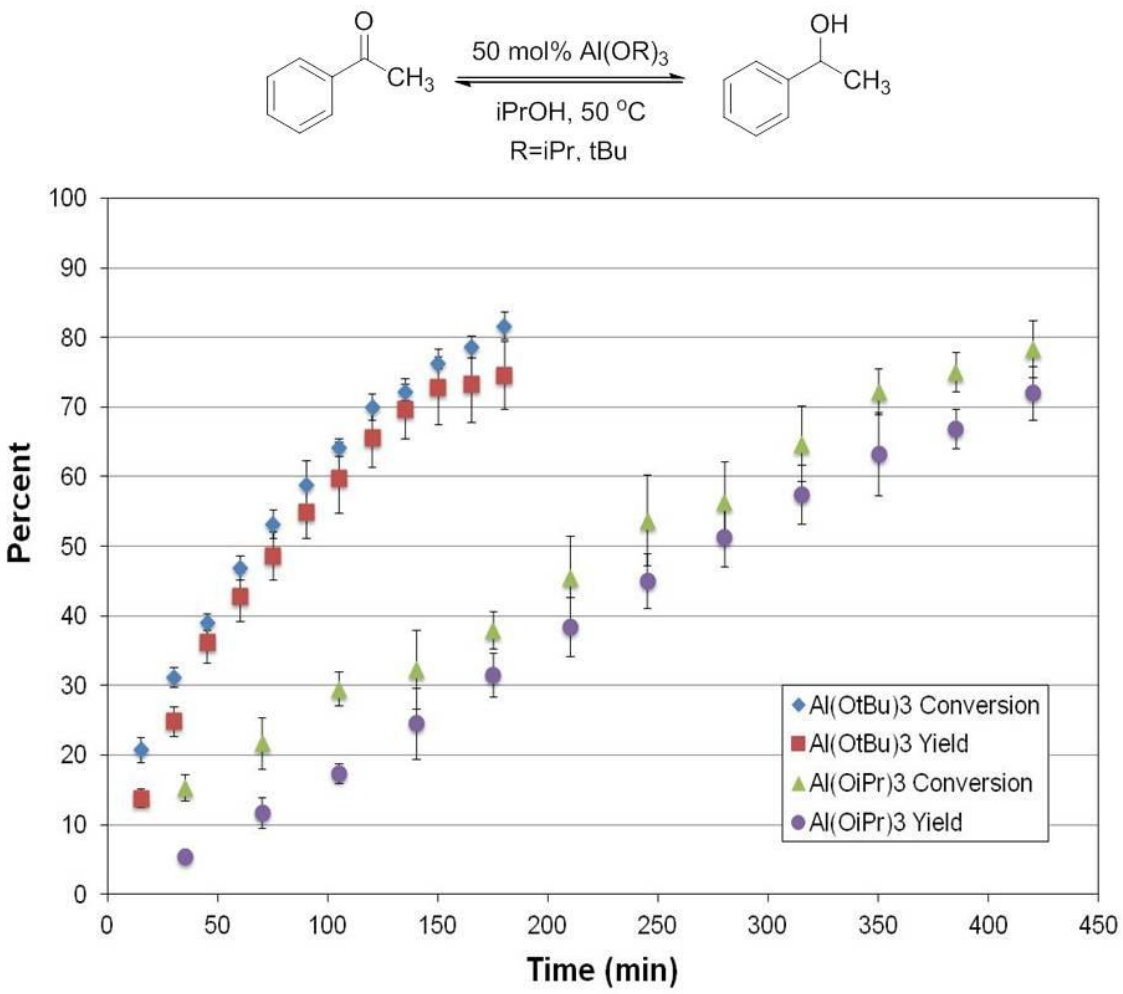


**Figure 2.10.** Reduction of acetophenone with 50 mol% $Al(OtBu)_3$ and $Al(OiPr)_3$ in iPrOH at 50°C

The initial rates were calculated to be 0.0106 for the $Al(OtBu)_3$ reduction and 0.0032 for the $Al(OiPr)_3$ reduction and are displayed in Table 2.4. This shows that the $Al(OtBu)_3$ catalyzed reaction is 3 times faster than the conventional MPV catalyst.

**Table 2.4.** Apparent rate constants in the reduction of acetophenone at 50°C

| Structure | Catalyst | $k_{app}$ ($min^{-1}$) |
|---|---|---|
| Acetophenone | $Al(OtBu)_3$ | 0.0106 |
| | $Al(OiPr)_3$ | 0.0032 |

It was initially thought that the reduction of acetophenone would be on the same order of rate as the (*S*)-CMK so the intervals between reaction quenches were not long enough to see the reaction reach completion. An experiment was run to look at the disappearance of acetophenone over time and it was found that even after 4300 minutes, acetophenone was still present. These results are plotted in Figure 2.11. The fact that the (*S*)-CMK reduction is so much faster with either catalyst system than acetophenone may be a combination of the CMA products precipitating out of reaction, the increased electrophilicity of the carbonyl in (*S*)-CMK due to the α-chlorine atom, and the amine hydrogen bonding interaction with the alkoxide units.

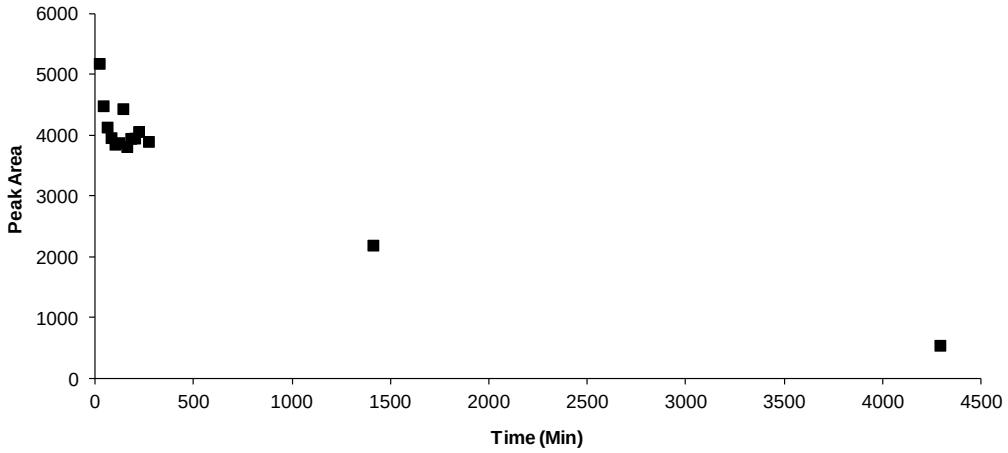


**Figure 2.11.** Reduction of acetophenone as a function of time

Rate enhancements were noted with all of the compounds investigated when utilizing $Al(OtBu)_3$ as a catalyst compared to $Al(OiPr)_3$. It was expected that the amount of iPrOH used in these systems, which was used as a solvent and co-reagant was promoting this enhanced rate through facile ligand exchange with the $Al(OtBu)_3$. To test this, reductions of (*S*)-CMK, acetophenone, and benzaldehyde were run with only 10% iPrOH in toluene. The reduction of iPrOH should promote competitive rates with the two catalysts if the ligand exchange is the key factor.

### 2.2.3 MPV Reductions in a mixed solvent system: toluene and iPrOH

2.2.3.1 Reduction of (*S*)-CMK with 10% iPrOH in toluene:

The reduction of (*S*)-CMK was conducted with both catalysts in a solution of toluene and iPrOH (9:1) (Figure 2.12).The $Al(OtBu)_3$ still outperformed the $Al(OiPr)_3$ catalyst, enabling reaction completion in 50 minutes whereas the $Al(OiPr)_3$ catalyst enabled 95% reaction completion in  300 minutes.

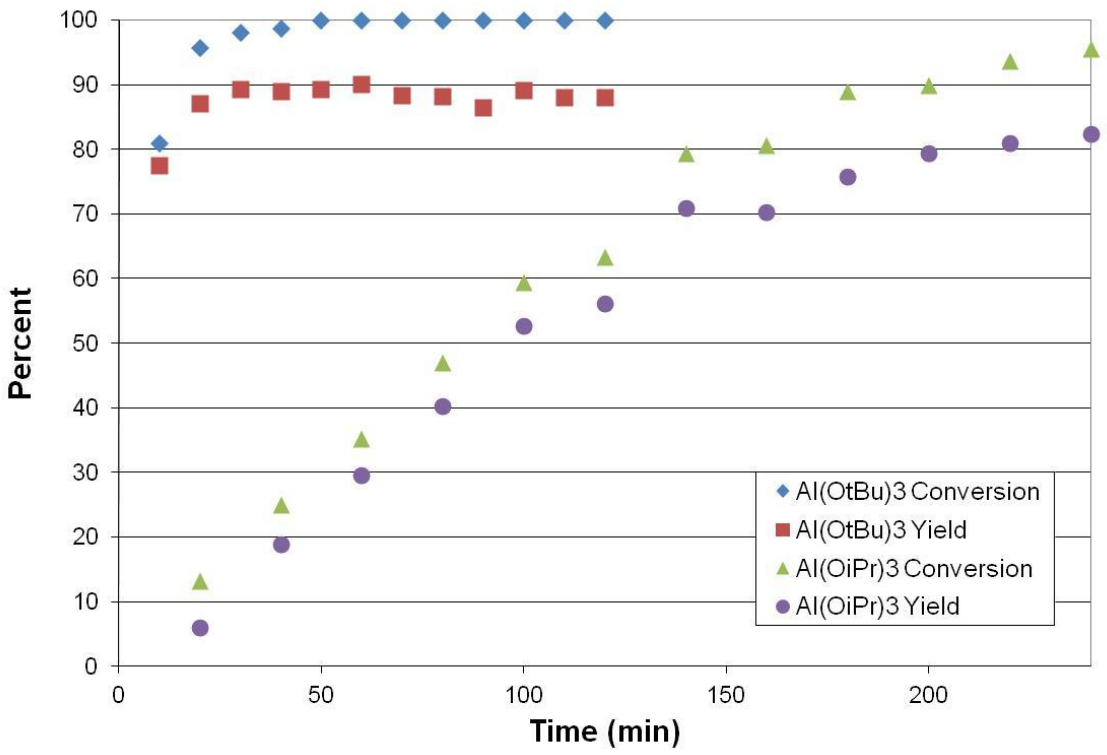


**Figure 2.12.** Reduction of (*S*)-CMK with 50 mol% $Al(OtBu)_3$ and $Al(OiPr)_3$ with 10% iPrOH in toluene at 50°C

Although it was noted that lower loadings of iPrOH still led to enhanced rates in the reduction of (*S*)-CMK, precipitation of the product alcohols during the course of the reaction could not be ruled out to be the driving force of the reaction rate. Furthermore, if the MPV reduction of (*S*)-CMK were to be converted from batch to continuous flow, precipitation of the alcohols would be detrimental. To validate the rate enhancement of $Al(OtBu)_3$ for the MPV reduction of ketones and aldehydes, two model compounds, benzaldehyde and acetophenone were reduced with both $Al(OtBu)_3$ and $Al(OiPr)_3$ in iPrOH and toluene:iPrOH (9:1) systems.

2.2.3.2 MPV reduction of benzaldehyde with 10% iPrOH in toluene:

When the reductions were run in 10% iPrOH in toluene, the same trend followed for the reduction of benzaldehyde. The $Al(OtBu)_3$ catalyzed reduction reached 90% completion in 50 minutes, taking 180 minutes to reach the same conversion with $Al(OiPr)_3$, shown in Figure 2.13 below.

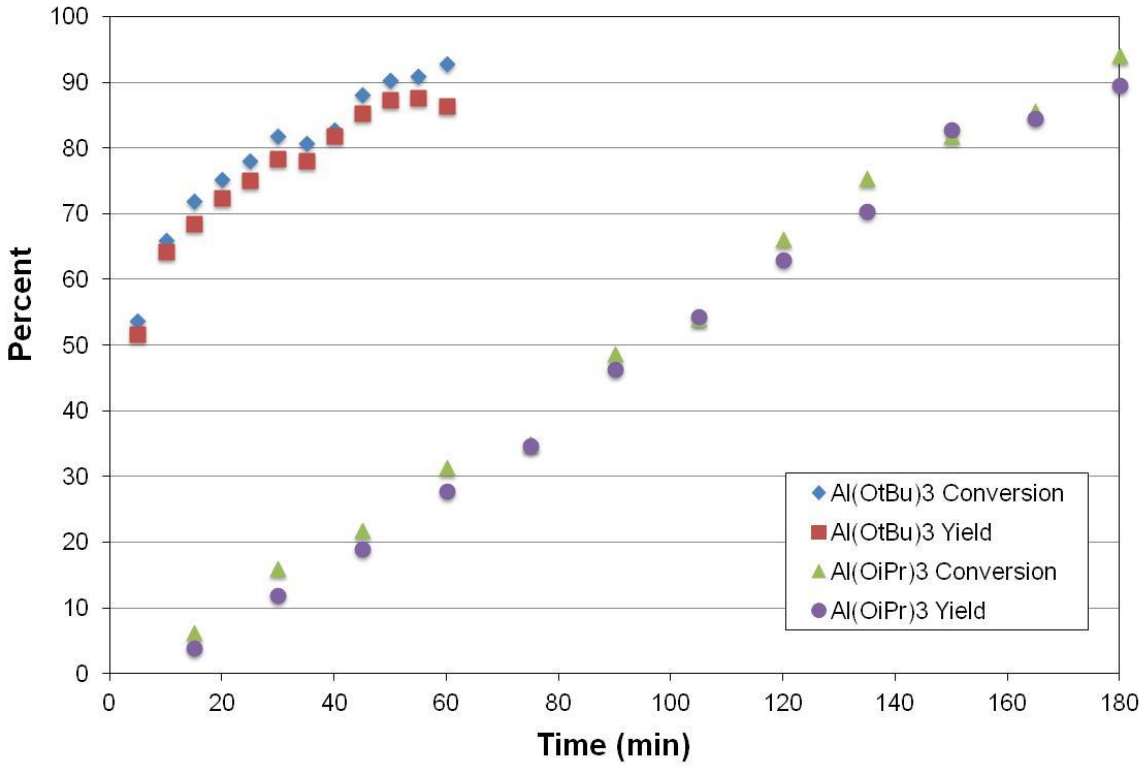


**Figure 2.13.** Reduction of benzaldehyde with 50 mol% $Al(OtBu)_3$ and $Al(OiPr)_3$ in 10% iPrOH in toluene at 40°C

2.2.3.2. MPV Reduction of acetophenone with 10% iPrOH in toluene:

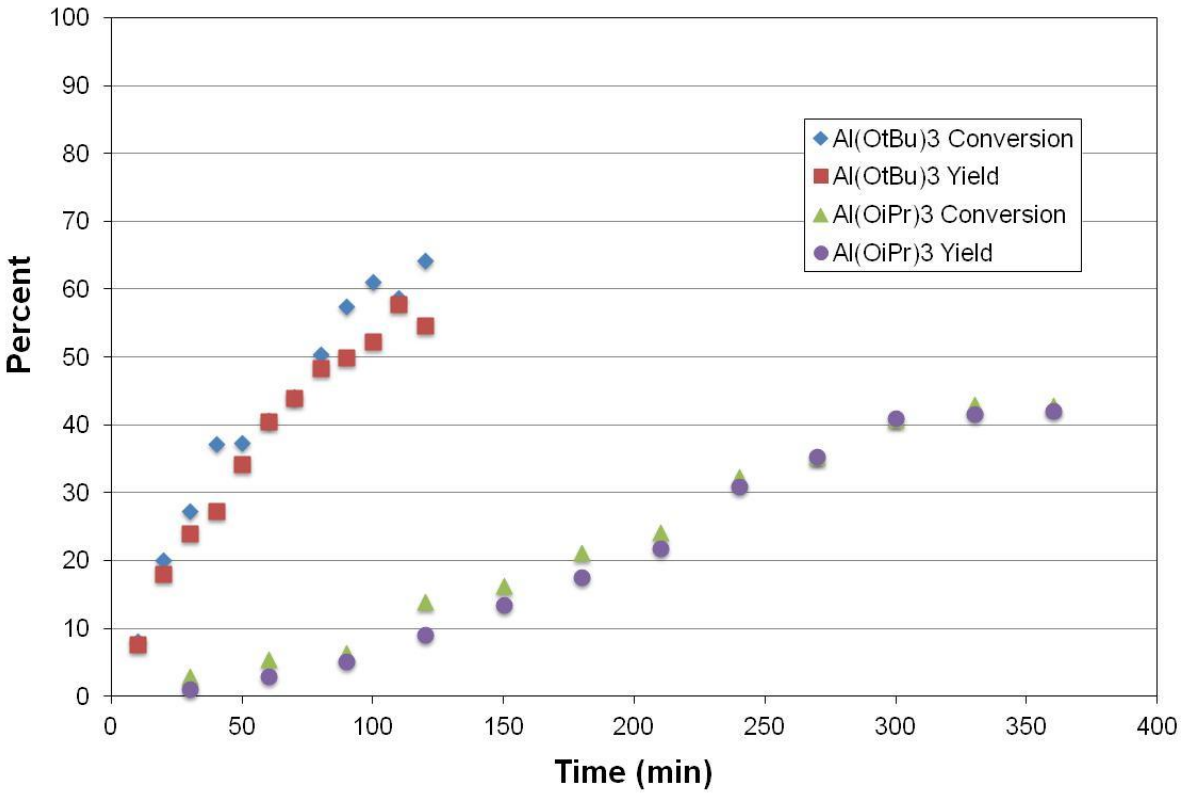


**Figure 2.14.** Reduction of acetophenone with 50 mol% $Al(OtBu)_3$ and $Al(OiPr)_3$ in 10% iPrOH in toluene at 50°C

Figure 2.14 displays the percent conversion and yield as a function of time in the mixed solvent reduction of acetophenone. The $Al(OtBu)_3$ reduction reached only 60% completion after 110 minutes whereas after 360 minutes of reaction, the $Al(OiPr)_3$ catalyzed system had only reached just over 40% completion. With less iPrOH, an induction period can be noted in the slope change of the $Al(OiPr)_3$ catalyzed reaction.

Lowering the amount of reactive iPrOH in these systems still promotes enhanced kinetic activity in the reduction of all three model compounds! It is also important to note that mixed solvent systems can be used in the MPV reduction with $Al(OtBu)_3$ to achieve fast reactions. This is beneficial for industry because solvent systems can be tuned to meet the needs of the reactions. Because the rate enhancement was observed with lower loadings of iPrOH, the actual structure of the aluminum complex was expected to have a pronounced effect on the rate. The aggregation states of the aluminum alkoxide complexes were then investigated.

### 2.2.4 Aggregation state of aluminum alkoxide complexes

#### 2.2.4.1 $^1$HNMR explanation of rate enhancement

To explain the observed trend in rate enhancement, investigation into the aluminum alkoxide structures themselves was done. It has been reported previously that the aggregation states of the $Al(OtBu)_3$ and $Al(OiPr)_3$ are different, the first being a cyclic dimer while the latter is a tetramer and are shown in Figure 2.15.[22] The dimer is linked through the Lewis interaction of an alkoxide oxygen lone pair with the aluminum centers. The tetramer is linked through the same interactions but has a hexavalent aluminum center at its core. These aggregation states were confirmed by $^1$HNMR because two types of ligands are apparent in the dimer and tetramer, Lewis-coordinated or bridging ligands and non-bridging ligands.

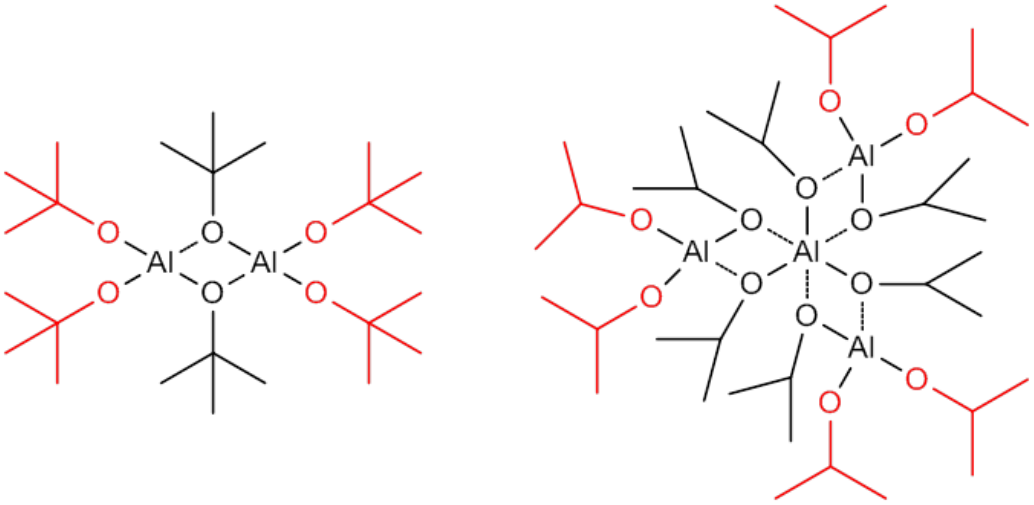


**Figure 2.15.** Aluminum alkoxide states of aggregation

The alkoxide ligands shown in red are non-bridging and the alkoxide ligands shown in black are bridging ligands. Because these ligands are in two different environments, their ratios were measured by $^{1}$HNMR.

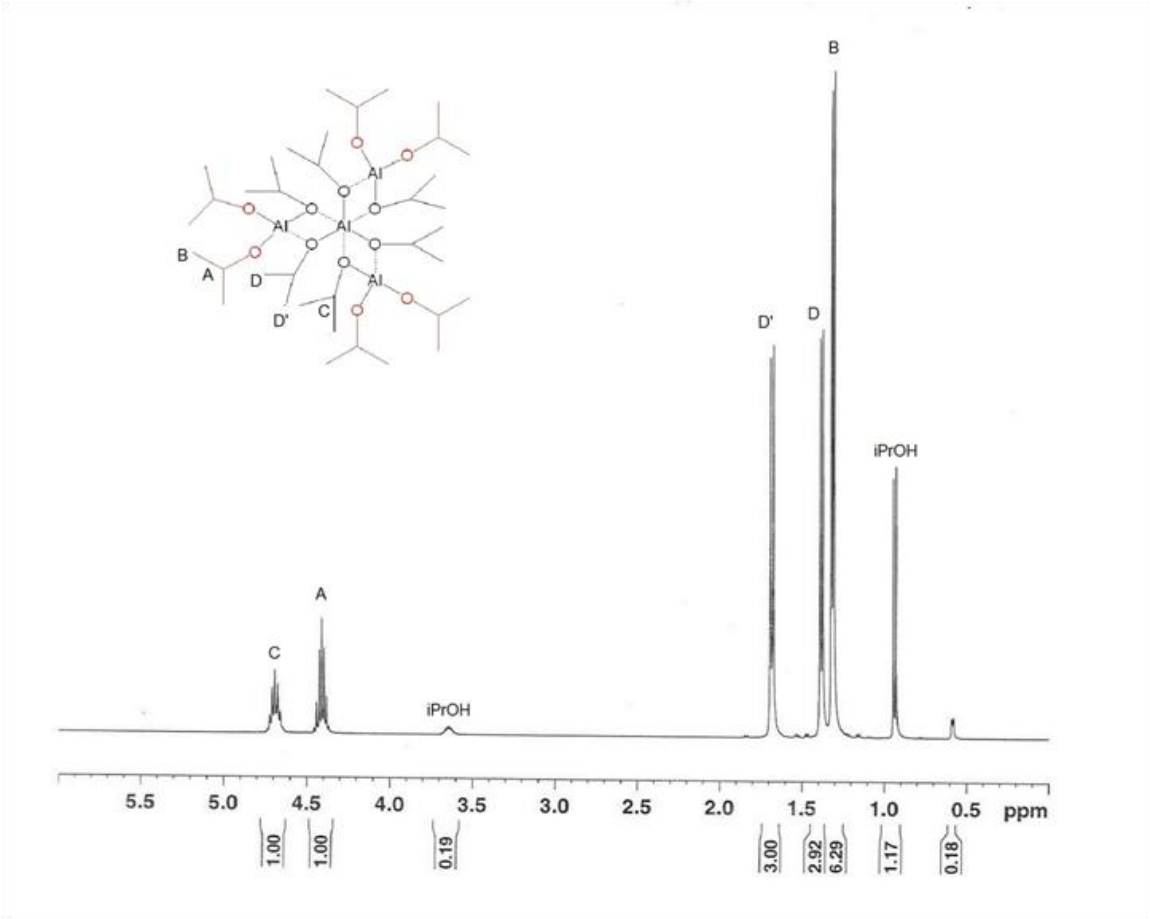


**Figure 2.16.** $^{1}$HNMR of $Al(OiPr)_3$ tetramer in $d_6$-benzene

Figure 2.16 shows the $^{1}$HNMR for the $Al(OiPr)_3$ tetramer in benzene. The non-bridging ligands in the tetramer are more shielded by electron density from the alkoxide oxygen and the methyl groups appear at about 1.3 ppm and integrate to 6 protons. The methyl groups of the bridging alkoxides are in two different environments and appear at 1.4 ppm and 1.7 ppm respectively and account for 6 protons as well. The equal integrations confirmed the tetrameric state of aggregation. The dimeric structure of $Al(OtBu)_3$ was also confirmed by the investigation of the $^{1}$HNMR and shown in Figure

2.17. The bridging and non-bridging alkoxides have different chemical environments and therefore, the methyl groups on the *tert*-butoxide ligands for each of these are different.

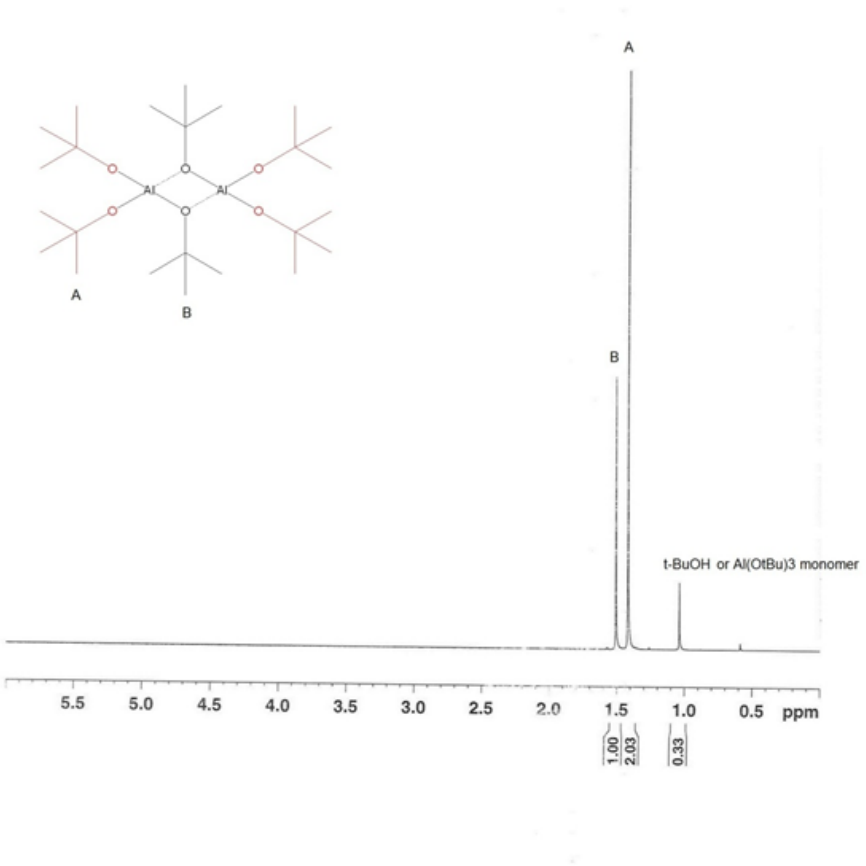


**Figure 2.17.** $^{1}$HNMR of $Al(OtBu)_3$ dimer in $d_6$-benzene

The peaks labeled A correspond to the non-bridging *tert*-butoxy methyl groups and have an integration of 2 protons, normalized. The bridging methyl groups are further downfield as expected and integrate for 1 proton, normalized. This 2:1 ratio is indicative of the dimeric state.

These two different aggregation states are expected to be responsible for the difference in rate. If the ratio of reactive to non-reactive ligands is compared for each catalyst, we find that $Al(OtBu)_3$ has a 2:1 ratio whereas $Al(OiPr)_3$ has a 1:1 ratio. This is important because it has been shown that only the non-bridging ligands are reactive.[16] This means that $Al(OtBu)_3$ in this aggregation state has twice as many reactive sites per mole of catalyst if complete exchange with the iPrOH of the *tert*-butoxy groups occured and the state of aggregation remained intact. Sterics in the aggregation state may also play an important role. The tetrameric state of aggregation has more steric hindrance around the reactive aluminum sites because of the number of alkoxide units bridged compared to that of the dimeric structure. It has been reported that lower states of aggregation are attribute to faster rates in other systems.[23]

2.2.4.2. Addition of iPrOH to $Al(OtBu)_3$

We engaged in NMR studies to gain information relative to the active species formed in solution when $Al(OtBu)_3$ and iPrOH were reacted. Experimentally, $Al(OtBu)_3$ was dissolved in benzene and equivalents of iPrOH were added sequentially with $^1$HNMR analysis between each addition to monitor the change in the catalyst. Upon successive additions, in general, broadening of the peaks was observed. This may be attributed to a dilution effect. The spectrum of $Al(OtBu)_3$ in benzene has already been shown. Shown in Figures 2.18 and 2.19 below is the $^1$HNMR spectrum after one equivalent of iPrOH had been added. The methyl groups on the *tert*-butoxy ligands represented by the broad peak at 1.03 ppm were still present. Between 1.2 and 1.6 ppm, overlapping peaks made it difficult to distinguish specific structural characteristics. The methylene proton in iPrOH is seen at 3.67 ppm in Figure 19. The appearance of two more unique multiplets at 4.19 and 4.31 indicate two isopropoxide peaks. This data

indicates that there may be a mixture of aluminum *tert*-butoxide and isopropoxide ligands after 1 eq. of iPrOH is added.

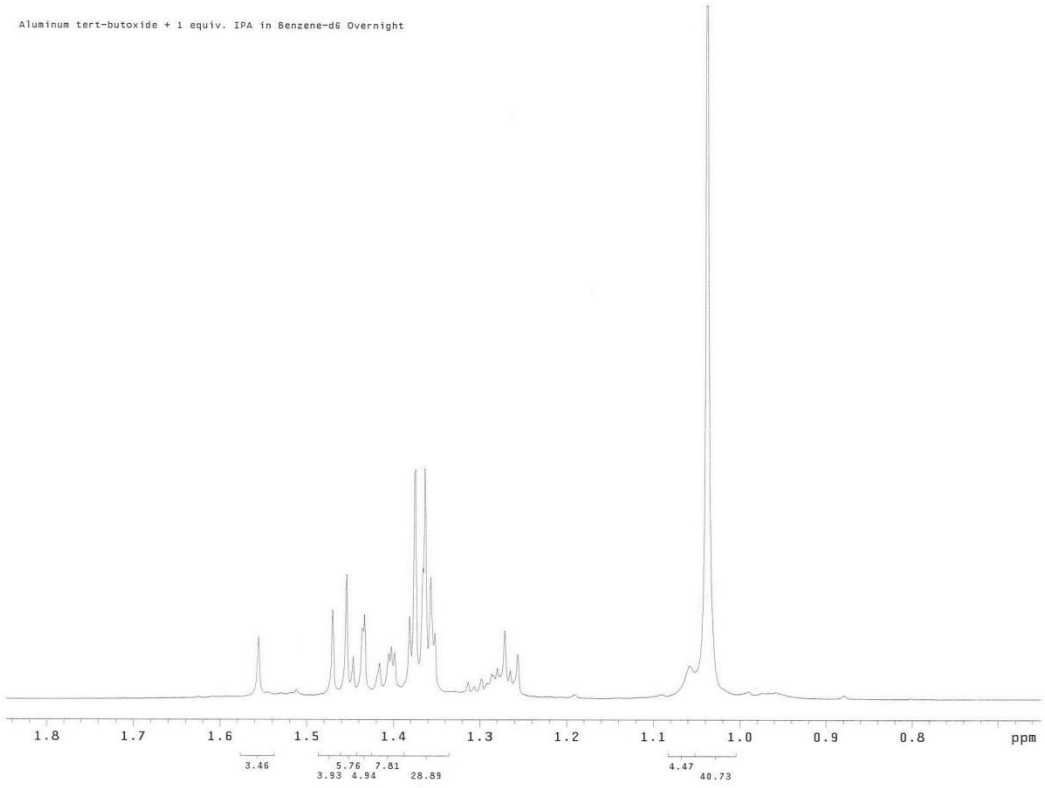


**Figure 2.18.** Upfield shifts of a single addition of iPrOH to $Al(OtBu)_3$

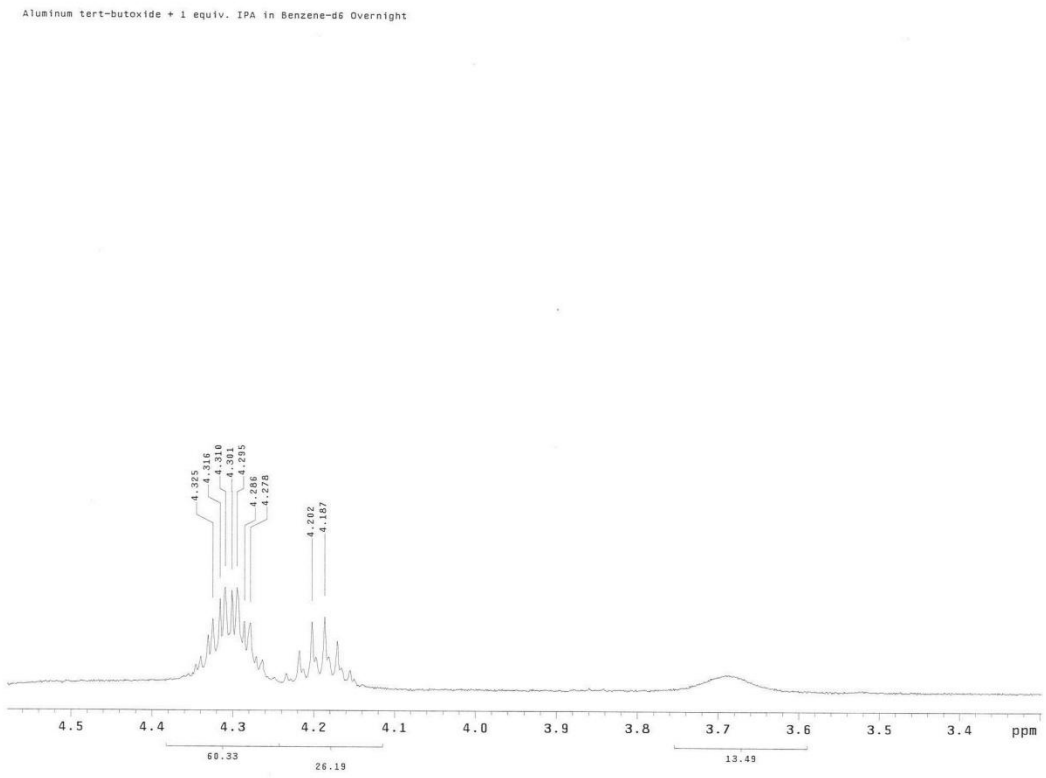


**Figure 2.19.** Downfield shifts of a single addition of iPrOH to $Al(OtBu)_3$

After a second addition of iPrOH, the doublet corresponding to the methyl groups in isopropanol does appear at 0.95 ppm. There is definite exchange of *tert*-butoxide and isopropanol evidenced by the overlapping broad peaks between 1 ppm and 2 ppm in each equivalent of iPrOH added (Figure 2.20). Furthermore, only one methylene shift is noted at 3.75 ppm indicating that isopropoxide as opposed to iPrOH is present.

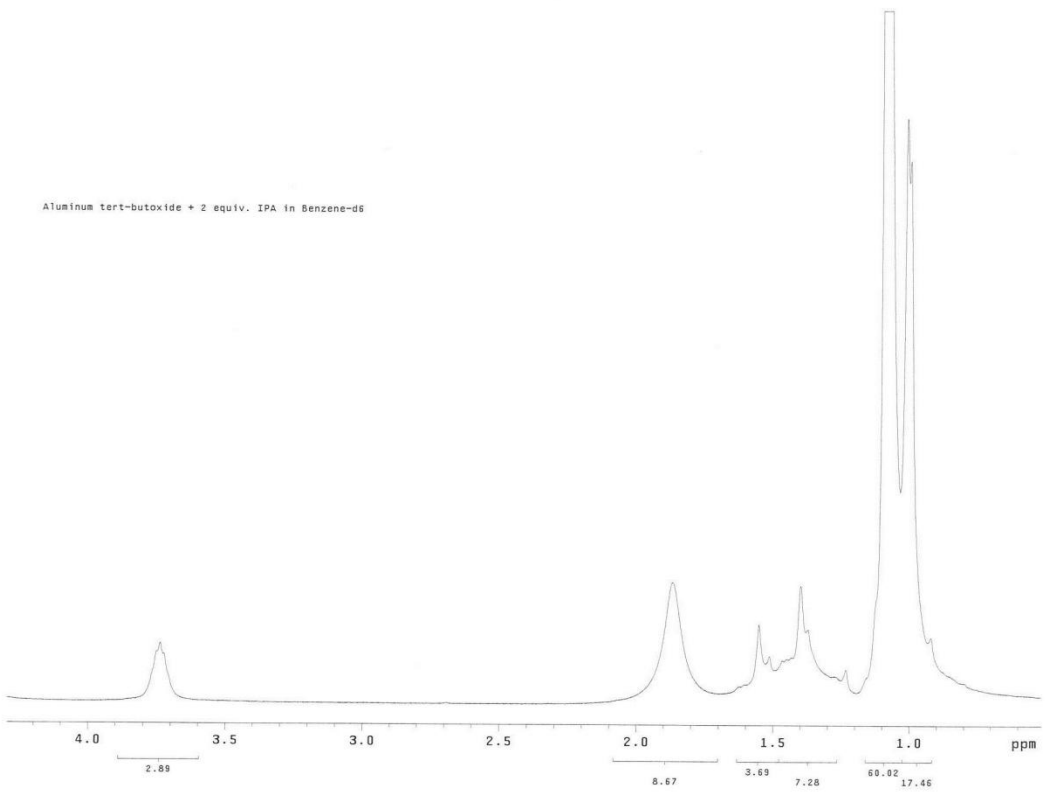


**Figure 2.20.** Addition of two equivalents of iPrOH to $Al(OtBu)_3$

By $^1$HNMR, after all three equivalents of iPrOH were added (Figure 2.21) the integration of the methyl doublets of the isopropoxide groups at 0.95 has increased compared to the integration after 2 eq. Still only one methylene shift is observed at 3.75 ppm.

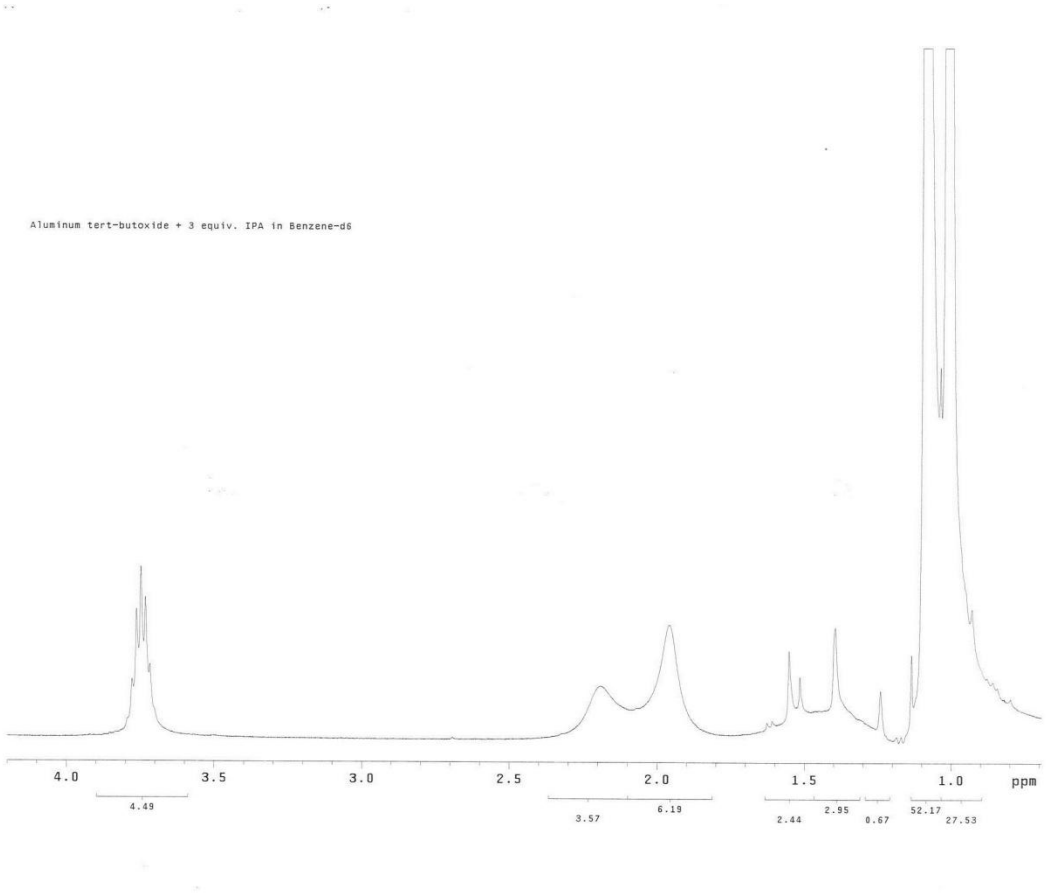


**Figure 2.21.** Addition of three equivalents of iPrOH to $Al(OtBu)_3$

These results are consistent with iPrOH exchanging with the *tert*-butoxy groups to form a more active catalyst for MPV reductions. Due to complex overlaps and peak broadening it was not possible to discern how many ligands were exchanged or the exact structure of the catalyst *in-situ*, but confirmation of ligand exchange was seen. It is also important to note that upon addition of all three equivalents of iPrOH, the $^1$HNMR was not consistent with pure $Al(OiPr)_3$.

### 2.2.5 Reduction rates of (*S*)-CMK with catalyst loading

2.2.5.1 Rate changes with catalyst loading in the reduction of (*S*)-CMK

The enhanced catalytic activity of the aluminum *tert*-butoxide opened the door to lower the amount of catalyst loading. Generally, close to stoichiometric quantities of $Al(OiPr)_3$ are used to drive the equilibrium towards the alcohol products. Since the $Al(OtBu)_3$ catalyst in iPrOH had proven more effective, lower catalyst loadings could be used to reduce (*S*)-CMK while maintaining reasonable rate and high conversion. The reduction of (*S*)-CMK was conducted with catalyst loading ranging from 5 to 50 mol%. Industrially, 50 mol% $Al(OiPr)_3$ is used and was implemented as our "standard" catalyst loading. As a result, (*S*)-CMK was reacted with 50, 40, 30, 20, 10, and 5 mol% $Al(OtBu)_3$ in iPrOH at 50°C. Plotted below in Figure 2.22 is the conversion from (*S*)-CMK starting material to product alcohols as a function of time. It can be seen from the graph that the reaction rate remained relatively unchanged from 50 mol% to 20 mol%. However, below 20 mol%, the reaction and conversion decreased significantly.

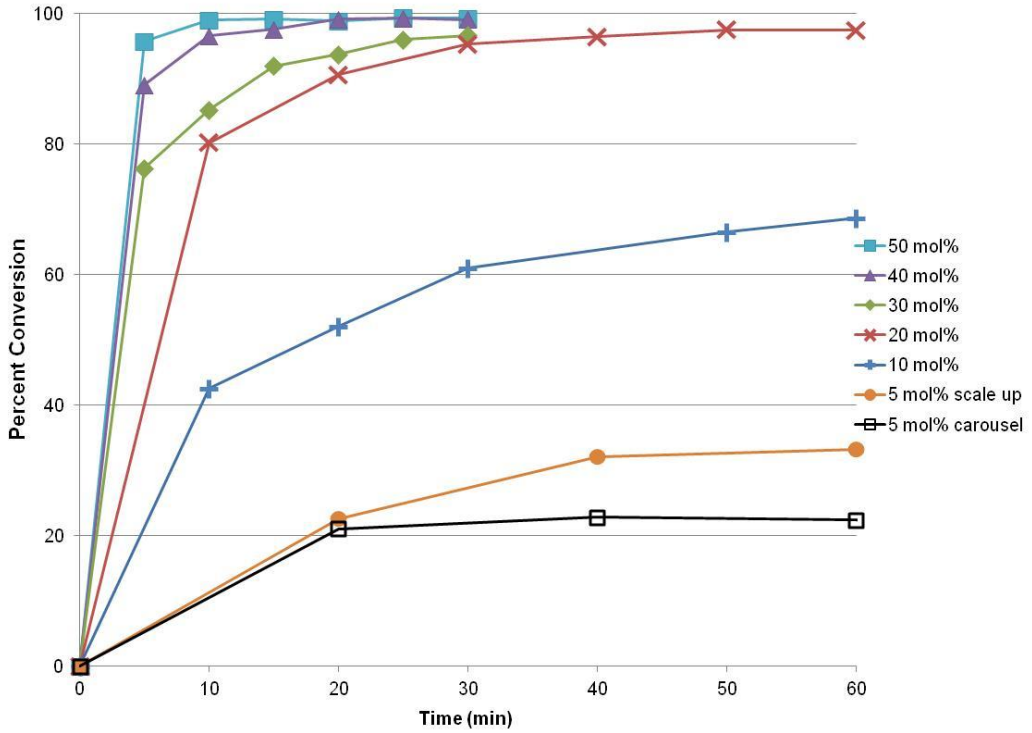


**Figure 2.22.** Catalyst loadings of $Al(OtBu)_3$ in the MPV reduction of (S)-CMK at 50°C in iPrOH

Specifically, from 50 mol% $Al(OtBu)_3$ to 20 mol%, the reaction reached completion before 60 minutes. Unquestionably, 20 mol% $Al(OtBu)_3$ effectively catalyzed the MPV reduction of (*S*)-CMK without compromising the reaction efficiency (yield and time). The lower loadings, 10 mol% and 5 mol%, did not enable the reaction to reach completion after one hour and I expect that the reaction equilibrium does not lie fully to the products because the kinetic curves begin to level. Under these conditions, the Oppenauer oxidation may become a competitive back reaction.

*2.2.5.1.1. Reductions with 5 mol% $Al(OtBu)_3$ on a large and small scales*

There are two kinetic curves in Figure 2.22 corresponding to the reduction of (S)-CMK with 5 mol% $Al(OtBu)_3$ loading. One is the 5 mol% loading in the carousel and the

other 5 mol% loading scaled up. Initially, a carousel reduction was run on a 5-mL scale with a mass of the catalyst being 20.5 mg. It was seen that the activity of the catalyst dropped as the reaction was conducted for longer periods of time. Shown in the graph is the reduction up to 60 minutes but it was found after 240 minutes, the conversion had dropped from around 20% to 9%. This was attributed to small amounts of water that can effectively quench the aluminum alkoxide catalyst *in-situ* and prevent the reaction from continuing as well as catalyst adhering to the walls once added through the reaction inlet. Even though the iPrOH used was anhydrous, any inherent moisture can quench the catalyst at the 5 ml scale.

As a result, a larger (250-mL) scale reaction was run with 5 mol% $Al(OtBu)_3$ loading. Under these conditions the reaction reached up to 48% conversion after 4 hours of reaction. The progression is represented by the 5 mol% curve in Figure 2.22 and shown to 60 minutes as a comparison. 1 mL samples were taken every 20 minutes, quenched with 2M HCl, diluted with MeOH and analyzed with HPLC. On a larger scale, it can be seen that the 5 mol% catalyst loading is effective to promote the reduction without losses in activity due to quenching.

A 250-mL scale reaction was also run with 10 mol% catalyst to validate the lower activity compared to that from 50-20mol%. However, precipitation occurred prior to the first sampling and the catalyst loading was concluded to be accurate in the carousel experiments.

### 2.3 Industrial advantages to using $Al(OtBu)_3$

The enhanced activity of the $Al(OtBu)_3$ can be implemented in industry with significant advantages over the traditional MPV protocol by capitalizing on (1) the enhanced rate of the reaction and (2) the decrease in catalyst loading. I have shown that

the rate of reaction can be drastically increased by substituting the conventional $Al(OiPr)_3$ catalyst with $Al(OtBu)_3$. In the case of the reduction of (*S*)-CMK, the reaction reached completion after 20 minutes whereas the conventional catalyst required 120 minutes. An even more important factor is the ability to reduce the catalyst loading and still have fast reaction times. I have shown with the reduction of (*S*)-CMK to as low as 20 mol% catalyst loading that the reaction reaches completion in 60 minutes, half the time and less than half the amount of aluminum alkoxide catalyst that the current industrial method requires. The significant lowering of catalyst can contribute to the reduction in material cost as well as the generation of aluminum containing waste, a positive step in making the process greener. Another avenue that was opened by the enhanced activity of aluminum *tert*-butoxide was to move the process toward continuous mode. These studies were conducted and are presented in the next chapter.

## 2.4 Conclusions

This work established $Al(OtBu)_3$ as a highly active catalyst toward MPV reduction. In this chapter, I presented the enhanced MPV reduction of three model carbonyl compounds (*S*)-CMK, benzaldehyde, and acetophenone. The standard method where $Al(OiPr)_3$ is the catalyst was compared to a new catalyst, $Al(OtBu)_3$, for MPV reduction for all three models. In all cases, $Al(OtBu)_3$ outperformed $Al(OiPr)_3$ by increasing reaction rates(up to 20 times in the case of benzaldehyde) and enabling high yield with as low as 20 mol% loading. It was found that the dimeric aggregation state of the $Al(OtBu)_3$ coupled with solvent exchange of the iPrOH resulted in the *in-situ* formation of a highly active catalyst. This research was significant because it enables a more sustainable pharmaceutical process (less time, less metal catalyst, high yields, and short reaction times) and also enables the technologic transfer to continuous mode.

## 2.5 Experimental methods

### 2.5.1 Experimental procedure for kinetic analysis

Experiments were run in a Radley's 12-tube carousel reactor under an inert argon atmosphere.

**Figure 2.23.** Radley's carousel reactor

2.5.1.1 (*S*)-CMK Reduction

(*S*)-CMK (0.475 g, 1.59 mmol) was added to a carousel tube and placed under argon atmosphere. 5 mL of anhydrous iPrOH was added and the mixture was brought to 50$^{o}$C. After the temperature had equilibrated at this temperature, Al(O*i*Pr)$_3$ (0.170 g, 0.83 mmol) or Al(O*t*Bu)$_3$ (0.205 g, 0.83 mmol) was added through the inlet port of the carousel tube to begin the reaction. After the allotted reaction time, the tube was removed from the carousel and placed in an ice bath. 2 mL of 2M HCl was then added to quench the reaction and the reaction mixture was then diluted with MeOH to achieve homogeneity (either 20 or 30 mL). A 0.25 mL or 0.35 mL aliquot depending on dilution (27 or 37 mL total reaction solution) was taken and diluted to 1 mL with MeOH in a GC Vial. The sample was analyzed by HPLC. Samples were taken every 10 minutes. Reaction samples were quenched every 10 min when Al(O*i*Pr)$_3$ was used as the catalyst and every 5 min when Al(O*t*Bu)$_3$ was used.

2.5.1.2 Benzaldehyde Reduction

Al(O*i*Pr)$_3$ (0.170 g, 0.83 mmol) or Al(O*t*Bu)$_3$ (0.205 g, 0.83 mmol) was added to a carousel tube and placed under argon atmosphere. 5 mL of anhydrous iPrOH was added and the mixture was brought to 40$^{o}$C. After the solution had equilibrated at this temperature, freshly distilled benzaldehyde (165 μL, 1.59 mmol) was syringed through the inlet port of the carousel tube to initiate the reaction. After the allotted reaction time, the tube was removed from the carousel and placed in an ice bath. 2 mL of 2M HCl was added to quench the reaction and the reaction mixture was then diluted with 10 mL MeOH. A 0.15 mL aliquot was taken from the reaction solution and diluted with 0.85 mL of MeOH in a GC Vial. The sample was analyzed by HPLC. Reaction samples were quenched every 10 min when Al(O*i*Pr)$_3$ was used as the catalyst and every 3 minutes when Al(O*t*Bu)$_3$ was used.

2.5.1.3 Acetophenone Reduction

$Al(O\textit{i}Pr)_3$ (0.170 g, 0.83 mmol) or $Al(O\textit{t}Bu)_3$ (0.205 g, 0.83 mmol) was added to a carousel tube and placed under inert atmosphere. 5 mL of anhydrous iPrOH was added and the mixture was brought to 50°C. After the solution had equilibrated at this temperature, freshly distilled acetophenone (190 μL, 1.59 mmol) was syringed through the inlet port of the carousel tube to begin the reaction. After the allotted reaction time, the tube was removed from the carousel and placed in an ice bath. 2 mL of 2M HCl was added to quench the reaction and the reaction mixture was then diluted with 10 mL of MeOH. A 0.15 mL aliquot was taken from the reaction solution and diluted with 0.85 mL of MeOH in a GC Vial. The sample was analyzed by HPLC. Reaction samples were quenched every 35 min when $Al(O\textit{i}Pr)_3$ was used as the catalyst and every 15 min when $Al(O\textit{t}Bu)_3$ was used.

2.5.1.4 MPV Reductions in toluene:iPrOH (9:1)

The same reaction conditions and experimental methods were used as the previous carousel reactions with 4.5 mL of anhydrous toluene and 0.5 mL of iPrOH instead of 5 mL of iPrOH. The work up was the same for each compound investigated. The reaction quench times for benzaldehyde in the mixed solvent system for $Al(OiPr)_3$ was every 15 minutes and for $Al(OtBu)_3$ was every 5 minutes. For acetophenone the quench times were every 30 minutes for $Al(OiPr)_3$ and every 10 minutes for $Al(OtBu)_3$. For the reduction of (*S*)-CMK with mixed solvent, the quench interval was every 20 minutes for $Al(OiPr)_3$ and every 10 minutes for $Al(OtBu)_3$.

2.5.1.5 (*S*)-CMK Reduction at Varying Catalyst Loadings (Carousel)

For the reduction of (*S*)-CMK at varying catalyst loadings, the general procedure follows: (*S*)-CMK was added to a carousel tube and purged with nitrogen. 5 mL of anhydrous

iPrOH was then added and the solution was brought to 50°C. To start the reactions, $Al(OtBu)_3$ was added through the inlet port at the top of the tube and quenched with 2 mL of 2M HCl in an ice bath and diluted with MeOH until homogeneous. Samples were then run following the same HPLC method. Quench times for each catalyst loading is shown in Table 2.5 below.

**Table 2.5.** Time interval in the quench of (*S*)-CMK reductions with various loadings of $Al(OtBu)_3$ in the carousel

| $Al(OtBu)_3$ Catalyst Loading | Quench interval at 50°C (min) |
|---|---|
| 50 mol% | 5 |
| 40 mol% | 5 |
| 30 mol% | 5 |
| 20 mol% | 10 |
| 10 mol% | 10 |
| 5 mol% | 20 |

2.5.1.6 (*S*)-CMK Reduction at 5 mol% catalyst loading Scale-Up (Batch)

In a 500 mL RB flask under nitrogen, (*S*)-CMK was stirred in 250 mL of anhydrous iPrOH at 50°C. When the solution reached temperature, $Al(OtBu)_3$ was added and the reaction was started. 1 mL aliquots were taken every 20 min and the contents of each aliquot was quenched with 2M HCl and diluted with MeOH. Analysis was conducted following the general HPLC method.

2.5.1.7 HPLC Analysis: Calibration Curves and Experimental

HPLC analysis was done following a method established by AMPAC. Samples were run through a Phenomenex Luna 5μ C18 reverse phase column equipped with a guard column at 40oC with a flow rate of 1.5 mL/min. Two solvent systems were used, HPLC grade acetonitrile and HPLC grade water with a 0.1% trifluoroacetic acid buffer. The method had a 15 minute run time with a 4 minute post-run time. The solvents were used on a gradient during this 19 minute complete run time which is shown in Table 6.

**Table 2.6.** HPLC solvent gradient method

| Time (min) | Acetonitrile:$H_2O$ |
|---|---|
| 0 | 48:52 |
| 8 | 48:52 |
| 11 | 80:20 |
| 15 | 80:20 |

UV-detection was used to monitor the starting material and products for all reactions at two wavelengths, 210 and 254 nm.

Calibration curves were used to analyze the concentrations of starting materials benzaldehyde, acetophenone, and (*S*)-CMK and the products benzyl alcohol, 1-phenylethanol, (*R,S*)-CMA and (*S,S*)-CMA in MeOH and are shown in Figures 2.24-2.30.

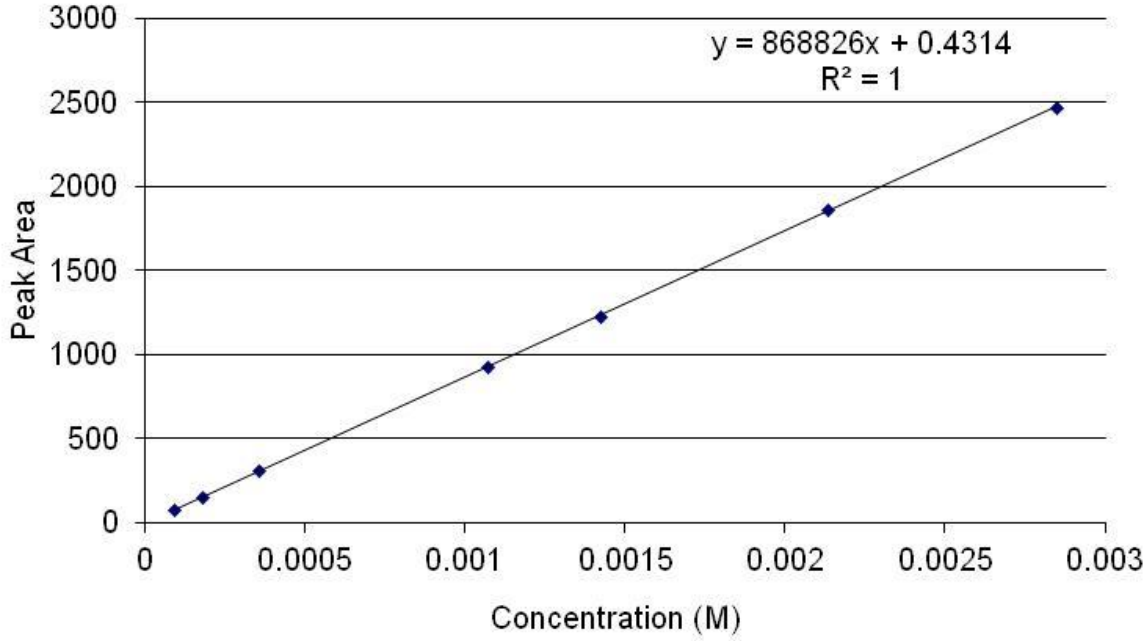


**Figure 2.24.** Calibration curve for benzaldehyde in MeOH

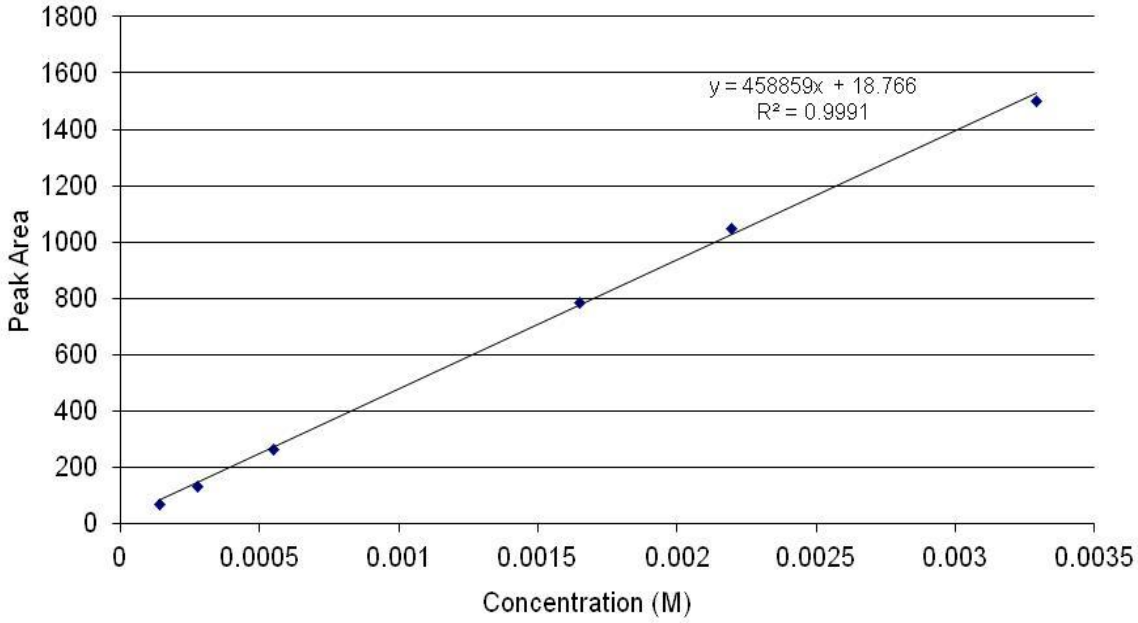


**Figure 2.25.** Benzyl alcohol calibration curve in MeOH

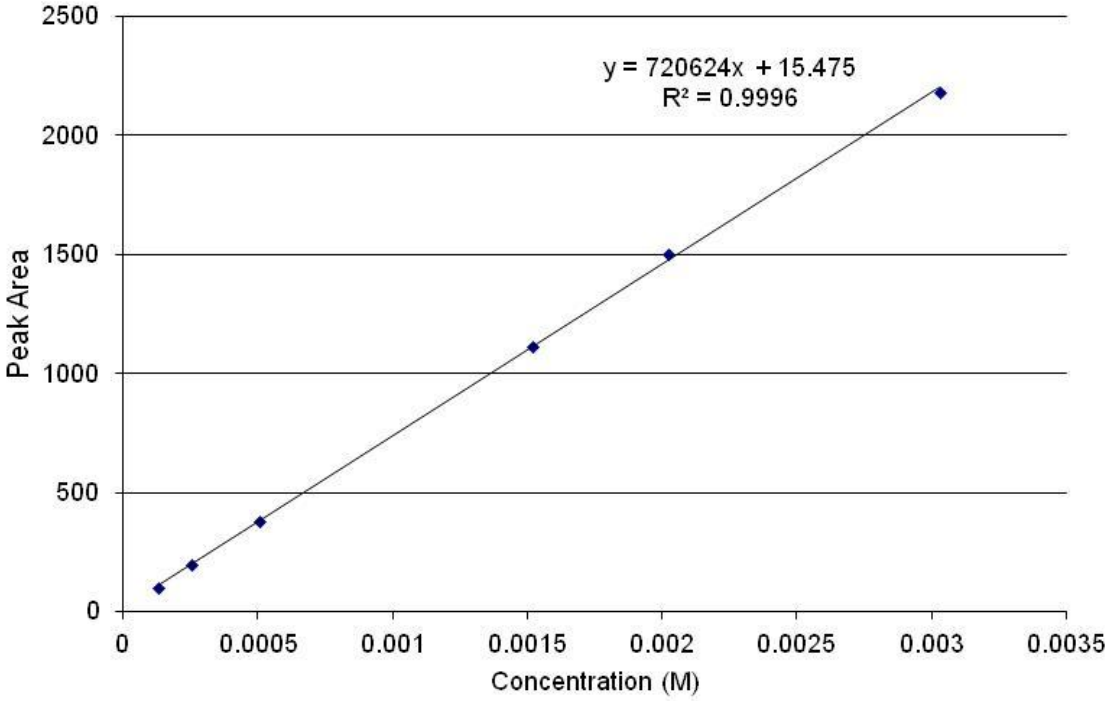


**Figure 2.26.** Calibration curve for acetophenone in MeOH

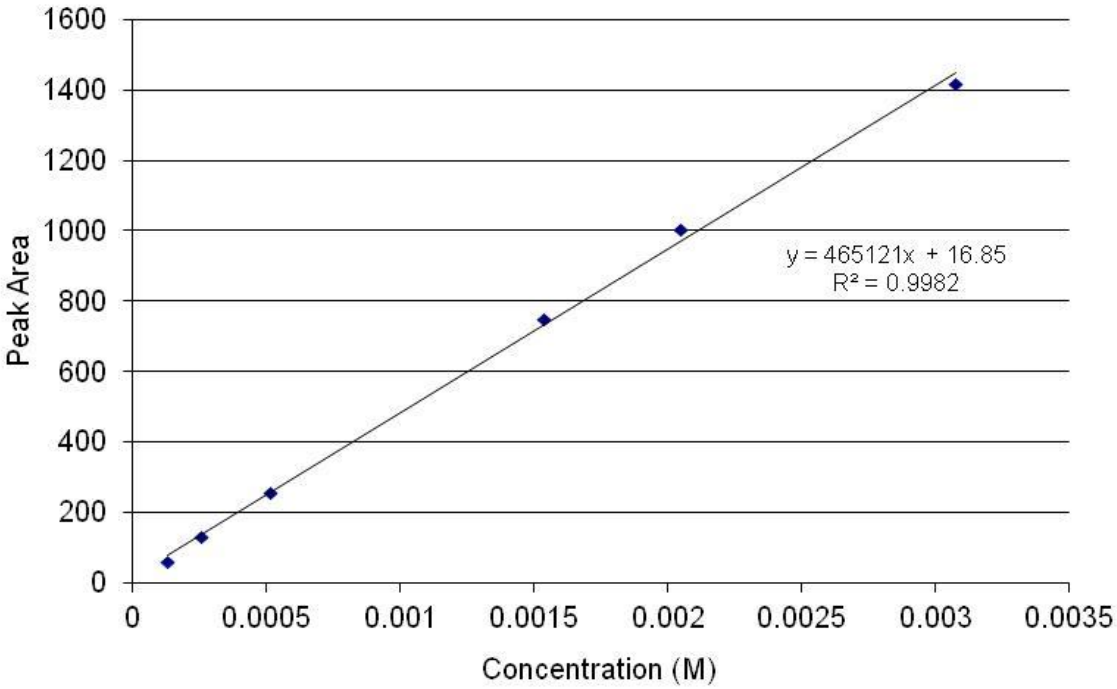


**Figure 2.27.** Calibration curve for *sec*-phenylethanol in MeOH

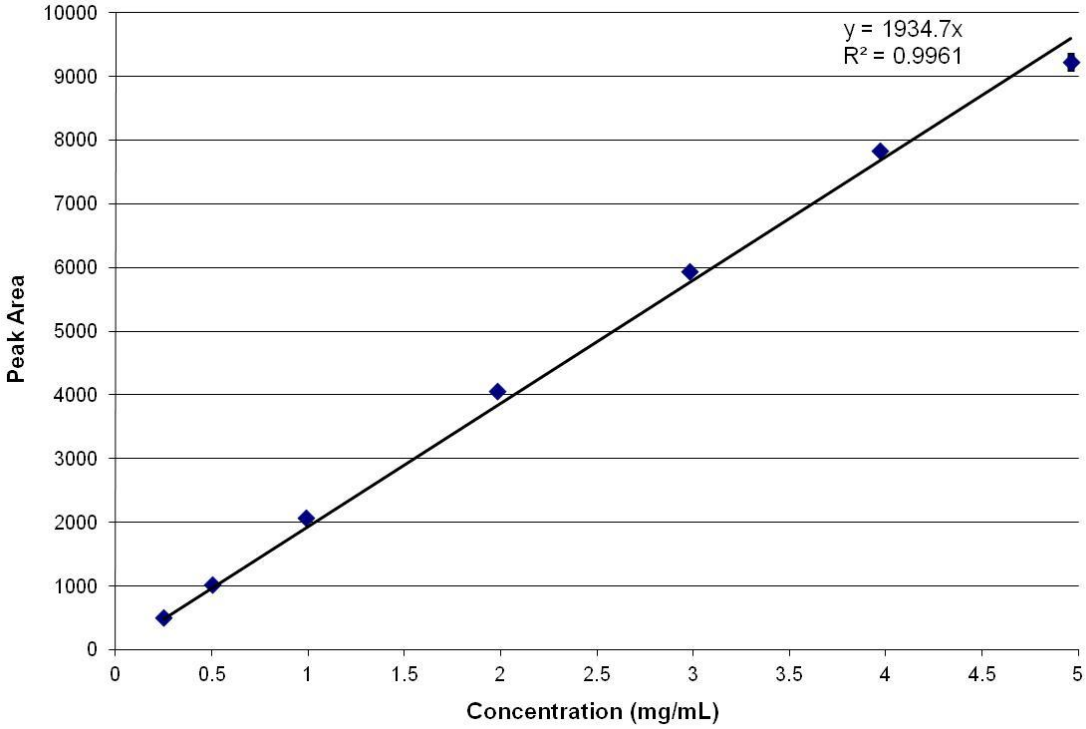


**Figure 2.28.** Calibration curve for (*S,S*)-CMA in MeOH

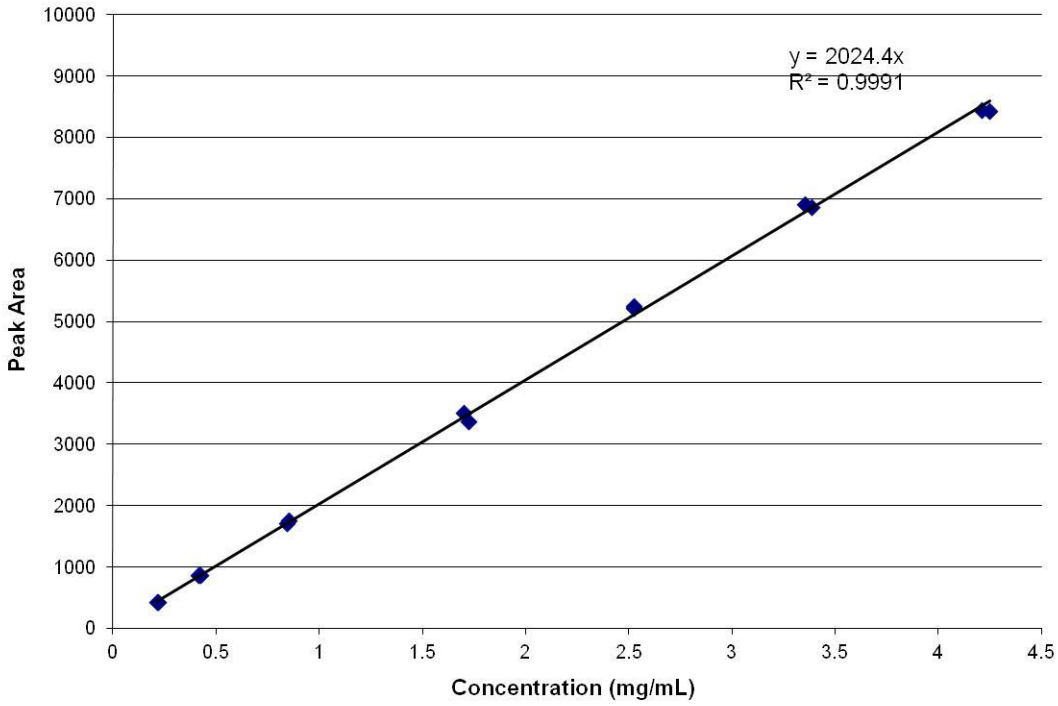


**Figure 2.29.** Calibration curve for (*R,S*)-CMA in MeOH

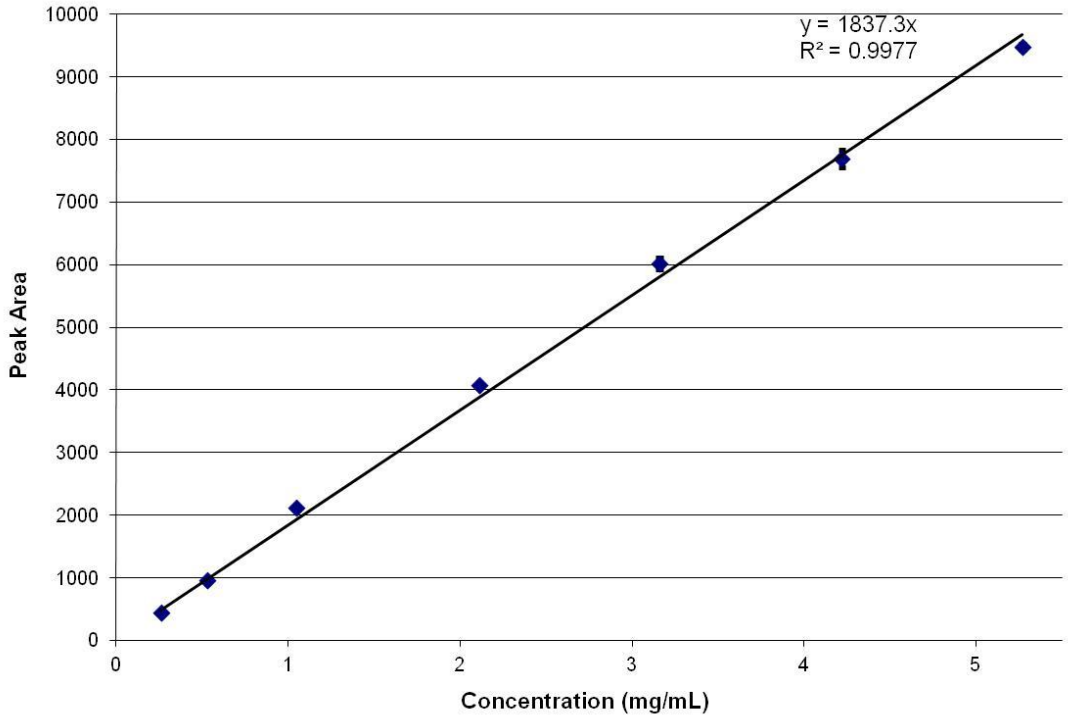


**Figure 2.30.** Calibration curve for (*S*)-CMK in MeOH

2.5.1.8 Calculation and Equation of Initial Rates

The kinetics of the MPV reductions of many carbonyls at different concentrations and temperatures has been reported but there is still no definitive order established for each reactant or reagent. Because the MPV reduction is an equilibrium reaction based on solvent concentration (which changes throughout the reaction due to alkoxide exchange), starting material concentration, and catalyst concentration, the kinetics are fairly difficult to understand. As a more simple approximation, initial rates were established for each system investigated. Since the rate approximation follows the equation below, the slope of the line generated through the initial points is the initial rate. All of the linear plots began with a line starting at (0,0) which is no elapsed time and full

concentration of starting material. The initial rate expression for the MPV reduction of any aldehyde or ketone with an aluminum alkoxide catalyst in iPrOH is shown in Equation 2.1.

**Equation 2.1.** General rate expression for an MPV reduction

$$\frac{-d[SM]}{dt} = k[SM]^x[Al(OR)_3]^y[iPrOH]^z$$

The rate is a function of starting material, catalyst, and iPrOH (solvent too) concentrations. If the assumption is made that because we perform the reactions in a large excess of iPrOH at a given time, there is little change in the concentration then the order is zero and the concentration is 1. If we also make the assumption, for simplicity, that the catalyst concentration has zero order as well then the simplified expression is shown in Equation 2.2.

**Equation 2.2.** Rate expression for an MPV reduction with pseudo-first order approximation

$$\frac{-d[SM]}{dt} = k_{app}[SM]$$

The rate constant is now an apparent rate constant because the calculation is only based on the linear area of the curve when concentration is plotted versus time. This slope of the plot is [SM]/t. The linear area is the initial rate, which is shown in Figure 2.31 for the example of (*S*)-CMK being reduced with $Al(OtBu)_3$, and is dependent on the starting ketone or aldehyde concentration.

**Equation 2.3.** Pseudo-first order rate approximation solved for $k_{app}$

$$k_{app} = \frac{\frac{-d[SM]}{dt}}{[SM]} = \frac{-slope}{[SM]}$$

When the slope is multiplied by -1 (because the concentration decreases over time) and then divided by the initial concentration, the result is $k_{app}$ (Equation 2.3). $K_{app}$ is not the true rate constant for this reaction but is an apparent initial rate constant that can be compared for both catalysts used.

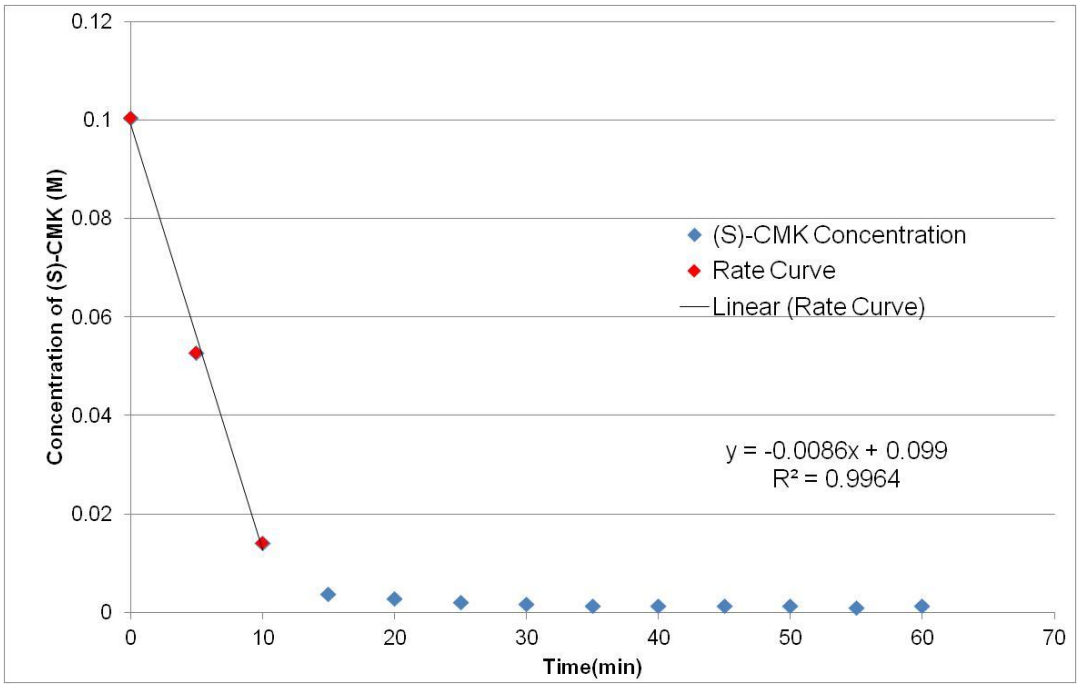


**Figure 2.31.** Trendline for initial rate of the disappearance of (*S*)-CMK with time with 50 mol% $Al(OtBu)_3$ at 50°C

The slope of the line plotted between the first three data points in the reduction of (*S*)-CMK with $Al(OtBu)_3$ was calculated to be -0.0086. Multiplying the slope by -1 and dividing by an initial concentration of 0.1005 M, the $k_{app}$ was found to be 0.0856 $min^{-1}$.

## 2.6 References


(1) Smith, M. B.; March, J. *March's Advanced Organic Chemistry: Reactions, Mechanism, and Structure*, **2007**.

(2) Chaikin, S. W.; Brown, W. G. *Journal of the American Chemical Society* **1949**, *71*, 122.

(3) Noyori, R.; Hashiguchi, S. *Accounts of Chemical Research* **1997**, *30*, 97.

(4) Namy, J. L.; Souppe, J.; Collin, J.; Kagan, H. B. *Journal of Organic Chemistry* **1984**, *49*, 2045.; Lebrun, A.; Namy, J. L.; Kagan, H. B. *Tetrahedron Letters* **1991**, *32*, 2355.

(5) Meerwein, H.; Schmidt, R. *Justus Liebigs Annalen Der Chemie* **1925**, *444*, 221,; Verley, M. *Bulletin de la Societe Chemique de France* **1925**, *37*, 871.; Ponndorf, W. *Angewandte Chemie* **1926**, *39*, 138.

(6) Wilds, A. *Organic Reactions* **1944**, *2*, 178.; Degraauw, C. F.; Peters, J. A.; Vanbekkum, H.; Huskens, J. *Synthesis-Stuttgart* **1994**, 1007.; Djerassi, C. *Organic Reactions* **1951**, *6*, 207.

(7) Cohen, R.; Graves, C. R.; Nguyen, S. B. T.; Martin, J. M. L.; Ratner, M. A. *Journal of the American Chemical Society* **2004**, *126*, 14796.

(8) Oppenauer, R. V. *Recueil Des Travaux Chimiques Des Pays-Bas* **1937**, *56*, 137.

(9) Cha, J. S. *Bulletin of the Korean Chemical Society* **2007**, *28*, 2162.

(10) Ooi, T.; Miura, T.; Maruoka, K. *Angewandte Chemie-International Edition* **1998**, *37*, 2347.

(11) Graves, C. R.; Zhou, H.; Stern, C. L.; Nguyen, S. T. *Journal of Organic Chemistry* **2007**, *72*, 9121.

(12) Uysal, B.; Buyuktas, B. S. *Chemical Papers* **2010**, *64*, 123.

(13) Cha, J. S.; Park, J. H. *Bulletin of the Korean Chemical Society* **2002**, *23*, 1051.

(14) Zeror, S.; Collin, J.; Zouioueche, L. A. *Inorganica Chimica Acta* **2009**, *362*, 2402.

(15) Bach, G.; Capitain.J; Engel, C. R. *Canadian Journal of Chemistry* **1968**, *46*, 733; Bouchard, R.; Engel, C. R. *Canadian Journal of Chemistry* **1968**, *46*, 2201.

(16) Kow, R.; Nygren, R.; Rathke, M. W. *Journal of Organic Chemistry* **1977**, *42*, 826.

(17) Gills, J.; Lo Piccolo, J.; Tsurutani, J.; Shoemaker, R. H.; Best, C. J. M.; Abu-Asab, M. S.; Borojerdi, J.; Warfel, N. A.; Gardner, E. R.; Danish, M.; Hollander,

M. C.; Kawabata, S.; Tsokos, M.; Figga, W. D.; Steeg, P. S.; Dennis, P. A. *Clinical Cancer Research* **2007**, *13*, 5183.

(18) Malik, A. A.; Clement, T. E.; Palandoken, H.; Robinson III, J.; Stringer, J. A. "Clean, High-yield Preparation Of S,S- and R,S- Amino Acid Isosteres." US Patent 6,867,311 B2, Mar. 15, **2005.**

(19) Hoffman, R. V.; Maslouh, N.; Cervantes-Lee, F. *Journal of Organic Chemistry* **2002**, *67*, 1045.

(20) Kitagawa, K., Ph.D. dissertation. Georgia Institute of Technology, **2010**.

(21) Ma, H. Y.; Okuda, J. *Macromolecules* **2005**, *38*, 2665.

(22) Shiner, V. J.; Whittaker, D.; Fernande, V. P. *Journal of the American Chemical Society* **1963**, *85*, 2318.

(23) Campbell, E. J.; Zhou, H. Y.; Nguyen, S. T. *Organic Letters* **2001**, *3*, 2391.

# CHAPTER 3: TRANSFER OF BATCH MPV REDUCTION MODEL COMPOUNDS BENZALDEHYDE AND ACETOPHENONE TO CONTINUOUS FLOW

## 3.1 Introduction

Industrial processing including the synthesis of chemicals and the separation of products and waste by-products has been thoroughly implemented through multiple facets of the chemical and pharmaceutical industries. Many operations include the transfer of materials from one place to another, generally using flow type systems. This technology of continuous flow has been around for decades but has not seen sufficient light for many chemical reactions. Many reactions are conducted in large reaction vessels, often called batch processing. The size and configuration of the vessels can be modified to fit the reactions being conducted. Optimization of these reactions is often scaled from small laboratory experiments. This process to convert from small lab scale reactions to large industrial size process reactors is called **scaling-up**. Scale up has led to thousands of functional procedures on industrial scales but in the effort to implement sustainable practices and efficient reactions, scale up approaches may not be appropriate.

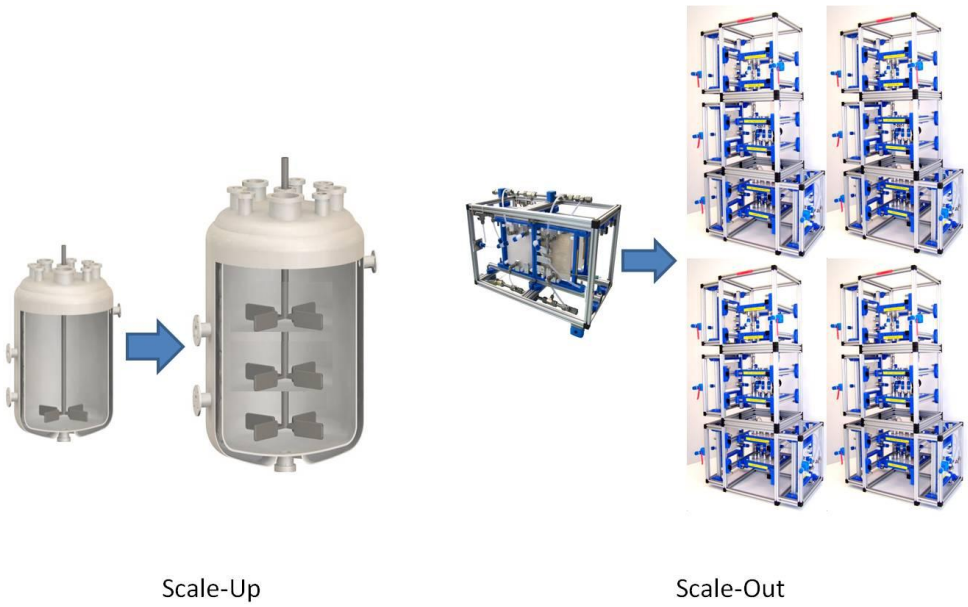


**Figure 3.1.** Scale-up versus scale-out processing approaches

The counter-point to scale up is **scaling-out**. Scaling-out is the process often used in continuous flow systems. Scale out places continuous flow processes in parallel rather than increasing the size of one single reaction. Both types of processes are shown in Figure 3.1. Because these modules operate continuously, production can be superior to standard batch processes. Scaling out reduces the time from discovery to production by eliminating the optimization time associated with the batch scale up. This is extremely important in industrial patent life. The time to production is not nearly the only advantage to converting from batch processing to continuous flow. Improvements in mixing efficiency, heat transfer, atom economy and reaction efficiency are all areas that continuous flow technology has addressed.

Large reaction vessels stirred by paddles can present poor mixing in certain situations that can lead to inefficiency in reaction time and atom efficiency, especially heterogeneous systems.[1] Heat transfer issues are also of concern because uneven

heating and a large volume to heat area in large reactor vessels can lead to hot spots in the reaction or thermal gradients. These thermal gradients can lead to undesired degradation of materials and side products which lower the efficiency of reactions.

Of particular interest are pharmaceutical syntheses, which have been dominated by batch processing. Design of flow reactors and reactions to improve upon current methods have seen a surge of activity in the past couple of decades. These designs have focused on addressing or even eliminating the drawbacks of large-scale batch reactors toward pharmaceutical applications, including: heat transfer issues, mixing issues, atom economy, and reaction efficiency mentioned before.

Continuous flow technology has been recently highlighted by the Green Pharmaceutical Roundtable as the number one priority in continuing research.[2] Continuous flow technology is often aimed at addressing the key issues that were mentioned previously in that the reactor volumes are often on the order of milliliters, allowing for efficient heat transfer which contributes to improved reaction efficiency and atom economy, lower overall volumes of toxic and hazardous materials or alternatives to these materials to improve safety of processes, and improved mixing designs.

Particular advances in the transfer of batch to continuous flow have been shown with the use of lab on a chip designs, continuous microwave reactors, multistep synthesis reactors, and in our labs previously, homemade reactor devices for the formation of energetic intermediates. Most of these areas have focus on pharmaceutically relevant reactions and processes and the goal is to demonstrate the effectiveness of this method as a replacement for current batch reactions. There are whole journals now dedicated to flow devices and reactions including “Lab on a Chip” and “Journal of Flow Chemistry” to name a few.

Lab on a chip designs have primarily been used in biological applications with microliter flows and are really designed for combinatorial chemistry and biological studies with limited applications to larger scale synthesis.[3] One group that has shown promising homemade designs that incorporate multistep syntheses with built in separations and reaction quenches on a larger scale is Jensen's group at MIT. For example Suzuki-Miyura couplings were conducted with phenols and triflic anhydride under basic conditions with a built in acid quench, organic/aqueous separator followed by addition of boronic acid in a second connected reactor.[4] Jensen's group is not by any means the only contributor to multistep organic synthesis in flow and a mini-review highlighting multistep continuous flow synthesis has been published by Webb.[5] Kappe[6] and Ley[7] have also been instrumental in improving standard batch reactions with microwave conditions, and then translating those to continuous processes. For example Kappe has demonstrated the effective formation of hydrazoic acid, an extremely energetic and dangerous compound, *in-situ* under flow conditions followed by an organic quench which decomposes the remaining acid safely. The Eckert/Liotta group has also had experience with continuous synthesis in the production of a pharmaceutically important diazoketone-intermediate through a homemade reactor.[8] The importance of the transfer of reactions to continuous flow, at least for the pharmaceutical industry, is the level of production possible. It is imperative that flow designs allow for large-scale production.

## 3.2 Continuous flow equipment

### 3.2.1 Corning® Continuous Flow Reactor

One particular example of a commercially available continuous flow system that allows for large throughputs has been pioneered by Corning®.

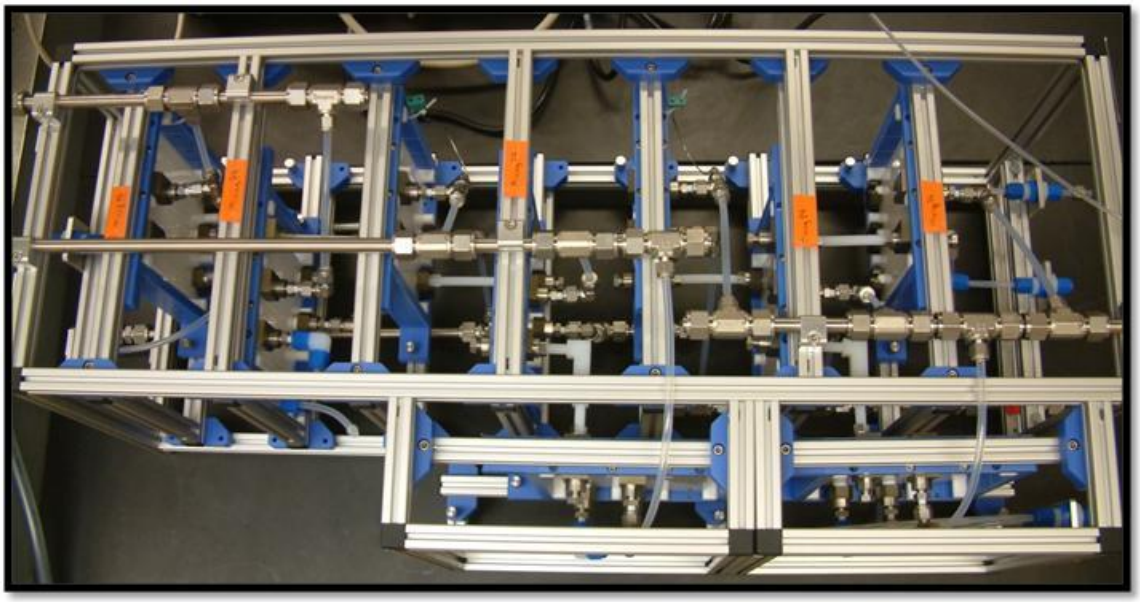

**Figure 3.2.** Photograph of the Corning® Continuous Flow Reactor in the lab hood

The Eckert-Liotta Research Group was one of two recipients to receive of a gift in the form of a Corning® Glass Continuous Flow Reactor (Figure 3.2). This reactor was specifically designed by Corning® to enable efficient mixing and heat transfer toward the implementation of multi-step synthesis. By analogy with continuous reactors, the reaction can be easily "scaled-out" to enable direct technology transfer from lab bench to pilot-plant scale. The reactor is modular and is equipped with multiple temperature zones, multiple reagent/reactant inlets, and enhanced mixing plates and linear plates for increased residence times. The mixing modules have specifically designed "heart shaped" motifs which make mixing exceptionally rapid and efficient. In fact, it was originally designed for biphasic liquid-liquid processes (Figure 3.3). Literature reports document the flexibility and breadth of the Corning® reactor as it has been used for the scale up of Diels-Alder reactions (translated from microscale homemade reactor kinetics), Grignard additions to acyl chlorides, and many other applications.[9]

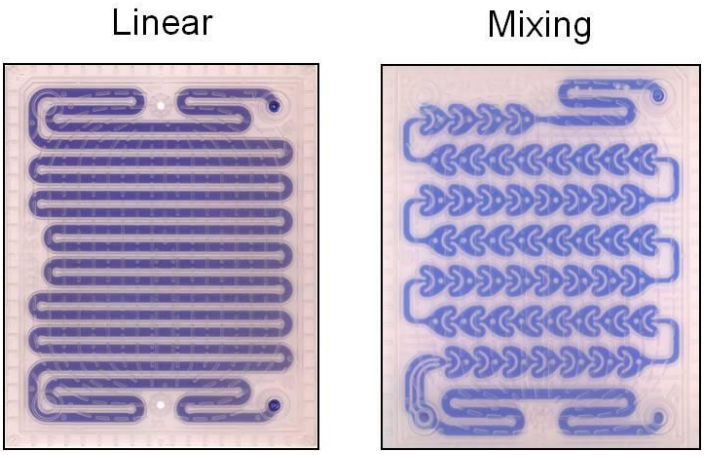


**Figure 3.3.** Mixing and linear plates

The reaction plates are connected through heat and chemical tolerant plastic fittings. The plastic used is perfluoroalkoxy polymer, known as PFA. The configuration can be altered to meet the needs of most chemical reactions. The reactor in our laboratories is capable of having a maximum of six inlets and three temperature regions which is displayed in a simplified graphic in Figure 3.4.

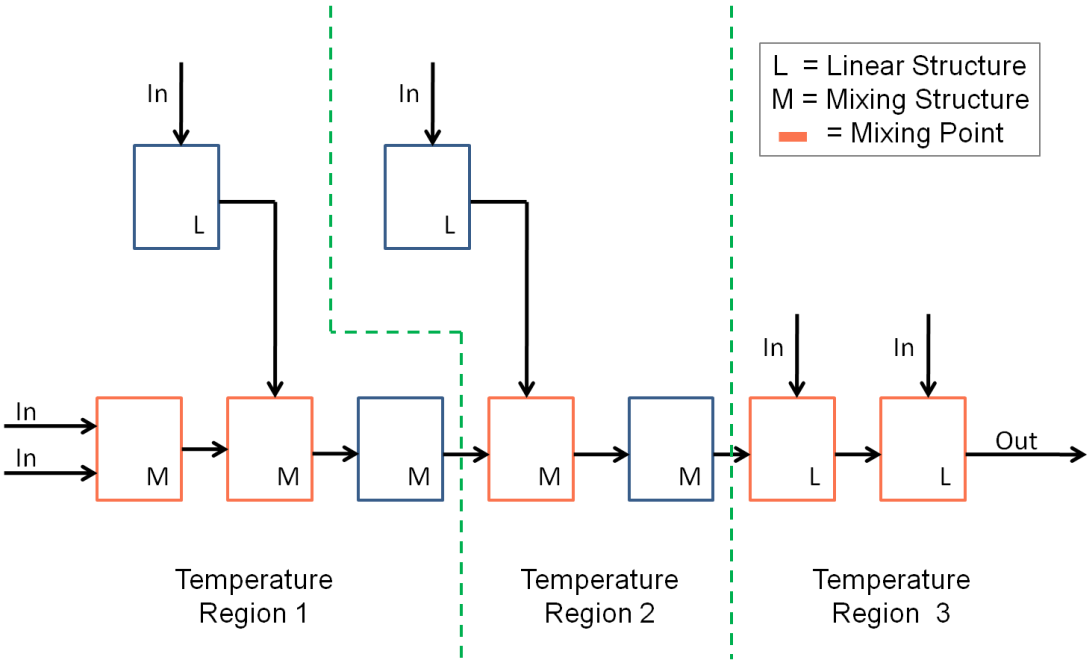


**Figure 3.4.** Continuous flow schematic with multiple inlets and temperature regions

I described in the previous chapter that $Al(OtBu)_3$ exhibited enhanced activity toward MPV reductions enabling lower loadings of catalyst with competitive reaction times and the ability to run the reduction in mixed solvent systems. As a consequence, we investigated $Al(OtBu)_3$ catalyzed MPV reductions of model compounds, benzaldehyde and acetophenone, in continuous flow. Benzaldehyde was selected for the transfer of the MPV reduction because the reaction is fast compared to ketones. Actually, the reduction of a pharmaceutical intermediate (*S*)-CMK is also fast and would be a great candidate for continuous flow, however, limitations arise as the (*S,S*)-CMA and (*R,S*)-CMA products precipitate out of solution as the reaction progresses. Precipitation must be avoided in a continuous flow reactor as shown because of clogging. As a result, CMK reduction in continuous flow will be investigated at later stage.

## 3.3 Results and Discussion

### 3.3.1 Initial reduction of benzaldehyde in continuous flow

It was found in prior research that $Al(OtBu)_3$ outperformed $Al(OiPr)_3$, the conventional MPV reduction catalyst, in terms of rate and catalyst loading in the reduction of benzaldhyde. Therefore, it was pursued in the transfer from batch to continuous flow. Initial experiments were conducted in continuous flow by employing 50 mol% catalyst loading of $Al(OtBu)_3$ in anhydrous iPrOH at 55$^{o}$C. These are the industrial conditions used in batch reactions by AMPAC (shown in Figure 3.5).[10] The batch conditions used industrially was the starting point for the transfer of enhanced MPV technology to continuous flow. Temperature, reaction time, catalyst loading and solvent were all investigated to optimize the continuous flow reduction of the model benzaldehyde.

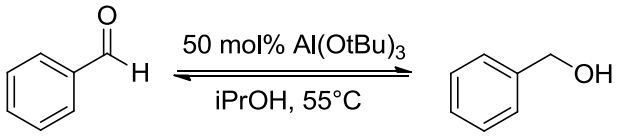


**Figure 3.5.** Conditions of the MPV reduction of benzaldehyde initially run in the continuous flow reactor

These initial investigations into the MPV reduction of benzaldehyde in continuous flow were conducted using the Corning® Continuous Reactor with a two plate design. The two solutions, one with benzaldehyde in iPrOH and the other with 50 mol% $Al(OtBu)_3$ in iPrOH were combined in the initial plate and flowed through both plates. The schematic of this setup is shown in Figure 3.6.

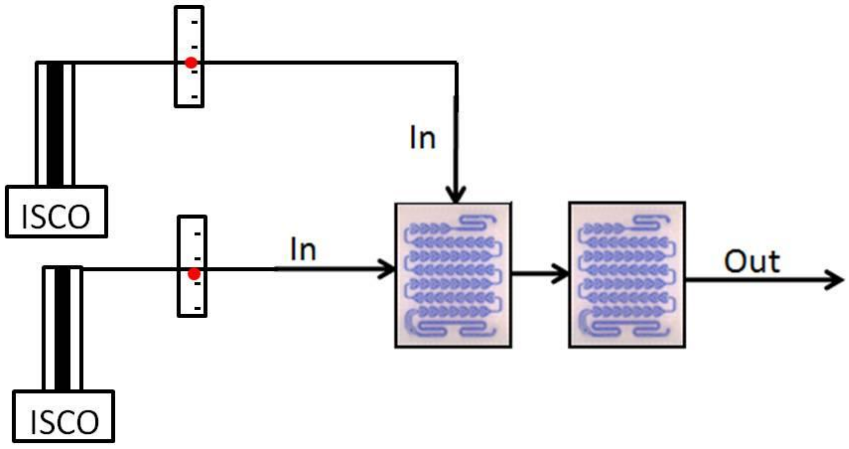


**Figure 3.6.** Two-plate reactor setup for initial experiments

3.3.1.1 The role of catalyst loading on the feasibility of continuous flow MPV reductions

An initial continuous flow reaction was attempted by reacting a homogeneous solution of benzaldehyde in iPrOH, pumped with an ISCO pump through one inlet and a slurry of 50 mol% $Al(OtBu)_3$ in pure anhydrous iPrOH pumped through the second inlet with a Fuji pump at 55$^{o}$C, shown in Figure 3.6. Use of slurries in this particular reactor has been previously reported by Corning®.[11] Upon pumping, however, the Fuji pump and reactor quickly clogged. The Fuji pump suffered from gasket failure due to the building of pressure from clogging and an ISCO was used from that point on. Deposited aluminum species within the reactor channels formed a white film on the channel walls. The film was expected to by hydrolyzed catalyst of $Al(OH)_3$. Flushing with iPrOH and water did not remove the film but 2M HCl did.

The reactor was thoroughly cleaned and it was realized that 50 mol% catalyst loading was clearly inadequate for our system. Moving forward, reaction conditions were optimized to enable the reaction to be conducted in the continuous reactor: We

focused on (1) temperature, (2) solvent, (3) concentration, and (4) catalyst loading to eliminate precipitation in the reactor while maximizing reaction efficiency. As a consequence, we first conducted investigations in batch mode to establish the optimal conditions before technology transfer to continuous mode.

### 3.3.2. MPV reductions with a mixed solvent system

#### 3.3.2.1.Toluene/iPrOH solvent system for MPV reductions

In Chapter 2, I demonstrated that the MPV reductions of benzaldehyde and acetophenone could be successfully conducted in a mixed toluene-isopropanol solvent system. Toluene was the solvent of choice to enhance the solubility of $Al(OtBu)_3$ in the reaction solution. Displayed in Figure 3.7, the reduction of benzaldehyde at $40^oC$ with a 9:1 ratio of toluene:iPrOH was compared for both $Al(OtBu)_3$ and $Al(OiPr)_3$ catalysts. The catalyst loading with respect to benzaldehyde was 50 mol%. The reduction using this mixed solvent system is still fast with $Al(OtBu)_3$ as compared to reduction in strictly iPrOH. It had been shown that in the conversion to continuous flow, 50 mol% loading of catalyst was not applicable. Because the residence time in the continuous flow reactor is maximum 11.2 minutes, efforts were made to optimize the mixed solvent system to increase the reduction rate by investigating both catalyst loading and reaction temperature.

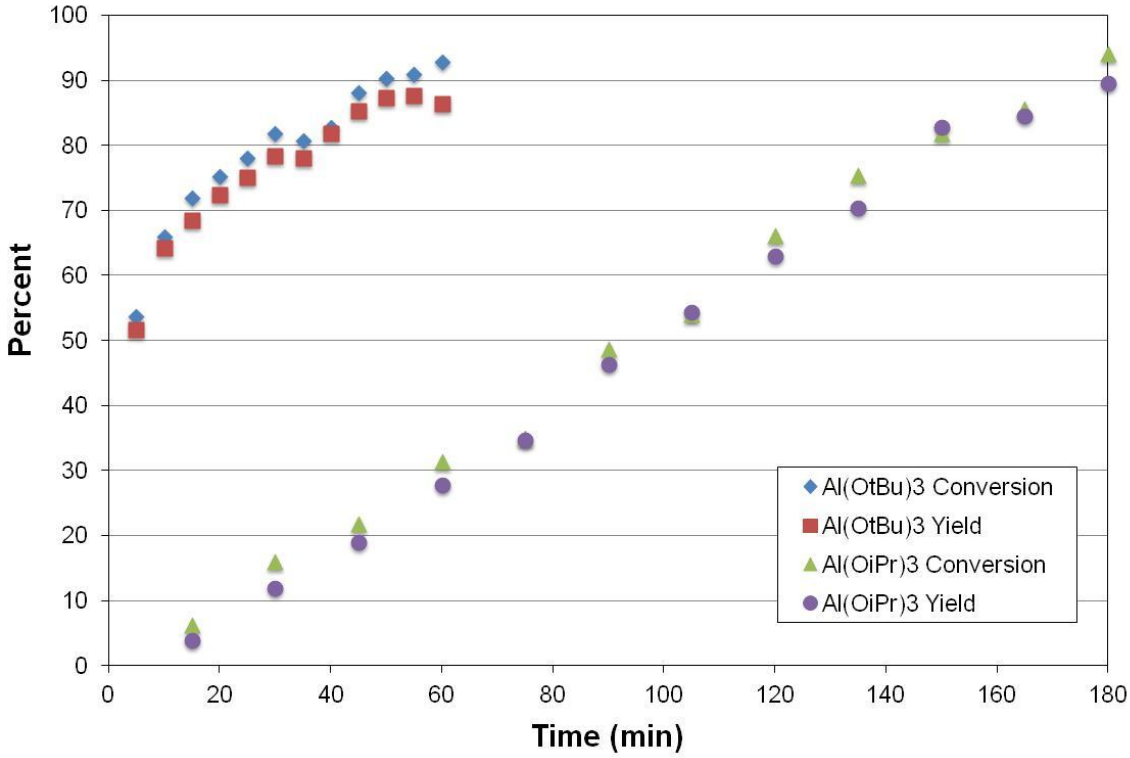


**Figure 3.7.** MPV reduction of benzaldehyde with a 9:1 ratio of toluene:iPrOH as a function of catalyst loading and time

Upon optimization in batch, it was found that a mixed solvent system of 3:2 toluene:iPrOH was effective in solubilizing catalyst loadings as high as 20 mol% $Al(OtBu)_3$ and providing fast reductions of benzaldehyde. These conditions were directly translated to continuous flow reactions.

### 3.3.3 Experimental method of all continuous flow experiments and analysis

For all subsequent continuous flow experiments, two solutions were pumped through two separate pumps at a ratio of 3:2. Distilled benzaldehyde (43 mL) was added to 500 mL of anhydrous iPrOH with a 1 volume % addition of dodecane. $Al(OtBu)_3$ ( 15.2 g for 20 mol %) was added to 600 mL of anhydrous toluene and was stirred vigorously.

A 1 volume % aliquot of nonane was added. The benzaldehyde solution was added to a 500 mL ISCO pump. The $Al(OtBu)_3$ solution was drawn into a 500 mL ISCO pump with a filter to prevent aluminum bi-products found in the commercial catalyst from entering the pumps.

A 3:2 ratio of toluene:iPrOH, was used for all flow rates investigated, for example, for the 30 mL/min total flow rate, the toluene solution was pumped at 18 mL/min while iPrOH was pumped at 12 mL/min. Samples were collected from the outlet tube of the reactor at the end of each residence time. It was found that two residence times were sufficient for equilibration of the reaction so samples were collected for each residence time after the first two had been passed through. 1 mL aliquots of samples were quenched with 2M HCl and diluted with MeOH. HPLC samples were made by diluting a 0.15 mL sample of the reaction solution with 0.85 mL of MeOH. HPLC analysis was conducted to quantify the amount of starting material and product to determine conversion and yield based on pre-formed calibration curves. GC was used to verify flow rate based on the internal nonane and dodecane standards in the solutions.

### 3.3.4 Continuous flow reduction of benzaldehyde with two plates

The simplified configuration that was shown in Figure 3.6 was used as a preliminary design to test the conversion of benzaldehyde to benzyl alcohol through MPV reduction in continuous flow. Figure 3.8 shows the reduction of benzaldehyde with a 3:2 ratio of toluene:iPrOH which was optimized in batch to gain an understanding of the reaction kinetics and then implemented in continuous flow experiments.

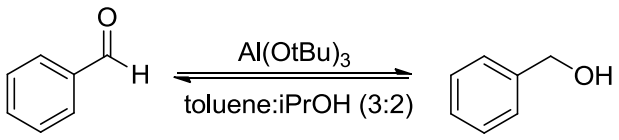


**Figure 3.8.** General reduction scheme for the MPV reduction of benzaldehyde in continuous flow and batch reactions

Total flow rates of 90, 60, 30, 15, and 6 mL/min with the reactor at a reaction temperature of 65$^{o}$C were investigated. It was found that with the maximum residence time of 3 minutes, a total flow rate of 6 mL/min, the conversion reached 45%, shown in Figure 3.9. These preliminary experiments were encouraging and most importantly did not show clogging or pressure build-up.

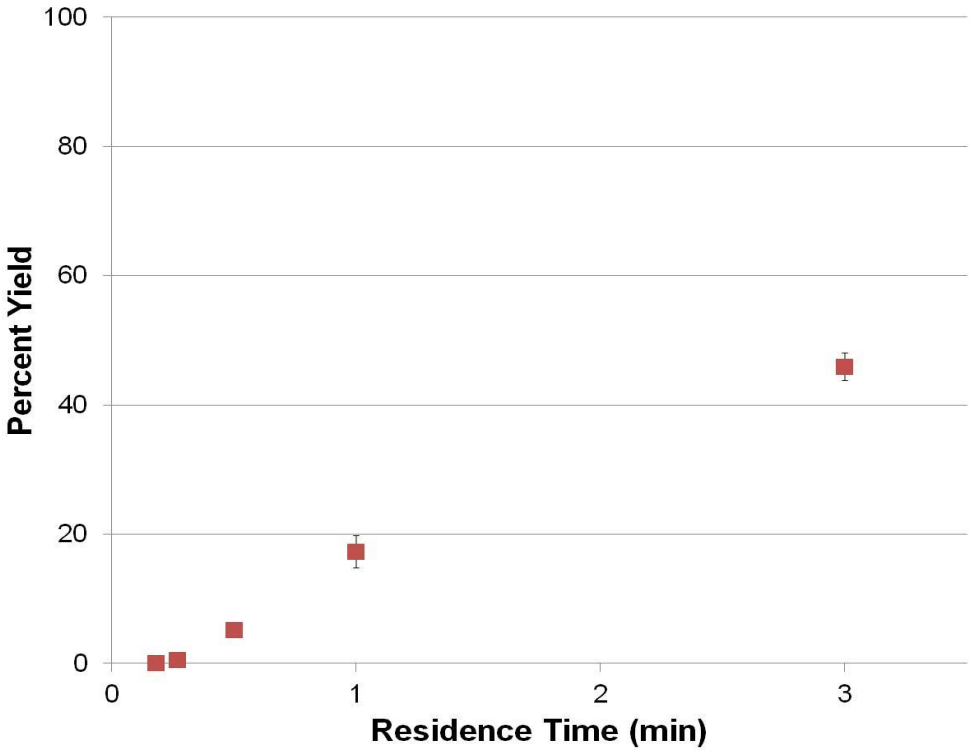


**Figure 3.9.** Yield as a function of residence time in the continuous flow reduction of benzaldehyde with 20 mol% $Al(OtBu)_3$ at 65°C

Therefore, we extended the reactor design to incorporate 6 plates allowing for residence time of 11.2 minutes at a total flow rate of 5 mL/min. These experiments will be addressed later in the chapter.

In a parallel effort, the reaction kinetics were gathered. The MPV reductions of benzaldehyde were conducted with 20 mol% and 5 mol% $Al(OtBu)_3$ at 65°C and 80°C. All four of these experiments were monitored with respect to reaction time and repeated in triplicate in batch and continuous flow. The batch reactions are introduced first.

### 3.3.5 Batch Reductions of model carbonyl compounds with toluene/iPrOH

3.3.5.1 Reductions of benzaldehyde at 65$^{o}$C with 5 and 20% Al(OtBu)$_3$

Two sets of MPV reactions were carried out at 65$^{o}$C in a 12-tube carousel reactor with toluene:iPrOH (3:2). Catalyst loadings of 20 and 5 mol% Al(OtBu)$_3$ were used and quenched with 2M HCl every 2 minutes and 5 minutes, respectively. The samples were analyzed by HPLC using calibration curves of benzaldehyde and benzyl alcohol to gain quantitative results. The results are displayed in Figure 3.10. At 65$^{o}$C, the reduction with 20 mol% catalyst reached 95% yield after 24 minutes while the 5 mol% reaction reached 62% yield after 25 minutes. There is indeed a noticeable rate advantage with increasing amounts of catalyst and even low loadings of 20 mol% are effective at promoting the complete reduction in about 25 minutes.

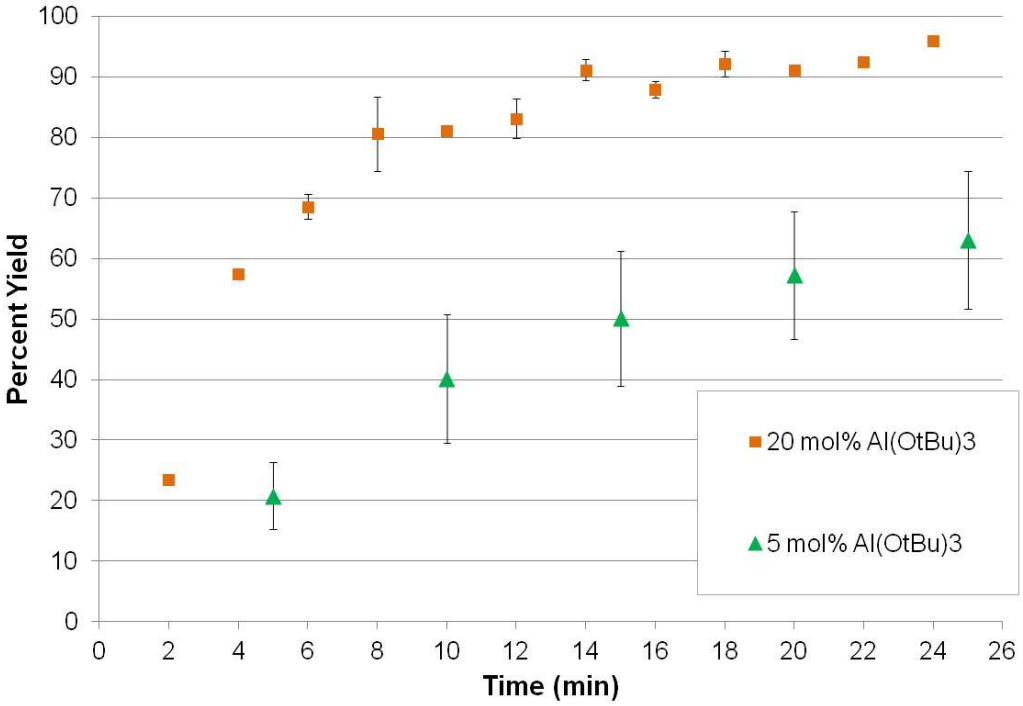


**Figure 3.10.** Batch MPV reductions of benzaldehyde at 65°C with 20 and 5 mol% $Al(OtBu)_3$

3.3.5.2 Reductions of benzaldehyde at 80°C with 5 and 20 mol% $Al(OtBu)_3$

The same set of reactions were conducted at 80°C using the (3:2) toluene:iPrOH system with catalyst loadings of 20 and 5 mol% $Al(OtBu)_3$ quenched with 2M HCl every 1 and 3 minutes. These reductions were also analyzed quantitatively by HPLC. The reaction with 20 mol% $Al(OtBu)_3$ catalyst was complete after 12 minutes and the 5 mol% catalyzed reaction was 70% complete after 12 minutes (Figure 3.11). From 65°C to 80°C, the reaction completion only took half of the time, from 24 minutes to 12 minutes--an important advantage in continuous flow.

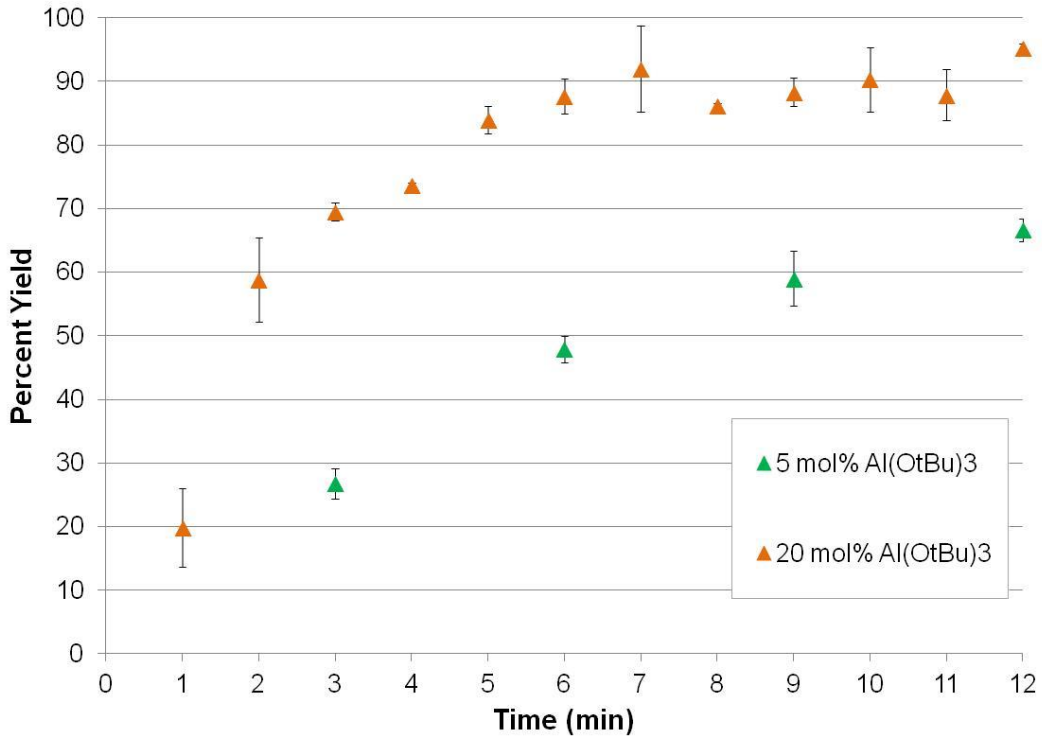


**Figure 3.11.** Batch MPV reductions of benzaldehyde at 80°C with 20 and 5 mol% $Al(OtBu)_3$

3.3.5.3 Batch Reactions of acetophenone at 80°C with 20 mol% $Al(OtBu)_3$

The reduction of acetophenone, a model ketone in the MPV reduction had been shown in Chapter 2 to be slower than its benzaldehyde counterpart. Benzaldehyde reductions are complete with 50 mol% catalyst at 40°C in about 30 minutes. Acetophenone at 50°C required almost 300 minutes to reach completion with 50 mol% $Al(OtBu)_3$. As a result, the batch reaction of acetophenone was directly carried out at 80°C with 20 mol% catalyst loading. The experiment was conducted once with quenching every 10 minutes and once with quenching (the example in Figure 3.12) at

varying intervals. The overlapping points between the two runs were in agreement with each other. The results were that the reaction reached about 85% completion at 120 minutes and then appeared to plateau. This is most likely due to the reverse Oppenauer oxidation competing with the forward reduction. This is consistent with previous experiments. In fact with 50 mol% catalyst loading, acetophenone also began to plateau.

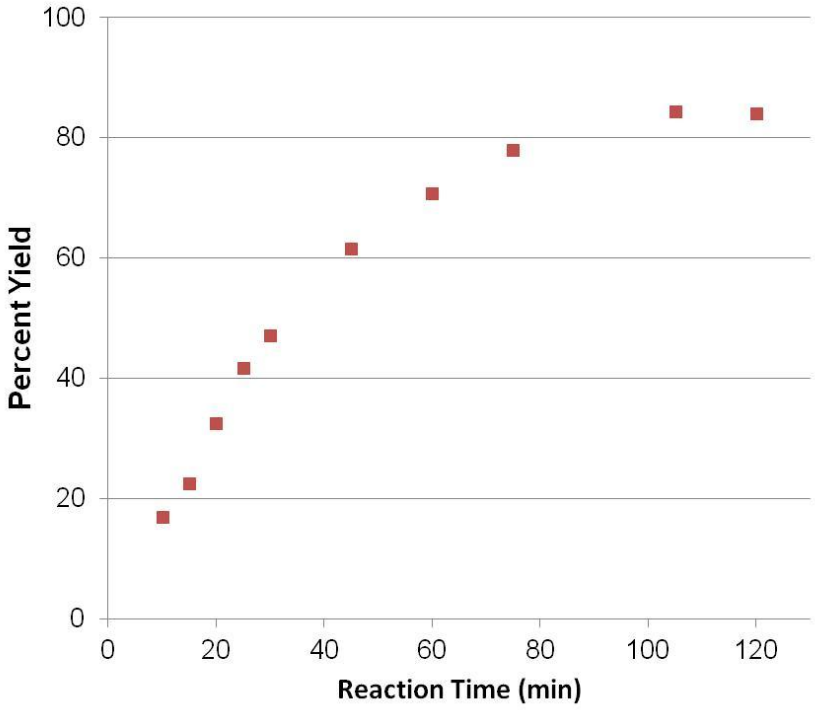


**Figure 3.12.** Batch MPV reduction of benzaldehyde at 80°C with 20 mol% $Al(OtBu)_3$

The reductions implemented and studied in batch reactions were converted to continuous flow with the under the same conditions.

### 3.3.6 MPV reductions of benzaldehyde and acetophenone in continuous flow

#### 3.3.6.1 Reactor design

The MPV reduction of benzaldehyde was conducted in continuous flow at 55$^{o}$C using a configuration of eight plates (Figure 3.13). Two plates were used as preheating plates for the solutions prior to mixing and the actual reaction ran through six plates. The two temperature regions were set to the same temperature so that the reaction was isothermal throughout. ISCO pumps supplied the reagents, and rotometers and pressure gauges were installed in between the pumps and the preheating plates. Heat exchangers supplied two temperature regions, the first covering plates 1-6 and the second regulating temperature in the last two plates. Thermocouples were also placed in the reactor between the inlet and outlet of each heat exchanger.

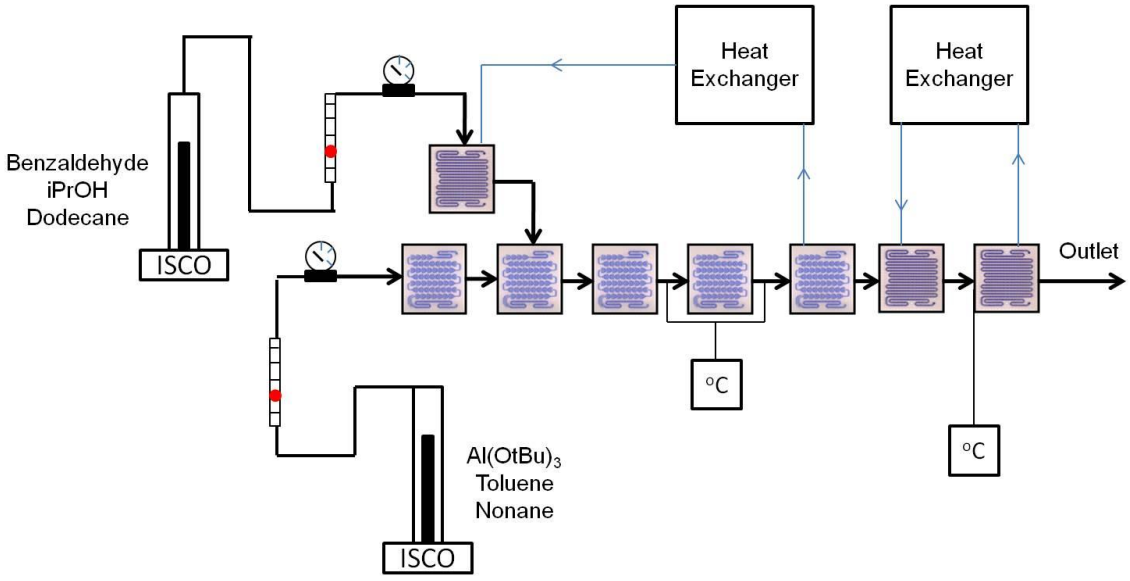


**Figure 3.13.** Schematic of the complete eight plate continuous flow setup

A simplified model of the reactor design for the reduction of benzaldehyde with six reaction plates is shown in the Figure 3.14 below.

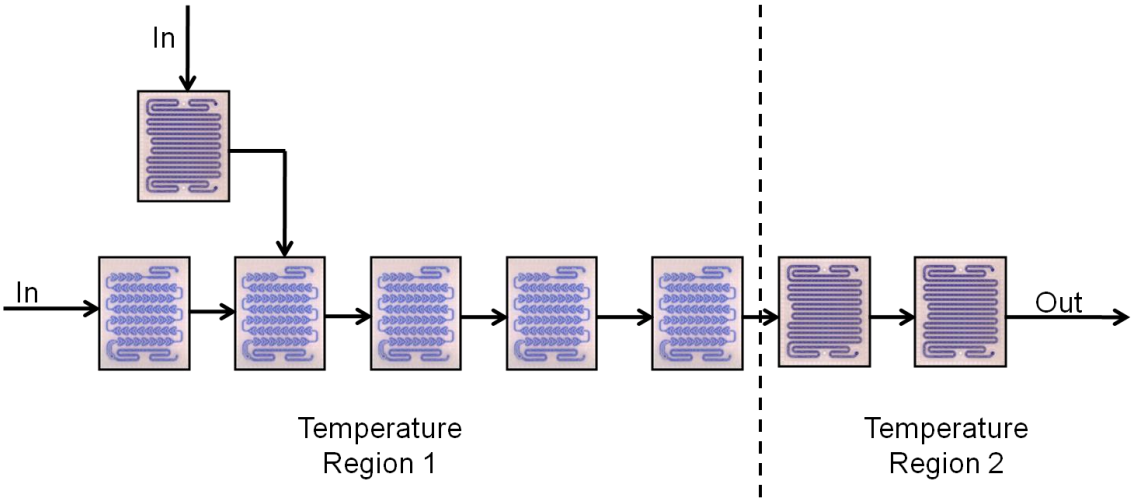


**Figure 3.14.** Mixing plate reactor setup for the continuous flow MPV reductions

3.3.6.2 Analysis of conversion and yield in continuous flow

The MPV reduction of benzaldehyde was conducted with 20% $Al(OtBu)_3$ in continuous flow at 55$^{o}$C. At a 5 mL/min total flow rate or 11 minute residence time, samples were collected. The HPLC analysis was quantified with calibration curves to monitor conversion (loss of benzaldehyde) and yield (formation of benzyl alcohol). Both conversion and yield should be identical since the MPV reduction of benzaldehyde did not lead to side products and evidence of other peaks were not noted in the HPLC chromatograph.

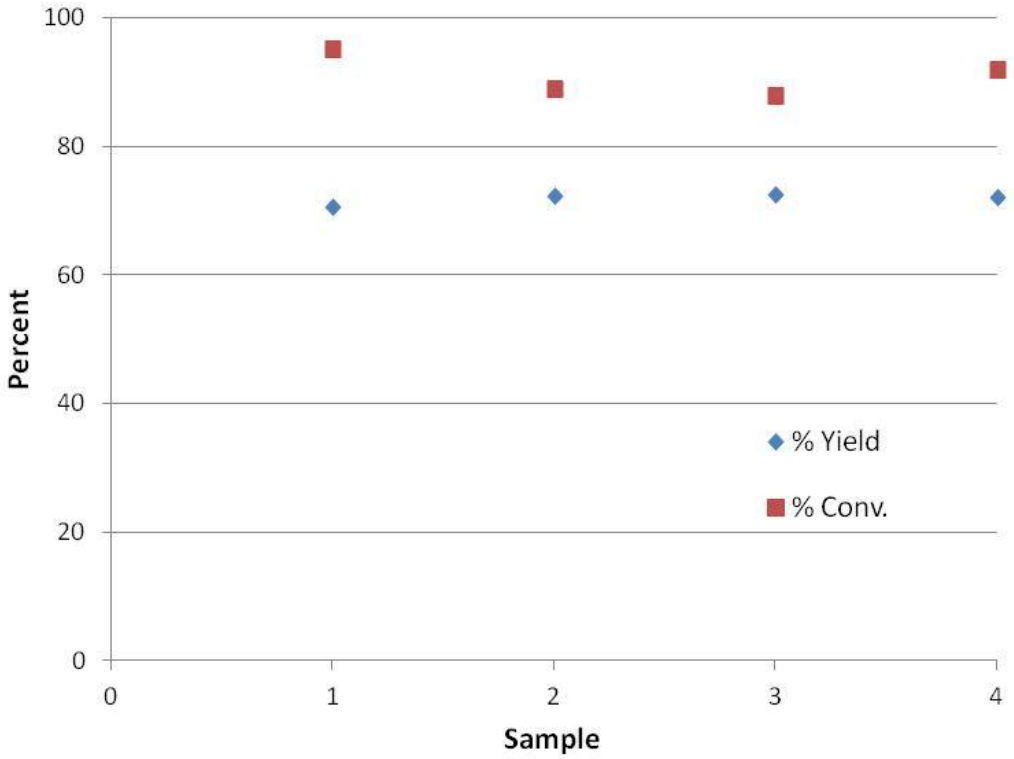


**Figure 3.15.** Yield error in the reduction of benzaldehyde with 20 mol% $Al(OtBu)_3$ in continuous flow at 55°C

It was found that conversion and yield had a discrepancy of about 25% in the reductions of benzaldehyde at 55°C in continuous flow (Figure 3.15). This was addressed prior to any other reactions being investigated. The calibration curves were checked for accuracy and proved not to be the problem. We also considered that the actual concentration expected to be introduced was not consistent with small changes in flow rate. Because the pump flow determines the amount of introduction of material through the reactor if it is set to 5 mL/min and provides a 4.8 mL/min actual flow, the theoretical concentration used to calculate loss of starting material would be incorrect. A

solution was easily implemented: alkanes, nonane and dodecane were introduced in 1 vol% to each of the reagents and monitored by GC to monitor the actual flow rates in the future experiments. A look into the mechanism of the reduction provided the solution to the yield and conversion discrepancy.

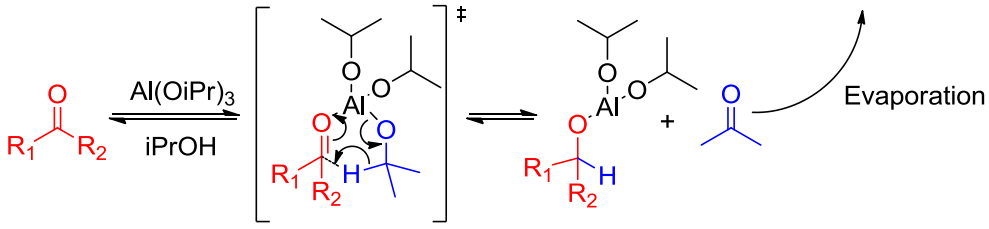


**Figure 3.16.** Mechanistic loss of acetone in the general MPV reduction

Acetone is a product of the reaction formed as the isopropoxide groups are oxidized. At 55°C, the evaporation of acetone may cause error in the concentrations (Figure 3.16). It was found that at faster flow rates, the amount of error was increased over the slower flow rates. This was expected because the slower the solution is moving, the longer time it has to cool before exiting, re-condensing the vaporized acetone. As a solution to this problem, the outlet spout on the continuous flow reactor was chilled with an ice bath. Having the outlet chilled as it exited proved to be a success in fixing this problem. One could imagine having the last few plates on the reactor being cooled to re-condense any of the volatile components. Because the reaction rate is a function of temperature, the reaction would slow down in those chilled plates, limiting the conversion of starting material so this was not explored as a way to address the problem.

3.3.6.3 MPV Reduction of benzaldehyde in continuous flow as a function of time, temperature, and catalyst loading

Continuous flow experiments of the MPV reductions of benzaldehyde were conducted as follows: Benzaldehyde was dissolved in anhydrous iPrOH and $Al(OtBu)_3$ was dissolved in anhydrous toluene. The two solutions were flowed together at a 2:3 ratio of carbonyl starting material in iPrOH to $Al(OtBu)_3$ in toluene with total flow rates of 5, 15, and 30 ml/min. Experiments were conducted with 5 and 20 mol% $Al(OtBu)_3$ at both 65°C and 80°C and the results are plotted in Figure 3.17. HPLC was used to determine reaction yields and GC analysis was used to determine actual flow rates (through use of the nonane and dodecane internal standards).

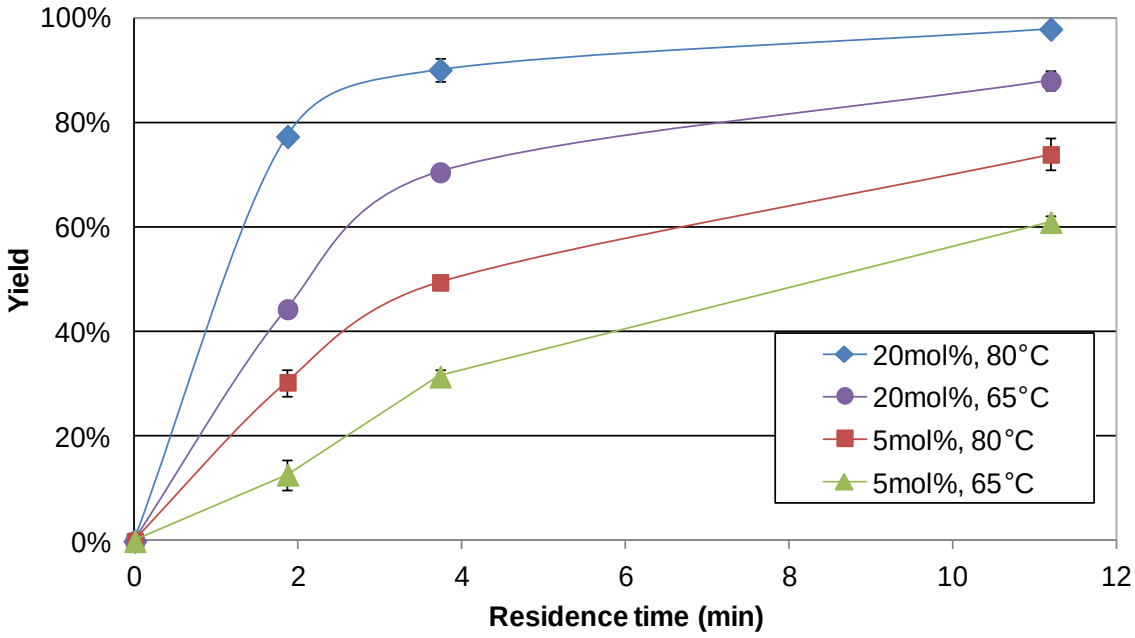


**Figure 3.17.** MPV continuous flow reduction of benzaldehyde with catalyst loading, temperature and residence time

As the flow rate was increased from 5 to 30 ml/min, the overall yield decreased from 60% to 15% when using 5 mol% $Al(OtBu)_3$ at 65$^oC$, as an example. As the flow rate increased, the residence time for the reaction to take place prior to quenching was shortened. By lowering the flow rate, the efficiency of mixing decreases, which in the case of homogeneous reactions like the mixed-solvent MPV reductions, was not a concern. This is a balance if one were to investigate heterogeneous reactions in this type of reactor. It was found in all experiments that a flow rate of 5 mL/min, which corresponded to 11.2 minutes of residence time, provided the highest yields. With 20 mol% $Al(OtBu)_3$ at 80$^oC$ in the (3:2) toluene:iPrOH ratio, full conversion to benzyl alcohol was achieved after only 11.2 minutes of reaction!

### 3.3.6.4 MPV reduction of acetophenone in continuous flow as a function of time

The MPV reduction of acetophenone was also conducted in continuous flow at 5, 15, and 30 mL/min flow rates. The MPV catalyzed reduction of acetophenone was conducted at 80$^oC$ with 20 mol% $Al(OtBu)_3$ and shown in Figure 3.18. The reaction reached about 18% yield at the maximum residence time of 11.2 minutes. Although the reaction did not reach completion under these conditions, higher concentrations of acetophenone or extending the residence time by incorporating more plates would enable full conversion. It is expected based on the batch reduction data at the same conditions that a residence time of about 150 minutes would be needed. This corresponds to about 80 plates at a flow rate of 5 mL/min.

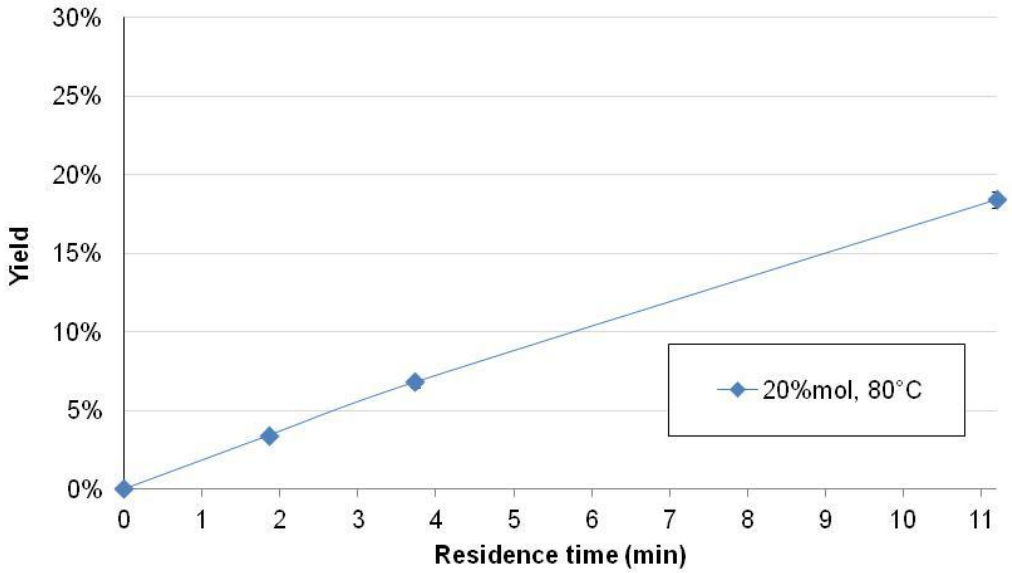


**Figure 3.18.** MPV continuous flow reduction of acetophenone with 20 mol% $Al(OtBu)_3$ at 80°C

### 3.3.7 Comparison of batch and continuous flow methodology

As mentioned in the introduction, continuous flow has been used to address not only improvements in batch conditions including superior mass and heat transfer, but also in its scale out approach. I was able to successfully enable an improved MPV reduction through $Al(OtBu)_3$ with lower catalyst loading as well as decrease the aluminum salt waste that would be generated. I was then able to convert the batch MPV reduction to a sustainable continuous flow process. To put into context the improvement of the continuous process as compared to batch conditions with the MPV reduction of benzaldehyde, I have compared the batch results with the continuous flow results under the same conditions for both variables investigated (catalyst loading and temperature).

The results show that the performance was equivalent, and therefore the pharmaceutical industry can appreciate that moving this process to continuous flow would maintain high efficiency while taking full advantage of a scale-out approach. I will highlight the conditions that provided the best results in continuous flow.

### 3.3.7.1 Benzaldehyde reductions in batch and continuous flow at 80°C and 20 mol% $Al(OtBu)_3$

Comparison of the batch and continuous reductions at 80°C with 20 mol% catalyst loading is plotted in Figure 3.19. With 20 mol% $Al(OtBu)_3$ at 80°C in the reduction of benzaldehyde, continuous flow proved to perform slightly better than in batch. The 11.2 minute residence time shows full conversion in continuous flow and in batch data, within error displays the same result.

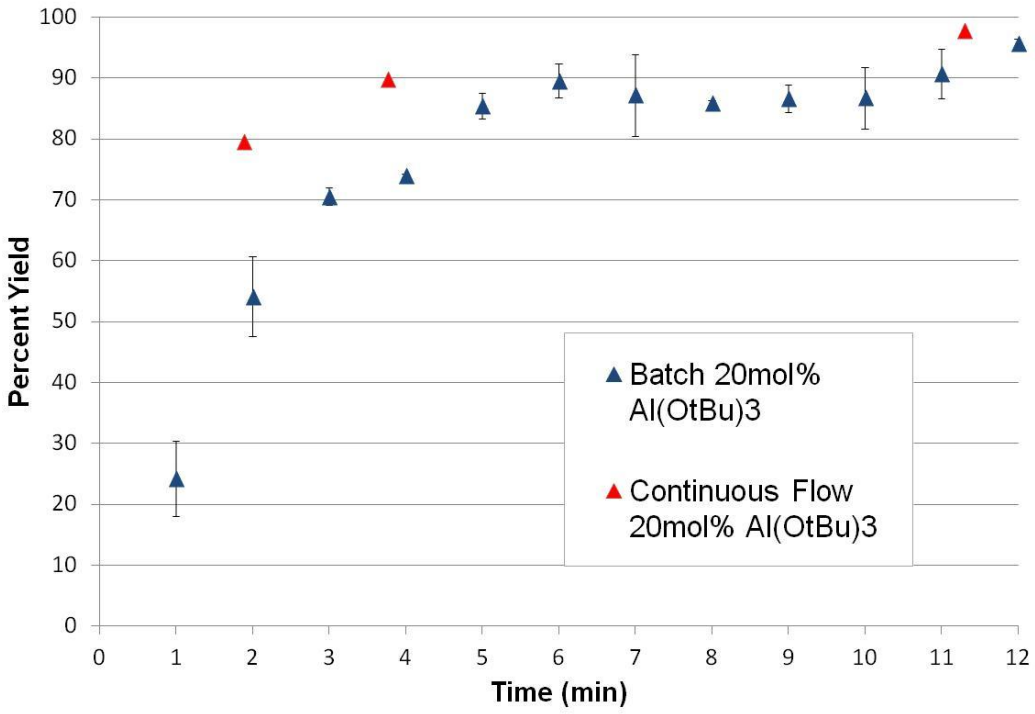


**Figure 3.19.** Comparison of batch and continuous flow in the MPV reduction of benzaldehyde with 20 mol% $Al(OtBu)_3$ at 80°C

Because of the mixed solvent system used (toluene:iPrOH 3:2), all of the reactants and catalyst are homogeneous. Therefore mixing is not a big concern for this particular reduction. Heat transfer is excellent which is noted by the difference between the continuous flow data points and the batch data points at lower residence times. At 2 minutes, the continuous flow reduction is at 80% where the batch is at 60%. The solutions in continuous flow are preheated prior to mixing and because of the instantaneous even heating in the Corning® Continuous Reactor, the reaction begins to take place faster than in batch, where the reactants require time to come to temperature once added. Since the reaction is comparable in continuous flow from batch, scale out of this reaction could be achieved!

3.3.7.2 Acetophenone reductions in batch and continuous flow at 80°C and 20 mol% $Al(OtBu)_3$

The reduction of acetophenone with conditions that provided the best yield in the reduction of benzaldehyde, 80°C and 20 mol% catalyst loading, gave a maximum of 18% conversion at 11.2 minutes of residence time, shown in Figure 3.20. The batch data and continuous flow data are consistent as in the benzaldehyde example.

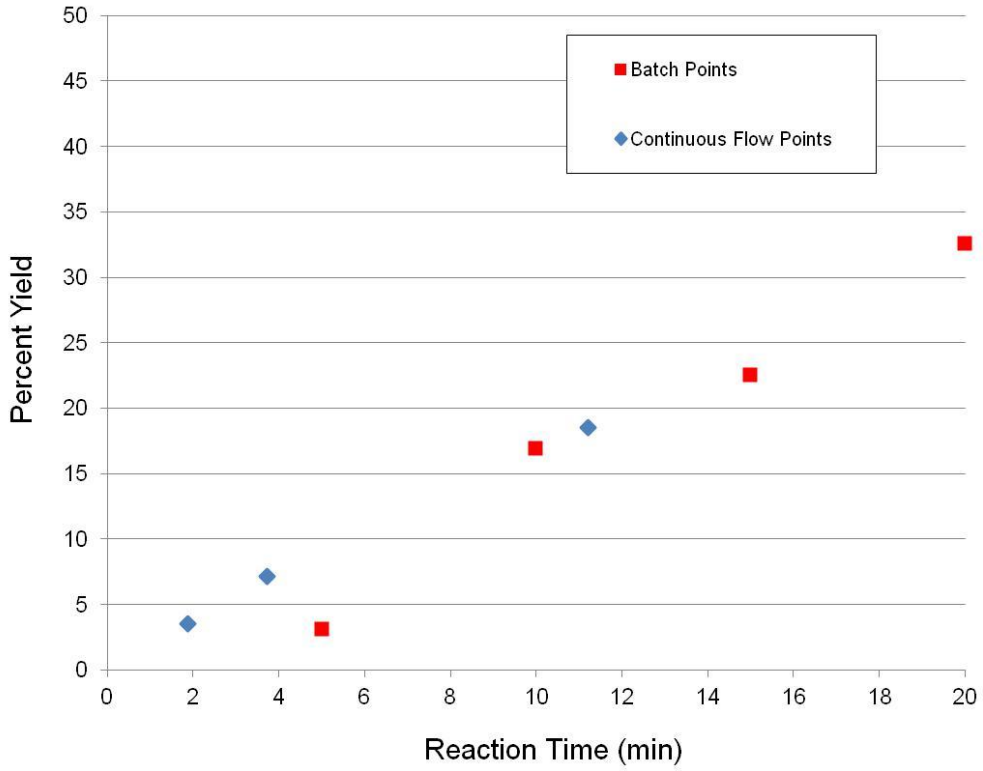


**Figure 3.20.** Comparison of batch and continuous flow in the MPV reduction of acetophenone with 20 mol% $Al(OtBu)_3$ at 80°C

## 3.4 Conclusions

It was found that continuous flow technology is a very useful tool for the conversion of batch reactions to greener processes. The reason that it can be an approach to green engineering is because the continuous flow reactions of benzaldehyde and acetophenone have been shown to have high reactivity at short reaction times (11 minutes for benzaldehyde) and this offers the benefit of a scale out approach as well improved atom economy and efficiency. We have been able to complete the reduction of benzaldehyde with 20 mol% $Al(OtBu)_3$ as opposed to 50 mol% commonly used in batch MPV processes and have even gone as low as 5 mol% catalyst loadings to effectively reduce carbonyls to their alcohols. Furthermore, mixed solvent systems have been demonstrated to be efficient at solubilizing all materials and achieving fast reactions with less amounts of iPrOH. These reductions can be demonstrated on a library of other ketones or aldehydes and scaled-out for large scale production which is particularly advantageous to the pharmaceutical industry. This, to our knowledge, is also the first successful MPV reduction to be converted to a continuous flow method.

## 3.5 Experimental procedures

### 3.5.1 General procedure for batch reactions:

Batch reactions were conducted in the carousel. Stock solutions were made under an atmosphere of nitrogen. Different stock solutions were made for both the 20 mol% and 5 mol% $Al(OtBu)_3$ loadings. For the 5 mol% $Al(OtBu)_3$ reactions, 0.2669 g of $Al(OtBu)_3$ was added to 40 mL of anhydrous toluene. For the 20 mol% $Al(OtBu)_3$ reactions, the solution was made in each carousel tube by adding 0.0810g of $Al(OtBu)_3$ to 3 mL of anhydrous

toluene. A stock solution of benzaldehyde was made by dissolving 2.5 mL in 30 mL of anhydrous iPrOH. For reductions with acetophenone, the stock solution was made by dissolving 2.87 mL of acetophenone in 30 mL of anhydrous iPrOH.

3 mL of the catalyst stock solution was added to each carousel tube and heated to the reaction temperature. Once the solution reached temperature, 2 mL of the benzaldehyde stock solution was added to begin the reaction. After the desired reaction time, each tube was placed in an ice bath with stirring. 2 mL of 2M HCl was added and the mixture was diluted with 30 mL of MeOH. 0.1 mL of the diluted reaction solution was added to 0.9 mL of MeOH in a GC Vial to be analyzed by HPLC.

### 3.5.2 General procedure for continuous flow reactions:

Continuous flow reactions were conducted using the same solvent regime as the batch reactions. Two stock solutions were made. Benzaldehyde (43 mL) was added to anhydrous iPrOH (500 mL) with a spike of dodecane (4.3 mL). 5 mol% $Al(OtBu)_3$ was created by adding 3.8 g of $Al(OtBu)_3$ to 600 mL of anhydrous toluene with a spike of nonane (6 mL). 20 mol% $Al(OtBu)_3$ was created by adding 15.5 g to 600 mL of anhydrous toluene with a spike of nonane (6 mL). The entire benzaldehyde solution was drawn into a 500D Model ISCO pump. The $Al(OtBu)_3$ solution was drawn into a 500D Model ISCO pump using a filter to keep insoluble aluminum species from clogging the pump and reactor. The continuous flow reactor was brought to the appropriate reaction temperature and allowed to stabilize. 0.1 mL samples were taken of each stock solution and diluted with 0.9 mL MeOH for GC analysis. The pumps were flowed at three total flow rates 5 mL/min (3 toluene:2 iPrOH), 15 mL/min (9 toluene:6 iPrOH), and 30 mL/min (18 toluene:12 iPrOH). The pumps were started at each flow rate and two reactor volumes were allowed to run prior to collection. After two volumes, collections were taken at every reactor volume. 1 mL samples were used for GC analysis. For HPLC, 1

mL aliquots were placed in tubes in an ice bath and diluted with 1 mL cold MeOH. After 1 minute, 0.4 mL 2M HCl was added. 15 mL MeOH were then added to dilute samples. 0.1 mL of reaction mixture was added to a GC vial with 0.9 mL MeOH and analyzed by HPLC. After the reactions are complete, the reactor and ISCO pumps were flushed with iPrOH and toluene and the heat exchangers cooled to room temperature.

### 3.5.3 Continuous flow sampling guide

| 80°C | 5 mL/min | 2 and 3 | | Total Residence Volumes | Volume Used | Total Time (sec) | Total Time (Min) | Time of Volume (hr:min:sec) | TR 1 (°C) | TR 2 (°C) | TR 3 (°C) | $P_{cat}$ (psi) | $P_{BA}$ (psi) | $RM_{Cat}$ | $RM_{BA}$ | Total Flow Rate (ml/min) |
|---|---|---|---|---|---|---|---|---|---|---|---|---|---|---|---|---|
| | | Isco | Fugi | | | | | | | | | | | | | |
| | BA Start Conc. Out of ISCO | | | 0 | 0 | 0 | 0 | 0 : 00 : 00 | ------ | | | | | | | |
| LAUDA Set Point= | 86.8 C | | | 1 | 56 | 672 | 11.20 | 0 : 11 : 12 | | | | | | | | |
| Thermo Set Point= | 82.9 C | | | 2 | 112 | 1344 | 22.40 | 0 : 22 : 24 | | | | | | | | |
| Vol. Cat= | | | | 3 | 168 | 2016 | 33.60 | 0 : 33 : 36 | | | | | | | | |
| Vol. BA= | | | | 4 | 224 | 2688 | 44.80 | 0 : 44 : 48 | | | | | | | | |

| 80°C | 15 mL/min | 6 and 9 | | Total Residence Volumes | Volume Used | Total Time (sec) | Total Time (Min) | Time of Volume (hr:min:sec) | TR 1 (°C) | TR 2 (°C) | TR 3 (°C) | $P_{cat}$ (psi) | $P_{BA}$ (psi) | $RM_{Cat}$ | $RM_{BA}$ | Total Flow Rate (ml/min) |
|---|---|---|---|---|---|---|---|---|---|---|---|---|---|---|---|---|
| | | Isco | Fugi | | | | | | | | | | | | | |
| | BA Start Conc. Out of ISCO | | | 0 | 0 | 0 | 0 | 0 : 00 : 00 | ------ | | | | | | | |
| LAUDA Set Point= | 86.8 C | | | 1 | 56 | 224 | 3.73 | 0 : 3 : 44 | | | | | | | | |
| Thermo Set Point= | 82.9 C | | | 2 | 112 | 448 | 7.47 | 0 : 7 : 29 | | | | | | | | |
| Vol. Cat= | | | | 3 | 168 | 672 | 11.20 | 0 : 11 : 12 | | | | | | | | |
| Vol. BA= | | | | 4 | 224 | 896 | 14.93 | 0 : 14 : 56 | | | | | | | | |

| 80°C | 30 mL/min | 12 and 18 | | Total Residence Volumes | Volume Used | Total Time (sec) | Total Time (Min) | Time of Volume (hr:min:sec) | TR 1 (°C) | TR 2 (°C) | TR 3 (°C) | $P_{cat}$ (psi) | $P_{BA}$ (psi) | $RM_{Cat}$ | $RM_{BA}$ | Total Flow Rate (ml/min) |
|---|---|---|---|---|---|---|---|---|---|---|---|---|---|---|---|---|
| | | Isco | Fugi | | | | | | | | | | | | | |
| | BA Start Conc. Out of ISCO | | | 0 | 0 | 0 | 0 | 0 : 00 : 00 | ------ | | | | | | | |
| LAUDA Set Point= | 86.8 C | | | 1 | 56 | 112 | 1.87 | 0 : 1 : 52 | | | | | | | | |
| Thermo Set Point= | 82.9 C | | | 2 | 112 | 224 | 3.73 | 0 : 3 : 44 | | | | | | | | |
| Vol. Cat= | | | | 3 | 168 | 336 | 5.60 | 0 : 5 : 36 | | | | | | | | |
| Vol. BA= | | | | 4 | 224 | 448 | 7.47 | 0 : 7 : 29 | | | | | | | | |

**Figure 3.21.** Sampling guide for the continuous flow experiments

### 3.5.4. Comparisons of batch and continuous flow

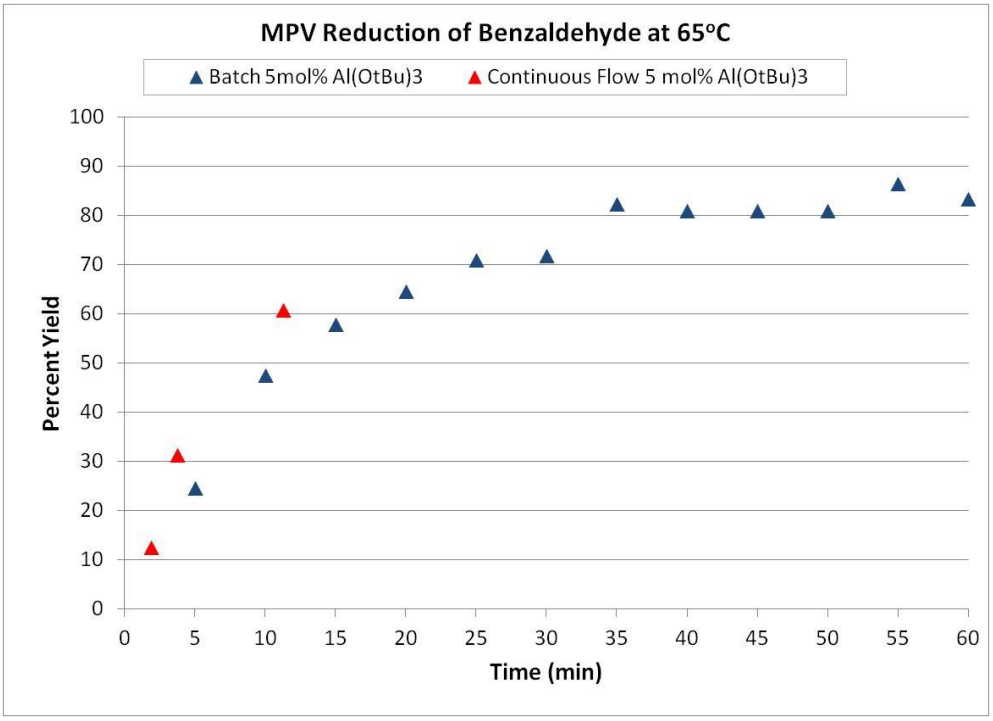


**Figure 3.22.** Comparison of batch and continuous flow in the MPV reduction of benzaldehyde with 5 mol% $Al(OtBu)_3$ at 65°C

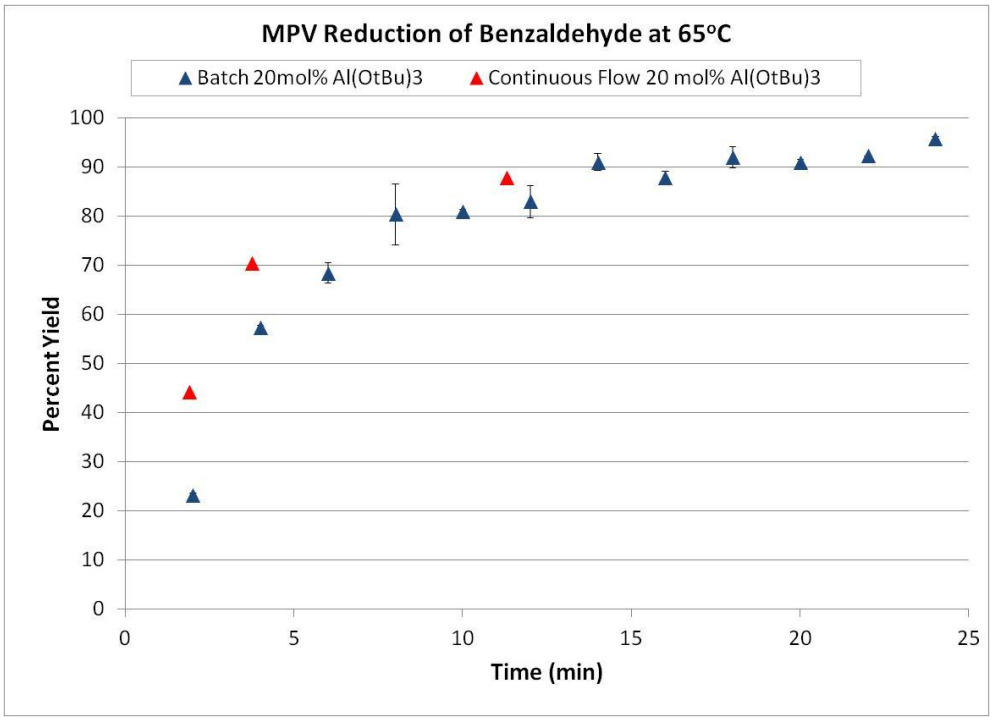


**Figure 3.23.** Comparison of batch and continuous flow in the MPV reduction of Benzaldehyde with 20 mol% $Al(OtBu)_3$ at 65°C

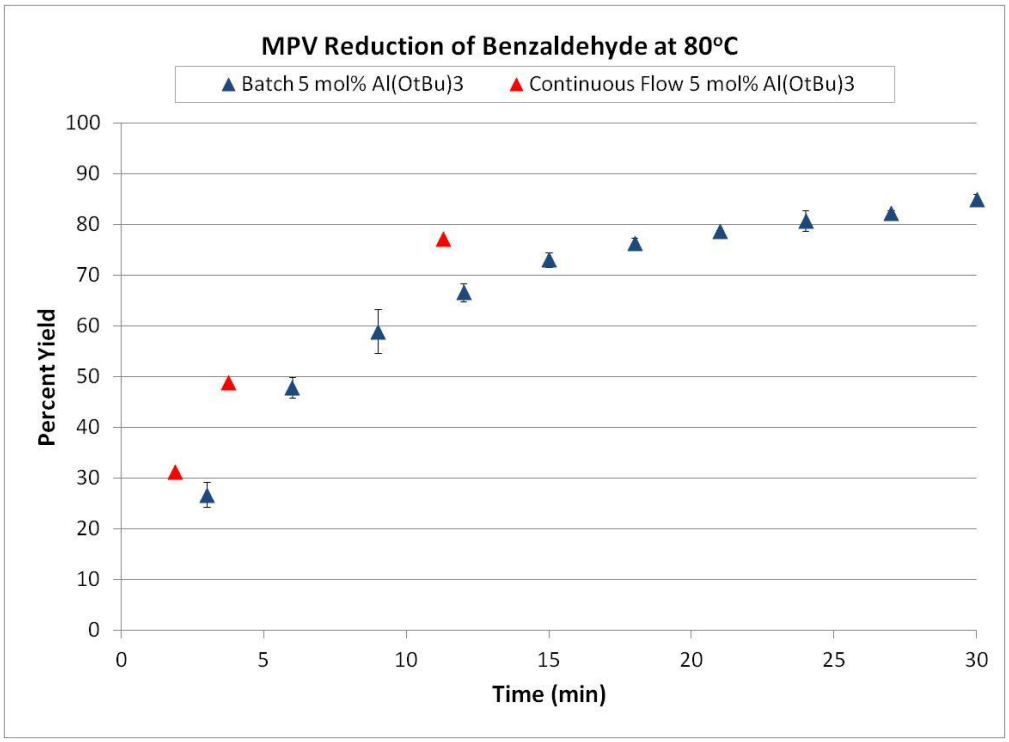


**Figure 3.24.** Comparison of batch and continuous flow in the MPV reduction of benzaldehyde with 5 mol% $Al(OtBu)_3$ at 80°C

## 3.6 References


(1) Baroud, C. N.; Willaime, H. *Comptes Rendus Physique* **2004**, *5*, 547.

(2) Jimenez-Gonzalez, C.; Poechlauer, P.; Broxterman, Q. B.; Yang, B. S.; Ende, D. A.; Baird, J.; Bertsch, C.; Hannah, R. E.; Dell'Orco, P.; Noorrnan, H.; Yee, S.; Reintjens, R.; Wells, A.; Massonneau, V.; Manley, J. *Organic Process Research & Development* **2011**, *15*, 900.

(3) Weigl, B. H.; Bardell, R. L.; Cabrera, C. R. *Advanced Drug Delivery Reviews* **2003**, *55*, 349.

(4) Noel, T.; Kuhn, S.; Musacchio, A. J.; Jensen, K. F.; Buchwald, S. L. *Angewandte Chemie-International Edition* **2011**, *50*, 5943.

(5) Webb, D.; Jamison, T. F. *Chemical Science* **2010**, *1*, 675.

(6) Glasnov, T. N.; Kappe, C. O. *Chemistry-A European Journal* **2011**, *17*, 11956.

(7) Baxendale, I. R.; Hayward, J. J.; Ley, S. V. *Combinatorial Chemistry & High Throughput Screening* **2007**, *10*, 802.

(8) Pollet, P.; Cope, E. D.; Kassner, M. K.; Charney, R.; Terett, S. H.; Richman, K. W.; Dubay, W.; Stringer, J.; Eckert, C. A.; Liotta, C. L. *Industrial & Engineering Chemistry Research* **2009**, *48*, 7032.

(9) McMullen, J. P.; Jensen, K. F. *Organic Process Research & Development* **2011**, *15*, 398.; Roberge, D. M.; Zimmermann, B.; Rainone, F.; Gottsponer, M.; Eyholzer, M.; Kockmann, N. *Organic Process Research & Development* **2008**, *12*, 905.; Chevalier, B.; Lavric, E. D.; Cerato-Noyerie, C.; Horn, C. R.; Woehl, P. *Chimica Oggi-Chemistry Today* **2008**, *26*, 38.; Monbaliu, J.-C. M. R.; Winter, M.; Chevalier, B.; Schmidt, F.; Jiang, Y.; Hoogendoorn, R.; Kousemaker, M.; Stevens, C. V. *Chimica Oggi-Chemistry Today* **2010**, *28*, 8.; Chevalier, B. *Chimica Oggi-Chemistry Today* **2008**, *26*, 2.

(10) Malik, A. A.; Clement, T. E.; Palandoken, H.; Robinson III, J.; Stringer, J. A. "Clean, High-yield Preparation Of S,S- and R,S- Amino Acid Isosteres." US Patent 6,867,311 B2, Mar. 15, **2005.**

(11) Buisson, B.; Donegan, S.; Wray, D.; Parracho, A.; Gamble, J.; Caze, P.; Jorda, J.; Guermeur, C. *Chimica Oggi-Chemistry Today* **2009**, *27*, 12.

# CHAPTER 4: $CO_2$ CAPTURE WITH TRIALKYLSILYLPROPYLAMINES

## 4.1 Introduction

### 4.1.1 Aqueous amines for $CO_2$ Capture

The capture of $CO_2$ from industrial effluents has become a major endeavor across multiple disciplines. Particular interest has been widely placed on the purification of the gaseous waste stream of coal-fired power plants.[1] Because the chemical reaction between both primary and secondary amines with $CO_2$ forms thermally reversible carbamate salts, shown in Figure 4.1, the use of amines as $CO_2$ scrubbing agents has become the industrial standard for gas sweetening in natural gas purification operations.[2] Because of the corrosive nature of pure amines, water is generally used to mitigate both corrosion and viscosity of the ammonium/carbamate salts formed.

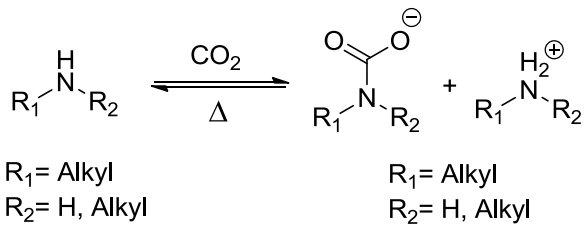


**Figure 4.1.** Reversible reaction of amines with carbon dioxide

Once the $CO_2$ is captured through reaction, the overall recycle process requires the removal of $CO_2$ from the solution by thermal decomposition of the ammonium/carbamate salt thereby regenerating the aqueous amine solution for successive capture cycles. Many aqueous amine based capture systems have been

developed over the past century. Many of these systems use alkanolamines.[3] Because of the tendency of alkanolamines to be corrosive and to undergo degradation (often through oxidation), many commercial solutions have included additives.[4] For example, the formation of acidic bi-products (such as formic acid and acetic acid) from the degradation of alkanolamines led to the need of mineral bases such as sodium carbonate.[5] Many blends including DOW MEA, Econamine FG[6], and Kerr-McGee MEA have been developed and studied for $CO_2$ capture.[7] In all cases, these in some capacity utilize monoethanolamine (MEA), shown in Figure 4.2.

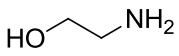


**Figure 4.2.** Monoethanolamine (MEA)

The accepted benchmarked amine system is a 30% solution of monoethanolamine (MEA) in water. Reaction of $CO_2$ with neat MEA leads to a very viscous liquid, not viable from an industrial standpoint. Additionally, MEA is used in dilute conditions to minimize corrosion and degradation. Furthermore, MEA degradation pathways has been studied and are found to be rather complex and involve both amine and alcohol groups. Thermal side reactions of MEA in the presence of water and $CO_2$ primarily lead to ring closed structures by reaction of the alcohol on MEA with the formed carbamate which produces hydroxide and results in an oxazolidin-2-one ring. The oxazolidin-2-one ring can then be further reacted with another mol of MEA to form ring-opened 2-(aminoethyl)ethanolamine which can undergo reaction with $CO_2$ and ring closure again to form cyclic ureas.[8] This is displayed in Figure 4.3 below.

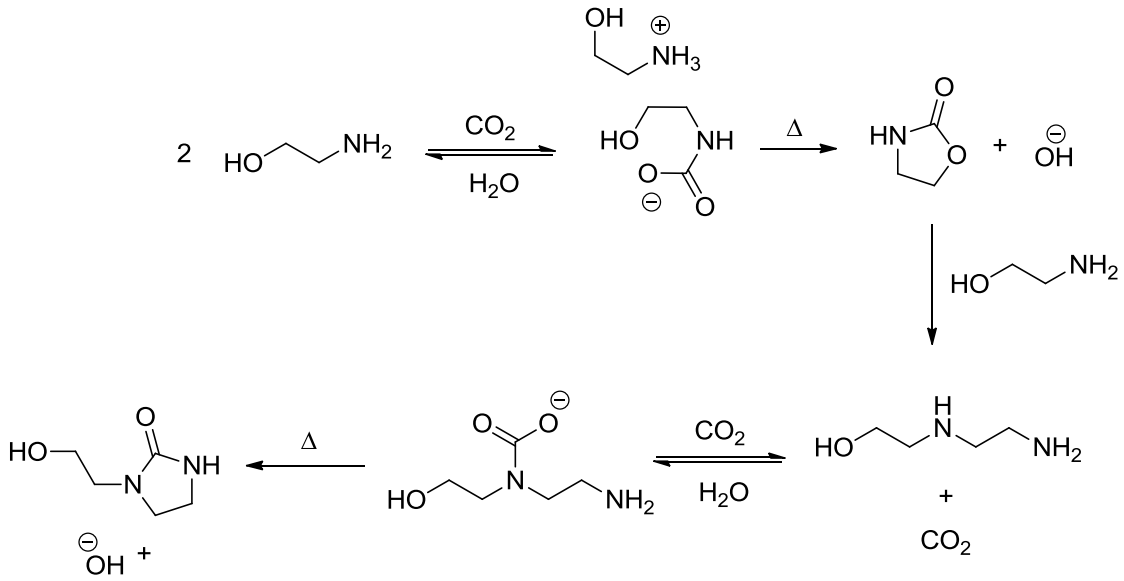

**Figure 4.3.** Thermal degradation in aqueous MEA systems

Oxidative pathways have also been studied and it has been found that radical formation leads to breakdown of MEA to small, volatile molecules such as ammonia and formaldehyde.[9] Oxidative degradation can be promoted by high levels of oxygen and is usually catalyzed by traces of iron. Degradation pathways from oxidation are shown in Figure 4.4 by radical formation and shifts from the amine to the α-carbon of the alcohol.

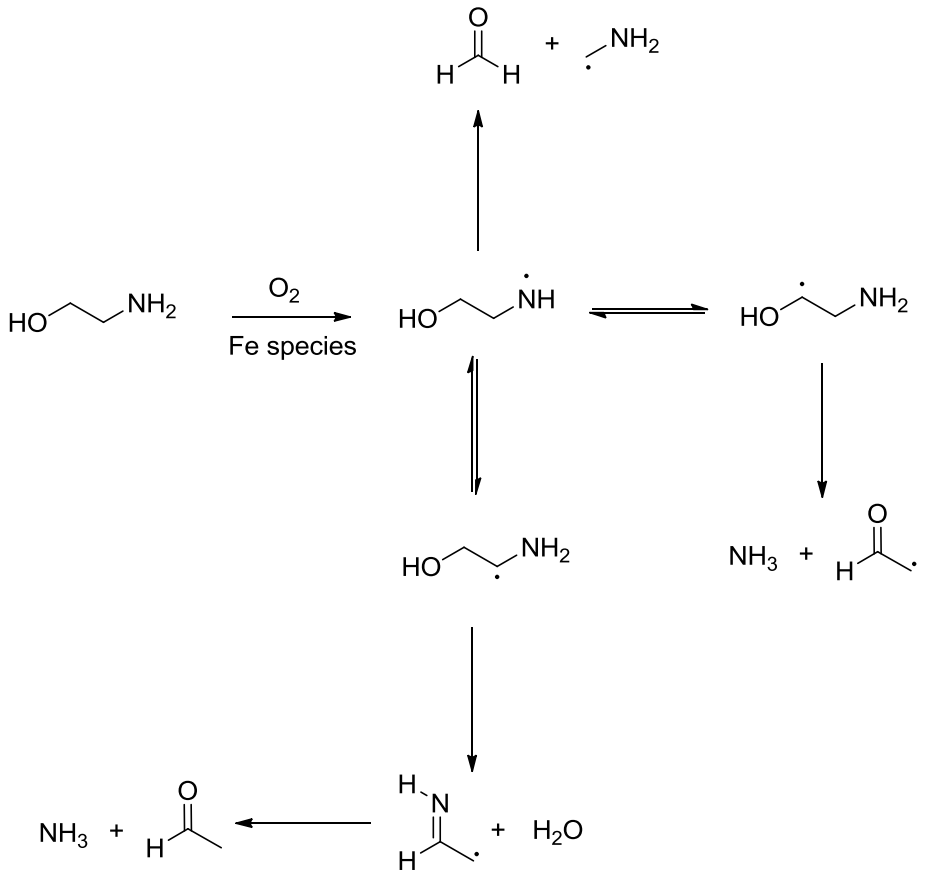


**Figure 4.4.** Oxidative degradation pathways in aqueous MEA systems

The inherent side reactions of MEA under operative conditions is addressed by implementing a make-up stream. This is a cost consideration as the make-up stream of MEA, as reported by Rao and Rubin, can be as high as 3.1 kg MEA/ton of $CO_2$ captured.[10] Regardless, MEA is still considered the benchmark $CO_2$ capture solvent. The intrinsic drawback of MEA strategy for $CO_2$ capture agent is the large energy requirements to operate the process.

Within this, the major cost of the entire $CO_2$ capture process comes from the reversal step.[11] This is both due to the heat required for reaction reversal as well as the

large excess of water, needed for corrosion and viscosity control, that also must be heated to a reversal temperature of 120°C. The ΔH of reversal at this temperature has been reported to be on the order of 96 kJ/mol $CO_2$ for loadings of 0.5 mol $CO_2$/mol MEA.[12] To address the large energy penalty associated with the use of aqueous MEA solutions, focus in industry and academia has been on developing alternative $CO_2$ capture solutions including: improved liquid sorbents including aqueous amines, solid sorbents, polymer membranes, and physical sorbent technologies which encompass ionic liquids. As a ConocoPhillips Fellow, my research has also been focused on the economical and realistic approaches to the capture of $CO_2$. I'll preface my work by introducing ionic liquids.

### 4.1.2 Ionic liquids (ILs) for $CO_2$ capture

Ionic liquids are molten salts with a melting point below 100°C. Ionic liquids have unique properties including negligible vapor pressures and tunable polarities.[13] Often, ILs are used as reaction solvents to coupling reactions and separations.[14] Generally, ILs consist of a cation and an anion species. By changing either of these, the properties of the IL can be altered. Examples of cations commonly used are imidazolium, phosphonium, tetraalkyl-ammonium, pyridinium, and guanidinium functionalities (Figure 4.5). Common anions include halides, sulfonamides, and phosphohalides (Figure 4.6).

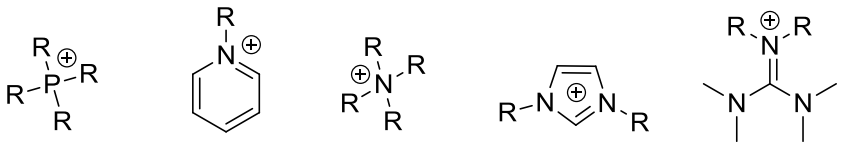

**Figure 4.5.** Common Ionic Liquid Cations

**Figure 4.6.** Common Ionic Liquid Anions

Such ionic liquids do not directly react with $CO_2$. However, they have been shown to have high solubility for some gases, particularly $CO_2$.[15] $CO_2$ has a preferential solubility in ionic liquids due to its large quadrupole moment, meaning it can be polarized in the direction of both oxygen atoms. The polarizability with interaction of predominately the anion of the IL, results in rather strong ion-dipole intermolecular interactions.[16] The characteristic with physical absorption is that the energy required to release the $CO_2$ is much lower than breaking a covalent bond, as in chemical capture. Additionally, as $CO_2$ pressure applied to ILs increases, $CO_2$ physisorption also increased. For $CO_2$ capture at flue gas conditions however, physical absorption may be low due to the low partial pressure of $CO_2$. Because of this, Dr. Brennecke's group at Notre Dame and Dr. Noble's group at UC-Boulder have been instrumental in designing task-specific ILs (Figure 4.7) which display both chemical and physical capture.[17]

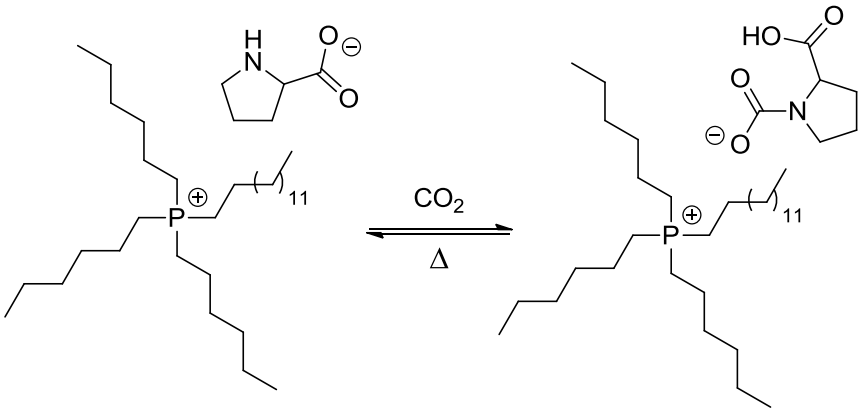

**Figure 4.7.** Proline Anion Functionalized Task-Specific Ionic Liquids

Specifically, recent efforts have been focused on incorporating tethered amines to either the cation or anion in the IL to enable chemical and physical capture, increasing overall capacity. Although capacities up to 1 mol $CO_2$/mol IL are approached with amine functionalized proline anions, the entire system remains in an IL form.[18,19] This is a downside, although later designed improvement enable to reduce the viscosity to 1000 cP upon complete reaction with $CO_2$. The major drawback remains the $CO_2$ capacity of these systems, which would require large amount of solvent to enable the level of capture expected for large scale. In the example in Figure 4.7, the alkyl chains on the cation alone are made of 32 carbon atoms and 68 hydrogen atoms—for a total IL molecular weight of 597.98 g/mol. Although favorable 1:1 ratios of mol $CO_2$/mol amine are achievable, actual capacities in terms of mol $CO_2$/kg amine solvent only reach 1.5.

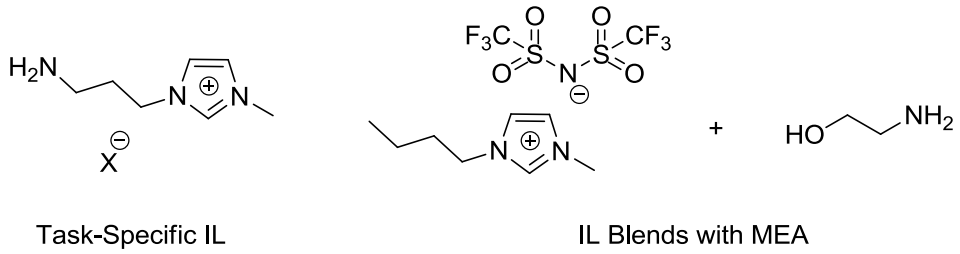


**Figure 4.8.** Amine functionalized cations and ionic liquid blends with MEA

Other task specific ionic liquids (TSILs) investigated are amine branched imidazolium cations coupled with an anion (Figure 4.8).[20] These amine functionalized imidazolium species suffer from very high viscosities.[21] Upon reaction with $CO_2$, they do have a dual-capture mechanism with both chemical and physical absorption, however physical absorption was almost negligible. Upon reaction, the viscosities spike

tremendously making industrial viability of these TSILs unfavorable, not to mention the multistep synthesis required to prepare them can be tedious. One approach that has been taken is to blend ILs with amines, like MEA.[20,22] It was found that ILs can solubilize MEA and do capture high loadings of $CO_2$ through dual capture. Unfortunately, at higher loadings especially, MEA salts can precipitate from the solution, yielding solid-liquid mixture which adds complexity to the handling and processing aspects—and ultimately to the cost and efficiency of the overall process.

In all cases mentioned regarding ILs, viscosity is a concern and limitation to their implementation, primarily because the starting material and products are both ionic. Our approach has been to design reversible ionic liquids, which are formed upon reaction of $CO_2$ with a molecular, neutral silylamine. Therefore, our strategy is to start with a non-ionic species (low viscosity) and then form a reversible ionic species (modular viscosity). One of the attractive aspects of our approach is that the (modular) viscosity of the ionic liquid form can be controlled by controlling the extent of reaction (an already well-established process-control parameter in many industries). The Eckert-Liotta and Jessop groups have pioneered “smart solvents” such as reversible ionic liquid systems.[23]

### 4.1.3 Reversible systems for $CO_2$ capture

#### 4.1.3.1 Two-component systems

A reversible ionic liquid (RevIL) is one where either one (silylamine) or two components, for example a guanidine and alkyl alcohol, react with $CO_2$ to form an ionic liquid which upon heating reverses back to the respective molecular liquid (Figure 4.9).[24]

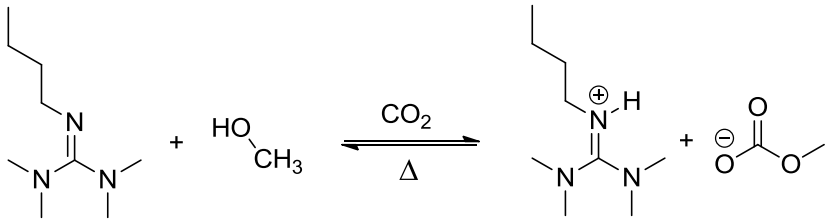


**Figure 4.9.** Guanidium and alcohol molecular liquids that form an ionic liquid upon $CO_2$ exposure

In the two-component systems, the molecular liquid properties can be modified by changing the alcohol and/or the guanidine counterpart. Shown in the figure is tetramethylbutylguanidine or TMBG but we have shown that amidines such as DBU can also be used.[25] It is recognized that a trade off exists between high capacity and low molecular weight alcohols. Specifically, methanol provides the highest $CO_2$ capacity in terms of $CO_2$/ kg ML components; however, it is low boiling (65°C) and water soluble. This means that methanol losses will occur during the $CO_2$ recovery and solvent regeneration step as well as from difficult recovery from water. It was also found that reversal temperatures were high for these systems, on the order of 80°C and above. Although the two-component systems are not optimum from a $CO_2$ capture perspective, we have developed silylamine, one component systems that show far-reaching capabilities to large scale $CO_2$ capture technologies.

4.1.3.2 One-component systems

One-component RevILs were originally based on commercially available 3-(aminopropyl)trialkoxysilanes.[26] Silylamines were chosen because it has been reported that incorporating silicon functionalities in conventional ionic liquids led to decreased viscosities. This was reported to be an effect of bond lengthening in silylated derivatives as well as electronic effects. The alkoxysilylamines were reacted with $CO_2$ to form

ammonium/carbamate ionic pairs that remain in a liquid state! They were also found to be thermally reversible (Figure 4.10). The real advantage is that with one-component systems such as these, volatility of the starting material or products is not a concern and in a preliminary approach the properties could be tuned by simply changing the alkoxy chain length.

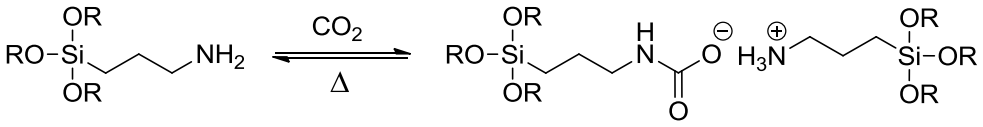


**Figure 4.10.** Alkoxysilylamines as one-component reversible ionic liquids

These systems seemed very promising as $CO_2$ capture alternatives to aqueous amines. Althought efficient for proof of concept, alkoxy silanes are water-sensitive. As we moved forward, we progressed toward trialkylsilylamines, shown in Figure 4.11. The carbon-silicon bond is stable to hydrolytic cleavage. Furthermore, trialkylsilylamines should exhibit a dual-capture, having both chemical reaction and physical absorption to capture $CO_2$. Although water tolerant, use of these trialkylsilylamines in anhydrous conditions was paramount in reducing the energy required for the $CO_2$ capture process.

### 4.1.4 Motivation and principles behind trialkylsilylamines for $CO_2$ capture

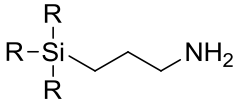


**Figure 4.11.** Trialkylsilylamine

The motivation behind this work was first to understand how structural modifications around the silicon atom affected the bulk properties of the RevILs formed under neat conditions and second to apply this knowledge to the design and development of optimum systems for commercial implementation. The properties of interest are (1) $CO_2$ capacity, (2) viscosity of the molecular liquid and resulting RevIL after reaction with $CO_2$, and (3) the reversal temperature and enthalpy of the reaction with $CO_2$. $CO_2$ capacities are often reported in two different manners in literature, in terms of mol $CO_2$/mol amine and mol $CO_2$/mol kg amine. The first is a measure of general capture effectiveness and the second is commonly use by industries as it may better translate to economic viability. Even if capacity is very high in molar ratio, the molecular weight may be so large that the capacity in terms of amount of reagent needed is extremely low. Both measures of capacity will be used and explicitly identified. The viscosity goals outlined by ConocoPhillips are that the molecular and reversible ionic liquids through the entire capture and reversal process remain below 200 cP.

The last area of study was the thermodynamic properties of the trialkylsilylamine $CO_2$ capture systems. The thermodynamic properties investigated were the reversal temperature which corresponds to the temperature required to reverse the ionic liquid back to the molecular liquid for recycle as well as the enthalpy of reversal. The enthalpy of reversal refers to the amount of heat required for reversal to take place. Both the reversal temperature and enthalpy of reaction have a large effect on the economics of the process. To develop this structure-property relationship, trialkylsilylamines were synthesized via a one-step hydrosilylation reaction, isolated and characterized prior to being reacted with $CO_2$. The formed ionic species were then characterized, and capacity, viscosity, and thermodynamic properties were measured. I will first discuss the synthesis of the molecular liquids prior to reaction with $CO_2$.

4.1.4.1 Dual capture mechanism

All of the RevIL systems introduced to this point were capable of the dual-capture mode (chemical and physical absorption). Chemical capture happens through reaction of the amine with $CO_2$ to form an ionic liquid. Because $CO_2$ solubilities in ILs are appreciable, it is expected that the formed ionic liquids physically absorb $CO_2$, resulting in a dual-capture mechanism for high capacities.

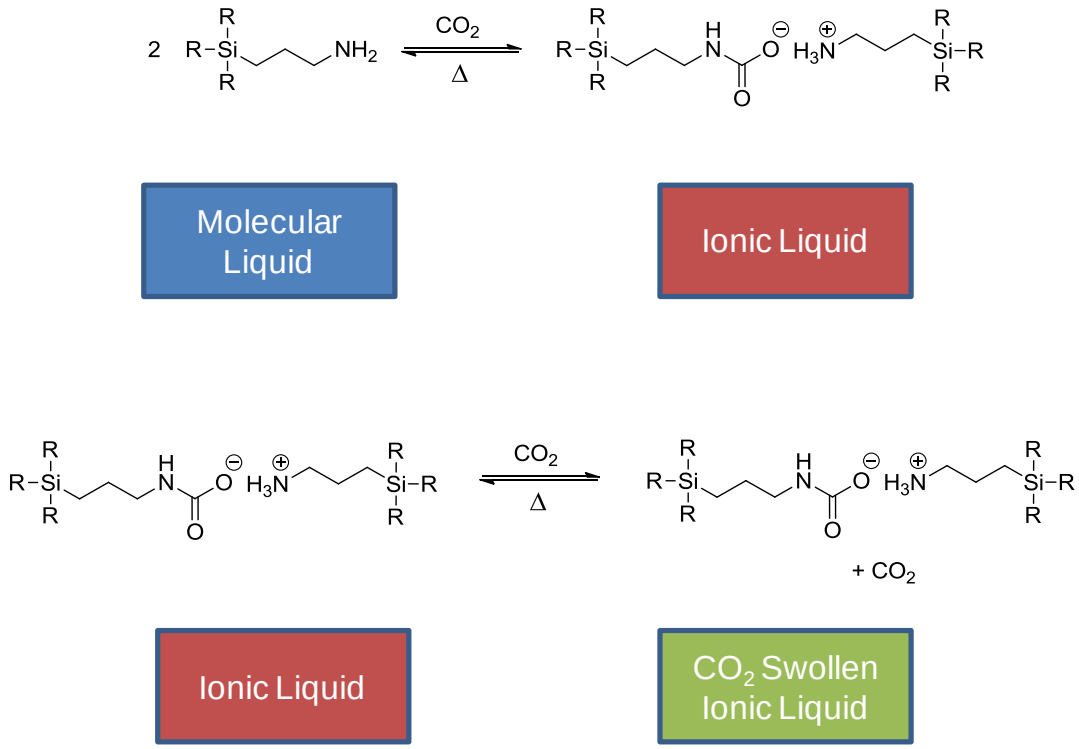


**Figure 4.12.** Dual capture mechanism of the reaction of trialkylsilylpropylamines with $CO_2$

It was expected that through reaction of silylated amines with $CO_2$, chemical reaction to form a RevIL will occur followed by physical absorption of $CO_2$, both being reversible processes. This dual capture mechanism (Figure 4.12) is a key feature of these systems. To explore this, trialkylsilylamines were synthesized.

## 4.2 Synthesis of trialkylsilylamines

### 4.2.1 Hydrosilylation reaction

Trialkylsilylamines are not commercially available. Therefore, a synthetic pathway was developed to efficiently design a range of molecular liquids. Although currently the synthesis of these derivatives was done on scales below 50 g for testing purposes on a lab scale, it was necessary to develop a pathway that could be commercially viable in the case that these amines were to be evaluated at the pilot plant level. A hydrosilylation reaction was developed by analogy with literature precedent.[27] Hydrosilylation is the addition of a silicon-hydrogen bond across an alkene. Commonly, hydrosilylations are conducted by reacting trialkylsilanes with allylamine in the presence of a platinum catalyst, either Speier's or Karstedt's catalysts (Figure 4.13). Speier's catalyst is the common name for chloroplatinic acid or $H_2PtCl_6$ and Karstedt's catalyst, or Pt-DVDS as it is referred to throughout this thesis work, is platinum-divinyltetramethyldisiloxane.

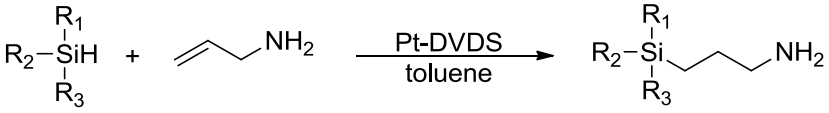


**Figure 4.13.** General hydrosilylation reaction scheme

The hydrosilylation procedure was chosen because of its versatility allowing for a structural library to be achieved via a one step procedure. Hydrosilylation of allylamine with trialkylsilanes produces specifically linear trialkylsilylpropylamines when using Pt-DVDS catalyst.

The hydrosilylation reaction mechanism is shown in Figure 4.14.[28] Trialkylsilanes are oxidatively added to the platinum(0) metal. Through coordination of the alkene, a migratory insertion of the hydride takes place. The migratory insertion step can add the hydride to either the primary or secondary carbon, and due to sterics, the addition to the secondary carbon is prevalent leading to linear structures. Reductive elimination of the platinum (II) propylamine-silane complex leads to the regeneration of the active platinum center as well as the desired trialkylsilylamine product.

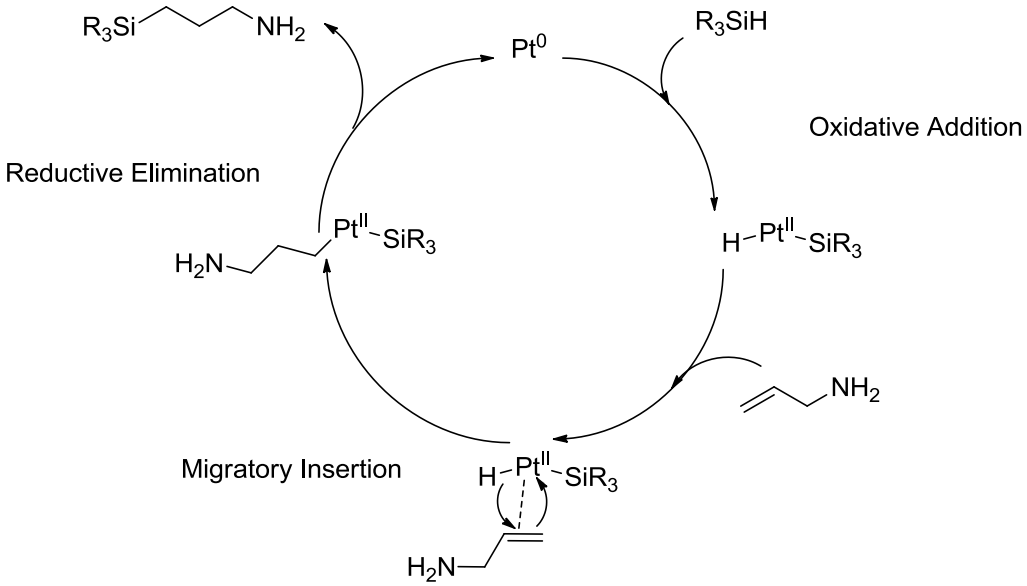


**Figure 4.14.** Hydrosilylation catalytic cycle

Synthesis of a library of trialkylsilylamines was accomplished through the hydrosilylation reaction with Pt-DVDS and allylamine. These structures are displayed in Table 4.1 with their corresponding acronyms that will be used throughout the chapter.

**Table 4.1.** Synthesized trialkylsilylpropylamines for $CO_2$ capture evaluation

| Structure | Name/ **Abbreviation** | Structure | Name /**Abbreviation** |
|---|---|---|---|
| 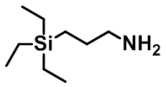 | 3-(aminopropyl)triethylsilane<br>**TEtSA** | 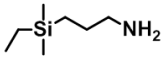 | 3-(aminopropyl) dimethylethylsilane<br>**DMESA** |
| 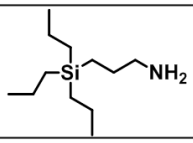 | 3-(aminopropyl)tripropylsilane<br>**TPSA** | 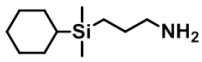 | 3-(aminopropyl)cyclohexyl-dimethylsilane<br>**CDMSA** |
| 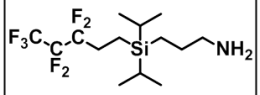 | 3-(aminopropyl)-(1H,1H,2H,2H-perfluoropentyl) diisopropylsilane<br>**FSA** | 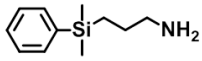 | 3-(aminopropyl) phenyldimethylsilane<br>**PDMSA** |
| 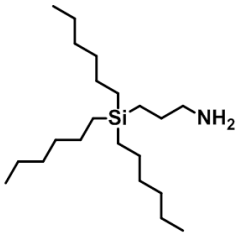 | 3-(aminopropyl)trihexylsilane<br>**THSA** | 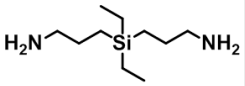 | *bis*-3-(aminopropyl)diethylsilane<br>**DESDA** |
| | | 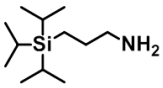 | 3-(aminopropyl) triisopropylsilane<br>**TIPSA** |

The structural modifications included: 1) increasing the alkyl chain length around the silicon atom, 2) introducing a $CO_2$-philic fluorinated alkyl chain on the silicon atom, and 3) altering the symmetry of the molecule by varying the substituents on the silicon. It was recognized that structures like THSA and FSA may not be commercially feasible; yet, they were key in understanding the structure/property relationship of the RevIL systems.

The structures that were chosen and synthesized represent a broad scope of modifications. All modifications to structure occurred at the silicon center. I sought to understand the role of alkyl chain length of RevIL properties by investigating length from ethyl to hexyl chains as well as bulky chain density with isopropyl groups through the molecules TEtSA, TPSA, THSA, and TIPSA. It was hypothesized that alkyl chain length may play an important role in decreasing viscosity of the formed ionic species by disrupting ion packing.

A series of dimethylalkyl derivatives were synthesized including dimethylethyl, dimethylcyclohexyl, and dimethylphenyl structures. These are abbreviated as DMESA, CDMSA, and PDMSA, respectively. The idea was that introducing asymmetry by having one of the substituent be different from the other two methyl groups would affect the capture properties. Small alkyl chains around the silicon were expected to increase capacities in terms of molecular weight. The introduction of ring structures including aromatic and aliphatic rings was investigated to provide insight into limiting degrees of freedom (in both rings) and incorporating aromatic functionality. Two unique derivatives were also designed, one with a perfluorinated pentyl tail (FSA) to effect the electronics of the silicon atom as well as increase physical $CO_2$ capture, and one with two amine linkages (DESDA). It has been shown that fluoroalkanes have large $CO_2$ solubilities which can lead to increased physical absorptions.[29] Likewise, with multiple reactive sites, the amount of $CO_2$ captured per molecule should be increased.

All of the amines introduced were synthesized by a common method, hydrosilylation of allylamine with trialkylsilanes. The general procedure for the synthesis of these compounds is shown below.

4.2.1.1 General Reaction Procedure

(0.2% eq) Pt-DVDS (2% in xylenes) was added to a trialkylsilane (0.08 mol, 1 eq) under nitrogen in a 3 neck flask and condenser. Anhydrous toluene was added to make a 2M solution of silane and the solution was stirred. In all cases the solution turned a dark yellow color. Allyl amine (0.16 mol, 2 eq) was then added slowly and the solution became a deep red. The solution was brought to reflux and allowed to react. Upon reaction completion (monitored by NMR) the solution was cooled and the solvent removed by vacuum evaporation. The remaining liquid was distilled under vacuum to provide pure colorless liquid products. *Reactions were not optimized and yields are isolated upon distillation. The purified trialkylsilylamines were then characterized by $^{1}$HNMR, $^{13}$CNMR, FTIR, and EA. It is important to store synthesized amines in the glove box after distillation to ensure limited absorption of moisture from the atmosphere. Reaction and purification conditions are displayed in Table 4.2.

**Table 4.2.** Synthesis and purification of molecular liquids

| Molecular Liquid | Reaction Temperature ($^oC$) | Isolated Yield (%) | Distillation Temperature ($^oC$)/mmHg |
|---|---|---|---|
| **TEtSA** | 110 | 89 | 75/4 |
| **TPSA** | 110 | 96 | 84/0.3 |
| **THSA** | 110 | 92 | 155/3 |
| **FSA** | 110 | 94 | 100/1 |
| **CDMSA** | 110 | 60 | 80/1 |
| **PDMSA** | 110 | 74 | 62/0.15 |
| **DMESA** | 110 | 58 | 38/2.5 |
| **DESDA** | 50 | 41 | 67/2.7 |
| **TIPSA** | 110 | -- | -- |

In the synthesis of TIPSA, the reaction of triisopropylsilane with allylamine in the presence of Pt-DVDS led to no reaction, even after 56 hours at 110°C. This non-reactivity was attributed to the bulky isopropyl groups on the silicon blocking the silicon-hydride bond, preventing the oxidative addition. With this exception, all molecular liquids were successfully synthesized and particular interest was placed in synthesizing TPSA on a larger scale.

4.2.1.2 Scaled up synthesis for the formation of TPSA

TPSA was seen as a promising candidate for $CO_2$ capture. ConocoPhillips expressed interest to perform $CO_2$ capture testing and corrosion testing at their site in Bartlesville, OK. Specifically, the studies performed at ConocoPhillips used mimic flue

gas streams with a wetted-wall column. For this purpose, I synthesized 2 liters of TPSA for their studies. The platinum catalyzed synthesis of TPSA was accordingly scaled up to 1 liter production (Figure 4.15).

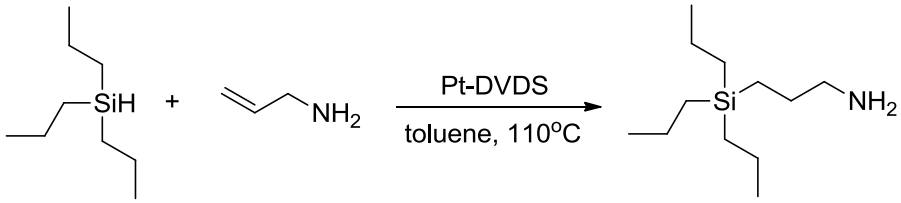


**Figure 4.15.** Scaled-up Synthesis of TPSA

In order to scale up to 1 liter, two separate batches were synthesized and combined. The larger batch is represented.

To a 3-neck 5L RB flask under argon was cannulated 1.25 L of anhydrous toluene. To the toluene was added 450 g of tripropylsilane. 32.5 mL of Pt-DVDS, (which represents 0.1 mol%) was added and the solution became a deep yellow color. 426 mL of allylamine, or 2 equivalents compared to the silane were cannulated via pressure. As the allylamine was added, the solution became a deep reddish brown color and the reaction was found to be exothermic, reaching 80°C upon addition with no heat. The solution was heated to 110°C for 4 hours. $^{1}$HNMR confirmed reaction completion. The toluene and excess allylamine were rotovapped and the remaining crude solution distilled at 83°C with a vacuum of 0.25 mmHg to provide 557.8 g of pure TPSA in a 91% yield.

It was realized that the hydrosilylation reaction of tripropylsilane with allylamine, although great on a lab scale, may be too expensive on an industrial scale due to the amount of platinum required. Studies on the amount of platinum catalyst or recycle of the

catalyst have not been performed at this time, but will be considered in future work. As an alternative, a copper catalyzed hydrosilylation has been proposed.

### 4.2.2 Copper catalyzed alternative formation of trialkylsilylamines

Efforts into developing an industrially feasible strategy without the need for the relatively expensive platinum-containing catalyst led to the investigations of a neat, copper catalyzed hydrosilylation followed by an amination step. A patent by DOW reports a copper catalyzed hydrosilylation of allyl chlorides with trialkylsilanes.[30] Shown in Scheme 4.1, trialkylsilanes were reported to react with allyl chloride in the presence of copper acetate under neat conditions. This coupling has been reported to proceed at temperatures upwards of 200°C and due to the volatility of allyl chloride, very high pressures. After cooling the reaction, the possibility of catalyst filtration and recycle was envisioned. The second step proposed was an amination reaction to form the hydrochloride salt of the trialkylsilylamine through reaction of the trialkylsilylpropylchloride with excess ammonia. The excess ammonia would simply be evaporated (and recycled). The amine could be obtained upon an aqueous NaOH treatment of the ammonium hydrochloride product.

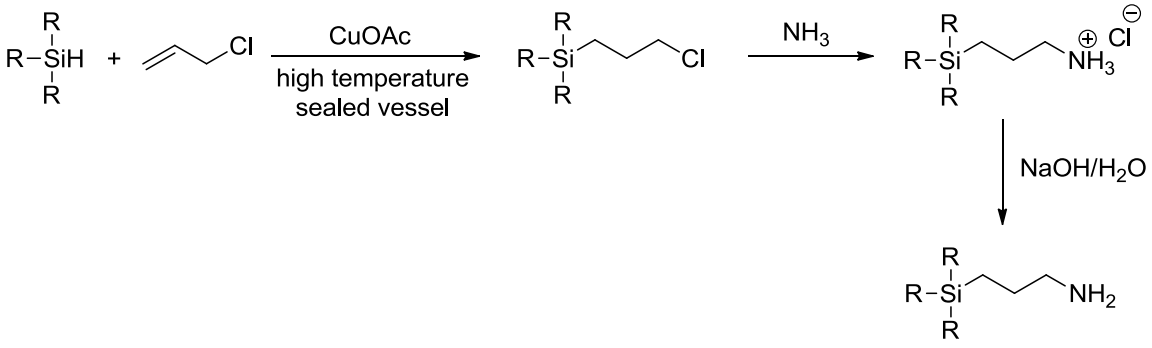


**Scheme 4.1.** Copper catalyzed hydrosilylation and amination for the formation of trialkylsilylpropylamines

An initial experiment was investigated by reacting tripropylsilane with allyl chloride in the presence of $Cu(OAc)_2$. The reaction was conducted in an Ace glass 48 mL pressure tube specifically equipped with one outlet with a pressure gauge and pressure release valve (Figure 4.16).

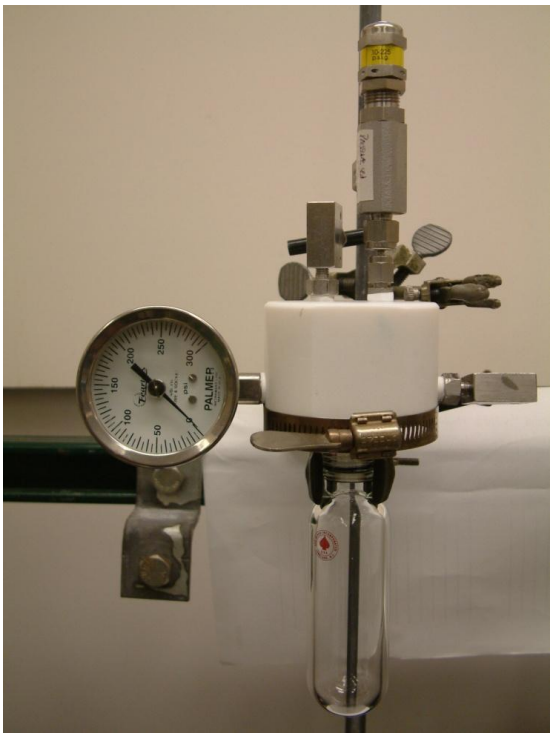


**Figure 4.16.** Customized pressure tube for copper catalyzed hydrosilylations

The first reaction was conducted for 48 hours at 100$^{o}$C. During the course of the reaction, the catalyst changed from blue to colorless and then precipitated as a white solid. After the reaction was cooled and filtered, the crude was analyzed with $^{1}$HNMR by dissolving 0.1 mL in 0.5 mL of $CDCl_3$. The $^{1}$HNMR did not show signals consistent with the desired product. However, allyl chloride seemed to have been fully consumed.

As a consequence, we decided to carry the reaction out in titanium reactors sealed with a titanium cap and heated in an aluminum block (Figure 4.17), to accommodate for higher pressures.

**Figure 4.17.** Titanium reactor with the aluminum block for high-pressure reactions

The reactors were loaded with tripropylsilane, allyl chloride and either CuOAc or $Cu(OAc)_2$. Reactions were run for 48hrs at 200$^{o}$C and after stopping the reactions by removing them from the aluminum block and cooling in ice water, the reactors were uncapped and the crude mixture analyzed. The mixtures, although starting out colorless, were dark brown. Regardless of the catalyst (Cu(I) or Cu(II)), the $^{1}$HNMR showed no indication of the formation of the desired product, the trialkylsilylpropylchloride. Nonetheless, the appearances of a doublet just above 1 ppm in the $^{1}$HNMR and of a single peak around 20 ppm in the $^{13}$CNMR were indicative of a reaction taking place.

GC-MS indicated the presence of two distinct products. The lower boiling product was identified as tripropylchlorosilane. The other product remains unidentified but has no chlorine atom present. In order to better understand this side reaction, a reaction was also run as a control with no copper catalyst. The analysis of this experiment showed that with no catalyst present, the tripropylchlorosilane was still formed as the predominant product. It is believed that the allylamine is essentially in the vapor phase at these reaction temperatures, with the silane in both the liquid and vapor phase and the catalyst, a solid phase. This is clearly hindering reaction from taking place, and enabling all reagents to be in the liquid phase may contribute to the efficient proceeding of the reaction.

### 4.2.3 Formation of RevILs through reaction with $CO_2$

In all cases, molecular liquids were synthesized through the hydrosilylation reaction with platinum catalysis and were purified and characterized. The molecular liquids were then reacted with $CO_2$. The resulting RevILs were studied for their properties including $CO_2$ capacity, viscosity, and thermodynamic properties. In order to gain an understanding of the structural modifications of the molecular liquids on the formation and properties of the RevILs, $CO_2$ capture studies were done with pure molecular liquids under neat conditions with a pure $CO_2$ stream.

#### 4.2.3.1 Experimental reaction of molecular liquids with $CO_2$

To investigate the capacity, viscosity, and thermodynamic properties of these RevILs, trialkylsilylamine molecular liquids were reacted with anhydrous $CO_2$. Experimentally, a known amount of molecular liquid was placed into a 4 dram vial with a rubber septum under argon atmosphere. $CO_2$ was flowed through a diffuser tube into the

molecular liquid with a 200 mL/min flow rate for 75 minutes unless otherwise noted. The diffuser tube was used to stir the sample while bubbling.

*4.2.3.1.1 Equilibrium experiments of formed RevILs*

The reactions of amines with $CO_2$ are equilibrium reactions. For consistency, the reaction equilibrium had to be achieved prior to analysis and characterization.

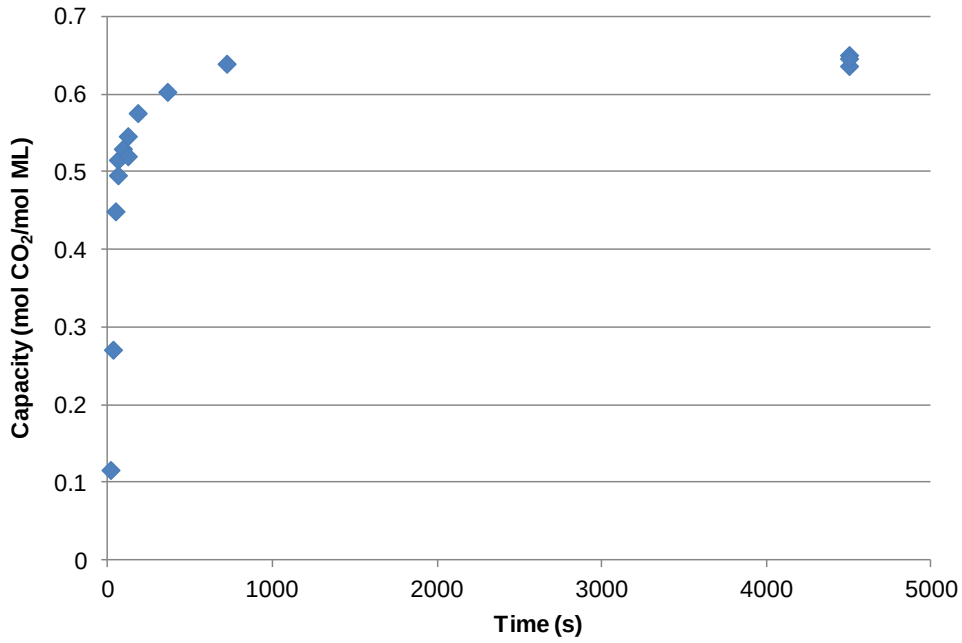


**Figure 4.18.** Equilibrium experiment in the reaction of TPSA with $CO_2$

We established that 75 minutes was the optimum reaction time to ensure that the reaction with $CO_2$ had reached equilibrium under our operating conditions. A representative profile of $CO_2$ uptake as function of time is shown in Figure 4.18 for the TPSA system. The reaction is shown to reach equilibrium at about 13 minutes of

reaction or about 800 seconds. 75 minute reaction times were used to ensure that equilibrium conversion had been reached for all systems. The reaction of these primary amines were extremely fast reactions and were only limited by mass transfer in their complete conversion.

## 4.3 Results and Discussion

Herein, I will described in detail each reversible system (ML and RevIL forms) and their specific profile in terms of $CO_2$ uptake capacity, physical properties (i.e. viscosity and melting points) and thermodynamic properties (i.e. reversal temperature and reaction enthalpy). First I will report the system that yielded salts with melting points higher than room-temperature. In all cases, melting occurred concurrently to the $CO_2$ release, limiting their applications as liquid sorbents. They could be of interest however for blend formulations. I did not investigate these systems further for my work. I will then discuss the systems that enabled the formation of salts with melting points below room temperature, i.e. reversible ionic liquids (RevILs). The effect of structure on the bulk physical properties and on the $CO_2$ capture properties will be discussed.

### 4.3.1 Reactions of molecular liquids with $CO_2$ producing salts with melting points above room temperature

Upon reaction with $CO_2$, four of the synthesized molecular liquids, namely CDMSA, PDMSA, DMESA, and DESDA, formed ionic species with melting points above room temperature (Table 4.3). Although as solid salts these systems would not be applicable to flue gas treatment, if the melting point was below 40$^{o}$C (flue gas and capture temperature), they could possibly be applied if the window between melting and reversal was substantial. Investigations into that possibility were evaluated.

**Table 4.3.** Trialkylsilylpropylamine derivatives that form solid salts upon reaction with $CO_2$

| Structures that Form Solid Salts Upon Reaction with $CO_2$ | | | |
|---|---|---|---|
| CDMSA | PDMSA | DMESA | DESDA |
| 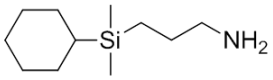 | 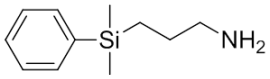 | 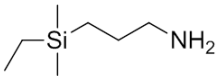 | 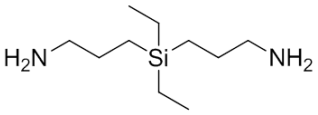 |

$CO_2$ capture capacities were not measured with these systems because it would provide information that will be difficult to accurately compare and interpret. Indeed, conversion can change significantly from system to system due to mass transfer limitations as the solid forms. This has been documented in literature for systems undergoing analogous phase changes.[31] Differential Scanning Calorimetry and a traditional melting point apparatus were both used to measure the melting temperature. Melting and reversal temperatures were measured at the intersection of the tangent to the initial endotherm curve and the baseline.

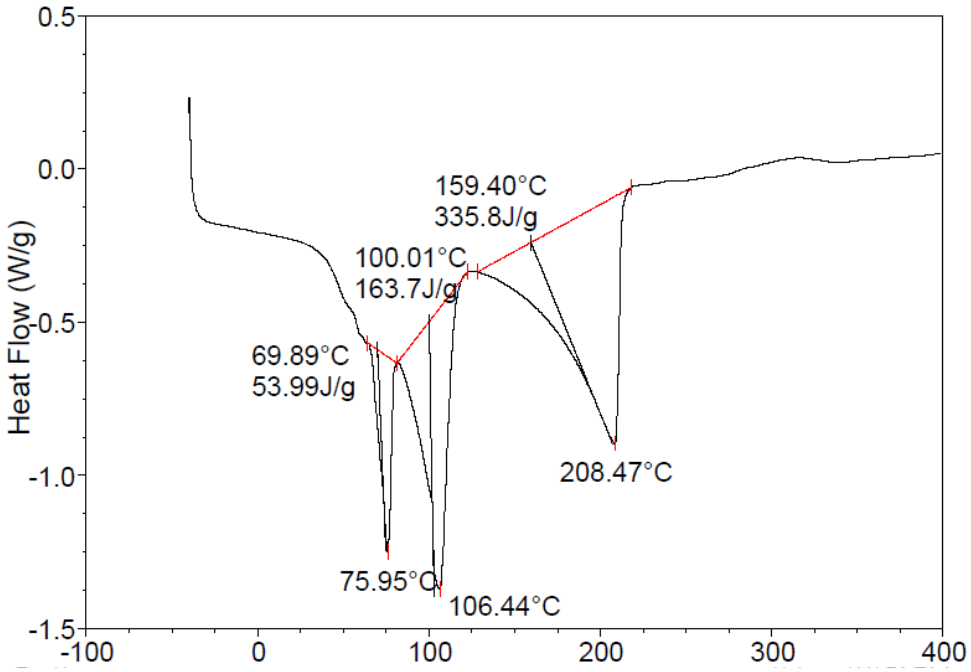


**Figure 4.19.** DSC thermogram of CDMSA-IL

The DSC thermogram of CDMSA-RevIL (Figure 4.19) shows three endothermic events: melting, $CO_2$ reversal, and molecular liquid evaporation. In this specific case, there were two distinct events for melting and reversal but some ionic solids from reaction of amines with $CO_2$ showed indistinguishable separation between melting and reversal. The two events actually overlapped making melting and reversal unable to be decoupled. With direct melting point analysis, bubbling indicative of reversal was noticed while the solid ammonium/carbamate salt melted. In fact, in all cases, $CO_2$ reversal occurs upon melting. The melting points are shown in Table 4.4.

**Table 4.4.** Melting points based on DSC for solid forming ILs

| Structure | Melting Point ($^{o}$C) |
|---|---|
| DMESA-IL | 63 |
| CDMSA-IL | 70 |
| PDMSA-IL | 35 |
| DESDA-IL | 98* |

*There was only one peak with a small shoulder whereas the others had two distinct melting and reversal peaks that overlapped

It is interesting to note that all of the silylamines with dimethyl substitutents on the silicon atom resulted in solid formation. The PDMSA had the lowest melting point at 35$^{o}$C. This supports the idea that less degrees of freedom, from the aromatic ring remaining in a planar confirmation around the silicon atom, resulted in a viscosity increase. The diamine, DESDA, was a solid upon reaction with $CO_2$. The role of symmetry is most likely the major contributing factor to its solid form upon reaction with $CO_2$. Intermolecular hydrogen bonding may also contribute since this structure can form a linear “ionic” polymer in principle.

### 4.3.2 Conversion of reversible ionic liquids systems

The four molecular liquids: TEtSA, TPSA, THSA, and FSA did form liquids upon reaction with $CO_2$. Analyses of their properties including equilibrium capture capacities, viscosities, and thermodynamic properties were completed. It is important that molecular liquid reactions with $CO_2$ were carried to their equilibrium conditions in order to have consistent measures of properties. $^{13}$CNMR, Refractive index, and gravimetry were used to characterize the RevIL formation.

4.3.2.1 $^{13}$CNMR as a tool for the verification of conversion

It can be seen in the $^{13}$CNMR spectrum of TPSA that conversion—through chemical reaction—from molecular liquid to ionic liquid is apparent.

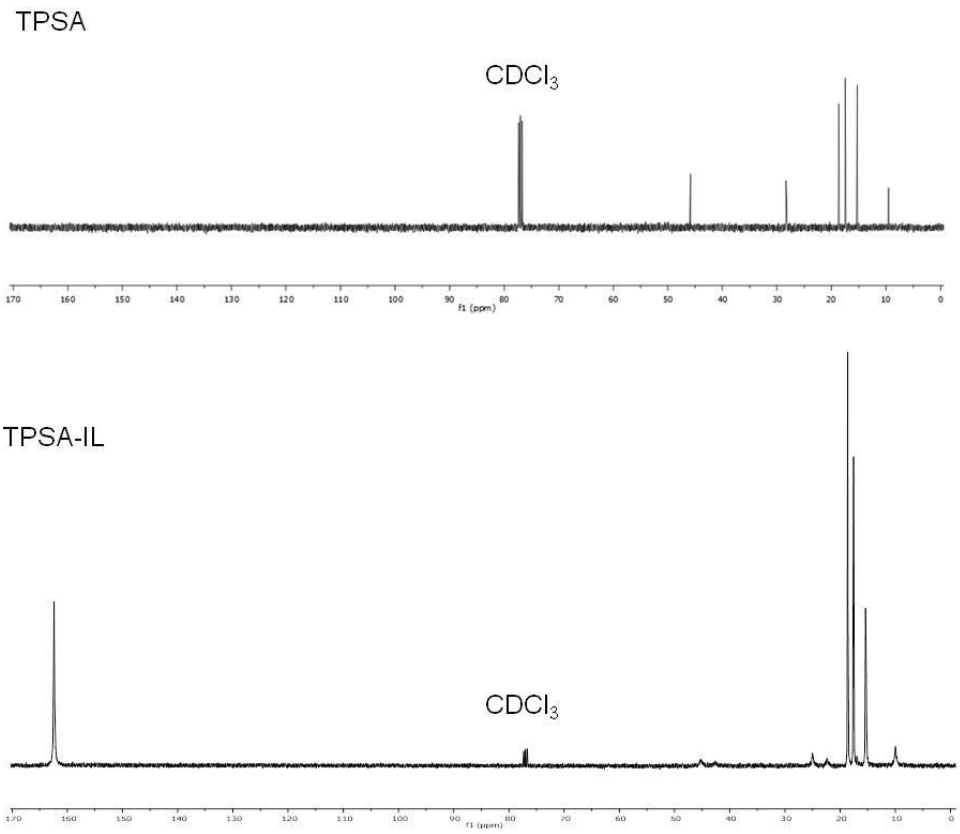


**Figure 4.20.** Comparison of $^{13}$CNMR spectra of TPSA-ML and TPSA-IL

Shown above in Figure 4.20, are the spectra of the TPSA molecular liquid (top) and TPSA-RevIL (bottom). The molecular liquid has six characteristic carbons and the ionic liquid has 9 distinct carbon signals. This reasoning is two-fold: (1) the formation of the carbamate, evidenced by the sharp peak at ~162 ppm in the bottom spectrum and (2)

the splitting of the carbons α (~48 ppm) and β (~28 ppm) to the amine. Furthermore, the spectrum indicated that the molecular liquid had been fully converted to the ionic liquid because no peaks corresponding to the molecular liquid were seen in the ionic liquid spectrum.

4.3.2.2 Refractive Index as a tool for the verification of conversion

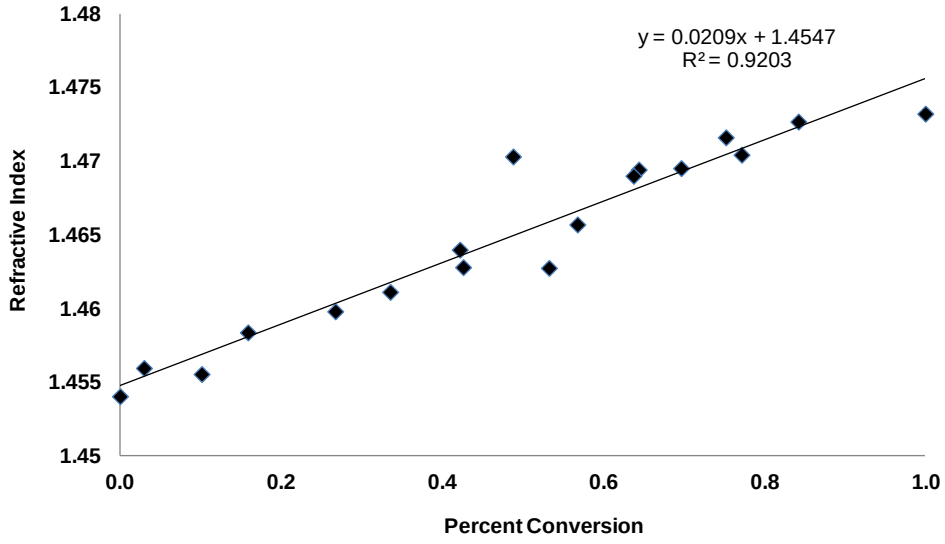


**Figure 4.21.** Refractive index as a function of conversion to IL in TPSA

Another reliable approach to monitoring conversion was refractive index. The refractive indices can be directly correlated to the composition of the sample, therefore providing a direct measurement of conversion. The refractive index of TPSA molecular liquid went from 1.4550 to 1.4732 in the fully formed ionic liquid in a linear fashion (Figure 4.21).

4.3.2.3 $CO_2$ Capture capacity evaluation for revIL systems

$CO_2$ capture capacity was measured by gravimetry, or mass uptake, after exposure to $CO_2$ for the TEtSA, TPSA, THSA, and FSA systems. The total $CO_2$ capacity is defined by the measured gravimetric uptake, which is the result of (1) the chemical reaction of the amines with $CO_2$, deemed chemisorption, and (2) physical capture (physisorption) through absorption of $CO_2$ into the ionic liquid formed. I will highlight that gravimetric capacity was used as an overall measure of capacity but it is also very important to decouple the respective contributions of each mode of capture as well. Herein, $CO_2$ capture will be reported in terms of mol $CO_2$/mol amine and mol $CO_2$/kg amine solvent. Industry often favors the latter, yet I found the former to be informative and therefore opted to report both.

### 4.3.3 $CO_2$ capture capacities

4.3.3.1 $CO_2$ capacity from gravimetric analysis

In comparing the theoretical chemical capacities dictated by the reaction stoichiometry, it was expected that the maximum theoretical absorption would be 0.5 mol $CO_2$/mol amine. With respect to capacity in terms of mol $CO_2$/kg amine (based on the molar theoretical uptake), TEtSA had the highest capacity at 2.89 mol $CO_2$/kg amine. In comparison, a 30% aqueous solution of MEA, was projected to have a capacity of 2.46 mol $CO_2$/kg amine.[32] Theoretical uptakes ranged from 1.35 to 2.32 mol $CO_2$/kg amine.

**Table 4.5.** Gravimetric capacities for the reaction of trialkylsilylpropylamines with $CO_2$

| Structure | Theoretical Chemical Capacity (mol $CO_2$/mol amine) | Experimental Capacity (mol $CO_2$/mol amine) | Theoretical Chemical Capacity (mol $CO_2$/kg amine) | Experimental Capacity (mol $CO_2$/kg amine) |
|---|---|---|---|---|
| Aq. MEA, 30% | 0.5 | 0.23* | 2.46 | 1.13* |
| TEtSA | 0.5 | 0.630 ± 0.006 | 2.89 | 3.66 ± 0.035 |
| TPSA | 0.5 | 0.640 ± 0.007 | 2.32 | 2.99 ± 0.034 |
| THSA | 0.5 | 0.670 ± 0.008 | 1.46 | 1.96 ± 0.024 |
| FSA | 0.5 | 0.62 ± 0.03 | 1.35 | 1.67 ± 0.07 |

Experimentally, it was observed that experimental uptakes exceeded the expected theoretical uptake for all four RevIL systems (Table 4.5). At full conversion, both TEtSA and TPSA displayed much higher capacities (up to 300 %) over MEA, with uptakes of 3.66 and 2.99 mol $CO_2$/kg amine, respectively. Although gravimetric measurements did not distinguish between physical and chemically reacted $CO_2$, the over-capacity relative to chemical adsorption alone suggested that physical absorption was occuring. In all cases, silylamine RevIL systems showed higher (up to 3 times) capacities than the accepted aqueous MEA benchmark. The MEA data reported in Table 4.5 are reported literature data obtained at flue gas conditions in a wetted wall column: 9M MEA at 40°C with a $CO_2$ pressure of 10.4 Pa.[32]

### 4.3.4 Decoupling chemical and physical absorption

4.3.4.1 Chemical absorption (reaction)

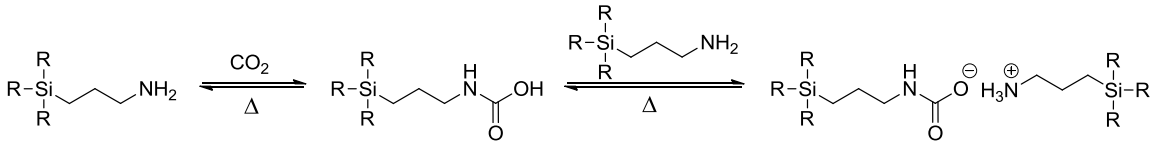

**Figure 4.22.** Trialkylsilylpropylamine chemical reaction with $CO_2$ to form an ammonium/carbamate ion pair

Reaction of 2 moles of trialkylsilylamines with $CO_2$ forms an ionic pair consisting of one mol of amine forming a carbamate anion and on mol forming the ammonium cation (Figure 4.22). One mole of primary amine reacts with $CO_2$ to first form a carbamic acid intermediate. An acid-base reaction with another mole of amine then forms the ionic pair. With this stoichiometry the equilibrium when lying completely to the right gives a capacity of 0.5 mol $CO_2$/ mol amine. Indeed, all of our analyses (NMR) were consistent with the chemical reaction going to full conversion for the ionic species.The discrepancy between the theoretical capacities and the experimental capacities were attributed to physical absorption. To unequivocally verify that this was indeed the case, we used ATR-FTIR to (1) decouple physisorption from chemisorption and (2) quantify physisorption for the RevILs via Henry constant measurements.

4.3.4.2 Physical absorption

Physical absorption is highly beneficial because it is low energy process and plays a significant role in certain applications of $CO_2$ capture, specifically in capture at high pressures, for example natural gas streams. With traditional ionic liquids this is the only method of capture and reversal energy is very low due to the weak interactions

which favor absorption. By analogy, it is expected that RevILs would physically absorb $CO_2$. It is important to decouple the amount of physically absorbed $CO_2$ to chemically absorbed $CO_2$ to accurately address the energy that will be required for the $CO_2$ recovery step. ATR-FTIR measurements were conducted on the four RevIL systems.

*4.3.4.2.1 Introduction to ATR-FTIR*

Attenuated Total Reflectance-Fourier Transform IR or ATR-FTIR measures the vibrational bond frequency unique to each chemical bond. ATR-FTIR offers the benefit of no sample preparation and solids and liquids can both be analyzed. This is possible because the penetrating wave is shown through a diamond plate where multiple penetrations of the wave are possible through the sample (Figure 4.23). Furthermore, a pressurizable reaction cell was fitted to the ATR cell for *in-situ* studies with small sample volumes.

**Figure 4.23.** ATR-FTIR attachment

FTIR is a sensitive analytical technique that enables the easy and accurate identification of functional groups. An example of an ATR-FTIR spectrum of TEtSA-ML and TEtSA-IL is shown in Figure 4.24 below.

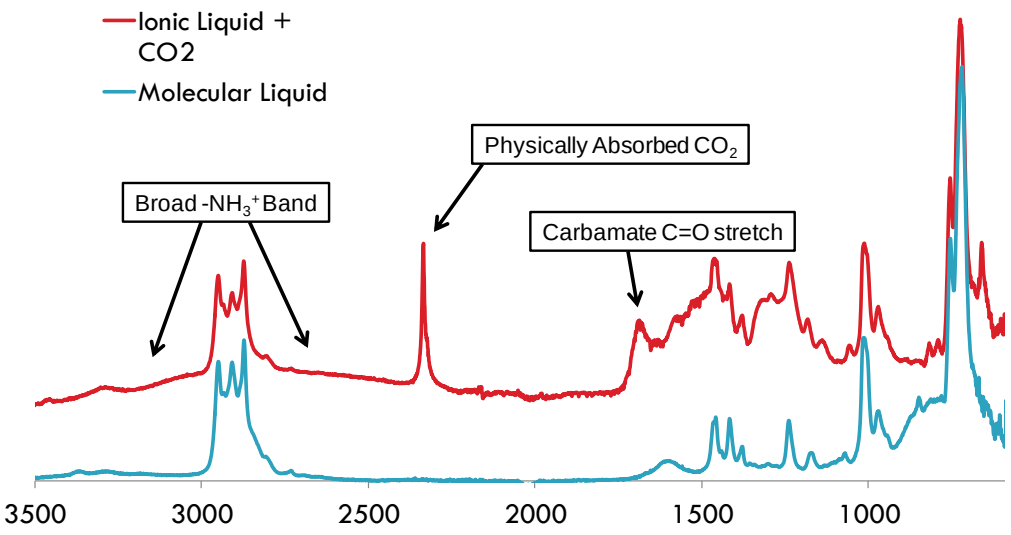


**Figure 4.24.** ATR-FTIR spectra of TEtSA-ML and TETSA-IL

Three regions were identified which correspond to (I) the ammonium shift region between 2400-3200 wavenumbers, (II) corresponding to the asymmetric $CO_2$ stretch at 2330 wavenumbers and (III) the carbamate carbonyl stretch at 1700 wavenumbers. These regions changed between the molecular and ionic liquid forms of TEtSA, particularly the appearance of the carbamate carbonyl stretch and the broad band of the ammonium stretching vibrations. Of particular interest was the peak that appears at 2330 wavenumbers. This peak represents the asymmetric stretch of carbon dioxide,

characteristic of physically absorbed $CO_2$. This unique stretch allowed for the quantification of free $CO_2$ absorbed versus the ammonium/carbamate stretches indicative of chemical reaction. To calculate the amount of physisorption and chemisorption in the RevIL systems, the C-H stretch was used as an internal standard. Since the reaction of these amines with $CO_2$ does not introduce any more C-H bonds or interfere with the existing carbon bonds, the peak area remained the same from molecular liquid to ionic liquid.

4.3.4.3 $CO_2$ physical absorption as a function of $CO_2$ pressure

For initial experiments, the physical absorption was measured from the preformed RevIL. As a result, the RevILs were loaded onto a custom-made pressurizable cell fitted to the ATR-FTIR (Figure 4.25).

**Figure 4.25.** High-pressure reactor for the ATR-FTIR

The ionic liquids were then subjected to increasing pressures of $CO_2$ from 5 to 55 bar. The asymmetric $CO_2$ stretch was used to quantify the mole fraction of $CO_2$ absorbed compared to the chemically reacted $CO_2$ in the preformed ionic liquids. This experiment

was completed for TEtSA, TPSA, THSA, and FSA. Data points at 0 bar were not measured.

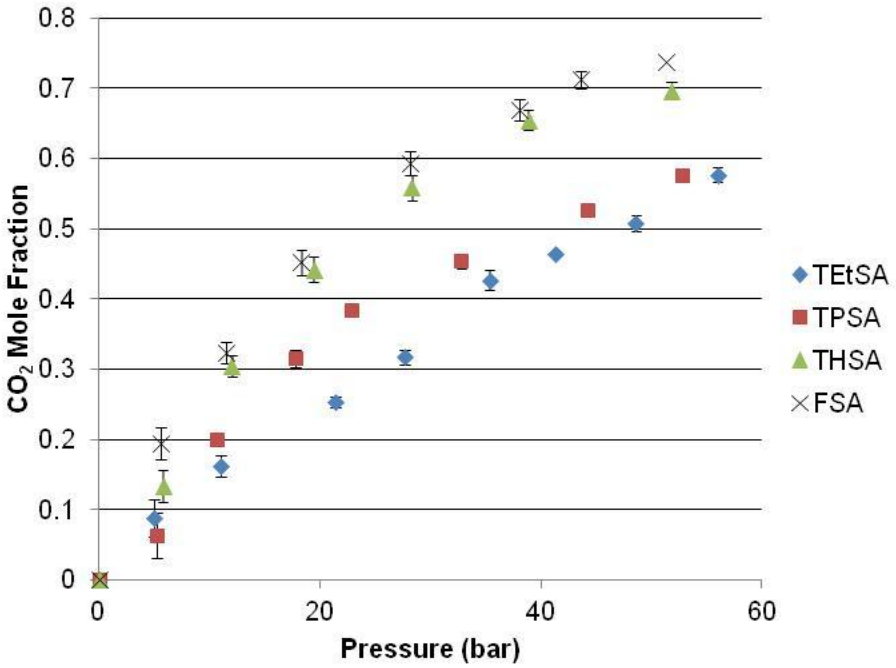


**Figure 4.26.** $CO_2$ physical absorption as a function of $CO_2$ pressure for RevILs

Shown above in Figure 4.26, is a plot of $CO_2$ mole fraction as a function of $CO_2$ pressure for four systems TEtSA, TPSA, THSA, and FSA. A linear trend existed up to about 30 bar of $CO_2$ for each of the systems. Higher than 30 bar, the vapor phase no longer behaved as an ideal gas phase. $CO_2$ absorption increased up to about 35% at 30 bar in the TEtSA system. At 30 bar, the other systems reached the following percentages: TPSA (about 42%), THSA (about 53%), and FSA (about 61%). This showed that not only can physical absorption be increased by increasing $CO_2$ pressure, but structural changes directly affected the amount of $CO_2$ that could be physically absorbed. At 1 bar of $CO_2$, the pressure that $CO_2$ capture experiments were conducted, physical absorption was calculated to account for  0.02% mol of the entire capture

capacity. This highlighted a discrepancy of about 15-20 % between the experimental capacities (>0.60) and the predicted overall capacities of 0.52 (taking into account both chemical and physical mode of absorption).

It was noted that although at very low pressures of $CO_2$, the physical absorption component was very tiny, the amount of physical absorption possible at higher $CO_2$ pressures varied with structure.

*4.3.4.3.1 Relationship between experimental physical absorption and predicted absorption*

Because a linear trend existed from 0 to 30 bar of $CO_2$ pressure, a relationship known as Henry's Law was used to establish a correlation between structure and physical absorption. Henry's Law is a limiting case of vapor-liquid equilibrium, valid for systems at low solubility, stating that the solubility of a gas in equilibrium with a liquid phase is directly proportional to the partial pressure of the gas in the vapor phase, where $x_{CO2}$ is the mole fraction of $CO_2$ in the liquid phase and $P_{CO2}$ is the partial pressure of $CO_2$ in the vapor phase (Equation 4.1).

**Equation 4.1.** Henry's Law

$$H_{CO2} = \lim_{x_{CO2} \to 0} \left( \frac{P_{CO2}}{x_{CO2}} \right)$$

Henry's Law constants were determined by the straight-line fit (through the origin) of the data points for which $P_{CO2} < 35$ bar and are reported in Table 4.7 below. Because of the relationship shown above, the lower the Henry constant, the more $CO_2$ physically absorbed. These Henry's constants were validated by comparing absorption in

conventional ionic liquids, specifically [Bmim]$PF_6^-$. The Henry's constant was calculated to be 58, which is within error of the reported value of 53.4.[33]

**Table 4.6.** Henry's constants at 35°C for each RevIL system

| Structure | Henry's Constant (bar) |
|---|---|
| TEtSA-IL | 73 |
| TPSA-IL | 60 |
| THSA-IL | 43 |
| FSA-IL | 44 |
| [Bmim]$PF_6^-$ | 58* |

*At 25°C

As a tool for prediction of physical absorption capabilities with changes in structure, "void volumes" were calculated.

4.3.4.4 Void Volumes as a trend for physical capture

Void volume was defined as the "free space" not occupied by a molecule in a given amount of ionic liquid. It was postulated that a direct relationship between void volume and physical absorption could be identified, toward the prediction of physisorption in the silylated amines systems. The molecular volumes were calculated by the summation of the Van der Waals molar volumes of individual single bonds, suggested by Bondi.[34] The ammonium/carbamate ion pair was calculated with a carbamic acid and amine because these values were known.

Experimental molar volumes were then calculated for each of the RevIL systems from the experimentally measured densities. From the densities (ρ) at 25°C, molar

volumes ($V_M$) were calculated by dividing by the molecular weight (MW), assuming that 2 moles of amine reacted with 1 mol of $CO_2$. The difference between the experimental and calculated molar volumes led to a "void volume" ($V_V$). Void volumes were calculated for all four systems and are displayed in Table 4.7 below.

**Table 4.7.** Void volumes for each RevIL system

| Structure | MW (g/mol) | ρ @ 25°C (g/cm$^3$) | $V_M$ (cm$^3$/mol) | $V_dW$ (cm$^3$/mol) | $V_V$ (cm$^3$/mol) |
|---|---|---|---|---|---|
| TEtSA-IL | 390 | 0.922 | 423 | 257 | 166 |
| TPSA-IL | 474 | 0.912 | 520 | 318 | 202 |
| THSA-IL | 727 | 0.884 | 828 | 502 | 320 |
| FSA-IL | 783 | 1.193 | 656 | 395 | 261 |

Void volumes differed between all four structures with TEtSA-IL having a void volume of 166 cm$^3$/mol and increased with alkyl chain length around the silicon atom up to 320 cm$^3$/mol for THSA-IL. To understand the correlation between these void volumes and actual physical absorption uptakes, amounts of physical absorption were measured with ATR-FTIR. The Henry's constants calculated by pressure experiments were compared to calculated "void volumes."

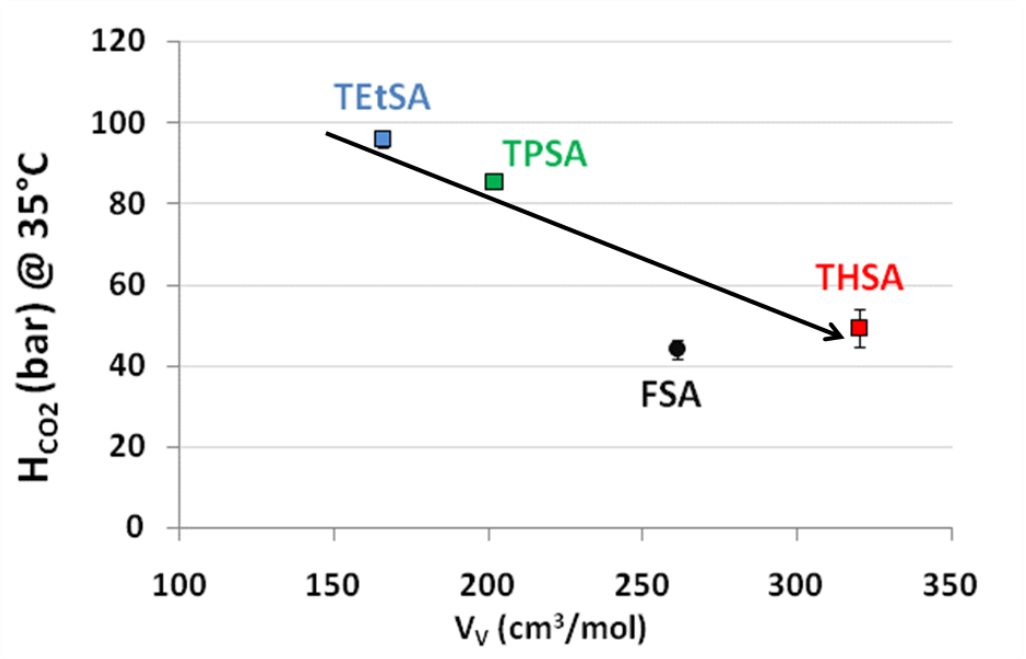


**Figure 4.27.** Henry's constant versus void volume for RevIL systems

From the graph of Henry's constants at 35°C compared to calculated void volumes, a linear relationshipwas apparent for the three symmetrical trialkylsilylamine species and is represented in Figure 4.27. FSA is an outlier from the linear relationship because of its enhanced capture through fluorocarbon-$CO_2$ interactions. This allows for predictions of other trialkylsilylamine species in regards to physical $CO_2$ capture with the caviat that the RevIL remains a liquid.

### 4.3.5 Understanding the experimentally enhanced $CO_2$ capture

Capacities higher than expected for chemical reaction (0.5 mol $CO_2$/ mol ML) and physisorption (from Henry's Law) were observed for all four RevIL systems. To identify the source of these enhanced capacities re-evaluation of the $CO_2$ capture setup and analytical technique were investigated.

Initially, it was hypothesized that residual water may be leading to increased weight gain that would provide false $CO_2$ uptakes. Not only would water accumulation add inherent mass but water and amines react with $CO_2$ to form ammonium carbonates with the amine to $CO_2$ ratio driven to 1:1 on a molar basis. The formation of carbonate by water would lead to increased capture capacities. Yet, the $CO_2$ source contained only ppb levels of water and a drying tube along the $CO_2$ line did not change the outcome of the capacity measurements. Another experimentally plausible cause was the formation of entrapped microscopic bubbles within the ionic liquids (due to their high viscosity at equilibrium capacities). Dynamic light scattering (DLS) experiments did not indicate microbubbles. There were no visible bubbles trapped in the samples so the possibility of entrainment is still possible but unlikely. From a chemical standpoint, one can think of the formation of additional reactions with $CO_2$.

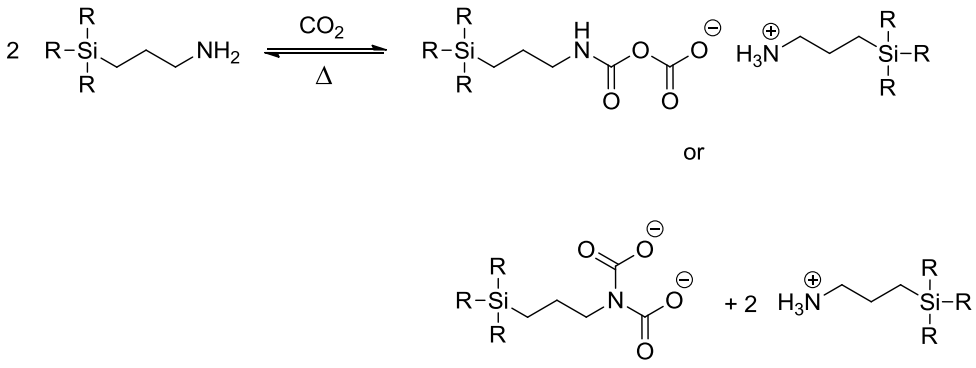


**Figure 4.28.** Proposed structures to understand enhanced capacity

Specifically, two different scenarios were considered (Figure 4.28), the first being a carbamic anhydride type species through the subsequent carbamate reaction with another mole of $CO_2$. The second scenario was that carbamate could react further with another mole of $CO_2$ to form a diamide species.This would be expected under more extreme conditions such as high $CO_2$ pressure. These two proposed structures were expected to be distinguishable by $^{13}$CNMR. The first structure is asymmetric, therefore displaying two different carbonyl peak shifts. The $^{13}$CNMR spectrum of TPSA-IL (prepared with $^{13}$C enriched $CO_2$ for maximum sensitivity) ruled out the formation of the first species because only the product (carbamate) peak was evident in the carbonyl region at 162.4 ppm (Figure 4.29).

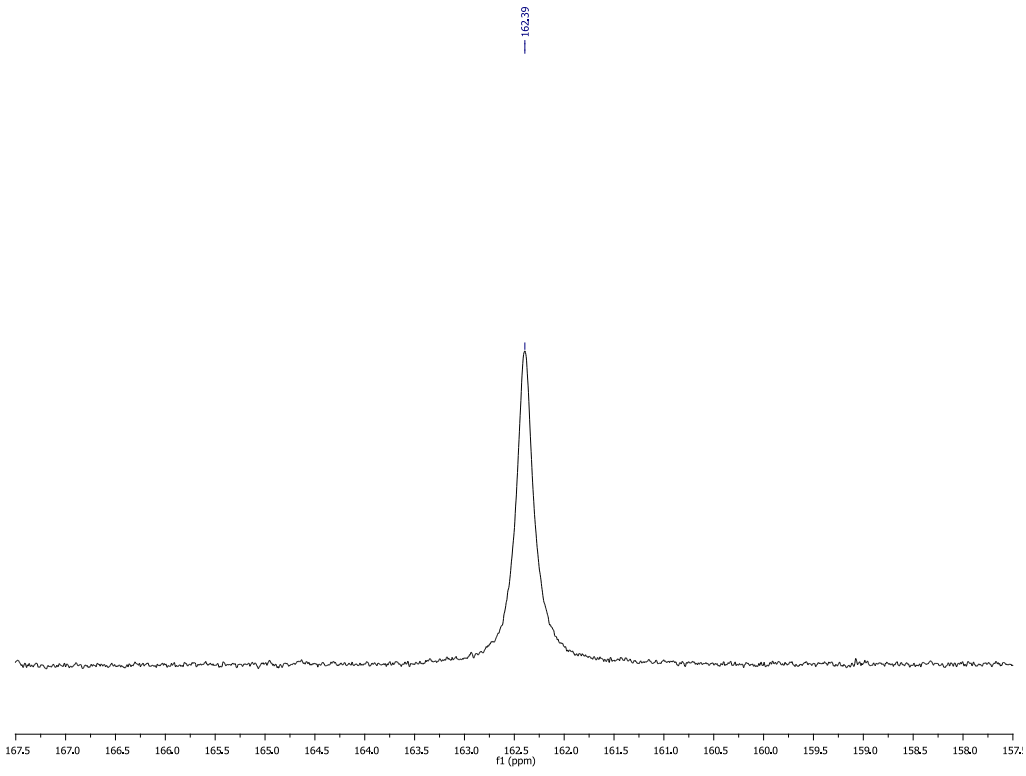


**Figure 4.29.** Single carbamate peak in the $^{13}$CNMR spectrum of TPSA-RevIL

Clearly, the NMR analyses did not support the formation of structurally different structure that the desired product.

4.3.5.1 Formation of carbamic Acid in the equilibrium reaction of primary amines with $CO_2$

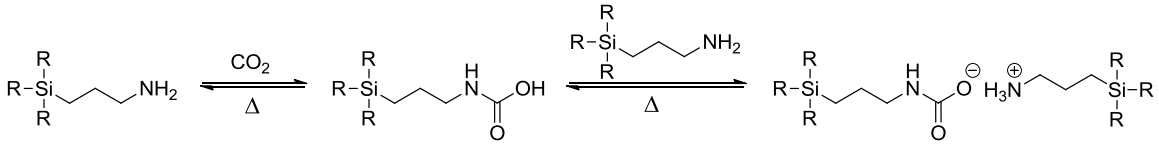

**Figure 4.30.** Equilibrium formation of carbamic acid in the reaction of amines with $CO_2$

We revisited the equilibrium reactions involved in the formation of the carbamate/ammonium ions. The first step is the reaction of the primary amine with $CO_2$ to form carbamic acid. The carbamic acid is then deprotonated by another mol of amine through an acid base reaction. If the reaction equilibrium did not lie fully to the ion paired product, then carbamic acid may be a contributing intermediate (Figure 4.30). The formation of carbamic acid from one mol of amine and one mol of $CO_2$ would yield capacities of 1:1 in terms of mol$CO_2$/mol amine, not 0.5 as theoretically expected when the equilibrium fully lies to the ionic products. As a consequence, carbamic acid was expected to be present. The overall capture capacity would be expected to be anywhere between 0.5 and 1 with inclusion of carbamic acid, as was observed.

Quantitative $^{13}$CNMR of TPSA RevIL, prepared with both enriched and non enriched $CO_2$, were conducted. In the case of the $^{13}CO_2$ enriched study, there existed only one peak in the carbonyl region attributed to the carbamate. However, if small amounts of carbamic acid were formed in the ionic liquid, hydrogen exchange between

the carbamate and carbamic acid would be much faster than the NMR scale, making the two species not differentiable. Because the carbons α and β to the ammonium and carbamate have distinctive chemical shifts, their integration provided information as to the relative concentration of ammonium and carbamate species. As a consequence, quantitative $^{13}C$ NMR experiments were conducted to monitor the ratio of the α and β peaks. If only the ionic species was formed and carbamaic acid was NOT present, this ratio was expected to be 1:1. In contrast, if carbamic acid was present, the α-carbon on the carbamate/carbamic acid should integrate to a value higher than the α-carbon corresponding to the ammonium cation. These two values should also sum to the total carbamate species present, indicated by the carbonyl peak.

*4.3.5.1.1 Quantitative $^{13}C$NMR to evaluate carbamic acid formation*

Integrations of the carbonyl peak, and α and β carbons of each ion were done and are shown in Figure 4.31. The α carbon of the ammonium species integrated to 0.5 whereas the α carbon on the carbamate/carbamic acid species integrated to 0.7. Furthermore, the carbonyl carbon integrated to 0.7 as well (not shown in Figure 4.31). These results strongly supported the presence of carbamic acid formation as well as ion-pair formation!

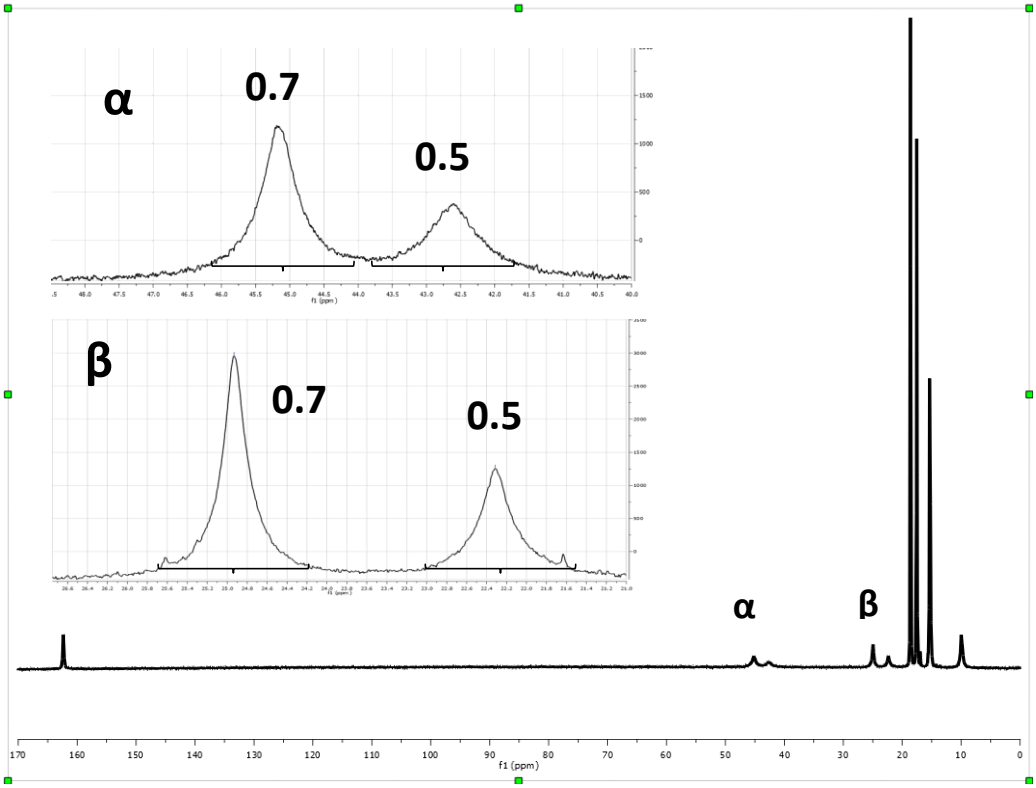


**Figure 4.31.** Quantitative $^{13}$CNMR in the evaluation of carbamic acid formation for TPSA-IL

*4.3.5.1.2 ATR-FTIR to evaluate carbamic acid formation*

Verification of the formation of carbamic acid as well as ammonium/carbamate ion pair was also supported by ATR-FTIR. It was expected that if carbamic acid was being formed, as $CO_2$ pressure was increased, the equilibrium would shift towards its formation, leading to less ionic pair formation. Therefore, the carbamate/carbamic acid stretch at 1700 wavenumbers should increase while the ammonium stretch between 2400-3200 decreases. The carbamate stretch was compared to that of the ammonium stretch and at increasing pressures. It was found that the area of the carbamate stretch

did in fact increase. Figure 4.32 shows that increasing from 0 bar to 20 bar of $CO_2$ pressure led to an increase of the absorbance of the carbamate/carbamic acid stretch.

The Beer-Lambert Law[35] states that absorbance is a direct function of path length through a sample, the molar absorptivity unique to that sample, and the concentration. The increase in absorbance was therefore attributed to the increase in carbamic acid concentration. It is noted that $CO_2$ pressure above 20 bar does not appear to further affect the concentration of carbamic acid, yet more experiments are being conducted to investigate these systems at higher pressures.

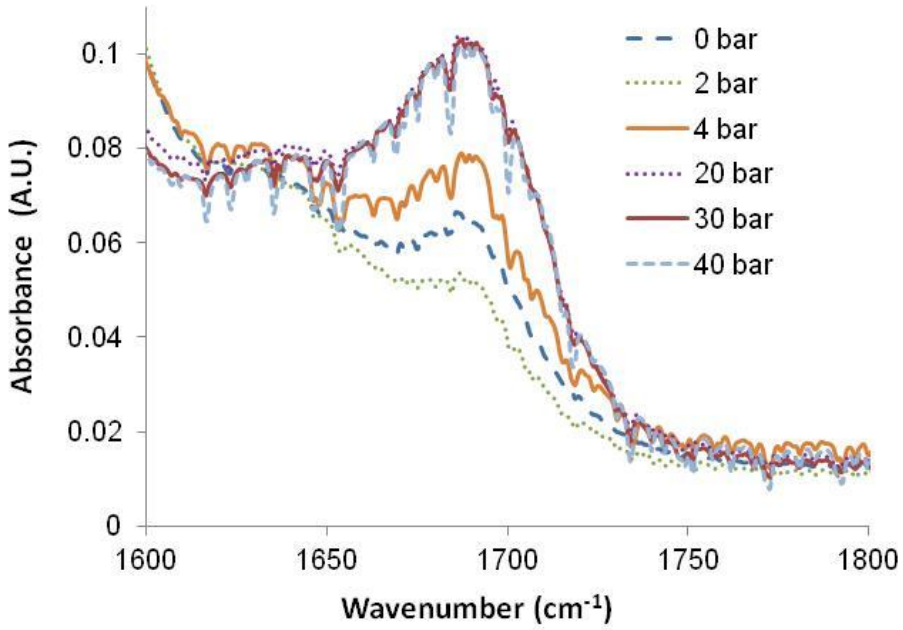


**Figure 4.32.** ATR-FTIR Spectra of TPSA carbamate stretch with $CO_2$ pressure

Both $^{13}$CNMR and ATR-FTIR supported the formation of up to 20% carbamic acid in trialkylsilylamines systems in addition to ammonium/carbamate ionic liquid. Unquestionably, RevIL systems have a unique and beneficial advantage in $CO_2$ capture. Although two reports in the literature allude to the formation of carbamic acid as a contributing product, experimental evidence was not conducted or proposed to support this conjecture.[19,36]

In terms of capacity, trialkylsilylamines display excellent ability to capture $CO_2$ both chemically through formation of ammonium/carbamate ionic liquids, carbamic acid, and physically absorbed $CO_2$. Viscosities of these unique ionic liquid systems at full capacity have been investigated (fundamental study) as well as the viscosity as a function of conversion from an applied standpoint. Presented in the next section are the viscosity studies of the RevIL systems.

### 4.3.6 Viscosity evaluation in formed RevILs

Viscosity of RevIL systems in an absorption/desorption process is a critical variable in industrial and commercial viability. It is accepted that viscosities below 200 cP is paramount but a viscosity of 100 cP or less is suitable for implementation. In contrast with conventional ILs, RevILs are “dynamic” systems in the sense that the molecular liquids are essentially not viscous while the RevIL at full conversion has relatively high viscosity. TEtSA, TPSA, THSA, and FSA viscosities were evaluated upon complete reaction with $CO_2$. The standard operating temperature of a flue gas stream has been reported to be 40$^{o}$C, therefore, viscosities at this temperature are pertinent, and the viscosities reported herein are for both 25 and 40°C.

A general trend in viscosity for most liquids is that viscosity is an inverse function of temperature thereby lowering viscosity by increasing temperature. If temperature could be increased to reduce viscosities, this could be an advantage. There is however a

balancing act with using temperature as a process variable because RevILs are thermally reversible. Reversal temperatures will be addressed later in the chapter, but all four of the systems evaluated reverse at higher temperatures than 40$^{o}$C.

Viscosity measurements were made using a Rheosys Merlin II viscometer equipped with a cone and plate. The pre-formed RevIL sample was placed on the sample plate and the temperature of the sample and plate was allowed to come to equilibrium prior to measurement. Shear rates between 10 and 2000 $s^{-1}$ were used and the average viscosity over that range was recorded.

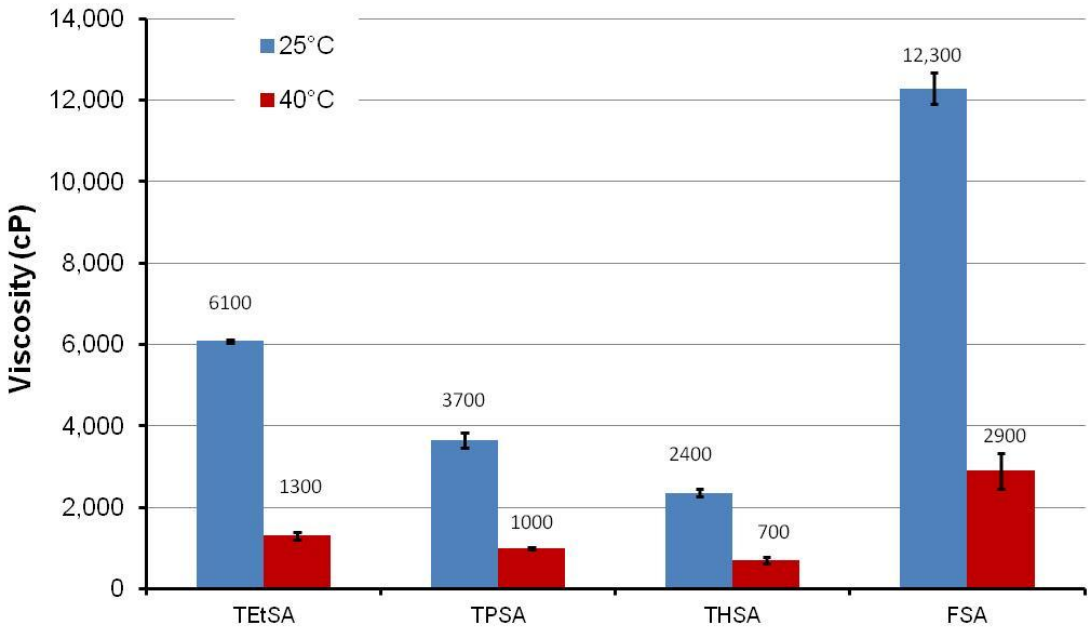


**Figure 4.33.** Viscosity Comparison at 25°C and 40°C for four RevIL systems

The highest RevIL viscosity at 25°C was found to be 12,300 cP for the FSA derivative. TEtSA, TPSA, and THSA ionic liquids had a linear decrease in viscosity from 6,100 cP to 2,400 cP (Figure 4.33). At 40$^{o}$C the trend remained the same. The viscosity of the FSA derivative was the highest of all four systems at 2,900 cP followed by linearly decreasing viscosities from TEtSA to THSA with viscosities between 1,300 cP to 700 cP respectively. There are two important findings with regard to viscosity measurements. First is that increasing the temperature from 25°C to 40°C led to drops in viscosity on the range of 70-80%. The second finding is that alkyl chain length around the silicon atom in the molecular liquids played a large role in viscosity. Particularly, by increasing the alkyl chain lower viscosities were achievable. It should be noted that decreasing the alkyl chain length any less that two carbons around the silicon led to solid formation of the ionic species.

It was hypothesized that stronger interactions of the carbamate/ammonium ion pair would lead to higher viscosities. As the alkyl chain length was extended and the liquid ion pairs have increased degrees of freedom, the alkyl chain flexibility was expected to compete with the ion pairing ability of the formed ions. FSA actually had the highest viscosity upon reaction with $CO_2$. This was surprising because of the bulk around the silicon atom and the flexibility of the fluorinated pentyl chain. This high viscosity may be due to ion-dipole interactions. In the case of the TEtSA, TPSA, and THSA, the main intermolecular interaction is the ionic bond between the ammonium and carbamate ions. In the case of FSA, the fluorine atoms are capable of interacting weakly with the ammonium cation so the solution consists of both ion pair interactions as well as ion-dipole interactions, leading to higher viscosities.

4.3.6.1 Viscosity as a function of conversion

Although the viscosities of these RevIL systems at full capacity were too high for a $CO_2$ capture process, a benefit of RevILs for $CO_2$ capture, as opposed to conventional ILs, is that viscosity is only an issue at high conversion. We therefore investigated the relationship between viscosity and extent of the reaction. It was expected that as the molecular liquids are converted to the RevILs, the viscosity would increase but it was not known if the viscosity would increase in a linear fashion. Shown below, in Figure 4.34, is an example of the increase of viscosity as a function of conversion in the formation of TPSA.

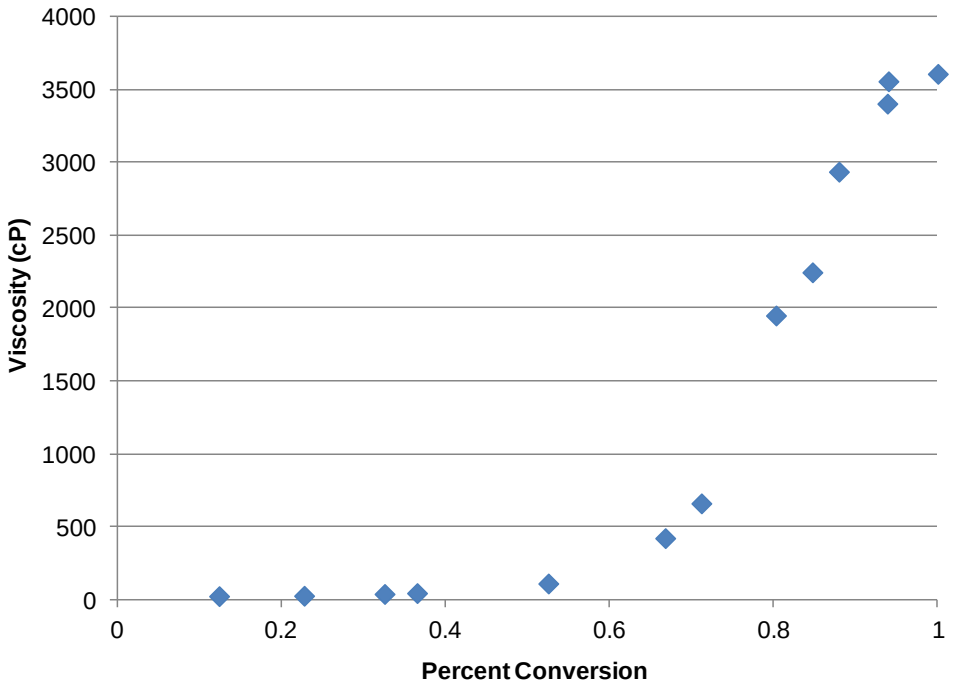


**Figure 4.34.** Viscosity as a function of conversion in the formation of TPSA-IL

The trend between viscosity and extent of conversion followed a “hockey-stick” shaped curve with two distinct regions. There was an initial region in which viscosity was essentially conversion independent and a second region for which viscosity was highly conversion dependent. For TPSA as representative example, the conversion independent region existed from 0% conversion (or pure molecular liquid) to about 60% conversion and exhibited a relatively linear behavior, well below the desired 200 cP limit. From 60% to 100% conversion to RevIL, the viscosity showed a marked exponential increase. This can be explained by solvation. As the RevIL is formed during the reaction, the ion pairs are solvated by the free amine molecular liquid. At 60% conversion, the ion pairs then solvate the free molecular liquid, that upon extension of reaction increases in viscosity. The same trend was observed in the study of the other three silylamine systems. This remarkable behavior is extremely important in industrial viability of these RevIL systems. Viscosity can now be controlled by not only tuning the trialkylsilylamine structure but by controlling the extent of reaction or reaction time in a capture vessel. Viscosities have been shown to be controllable with structure and conversion, and even at incomplete conversion, enhanced capacities still make these systems favorable. The last set of properties that were evaluated for trialkylsilylamines were thermodynamic properties, both enthalpy of reaction and reversal temperature.

### 4.3.7 Thermodynamic parameters in $CO_2$ capture evaluation

It is undisputed that the enthalpy of reaction of $CO_2$ with an amine, and the temperature required to regenerate the molecular liquid, play a large role in the overall energy required to employ an energy efficient $CO_2$ capture strategy. Our goal was to understand how structural changes at the molecular level of trialkylsilylamines affected

the overall capture properties including $CO_2$ uptake, viscosity, and the thermodynamic parameters. The latter of these are discussed in this section.

In a 30% aqueous MEA solution, the temperature required to reverse the captured $CO_2$ and recycle the reactive solvent is on the order of 110-120$^oC$. The reason these temperatures are required is because of the full vaporization of water. Our RevIL systems have a built in advantage that they are intended as non-aqueous systems. The enthalpy of reaction has been shown to be a function of not only dilution but of conversion as well. Reaction enthalpy associated with a 30% MEA solution is reported as 85 kJ/mol $CO_2$. Because the RevIL systems are conducted anhydrously, it was expected that enthalpies may be higher than the 30% MEA solution. The goal was to maintain relatively low enthalpy of regeneration balanced with low reversal temperature and high $CO_2$ capacity.

4.3.7.1 Differential Scanning Calorimetry (DSC) as a characterization tool

Thermodynamic parameters were investigated in the study of structure with respect to $CO_2$ capture. Two important parameters were measured, reversal temperature of the $CO_2$ as well as the enthalpy of reaction during reversal. In order to understand how the reaction enthalpy and reversal temperature change with small structural changes, Differential Scanning Calorimetry (DSC) was used as a primary analytical tool. During the reversal process, the reversal temperature and the enthalpies were obtained.

Upon complete formation of the RevILs through reaction with $CO_2$, samples were crimped in a hermetic aluminum pan and equilibrated at -40ºC in the DSC. The sample was then ramped at a rate of 5ºC/min from -40ºC to 300ºC. There are two endothermic events which occured during the temperature profile at which these RevIL systems were

conducted. The first event corresponds to the reversal of the ionic liquid to the molecular liquid and the second event corresponds to the vaporization of the molecular liquid.

The example shown below (Figure 4.35) is TPSA RevIL. From the DSC thermogram, the reversal temperature was found to be 63°C and the onset of evaporation, 180°C.

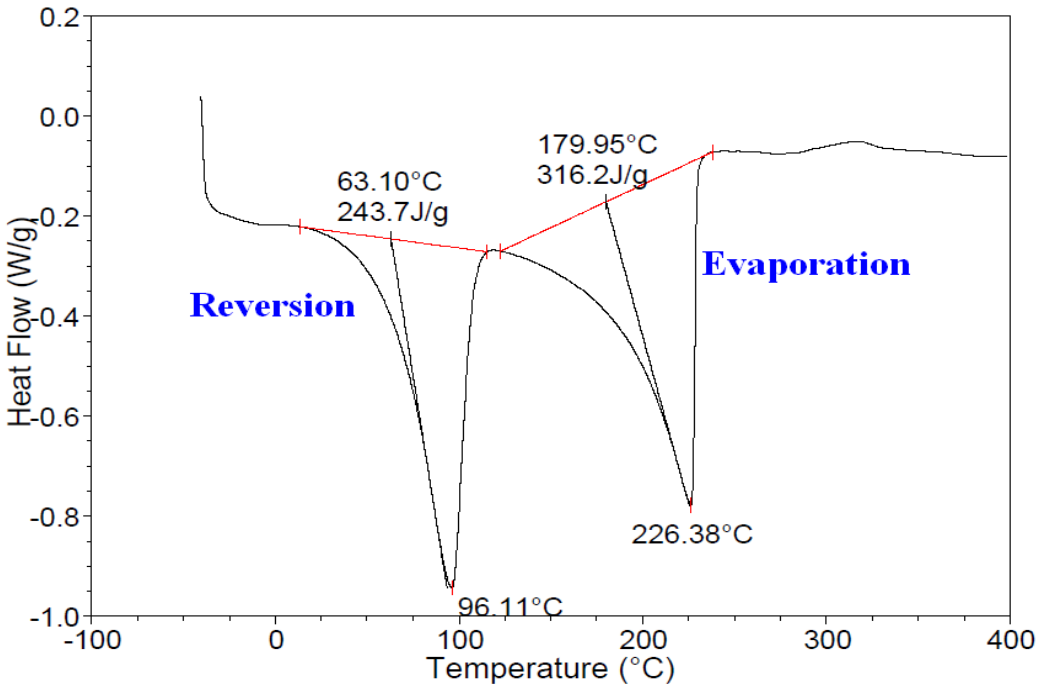


**Figure 4.35.** DSC thermogram showing $CO_2$ reversal and ML evaporation for TPSA

4.3.7.2 $CO_2$ reversal and molecular liquid evaporation in revIL systems

Reversal temperatures were calculated by extrapolating the tangent to the onset of the curve at its peak to the baseline. It should be said that actual onset temperatures of reversal and evaporation are lower because the temperature reported is taken with the linear tangent rather than the apex of the peak. In fact, there is some level of

reversal and evaporation before the reported temperatures. The average (over three runs) temperatures of reversal and evaporation for each of the RevIL systems are shown in Table 4.8 below.

**Table 4.8.** Comparison of reversal and evaporation temperature for four RevIL systems

| RevIL system | $T_{reversal}$ ($^oC$) | $T_{evaporation}$ ($^oC$) | $T_{evaporation}$-$T_{reversal}$ ($^oC$) |
|---|---|---|---|
| TEtSA | 71 ± 3 | 168 ± 12 | 97 |
| TPSA | 64 ± 2 | 180 ± 11 | 116 |
| THSA | 51 ± 1 | 233 ± 1 | 182 |
| FSA | 48 ± 3 | 147 ± 14 | 99 |

Of the four systems, TEtSA was found to have the highest reversal temperature at 71°C, followed by TPSA at 64°C, THSA at 51°C, and FSA at 48°C. The data indicated that as the alkyl chain length around the silicon atom was increased from TEtSA to THSA, the reversal temperature decreased. This is most likely an entropic effect. The alkyl chains on the silicon atom are essentially constrained through an ionic bond of the ammonium and carbamate. The longer these alkyl chains are, the more repulsive interactions are prominent and the degrees of freedom of the alkyl chains are then constrained by this ionic pairing. Upon reversal the constraint is eliminated, allowing for increased flexibility which is entropically favored.

As expected, the evaporation temperature increased with molecular weight. The evaporation temperatures are also reported in Table 4.8. The lowest onset of evaporation was surprisingly found in the FSA derivative at 147°C. This was surprising because the molecular weight of FSA exceeds that of TEtSA and TPSA. The increase

in evaporation temperature with increased alkyl chain length is advantageous because the higher the evaporation temperature and the lower the reversal temperature, the larger the gap between them. The temperature gap between ML and RevIL translates to loss of molecular solvent during the regeneration step. Evaporation of starting material is not desirable as it will demand a makeup stream -- an additional cost to the overall economics of the system and a possible an extra step for purification of the $CO_2$ stream.

4.3.7.3 Reaction enthalpy of $CO_2$ with trialkylsilylpropylamines

The enthalpy of these reactions is a very important variable in the optimization of new $CO_2$ capture systems. The reaction enthalpy controls the amount of heat necessary to reverse the process. It was a goal in designing these silylated amine RevIL systems that the enthalpy of reaction or enthalpy of reversal be competitive with current techonologies. Enthalpies of reaction were calculated from DSC experimental data. The amount of heat in J/g was calculated by integration of the endotherm area from baseline to baseline. Since the sample mass was known, the reaction enthalpy in kJ/mol can be easily calculated.

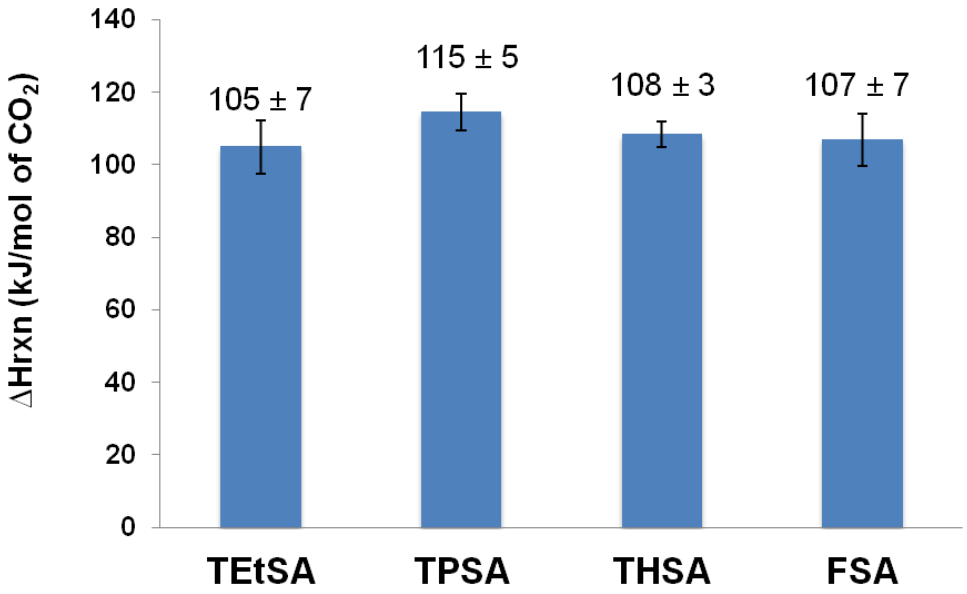


**Figure 4.36.** Reaction enthalpy versus RevIL structure in the reversal of $CO_2$

As expected, the reaction enthalpies did not change significantly between RevIL systems. The value obtained for each of these primary amines is shown in Figure 4.36 above. All of the silylated amine systems had enthalpy values of 110 kJ/mol $CO_2$, within error. These enthalpies were calculated based on the chemical reaction of 0.5 mol $CO_2$/ mol amine. The consistency in enthalpy between structures was both expected and a little surprising. It was expected that reaction enthalpies would not change much since these are all reactions of primary amines with $CO_2$.

4.3.7.4 Reversibility and recyclability in silylamine revIL systems

I have shown that silylamine RevILs are thermally reversible by analysis of the DSC thermograms of the ionic species. Coupled with DSC, TGA experiments provided an indication of mass loss as a function of temperature. The DSC measurements shown highlight the reversal temperature and vaporization temperature of the molecular liquids

systems and Table 8 shows the difference in temperature between reversal onset and evaporation. If these two events overlap at all, losses of molecular liquid are possible. TGA experiments were run to quantify the overlap between the two events. An example TGA experiment is shown in Figure 4.37 for TEtSA-RevIL.

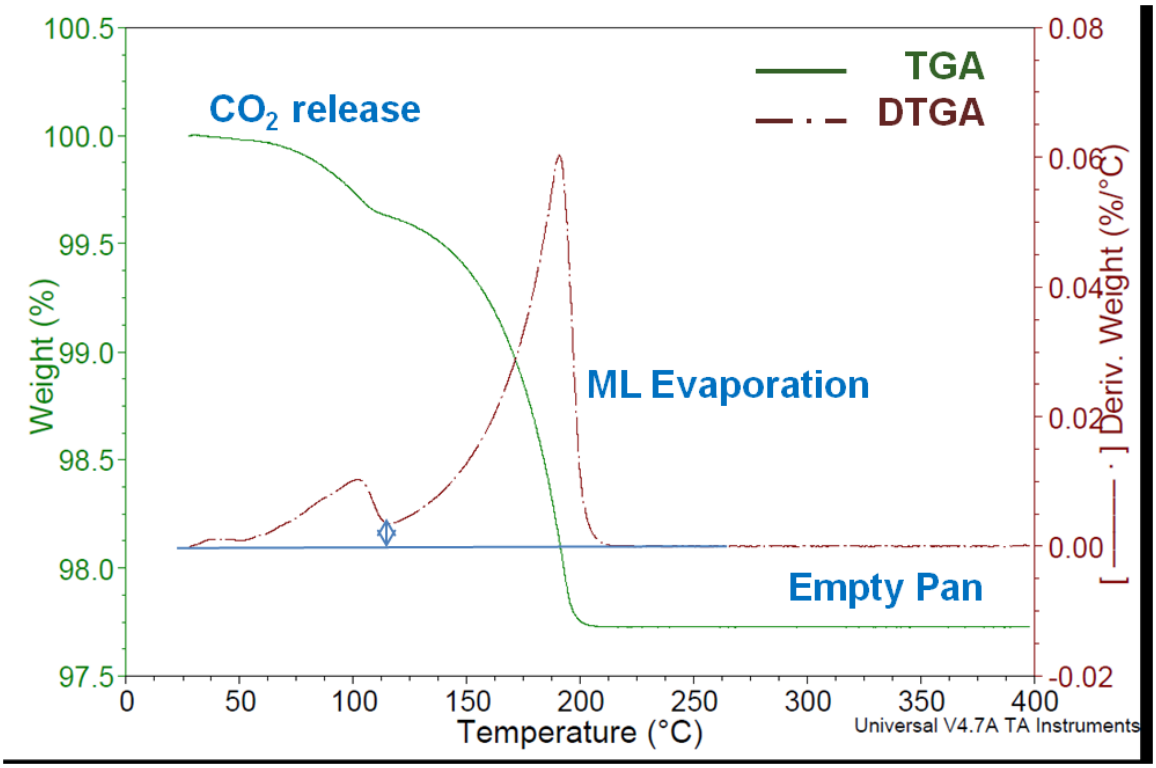


**Figure 4.37.** TGA and DTGA curves in the reversal of TEtSA-IL

There are two events in the TGA seen by the change in slope of the green curve. These two slopes correspond to same two endothermic events in the DSC, reversal of the ionic liquid and evaporation of the molecular liquid. In the case of TEtSA, Figure 4.37 shows the weight loss curve as well as its derivative. The $CO_2$ release can be seen between 25$^{o}$C and 110$^{o}$C and the loss of molecular liquid from 110$^{o}$C to just over 200$^{o}$C.

The derivative of the TGA curve, or the DTGA curve in red shows two distinct peaks. When the baseline was normalized to zero, it was apparent that the there was not a return to the baseline between events but actually overlap (blue diamond). This overlap translates to the amount of loss of molecular liquid expected during a capture and reversal cycle. From the data, the percentage loss of molecular liquid was calculated for each of these RevIL systems based on the overlap in the DTGA curves and is reported in Table 9 below, from lowest to highest. THSA had the lowest expected loss of 0.1% based on overlap of the two events, followed by increasing losses in FSA, TPSA, and TEtSA. TEtSA had the highest expected loss at 6.4% per cycle.

**Table 4.9.** Calculated losses of molecular liquids from DTGA curves

| RevIL | % ML loss | $T_{evaporation}$-$T_{release}$ (°C) |
|---|---|---|
| THSA | 0.10 ± .06 | 182 |
| FSA | 1.4 ± 0.5 | 99 |
| TPSA | 2.0 ± 0.5 | 116 |
| TEtSA | 6.4 ± 0.5 | 97 |

As expected, the larger the temperature difference in reversal and evaporation, the lower amounts of loss are to be expected. These values are the maximum losses expected and in fact reversing sharply at a given temperature within the reversal range may prevent any serious losses from occurring in an actual process. To evaluate the maximum quantitative losses experimentally, a recyclability study was conducted on both TPSA and THSA.

*4.3.7.4.1 Recyclability of trialkylsilylpropylamine revILs*

Recyclability is extremely important in a viable $CO_2$ capture process. If a process is not recyclable then a steady supply of amine would need to be used to account for losses, an energetic and economic disadvantage. To test recyclability of our silylamine RevILs, formation of ionic liquids through reaction of $CO_2$ followed by reversal was done. Again, refractive index was used as a reliable measure of conversion of molecular liquid to ionic liquid because of the linear relationship between the two. A representative example, TPSA, is shown in Figure 4.38 below. The refractive index of TPSA molecular liquid was recorded prior to exposure to $CO_2$ at a value of 1.4540.Upon complete reaction, the refractive index was measured at 1.4735. The TPSA-IL was then reversed back to the molecular liquid by heating at 100°C for 90 minutes. Five cycles were successfully conducted with no noticeable change in performance.

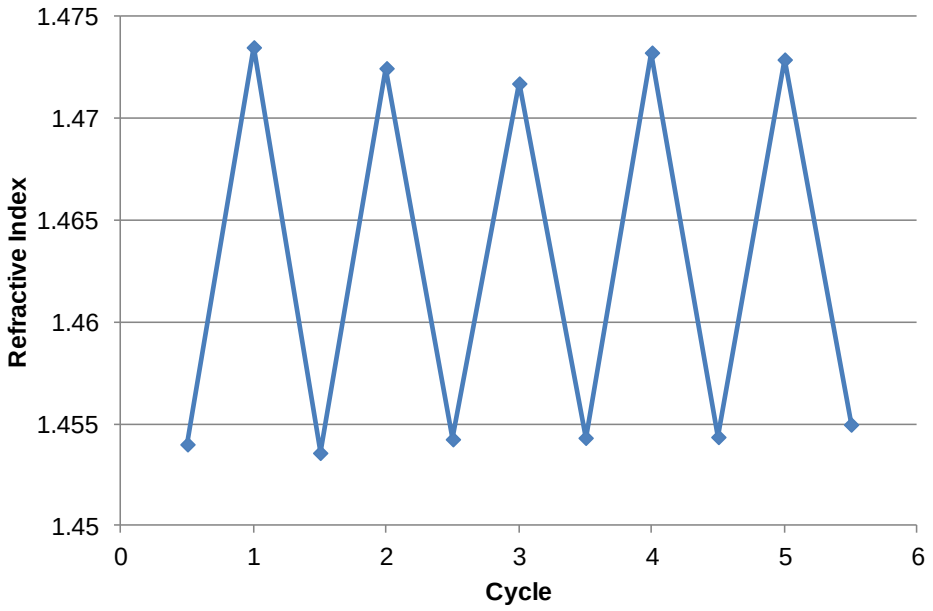


**Figure 4.38.** Recyclability study using RI over five cycles for TPSA

Recyclability by gravimetric techniques were also obtained. TPSA molecular liquid was reacted with $CO_2$ and the gravimetric uptake recorded. Reversal was done by heating the formed RevIL at 100ºC for 90 minutes. This cycle was successfully repeated five times.

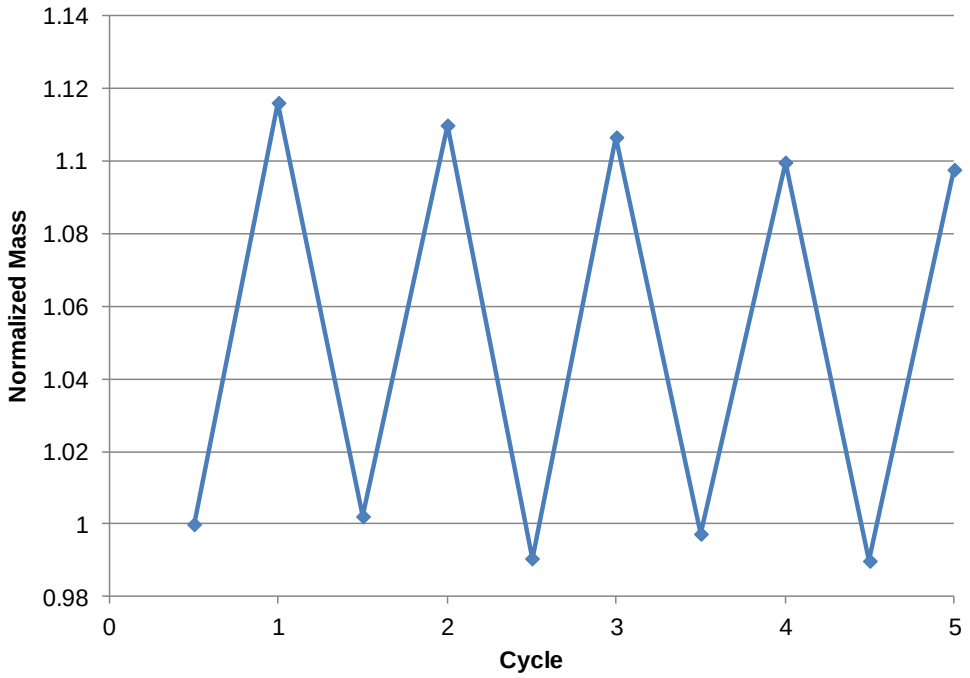


**Figure 4.39.** Recyclability study investigating mass loss over five cycles for TPSA

As expected, there is a slight loss in TPSA molecular liquid when reversing for a long period of time at 100$^{o}$C, as seen by the dip in some cycles below the normalized value 1 in Figure 4.39. The mass uptake also decreased slightly. This may have been due to some incomplete reversal which would lead to less $CO_2$ uptake but could also could have been due to small losses in TPSA (evaporation during capture step). $^{1}$HNMR indicated that no detectable degradation had occurred after the five cycles.

Also to note, degradation in aqueous amine solutions remains a challenge. Degradation occurs in MEA solutions thermally and oxidatively. The alcohol functionality plays a critical role in the major degradative chemistries. In the case of trialkylsilylamines, alcohol functionalities are not present and thermal and oxidative degradation are expected to be much less than aqueous MEA systems but extensive testing of these systems under degradative conditions would be informative.

### 4.3.8 Theoretical calculations for molecular liquid development

Calculations were conducted on the molecular liquid forms of TEtSA, TPSA, THSA, and FSA using Spartan® software. Possible correlation with calculated values and experimental values could lead to better optimization without synthesizing large libraries of compounds. The two main parameters investigated in these calculations were the available amine area and the Milliken charge on the amine,shown in Table 4.10. These parameters were investigated to shed light on the reactivity of these amines with $CO_2$ as well as give an indication into the reversal process. The exposed nitrogen area and the nitrogen atomic charge were calculated using DFT with a basis set B3LYP 6-31G* with Spartan® 2010 software. All four models were optimized to their lowest energy confirmations prior to calculation.

**Table 4.10.** DFT calculations of nitrogen area and atomic charge for RevIL systems

| **Reversible Ionic Liquid** | **Nitrogen Exposed Area** ($Å^2$) | **Nitrogen Atomic Charge** (Mulliken charge) |
|---|---|---|
| TPSA | 8.274 | -0.717 |
| TEtSA | 8.277 | -0.716 |
| THSA | 8.279 | -0.716 |
| FSA | 8.258 | -0.716 |

The charge on the amine did not change with respect to substitution around the silicon atom, staying consistent at -0.716. Even the fluorinated derivative had no electronic effect on the reactive amine. With respect to the exposed nitrogen area, there was a slight change with respect to alkyl chain length. FSA had the lowest exposed area at 8.258 squared Angstroms. This is probably because the two isopropyl groups are relatively bulky and rigid. The THSA, by calculation had the highest nitrogen exposed area at 8.279 squared Angstroms but TPSA and TEtSA had areas of 8.274 and 8.277, respectively.

It did not appear that there was a straightforward correlation between experimentally obtained results and calculated values for reversal temperature and viscosity. Enthalpy of reaction did not change significantly between silyl-substitutions and the exposed area didn't either. Computational trends could give an indication into reaction enthalpies. In order to truly have a marked effect on the amine reactive site, other structural modifications with silicon and amine functionalities needed to be explored.

## 4.4 Conclusions

Current aqueous amine technology is a benchmark but is far from being the optimum technology to meet the increasingly stringent regulations set forth by the DOE and EPA. Silylated amines were used to successfully capture $CO_2$. It was found that these systems had a dual capture mechanism through both chemical reaction and physical absorption. The chemical reaction of the amines with $CO_2$ was found to lie incompletely to the ionic products and instead remained partially as carbamic acid. This led to increased capacities, higher than predicited by stoichiometry. Viscosities of the formed RevILs were higher than desirable but were found to be tunable by conversion. Reversal temperatures were found to be far lower than temperatures required to reverse

aqueous amine solutions, an energetic advantage. It was found that all properties investigated were variable through structural changes around the silicon atom. There still existed a definite balance between desirable properties with a trade-off between viscosity and capacity. To address this, alternate modifications to the silylamine structure were identified and are presented in the remaining chapters.

## 4.5 Experimental Methods

### 4.5.1 Hydrosilylation reactions

(0.2% eq) Pt-DVDS (2% in xylenes) was added to a trialkylsilane (0.08 mol, 1 eq) under nitrogen in a 3 neck flask and condenser. Anhydrous toluene was added to make a 2M solution of silane and the solution was stirred. In all cases the solution turned a dark yellow color. Allyl amine (0.16 mol, 2 eq) was then added slowly and the solution became a deep red. The solution was brought to reflux and allowed to react. Upon reaction completion (monitored by NMR) the solution was cooled and the solvent removed by vacuum evaporation. The remaining liquid was distilled under vacuum to provide pure colorless liquid products. *Reactions were not optimized and yields are isolated upon distillation. The purified trialkylsilylamines were then characterized by $^{1}$HNMR, $^{13}$CNMR, FTIR, and EA.

### 4.5.2 Molecular liquid characterization

***3-(aminopropyl)triethylsilane (TEtSA)**:*

89% yield, distilled at 75$^{o}$C at 4mmHg

$^{1}$HNMR (400 Hz, $CDCl_3$) 2.63 (t, 2H), 1.39 (sex, 6H), 1.08 (s, 2H), 0.90 (t, 9H), 0.49 (q, 8H) $^{13}$CNMR (400 Hz, $CDCl_3$) 45.47, 27.88, 18.63, 7.90, 6.95, 2.87

Expected: C(62.35), H(13.37), N(8.08) Actual: C(62.41), H(13.42), N(7.94)

***3-(aminopropyl)tripropylsilane (TPSA):***

96% yield, distilled at 84$^{o}$C at 0.3 mmHg

$^{1}$HNMR (400 Hz, $CDCl_3$) 2.63 (t, 2H), 1.39 (p, 2H), 1.30 (sex, 6H), 1.05 (s, 2H), 0.93 (t, 9H), 0.48 (m, 8H) $^{13}$CNMR (400 Hz, $CDCl_3$) 45.85, 28.30, 18.63, 17.45, 15.27, 9.55

Expected: C(66.90), H(13.57), N(6.50) Actual: C(66.74), H(13.64), N(6.35)

***3-(aminopropyl)trihexylsilane (THSA):***

92% yield, distilled at 155$^{o}$C at 3 mmHg

$^{1}$HNMR (400 Hz, $CDCl_3$) 2.62 (t, 2H), 1.37 (p, 2H), 1.25 (s(br), 26H), 1.17 (s, 2H), 0.86 (t, 9H), 0.47 (m, 8H) $^{13}$CNMR (400 Hz, $CDCl_3$) 45.87, 33.58, 31.53, 28.34, 23.84, 22.61, 14.11, 12.40, 9.45

Expected: C(73.82), H(13.86), N(4.10) Actual: C(72.87), H(13.59), N(4.07)

***(3-(aminopropyl)-(1H,1H,2H,2H-perfluoropentyl))diisopropylsilane (FSA):***

94% yield, distilled at 100$^{o}$C at 1 mmHg

$^{1}$HNMR (400 Hz, $CDCl_3$) 2.68 (t, 2H), 2.03 (m, 2H), 1.45 (sex, 2H), 1.02 (s(br),14H), 0.79 (m, 2H), 0.58(m,2H)

$^{13}$CNMR (400 Hz, $CDCl_3$) 45.83, 28.21, 25.79(t), 18.15, 18.14, 17.24, 17.20, 12.91, 11.00, 6.53, -1.01

Expected: C(45.52), H(7.09), N(3.79) Actual: C(45.29), H(7.12), N(3.84)

***3-(aminopropyl)dimethylethylsilane (DMESA):***

58% yield, distilled at 38$^{o}$C at 2.5 mmHg

$^{1}$HNMR (400 Hz, $CDCl_3$) 2.61 (t, 2H), 1.37 (m, 2H), 1.15 (s(br), 2H), 0.44 (m, 4H), -0.09 (s, 6H)

$^{13}$CNMR (400 Hz, $CDCl_3$) 45.61, 28.22, 11.74, 7.24, 6.77, -4.04

Expected: C(57.86), H(13.18), N(9.64) Actual: C(57.50), H(13.01), N(8.94)

***3-(aminopropyl)dimethylphenylsilane (PDMSA):***

74% yield, 62$^{o}$C at 0.15 mmHg

$^{1}$HNMR (400 Hz, $CDCl_3$) 7.51(m ,2H), 7.35(m, 3H), 2.65 (t, 2H), 1.45 (m, 2H), 1.26 (s(br), 2H), 0.74 (m, 2H), 0.28 (s, 6H)

$^{13}$CNMR (400 Hz, $CDCl_3$) 139.24, 133.84, 133.52, 128.84, 127.74, 45.51, 28.22, 12.80, -3.10

Expected: C(68.33), H(9.90), N(7.24) Actual: C(68.25), H(10.07), N(7.14)

***3-(aminopropyl)dimethylcyclohexylsilane (CDMSA):***

60%, distilled at 80$^{o}$C at 1 mmHg

$^{1}$HNMR (400 Hz, $CDCl_3$) 2.61 (t, 2H), 1.67 (m, 3H), 1.63 (s(br),1H), 1.60(s(br), 1H), 1.37(m,2H), 1.16 (m, 5H*overlap with amine), 1.05 (m, 3H), 0.55 (t of t, 1H), 0.42 (m, 2H), -0.12 (s, 6H)

$^{13}$CNMR (400 Hz, $CDCl_3$) 45.82, 28.40, 28.16, 27.50, 27.04, 25.53, 10.55, -5.35

Expected: C(66.25), H(12.64), N(7.02) Actual: C(65.45), H(12.55), N(6.53)

***bis-(3-aminopropyl)diethylsilane (DESDA):***

41% yield, 67$^{o}$C at 2.7 mmHg *reaction conducted at 50$^{o}$C

$^{1}$HNMR (400 Hz, $CDCl_3$) (2.63 (t, 4H), 1.39 (m, 4H), 1.14 (s(br), 4H), 0.90 (t, 6H), 0.49 (m, 8H))

$^{13}$CNMR (400 Hz, $CDCl_3$) 45.82, 28.20, 11.74, 8.63, 7.42, 3.56

Expected: C(59.34), H(12.95), N(13.84) Actual: C(57.66), H(12.94), N(12.92)

### 4.5.3 Copper catalyzed reactions

Hydrosilylation reactions were conducted following a procedure from patent literature. A 48 mL Ace® glass pressure tube was outfitted with a cap containing a pressure gauge, a pressure relief valve, and an outlet and inlet line with needle valves. A general procedure is as follows:

Reactions in the glass tube were run at 100°C with a silicon oil bath. To the pressure tube was added triethyl or tripropylsilane (6.0 mmol) followed by allyl amine (0.59 mL) in an ice bath. Either CuOAc or $Cu(OAc)_2$ (0.021 g or 0.031 g) was added and the tube was sealed and placed in the oil bath. Reactions were carried out for 48 hours. After 48 hours, the glass tube was removed from the oil bath and allowed to cool. 0.1 mL of sample were added to 0.5 mL of hexane and analyzed by GC-MS.

Because the reactions in glass were not expected to be at high enough temperature to conduct the reaction, titanium reactor vessels (3 mL volume) were used for the reactions. These reactions were run at 200°C in a custom aluminum block. A stir bar was placed in the reactor followed by either CuOAc or $Cu(OAc)_2$ (0.0139 g or 0.0205 g) and a septum was fitted to the top of the reactor. Argon was flowed through the reactor and the reactor was then placed in an ice bath. Either triethyl or tripropylsilane (4.1 mmol) was added followed by allyl amine (0.39 mL). The septum was then removed and the cap tightly sealed. The reactions were run for 48 hours and then analyzed by cooling the reactors, removing the cap and sampling 0.1 mL, dissolved in 0.5 mL of hexane for GC-MS.

The products observed in any of these reactions was the trialkylsilylchloride (major) and an unidentified peak with a mass of 173 Da for the tripropylsilane derivatives and 216 Da for the triethylsilane reactions.

### 4.5.4 $CO_2$ reactions

Reactions of molecular liquids were performed by syringing a sample of the desired molecular liquid from the glove box into a dram vial. The vial was capped with a septum and a diffuser tube attached to a $CO_2$ line was used to introduce $CO_2$. $CO_2$ was flowed through the samples at a flow rate of 200 mL/min for 75 minutes. The diffuser tube was stirred in the solution as the reaction progressed to ensure mixing. The formed RevIL

was then subjected to analytical experiments to understand the role of structure on RevIL properties.

### 4.5.5 DSC/TGA

DSC measurements were performed in triplicate with a Q20 TA DSC Instrument. Sample weight was recorded in an aluminum hermetic pan crimped with an aluminum lid and measured against an empty pan. The DSC was calibrated with an Indium standard. Samples were held at -40$^{o}$C and ramped to 400°C at a ramp rate of 5°C/min. Reversal temperature was determined from the intersection of two tangents drawn at the beginning and bottom of the reversal endotherm. A similar treatment was used to determine the temperature of evaporation. Heat of regeneration was calculated by integrating the reversion endotherm with respect to time.

### 4.5.6 Viscometry

The viscosity of each ionic liquid was measured using a Rheosys Merlin II cone and plate viscometer. Samples were applied to the plate and were allowed to reach thermal stability prior to data collection. Shear rates varied between 10 and 2000 $s^{-1}$. The average viscosity over the shear range was recorded.

### 4.5.7 Densitometry

Density measurements were conducted in our laboratory using an Anton Paar DMA 38 Laboratory Density Meter.

### 4.5.8 Refractive Index

A Reichert Arias 500 Abbe-style refractometer, connected to a circulated cooling bath with glycol as the heat transfer fluid, enabling measurements from 0°C to 75°C was used. The refractometer is a semi-automatic design that eliminates the need for users to

interpret the shadowline intercept, resulting in an accuracy of ±0.0001. All measurements were run in triplicate.

### 4.5.9 ATR-FTIR

ATR-FTIR absorbance measurements were collected with a Shimadzu IRPrestige21 using a DLaTGS detector, with 32 scans and a resolution of 1 $cm^{-1}$. A Specac, Ltd. heated Golden Gate attenuated total reflectance (ATR) accessory with diamond crystal and zinc selenide (ZnSe) focusing lenses was used for the room temperature collection of the molecular and ionic liquid spectra. A custom built stainless steel reactor was designed in collaboration with Professor Sergei Kazarian of Imperial College London for the high pressure physical absorption studies.

### 4.5.10 Quantitative $^{13}$CNMR experiments

In our experimental study, we primarily used quantitative $^{13}$CNMR. A $T_1$ experiment was first conducted to determine the appropriate delay time between NMR scans to ensure full relaxation. $T_1$ represents the spin-lattice relaxation time, the time it takes the z-component of the magnetization vector to return to equilibrium after being pulsed. In order for the $^{13}$CNMR experiment to be quantitative, enough time must be allowed to ensure that the scan collected is representative of the equilibrium following the pulse and not a partial-return to equilibrium. The $T_1$ times of the TPSA IL are shown in Table 4.11 below and compared to the carbons labeled in Figure 4.40.

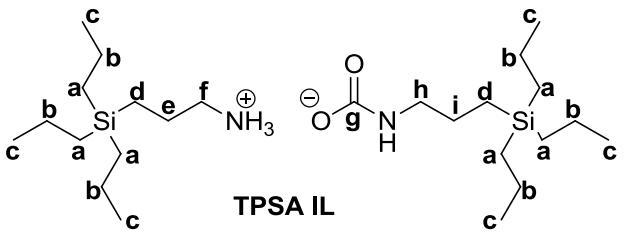


**Figure 4.40.** TPSA-IL ammonium/carbamate labeled

In order to allow sufficient time for relaxation it is recommended that the delay time between scans be five times the longest $T_1$ time; as a consequence, the delay time was set for 20 seconds. This insured that each peak could be used quantitatively. For the quantitative $^{13}$CNMR, $CO_2$ was introduced to TPSA in an NMR tube at 1 atm. In this particular experiment no external standard were used (to maximize signals); therefore, the spectrum was locked to the real-time FID (free induction decay).

**Table 4.11.** T1 experiment for TPSA-IL (relaxation times for each carbon)

| Atom / peak | a | b | c | d | e | f | g | h |
|---|---|---|---|---|---|---|---|---|
| $T_{1\,(s)}$ | 3.95 | 3.813 | 1.000 | 0.294 | 0.207 | 1.108 | 0.578 | 0.387 |

## 4.6 References


(1) EPA, Science and Technology: Climate Change. http://www.epa.gov/gateway/science/climatechange.html (accessed May 6, 2012).

(2) Kohl, A.; Neilsen, R. *Gas Purification*; Gulf Publishing Company: Houston, TX, 1997.

(3) Al-Juaied, M.; Rochelle, G. T. *Chemical Engineering Science* **2006**, *61*, 3830Hutchinson, A. J. L. US, 1939.

(4) Wolcott, R. A.; Pauley, C. R.; Pearce, R. L., 1984.

(5) Sherwood, T. K.; Pigford, R. L. *Absorption and Extraction*; 2nd ed.; McGraw-Hill Book Company: New York, 1952.

(6) Sander, M. T.; Mariz, C. L. *Energy Conversion and Management* **1992**, *33*, 341.

(7) Herzog, H. "An Introduction to $CO_2$ Separation and Capture Technologies," MIT Energy Lab, 1999.

(8) Strazisar, B. R.; Anderson, R. R.; White, C. M. *Energy & Fuels* **2003**, *17*, 1034.

(9) Bello, A.; Idem, R. O. *Industrial & Engineering Chemistry Research* **2005**, *45*, 2569.; Chi, S.; Rochelle, G. T. *Industrial & Engineering Chemistry Research* **2002**, *41*, 4178.

(10) Rao, A. B.; Rubin, E. S. *Environmental Science & Technology* **2002**, *36*, 4467.

(11) Rubin, E. S.; Chen, C.; Rao, A. B. *Energy Policy* **2007**, *35*, 4444.

(12) Kim, I.; Svendsen, H. F. *Industrial & Engineering Chemistry Research* **2007**, *46*, 5803.

(13) *Ionic liquids III : fundamentals, progress, challenges, and opportunities*; American Chemical Society :: Washington, DC :, 2005.

(14) Hart, R.; Pollet, P.; Hahne, D. J.; John, E.; Llopis-Mestre, V.; Blasucci, V.; Huttenhower, H.; Leitner, W.; Eckert, C. A.; Liotta, C. L. *Tetrahedron* **2010**, *66*, 1082.

(15) Baltus, R. E.; Culbertson, B. H.; Dai, S.; Luo, H. M.; DePaoli, D. W. *Journal of Physical Chemistry B* **2004**, *108*, 721.; Condemarin, R.; Scovazzo, P. *Chemical Engineering Journal* **2009**, *147*, 51.; Camper, D.; Scovazzo, P.; Koval, C.; Noble, R. *Industrial & Engineering Chemistry Research* **2004**, *43*, 3049.; Bara, J. E.;

Carlisle, T. K.; Gabriel, C. J.; Camper, D.; Finotello, A.; Gin, D. L.; Noble, R. D. *Industrial & Engineering Chemistry Research* **2009**, *48*, 2739.

(16) Gomes, M. F. C.; Padua, A. A. H. *Pure and Applied Chemistry* **2005**, *77*, 653.

(17) Lee, S. G. *Chemical Communications* **2006**, 1049.; Bates, E. D.; Mayton, R. D.; Ntai, I.; Davis, J. H. *Journal of the American Chemical Society* **2002**, *124*, 926.

(18) Gurkan, B. E.; de la Fuente, J. C.; Mindrup, E. M.; Ficke, L. E.; Goodrich, B. F.; Price, E. A.; Schneider, W. F.; Brennecke, J. F. *Journal of the American Chemical Society* **2010**, *132*, 2116.

(19) Goodrich, B. F.; de la Fuente, J. C.; Gurkan, B. E.; Zadigian, D. J.; Price, E. A.; Huang, Y.; Brennecke, J. F. *Industrial & Engineering Chemistry Research* **2011**, *50*, 111.

(20) Camper, D.; Bara, J. E.; Gin, D. L.; Noble, R. D. *Industrial & Engineering Chemistry Research* **2008**, *47*, 8496.

(21) Gutowski, K. E.; Maginn, E. J. *Journal of the American Chemical Society* **2008**, *130*, 14690.

(22) Zhang, F.; Fang, C. G.; Wu, Y. T.; Wang, Y. T.; Li, A. M.; Zhang, Z. B. *Chemical Engineering Journal* **2010**, *160*, 691.

(23) Jessop, P. G.; Heldebrant, D. J.; Li, X.; Eckert, C. A.; Liotta, C. L. *Nature* **2005**, *436*, 1102.

(24) Phan, L.; Chiu, D.; Heldebrant, D. J.; Huttenhower, H.; John, E.; Li, X. W.; Pollet, P.; Wang, R. Y.; Eckert, C. A.; Liotta, C. L.; Jessop, P. G. *Industrial & Engineering Chemistry Research* **2008**, *47*, 539.

(25) Heldebrant, D. J.; Koech, P. K.; Ang, M. T. C.; Liang, C.; Rainbolt, J. E.; Yonkera, C. R.; Jessop, P. G. *Green Chemistry* **2010**, *12*, 713.; Heldebrant, D. J.; Jessop, P. G.; Thomas, C. A.; Eckert, C. A.; Liotta, C. L. *Journal of Organic Chemistry* **2005**, *70*, 5335.

(26) Blasucci, V.; Hart, R.; Mestre, V. L.; Hahne, D. J.; Burlager, M.; Huttenhower, H.; Thio, B. J. R.; Pollet, P.; Liotta, C. L.; Eckert, C. A. *Fuel* **2010**, *89*, 1315.

(27) Marzinke, et al. "Method for the Preparation of Aminopropyl or Aminoalkyl Functional Polyalkyl or Aryl Siloxanes." US Patent 6,177,583 B1, Jan. 23, **2001**.

(28) Sakaki, S.; Mizoe, N.; Sugimoto, M. *Organometallics* **1998**, *17*, 2510.

(29) Gomes, M. F. C.; Padua, A. A. H. *Journal of Physical Chemistry B* **2003**, *107*, 14020.

(30) Nguyen, B. T., "Hydrosilylation with Platinum Free Neat Copper Containing Catalyst." US Patent 6,713,644 B1, Mar, 30, **2004.**

(31) Perry, R. J.; Grocela-Rocha, T. A.; O'Brien, M. J.; Genovese, S.; Wood, B. R.; Lewis, L. N.; Lam, H.; Soloveichik, G.; Rubinsztajn, M.; Kniajanski, S.; Draper, S.; Enick, R. M.; Johnson, J. K.; Xie, H.-b.; Tapriyal, D. *ChemSusChem* **2010**, *3*, 919.

(32) Dugas, R. E.; Rochelle, G. T. *Journal of Chemical & Engineering Data* **2011**, *56*, 2187.

(33) Anthony, J. L.; Maginn, E. J.; Brennecke, J. F. *Journal of Physical Chemistry B* **2002**, *106*, 7315.

(34) Bondi, A. *Journal of Physical Chemistry* **1964**, *68*, 441.

(35) Skoog, D.A.; Holler, J.F.; Crouch, S.R. *Principles of Instrumental Analysis,* 6th ed.; Thomson Brooks/Cole: United States, 2007.

(36) Aresta, M.; Ballivet-Tkatchenko, D.; Dell'Amico, D. B.; Bonnet, M. C.; Boschi, D.; Calderazzo, F.; Faure, R. E.; Labella, L.; Marchetti, F. *Chemical Communications* **2000**, 1099.; Pinto, M. L.; Mafra, L.; Guil, J. M.; Pires, J.; Rocha, J. *Chemistry of Materials* **2011**, *23*, 1387.

# CHAPTER 5: INVESTIGATION INTO $CO_2$ CAPTURE PROPERTIES OF TRIALKYLSILYLAMINES AS A FUNCTION OF SILICON-AMINE PROXIMITY AND AMINE ORDER

## 5.1 Introduction

The previous chapter discussed the effect of structural modifications at the silicon atom for 3-(aminopropyl)trialkylsilanes with respect to $CO_2$ capture pertinent properties. These propylamine derivatives were explored as the first structural modification; yet, these are not the only key structural feautures in silylamines that can be altered torward an optimum system for $CO_2$ capture. In this chapter, is highlighted the exploration of two more specific set of structural changes: (1) the length of the alkyl chain between the silicon atom and the amine reactive site, and (2) methylation of the reactive amine site (secondary amine). This chapter delves into the effect of each of these two structural changes onto the $CO_2$ capture properties of the resulting RevILs systems. First, the importance of the distance between the silicon and nitrogen atoms is reported followed by the methylation effect of the amine to yield the secondary amines analogs.

## 5.2 Length of the alkyl chain between the silicon atom and the amine reactive site

Silanes were incorporated as a key structural feature of our reversible systems because it has been reported that in conventional ionic liquids, silicon-containing substituents contribute to lowering viscosities, compared to their carbon analogs. The observed lower viscosity may be due to the Lewis acidic character of a silicon atom, but has also been reported as a function of the longer bond between silicon and carbon, giving the molecule more flexibility and electronic effects.[1] It has been documented that silicon can accept electron density into its low lying unfilled orbitals (Figure 5.1).[2] This has been shown primarily in halogenated and siloxylated silicon atoms.[3] There have also

been studies with evidence to support the lewis character of a silicon atom with carbonyl oxygen electron density creating chelation with the silicon atom.[4] Although there is no precedent or studies on systems analogous to alkylsilylamines, it is postulated that such interaction may contribute to the favorable properties observed.

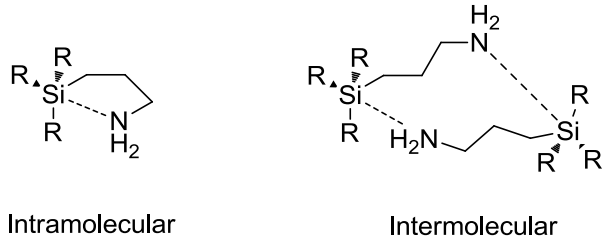


**Figure 5.1.** Silicon-amine interactions both inter and intramolecular in trialkylsilylamine systems

In general, most reports that investigate siloxylated amines for $CO_2$ capture have worked with propyl linkers between the nitrogen and silicon atoms, primarily due to the commercial availability of propyl-linked derivatives.[5] Poly-siloxylated amines have been shown to react reversibly with $CO_2$ and examples of reactions with both propyl and butyl derivatives between the silicon and nitrogen have been reported (Figure 5.2).[6] These amines, developed by GE, form solids upon reaction with $CO_2$.

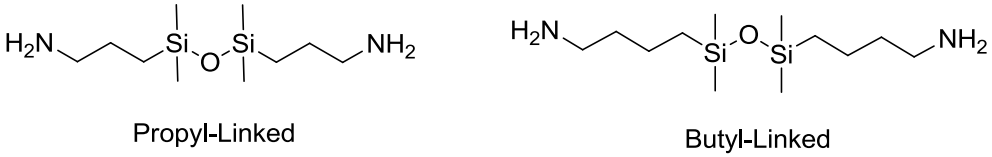


**Figure 5.2.** Propyl and butyl linked siloxanes developed by GE

The authors did not investigate other structures to enable solid or liquid systems—mostly because their focus is to form solids upon reaction with $CO_2$. Solid formation may be due to the bulkiness and the high molecular weight of the siloxyamines rather than an effect from the butyl linkage. In contrast, our goal was to remain liquid upon reaction with $CO_2$. It was shown in Chapter 4 that as alkyl chain length was varied on the silicon atom from ethyl to hexyl, there was in fact a substantial changes in bulk properties like viscosity, reversal temperature and capacity. As expected, no effect on the enthalpy of reaction was observed. Within this chapter are efforts to understand how the proximity of the amine to the silicon atom in trialkylsilylamines effect the RevIL properties pertinent to $CO_2$ capture. Because of the amine-silicon interactions, it was postulated that changing the chain length stepwise from a methyl to a butyl linker could limit intramolecular interactions resulting in marked differences in the reversal energies and viscosities of these systems. For the purpose of this study the silylamines derivatives were all synthesized with a triethylsilyl group because previous experiments show that TEtSA remains a liquid (albeit highly viscous) while having a higher capacity. It should be recognized that this is not a requisite and other functionalized silyl groups could be synthesized if desirable. A stepwise approach to the alkyl chain linker between the silicon and nitrogen was expected to give valuable information as to the specific effect of each of the small changes.

### 5.2.1 Synthesis of amines

**Table 5.1.** Structures investigated to understand the role of silicon-amine proximity on $CO_2$ capture properties

| Structures in the Investigation into Silane/Amine Proximity | | | |
|---|---|---|---|
| TESMA | TESEA | TEtSA | TESBA |
| 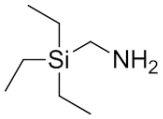 | 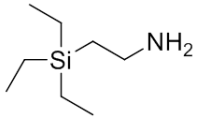 | 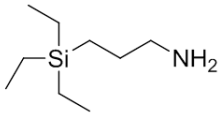 | 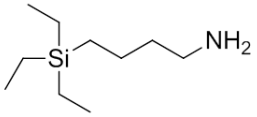 |

The specific synthesis of each the silylamines shown in Table 5.1 are described in the following section. Both (aminomethyl)triethylsilane (TESMA) and 2-(aminoethyl)triethylsilane (TESEA) required a custom preparation strategy, however, the 3-(aminopropyl)triethylsilane (TEtSA) and 4-aminobutyl)triethylsilane (TESBA) were synthesized via the one step “classic” hydrosilylation reaction presented in Chapter 4. Although the synthetic pathways and purification will be described briefly herein; a complete description is reported in the experimental methods section of the chapter. All molecular liquids were characterized by $^{1}$HNMR, $^{13}$CNMR, and EA.

5.2.1.1 Synthesis of (aminomethyl)triethylsilane (TESMA)

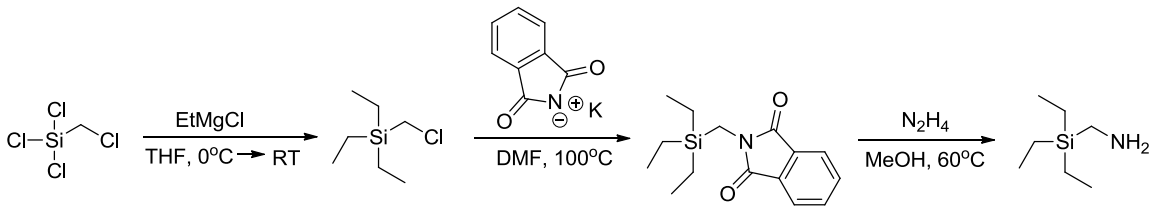


**Figure 5.3.** Synthetic methodology for the formation of TEMSA

TESMA was synthesized through a three-step scheme highlighted in Figure 5.3. The first step involved the Grignard displacement of the three chlorine atoms from the commercially available trichloro(chloromethyl)silane to form triethylchloromethylsilane.[7] Substitution of the chlorine atom from the methylene chloride group was achieved by reacting with potassium phthalimide under basic conditions. Finally, the triethylsilylphthalimidomethane was deprotected with hydrazine in methanol, yielding the desired triethylsilylaminomethane or TESMA. The distillation of the product for purification was achieved under vacuum at room temperature to minimize degradation.

5.2.1.2 Synthesis of 2-(aminoethyl)triethylsilane (TESEA)

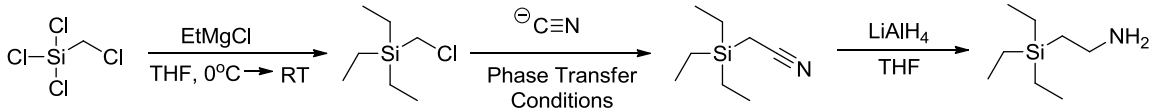


**Figure 5.4.** Synthetic methodology for the formation of TESEA

5.2.2.1.1 Nitrile formation promoted by phase transfer catalysis

The initial synthetic approach is shown in Figure 5.4. It was initially expected that because the phthalimide substitution of the chloride was successful, displacement with a nitrile group under phase transfer conditions could be achieved. The (triethylsilyl)cyanomethane reduction with $LiAlH_4$ was proposed to provide the desired product.[8] Grignard substitution, as shown in the formation of the TESMA derivative was straighforward. The displacement of the chloro group by the cyanide was then attempted under phase transfer conditions and in DMSO to form the (triethylsilyl)cyanomethane compound. Regardless of the conditions (solvent, time of reaction, PTC), the reaction failed to yield the desired product (Table 5.2). It was hypothesized that the nucleophilicity of the cyanide anion was not sufficient for the reaction to proceed despite the lower steric hindrance (with respect to the phthalimide for instance).

**Table 5.2.** Phase-transfer reaction conditions for the subsitution of triethyl(chloromethyl)silane

| Solvent System | Cyanide Salt | PTC | Temperature (°C) |
|---|---|---|---|
| No solvent | KCN | TBACl | 100 |
| Toluene | KCN | TBACl | 90 |
| Toluene | KCN | 18-crown-6 | 90 |
| DMSO | NaCN | -- | 100 |
| Toluene:$H_2O$ | NaCN | TBACl | 100 |
| THF | NaCN | TBACl | 66 |

All reactions were performed for 24 hrs under an inert atmosphere

*5.2.2.1.2 Boronation/Amination pathways to anti-Markovnikov amine synthesis*

An alternative one step route was considered by analogy with H.C. Brown's work.[9] His group's work has a large focus on alkenyl boronation to afford anti-Markovnikov additions of alcohols and amines. It was expected based on precedent that boronation with borane of commercially available triethylvinylsilane, followed by reaction of the trialkylborane species with hydroxylamine-*O*-sulfonic acid would yield the desired TESEA (Figure 5.5). The addition of hydroxylamine-*O*-sulfonic acid led to the reaction being heterogeneous presumably from the low solubility of hydroxylamine-*O*-sulfonic acid in THF. As a result, the reaction was conducted under vigorous stirring overnight. After quenching, the aqueous layer was basified and the product amine extracted with ether. GC-MS analysis of the organic layer prior and post basification showed a trace of product formation. MS analysis indicated however that the major product was boron-complexes with the starting material and complexed product.

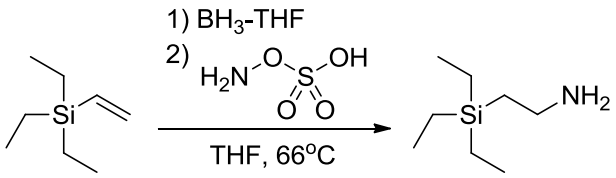


**Figure 5.5.** Hydroboration/amination from triethylvinylsilane

Brown's group suggested that incomplete amination of the boron complex can result in low reaction yields--especially the third amination. To overcome this problem, the formation of the mono-methyl borylated species has been reported.[10]

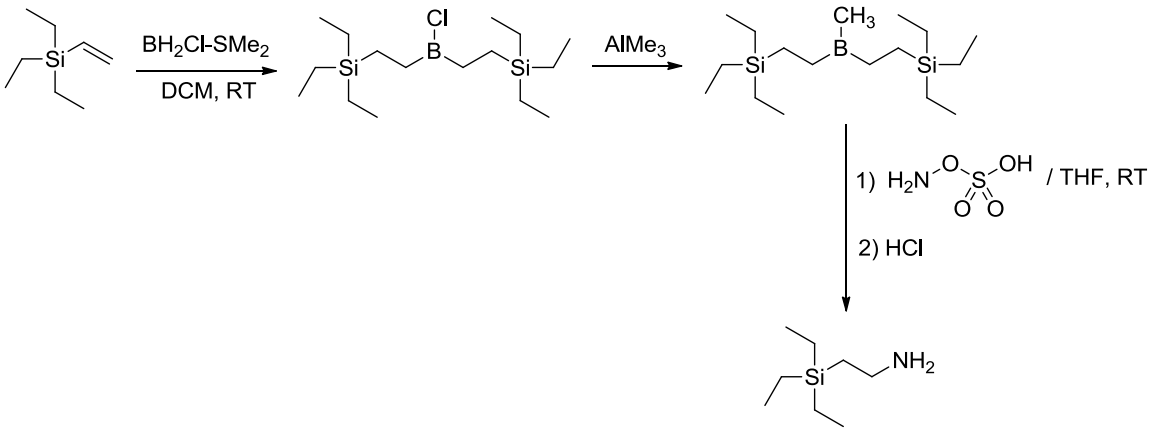


**Figure 5.6.** Modified boronation/amination from triethylvinylsilane with a methylated borane

This improved method was repeated in our labs to improve the yield of the original boronation/amination reaction (Figure 5.6). Triethylvinylsilane was reacted with chloroborane-dimethylsulfide complex to form the di-silylalkylchloroborane. This product was then reacted with 0.33 equivalent of trimethylaluminum to displace the chloride with a methyl group. The reaction was evidenced by the apparent formation of $AlCl_3$, which is insoluble in pentane. The resulting di-(silylalkyl)methylborane complex was then reacted with hydroxylamine-*O*-sulfonic acid following the previously described method.[10] Unfortunately, the amination and cleavage from the boron center did not take place.

To this point, synthesis of the TESEA derivative remained unsuccessful, however, recommendations for a potential synthetic pathway are presented in the conclusions and recommendations chapter.

5.2.1.3 Hydrosilylation of Reaction to form 3-(aminopropyl)triethylsilane (TEtSA)

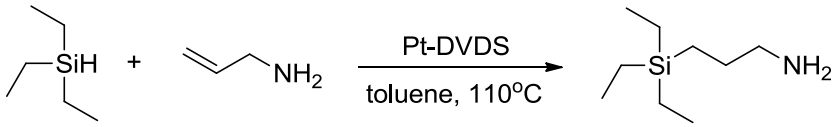


**Figure 5.7.** Hydrosilylation of triethylsilane and allylamine to form TEtSA

TEtSA was formed through hydrosilylation of allyl amine with Karstedt's catalyst (Pt-DVDS) in toluene at 110°C and is shown in Figure 5.7.[11] The reaction was monitored by $^{1}$HNMR and stopped after 24 hours of reaction. The toluene and excess allyl amine were removed and the product was purified by vacuum distillation.

5.2.1.4 Hydrosilylation Reaction to form 4-(aminobutyl)triethylsilane(TESBA)

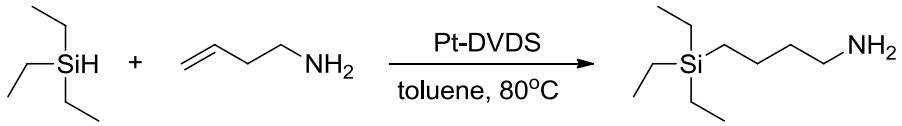


**Figure 5.8.** Hydrosilylation of triethylsilane and 4-amino-1-butene to form TESBA

Figure 5.8 shows the hydrosilylation reaction for the synthesis of TESBA.[11] In practice, TESBA was formed through hydrosilylation of 4-amino-1-butene with Pt-DVDS in toluene at 80°C. The product was then distilled under vacuum.

The three custom-made silylamines TEMSA, TEtSA, and TESBA were reacted with $CO_2$ and the resulting RevILs properties were measured and compared. The scope

of properties investigated included capture capacity, RevIL viscosity, and thermodynamic properties including reversal temperature and $CO_2$ reaction enthalpy.

## 5.3 Results and Discussion

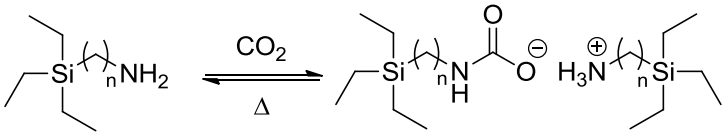


**Figure 5.9.** Equilibrium reaction of $CO_2$ with trialkylsilylamines with variable silicon-nitrogen linkages

Each of the three molecular liquids, TESMA, TEtSA, and TESBA were reacted with $CO_2$ as Figure 5.9 shows. A known mass of molecular liquid sample was added to a 4 dram vial under argon. A diffuser tube was used to sparge $CO_2$ through the system at a flow rate of 200 mL/min for 75 minutes. The gravimetric equilibrium capacity was then measured by direct measurement of the mass uptake of $CO_2$.

### 5.3.1 The role of Si-$NH_2$ distance in $CO_2$ capture capacity

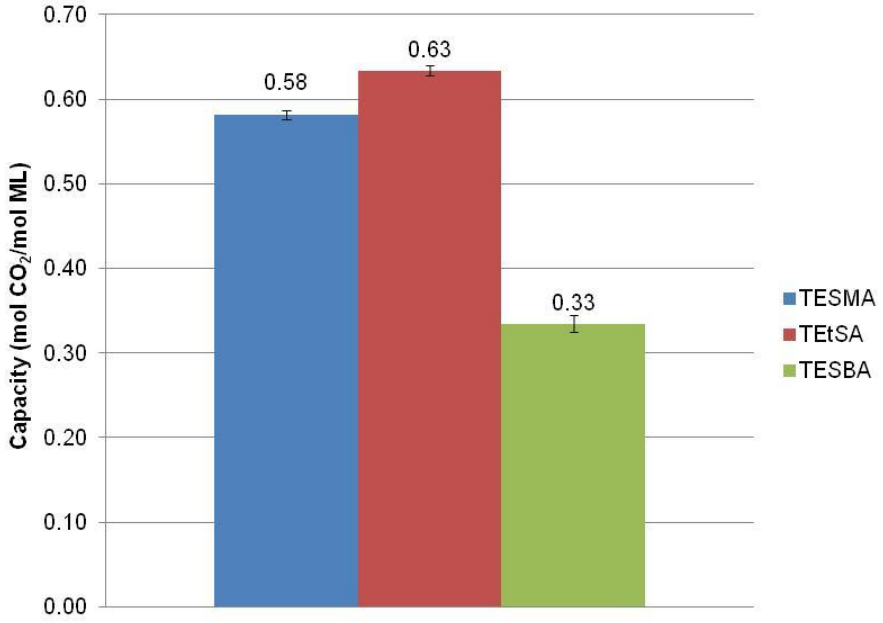


**Figure 5.10.** $CO_2$ capacity as a function of silicon-amine distance in trialkylsilylamines

Equilibrium capacities for the proximity studies show that both the TESMA and TEtSA are significantly superior to the theoretical (chemisorption) of 0.5 mol $CO_2$/mol amine in Figure 5.10. At equilibrium, TESMA and TEtSA had capacities of 0.58 and 0.63 mol $CO_2$/mol amine, respectively. The TESBA (butyl linker) formed a solid upon reaction with $CO_2$. The capacity reached about 66% of its theoretically predicted capacity due to mass transfer limitations upon solid formation. It was observed that TESMA was relatively volatile, significantly more volatile than the other silylamines. Because the initial acid/base reaction to form carbamate/ammonium salts is exothermic, small losses of TESMA by evaporation may have occurred during the $CO_2$ addition. An initial thought was that the steric hindrance from the triethylsilyl functionality on the same carbon that

the amine reactive site was on may hinder the complete reaction of the amine with $CO_2$, however the capacity remained above theoretical prediction. Like the trialkylsilylpropylamines, the formation of carbamic acid in the network of carbamate/ammonium ions was expected, leading to reaction of a percentage of the amine to a 1:1 ratio of $CO_2$:amine.

### 5.3.2 Effects of Si-$NH_2$ proximity on revIL viscosities

Viscosity differences in changing the alkyl chain linker was initially one of the effects that we felt may be the most pronounced. Indeed, it was expected that intra and intermolecular interactions of the silicon and aminewould both play a significant role. Viscosity measurements were conducted at 25°C and 40°C with a cone and plate viscometer.

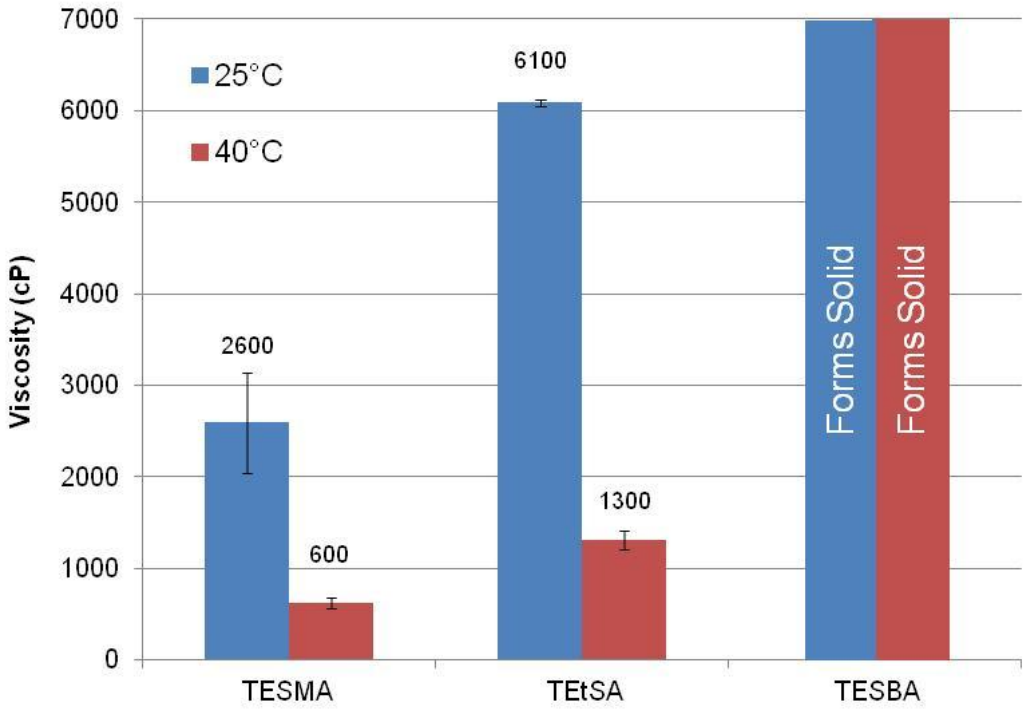


**Figure 5.11.** Viscosity as a function of temperature in trialkylsilylamines with varied silicon-amine distances

Figure 5.11 shows viscosity as a function of chain length between the silicon and nitrogen atoms at both temperatures investigated. Extending the linker chain from one methylene in TESMA to four methylenes in the TESBA, viscosity decreased drastically. In fact, at 25$^{o}$C the TESMA-RevIL exhibited a viscosity of 2600 cP, whereas TEtSA with a propyl linker had a viscosity on the order of 6100 cP. TESBA was a solid upon reaction $CO_2$.

At 40$^{o}$C, the viscosities were much lower with viscosities on the order of hundreds of cP. This was expected since viscosity is a function of temperature. TESMA-RevIL had a viscosity of 600 cP while the TEtSA derivative was slightly higher at 1300 cP.

This viscosity data supports the proximity of silicon and nitrogen play an important role. The interaction of silicon and nitrogen inter and intramolecularly was expected to be disfavored in the methylene linked derivative, TESMA, because of strain in the intramolecular interaction and steric hindrance in the intermolecular interaction. As the length of the alkyl linker was increased, the steric hindrance decreased and intramolecular interaction between the N and the Si also became less favored. This is conjectured to be why the butyl linker actually forms a solid because the amine lone pair can interact with a silicon atom on another molecule of silylamine as well as with itself with much less strain than the methylene linked TESMA.

### 5.3.3 Thermodynamic evaluation of silylamines as a function of silicon-amine proximity

Reversal temperature was measured following the same analytical protocol described in Chapter 4. DSC measurements were conducted on each of the formed RevIL systems. Two endotherms were observed. The first was the reversal of $CO_2$ from the RevIL to molecular liquid and the second was the vaporization of the molecular liquid. The temperature reported for reversal was calculated at the intersection of the tangent of the endotherm to the baseline. The DSC thermogram of TEMSA is shown in Figure 5.12.

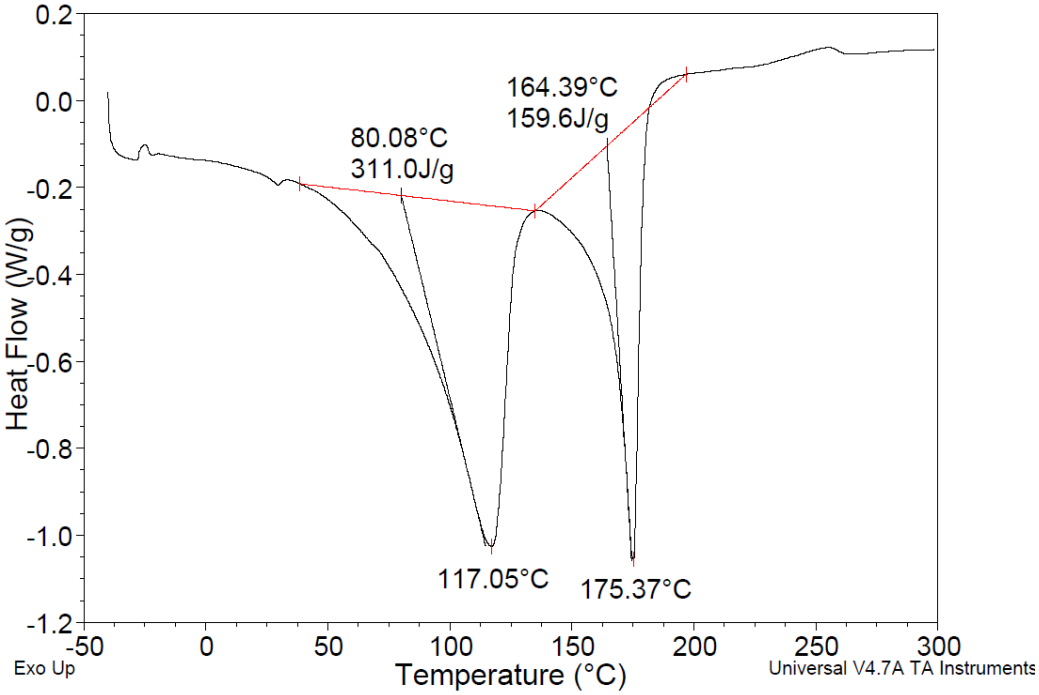


**Figure 5.12.** DSC thermogram of TESMA-RevIL

5.3.3.1 Reversal temperature as a function of Si-$NH_2$ proximity

Although each silylamine exhibited different reversal temperatures, no relationship was evident between reversal temperature and structural changes. The TEMSA-IL had a reversal temperature of about 80°C, the TEtSA at 71°C and the TEBSA melted and reversed beginning at 69°C. The DSC thermogram showing the melting and reversal overlap is shown in Figure 5.13. The TESMA had the highest reversal temperature at 80°C. This is beneficial because standard flue gas conditions operate at 40°C therefore full capture capacities are possible with minimal reversion.

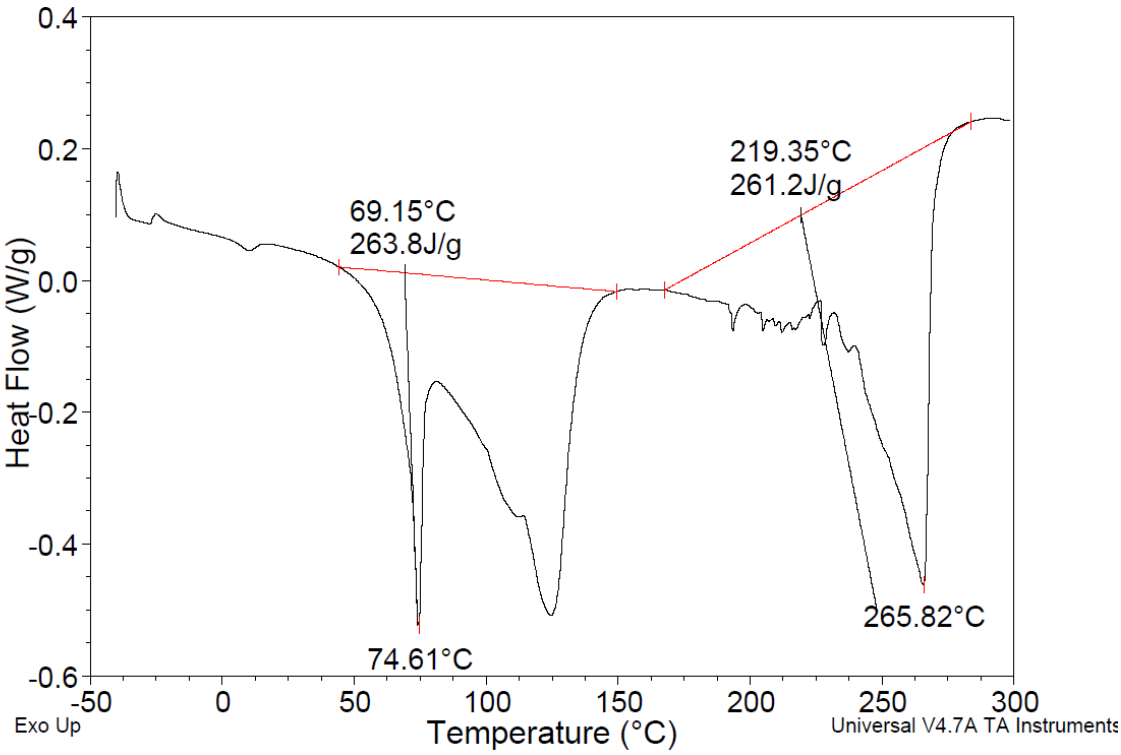


**Figure 5.13.** DSC thermogram of the solid forming TESBA-RevIL

In conclusion, the reversal temperature did not vary significantly between methyl and butyl chain extension.

5.3.3.2 Heats of reversal as a function of Si-$NH_2$ proximity

Enthalpies of reversal were calculated from the amount of heat required to reverse $CO_2$ from the DSC thermograms and are displayed in Table 5.3. The heat was then converted from J/g of sample to kJ/mol $CO_2$, a standard unit for comparison in literature.

**Table 5.3.** Calculated enthalpy of reversal as a function of Si-$NH_2$ proximity

| Structure | Gravimetric Capacity (mol $CO_2$/mol amine) | Enthalpy of Reversal (kJ/mol $CO_2$) |
|---|---|---|
| TESMA | 0.58 | 79 ± 8 |
| TEtSA | 0.63 | 83 ± 6 |
| TESBA | 0.33 | [a] |

[a] Enthalpy could not be calculated accurately based on overlap of melting and reversal peaks

Enthalpy of reaction was found to be the same, within experimental error between the TESMA and TEtSA derivatives. TESMA had a reversal enthalpy of 79 kJ/mol $CO_2$ and TEtSA had a reversal enthalpy of 83 kJ/mol $CO_2$. These enthalpies are on the same order of a 30% aqueous MEA solution (85 kJ/mol $CO_2$ as reported by Kim and Svendsen). TESBA enthalpy of reversal could not be calculated accurately due to overlap of the melting and reversal endotherms.

## 5.4 Conclusions

Understanding the role of the chain length between the silicon and amine $CO_2$ capture properties is extremely informative toward the identification of optimum systems. It was found that capacity higher than theoretical chemisorptions were obtained for two systems, TEMSA and TEtSA. It was also found that increasing the linker length led to increasing viscosity. This data suggests that the TESEA (ethyl linker) molecule could be an optimum candidate for $CO_2$ capture because the viscosity should be lower than the propyl derivative without being as volatile as the TEMSA derivative. The reversal temperature is to be optimum for a $CO_2$ capture system run at 40°C. Because the TESEA derivative seems promising based on the established trends in linker length, a

newly proposed synthetic pathway is highlighted in the conclusions and recommendations chapter.

### 5.5 The Role of order on $CO_2$ capture properties of silylamine revILs

#### 5.5.1 Introduction

The second structural key feature that I modified was the amine reactive site itself from a primary amine to a secondary amine. Order refers to the amine being primary, secondary, or tertiary. Amines used for $CO_2$ capture generally have at least one primary amine such as in MEA or DEA, a mixture of primary and secondary amines, or in the case of piperazine two secondary amines.[12] It has been shown previously that primary amines react instantaneously with $CO_2$. Secondary amines are usually slower, while the tertiary amines are unreactive toward $CO_2$.[13] If a secondary amine reacts at a reasonable rate, they could indeed be valuable candidates for $CO_2$ capture applications. And indeed, it has been documented that secondary amines with low steric hindrance (i.e. methyl groups) are practically faster than their primary counterparts. This may be in part due to their reactions in an aqueous environment. The basicity does increase with order in amines, however it would be expected that bulkier amines would be slower in reaction because they are actually protonated in aqueous conditions as opposed to reacting with $CO_2$. Secondary amines could also possibly limit the ion-pairing ability, expected of increasing the viscosity, and lower the enthalpy of reaction with $CO_2$. As a consequence, secondary silylamines were investigated and compared to their primary amine counterparts for $CO_2$ capture.

Secondary amine derivatives were optimized for low molecular weight trialkylsilylamines with the triethylsilyl and dimethylethylsilyl groups. In practice, formation of secondary amines were prepared from the respective primary amine analogs.

Four structures based on trialkylsilylamines with a propyl linker were selected for this study. Specifically, the structures investigated included TEtSA, *N*-methyl-3-(aminopropyl)triethylsilane (STEtSA), 3-(aminopropyl)dimethylethylsilane (DMESA), and *N*-methyl-3-(aminopropyl)dimethylethylsilane (SDMESA). Their structures are presented in Table 5.4.

## 5.6 Synthesis of secondary amines

**Table 5.4.** Structures of secondary and primary analogs of trialkylsilylamines for $CO_2$ capture

| Structures in the Investigation into Amine Order | | | |
|---|---|---|---|
| TEtSA | STEtSA | DMESA | SDMESA |
| 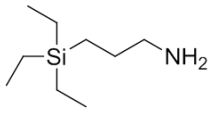 | 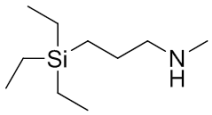 | 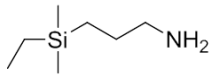 | 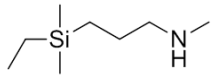 |

In order to keep capacity high, only single methylations were conducted. The synthesis of STEtSA and SDMESA were carried out following the same procedure and mono-methylation was insured by first formylation of the TEtSA or DMESA analogs followed by reduction with $LiAlH_4$. As in the formation of the amines for the proximity studies, detailed experimental procedures and characterization are presented in the experimental methods section at the end of the chapter.

### 5.6.1 Synthesis of STEtSA via formylation and reduction

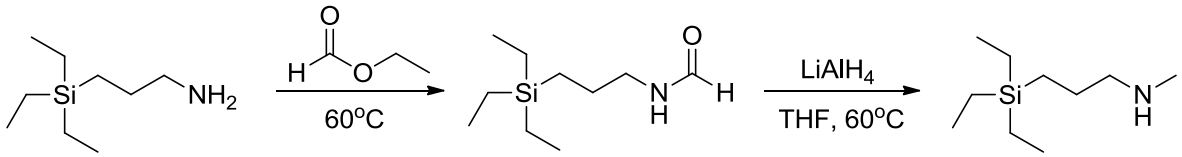


**Figure 5.14.** Synthetic pathway for the mono-methylation of TEtSA

Figure 5.14 shows the synthetic strategy for the formation mono-methylated TETSA derivative. Preformed TEtSA was reacted with ethyl formate under neat conditions in an argon atmosphere at 60°C.[14] Reaction was carried out for 4 hrs before cooling. The solvent and by-product (EtOH) were removed by rotary evaporation. The formamide was then reacted with a 1M $LiAlH_4$ in THF solution in THF at 60°C. After 18 hrs, water was added followed by addition of a 10% NaOH aqueous solution. The mixture was filtered through celite and the solid was washed with hexane and methanol. The filtrate was washed with brine, dried over $MgSO_4$ to provide the desired secondary amine which was purified by vacuum distillation.

### 5.6.2 Synthesis of SDMESA via formylation and reduction

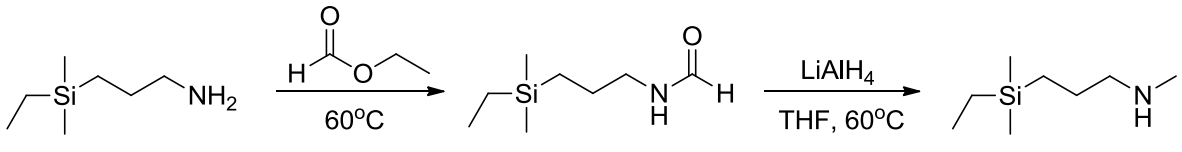


**Figure 5.15.** Synthetic pathway for the mono-methylation of DMESA

The synthesis of the SDMESA was synthesized by the same method as the STEtSA and is shown in Figure 5.15. Solid $LiAlH_4$ was added through solid addition funnel instead of a preformed 1M $LiAlH_4$ solution in THF. Vacuum distillation provided the pure product.

It was hypothesized that silylated secondary amines would have a lower enthalpy of reaction with $CO_2$ than their primary counterparts, lower viscosities and lower reversal temperature due to steric destabilization of the carbamate formed. Methylated secondary amines were also hypothesized to maintain high capacities. STEtSA and SDMESA were reacted with $CO_2$ and compared to their primary amine counterparts highlighted in the previous chapter.

## 5.7 Results and Discussion

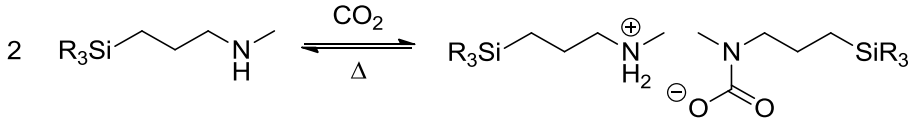


**Figure 5.16.** Reaction of secondary amines with $CO_2$ to form RevILs

The two secondary amines, SDMESA and STEtSA were reacted with $CO_2$ via standard protocol described in Chapter 4. The reaction of these amines with $CO_2$ is shown in Figure 5.16. A known amount of secondary amine was added to a dram vial and bubbled with $CO_2$ through a diffuser tube at a flow rate of $CO_2$ at 200 mL/min for 200 minutes. The diffuser tube was stirred to ensure good mixing during reaction. After conversion to the ionic liquid form, analytical measurements were taken to investigate capacity, viscosity, and thermodynamic parameters.

### 5.7.1 $CO_2$ capacity as a function of revIL structure and amine order

One of the key factors when choosing methylated secondary amines was that major changes in properties could be achieved while maintaining high capacity. It had been mentioned previously that methylated secondary amines had a faster rate of reaction than the primary counterparts in aqueous conditions. It was found that in anhydrous conditions, the rate of reaction was actually slower than the primary amine counterparts. It was found that for STEtSA, equilibrium capacities were reached after 200 minutes of reaction (Figure 5.17), whereas TEtSA, the primary amine only required about 13 minutes to reach equilibrium.

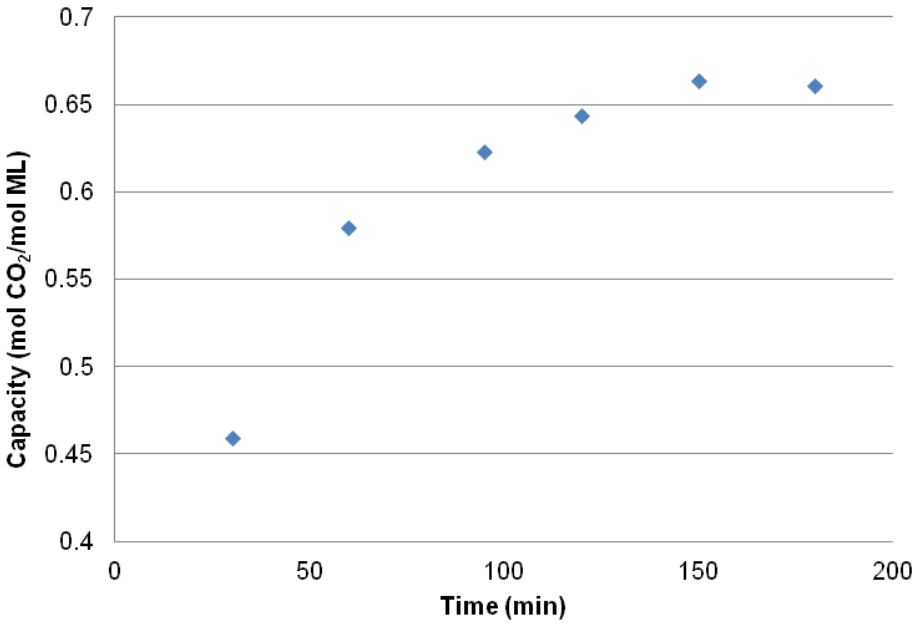


**Figure 5.17.** Capacity as a function of time for the formation of STEtSA-RevIL at 25°C

The secondary amines were sparged for 200 minutes and the primary amines in comparison were reacted for 75 minutes. The gravimetric capacities were then measured by direct measurements of the mass uptake. Shown in Figure 5.18 are the gravimetric capacities of both the primary and secondary amine derivatives of TEtSA and DMESA.

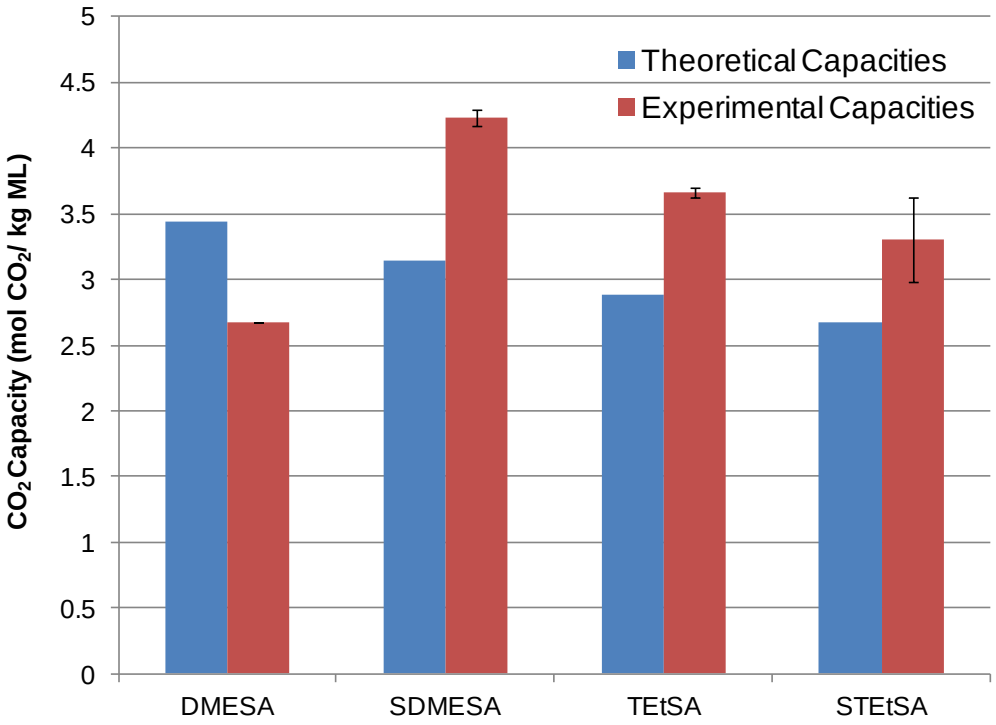


**Figure 5.18.** $CO_2$ capture capacity as a function of structure in primary and secondary trialkylsilylamines

Although the reaction of secondary amines with $CO_2$ is slower, it was found that they do go to completion, achieving capacities higher than expected from solely theoretical chemical absorption (based on 0.5 mol $CO_2$/mol amine). This enhanced

capacity was attributed to chemical and physical absorption, as well as carbamic acid formation. The SDMESA had the highest capacity at 4.2 mol $CO_2$/kg amine. The DMESA primary amine formed a solid upon reaction with $CO_2$ and did not go to completion because of mass transfer limitations. As expected, as molecular weight of the molecular liquid increased from DMESA to STEtSA, the overall capacity decreased. High capacities due to carbamic acid at these conditions of formation are valuable in maximizing $CO_2$ capture efficiency. The order of amine was not found to have an effect on the experimental capacities of these systems. Thermodynamic properties were then investigated of the formed RevILs.

### 5.7.2 Thermodynamic parameters (reversal temperature and reaction enthalpy) of secondary amine revILs

For comparison purposes, reversal temperatures of primary amines TEtSA and DMESA are compared along to the secondary amine analogs, STEtSA and SDMESA in this section. DSC measurements were taken for the formed STEtSA and SDMESA ionic liquids upon reaction with $CO_2$ and their thermograms are provided below. There were two distinct endothermic events in the thermograms corresponding to ionic liquid reversal to the molecular liquid and vaporization of the molecular liquid.

Figure 5.19 below is a representative thermogram of the DMESA-RevIL. Because this amine formed a solid with exposure to $CO_2$, there are three distinct endotherms corresponding to melting of the ionic solid, reversal of $CO_2$, and evaporation of the molecular liquid. It was found that melting and reversal partially overlapped.

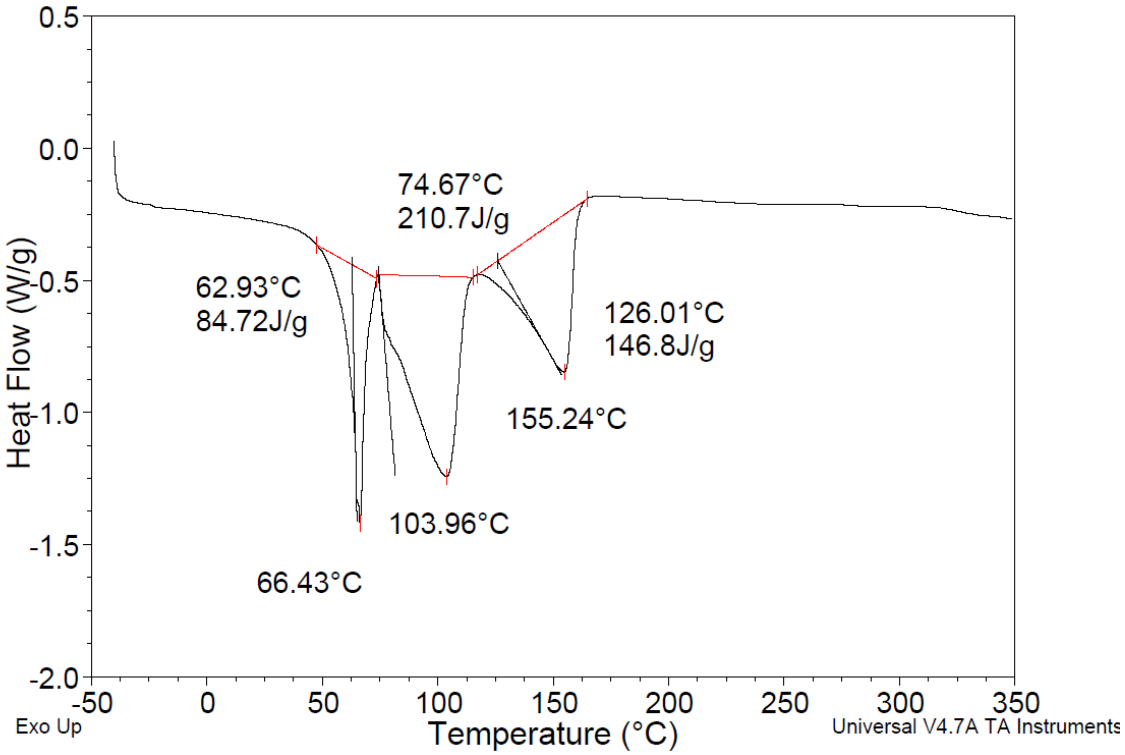


**Figure 5.19.** DSC thermogram of solid forming DMESA-RevIL

The TEtSA, STEtSA, and SDMESA did form liquids upon reaction with $CO_2$ and evidence of only two endotherms were present in their DSC thermograms.

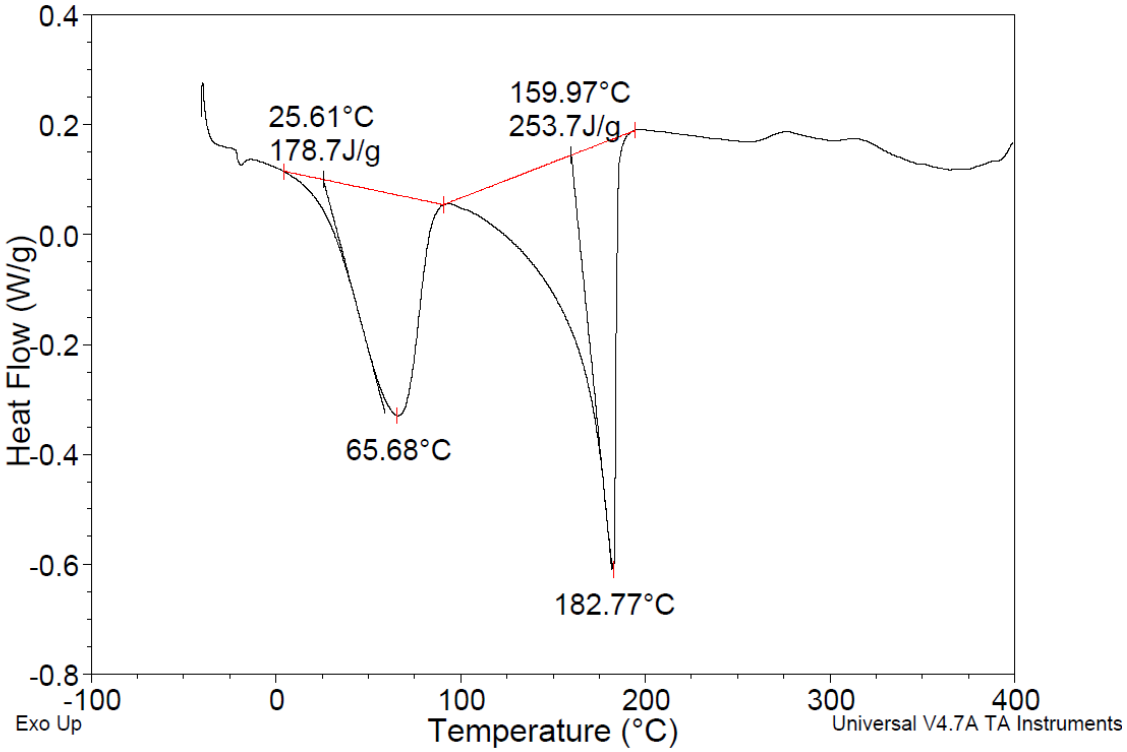


**Figure 5.20.** DSC thermogram of liquid forming STEtSA-RevIL

A representative example of the STEtSA-RevIL is shown in Figure 5.20 above. The reversal begins at 25°C. The relatively low reversal temperature was quite surprising even though a reversal temperature depression was expected due to the methyl groups steric hindrance and low carbamate stability.

**Table 5.5.** Reversal temperature and enthalpy of reaction as a function of structure

| RevIL system | Reversal Temperature (°C) | Enthalpy of Reaction (kJ/mol $CO_2$) | Evaporation Temperature (°C) | $T_{evap}$-$T_{rev}$ (°C) |
|---|---|---|---|---|
| **TEtSA** | 71 ± 3 | 81 ± 3 | 168 ± 12 | 97 |
| **STEtSA** | 25 ± 6 | 72 ± 14 | 140 ± 25 | 115 |
| **DMESA** | 63[a] | [b] | 126 | 63 |
| **SDMESA** | 36 ± 2 | 76 ± 3 | 134 ± 16 | 98 |

[a]Reversal and Melting are overlapping events and this system was run once [b]Enthalpic contributions could not be distinguished between reversal and melting

From the data presented in Table 5.5, it appeared that the order of the amine had a major effect on reversal temperature. From TEtSA, the primary amine, reversal temperature occured at 71°C whereas reversal in STEtSA occurs over 40°C lower at 25°C. As a result, the SDMESA was considered, synthesized, and reacted with $CO_2$. The SDMESA was expected to exhibit a higher reversal temperature than the STEtSA. In fact, this is exactly what was observed. The SDMESA reversal temperature was 36°C, about 11°C higher than the triethyl substitution around the silicon.

Secondary amine derivatives were expected to have lower enthalpies of reaction with respect to $CO_2$ absorption than the primary counterparts because secondary carbamates are less stable than primary carbamates. In fact, the enthalpy of reaction with $CO_2$ dropped almost 10 kJ/mol of $CO_2$ in the secondary derivatives in comparison to the primary derivatives.

### 5.7.3 Effect of amine order on RevIL viscosities

RevILs were subjected to $CO_2$ and allowed to reach full conversion and the viscosity of each RevIL system was measured at both 25°C and 40°C. The viscosity with respect to structure in shown in Figure 5.21.

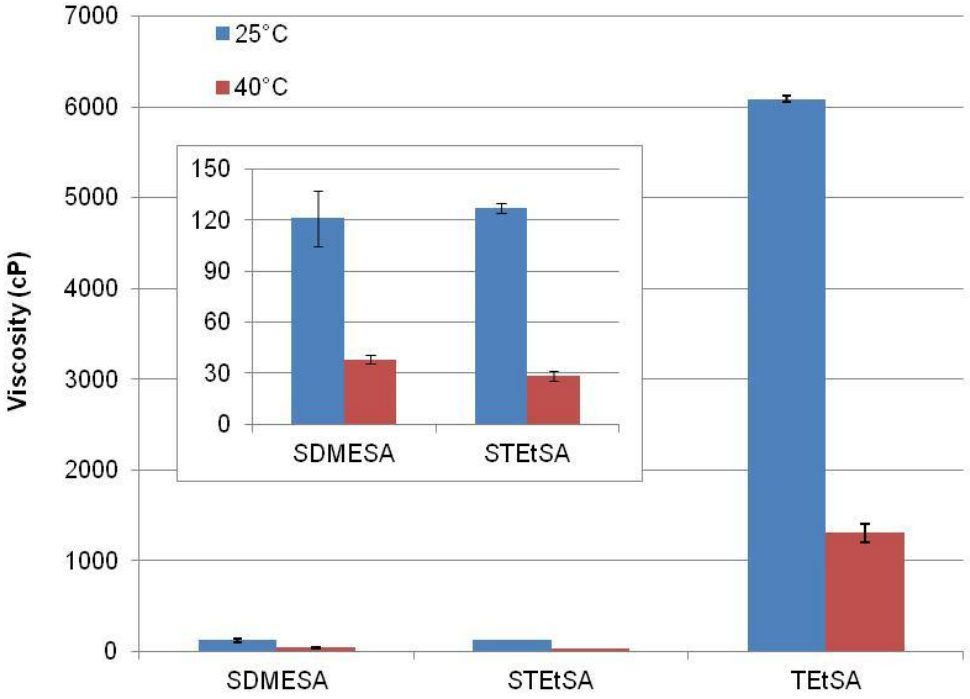


**Figure 5.21.** Viscosity as a function of RevIL structure at 25°C and 40°C for primary and secondary amines

As expected, viscosity decreased in all cases with increase in temperature from 25 to 40°C. The reaction of DMESA with $CO_2$ did form a solid which reversed upon melting and is not reported here. When adding a methyl group to the primary amine in DMESA to form the SDMESA, the viscosity did decrease tremendously.

The addition of a methyl group to the primary amine of trialkylsilylpropylamines decreased the viscosity at a given temperature drastically. At 25°C, TEtSA-IL had a viscosity of 6100 cP whereas the STEtSA-IL had a viscosity of 130 cP. It should be noted that viscosities could be lower due to partial reversal during the viscosity measurement leading to a viscosity measurement of an incompletely converted mixture of molecular and ionic liquid. Shown in the inset of the graph are the viscosities of the SDMESA and STEtSA at 25 and 40°C. At 40°C, complete reversal was documented by NMR analysis and therefore no accurate viscosity measurement can be reported.

## 5.8 Conclusions

Secondary amines were investigated in parallel to the primary amine counterparts and it was found that methylation of a primary amine resulted in systems having low reversal temperatures, as low as 25°C for the STEtSA derivative. Capture, although slower than the primary amine counterparts, resulted in capacities higher than predicted by chemical or physical absorption with both SDMESA and STEtSA having capacities of 4.2 and 3.3 mol $CO_2$/ kg amine which translates to molar ratios of 0.64 and 0.62, higher than 0.5 predicted by chemisorption. By analogy with our previous data, this was attributed to the formation of carbamic acid. The viscosities of these systems were much lower than the primary amine counterparts and partially could have resulted from reversal of $CO_2$ during the viscosity measurements. Although these low temperatures of reversal may not be conducive to flue gas capture applications, low temperature capture and release could be effective.

## 5.9 Experimental Methods

### 5.9.1 $CO_2$ reactions:

Reactions of molecular liquids were performed by syringing a sample of the desired molecular liquid from the glove box into a dram vial. The vial was capped with a septum and a diffuser tube attached to a $CO_2$ line was used to introduce $CO_2$. $CO_2$ was flowed through the samples at a flow rate of 200 mL/min for 75-200 minutes. The diffuser tube was stirred in the solution as the reaction progressed to ensure mixing. The formed RevIL was then subjected to analytical experiments to understand the role of structure on RevIL properties. Gravimetry was performed by preweighing the vial and septum as well as the diffuser tube. The mass of the starting material was weighed and the entire system reweighed upon reaction with $CO_2$. Uptakes were calculated by subtracting the initial mass from the final mass.

### 5.9.2 DSC/TGA:

DSC measurements were performed in triplicate with a Q20 TA DSC Instrument. Sample weight was recorded in an aluminum hermetic pan crimped with an aluminum lid and measured against an empty pan. The DSC was calibrated with an Indium standard. Samples were held at -40$^{o}$C and ramped to 400°C at a ramp rate of 5°C/min. Reversal temperature was determined from the intersection of two tangents drawn at the beginning and bottom of the reversal endotherm. A similar treatment was used to determine the temperature of evaporation. Heat of regeneration was calculated by integrating the reversion endotherm with respect to time.

### 5.9.3 Viscometry:

The viscosity of each ionic liquid was measured using a Rheosys Merlin II cone and plate viscometer. Samples were applied to the plate and were allowed to reach thermal

stability prior to data collection. Shear rates varied between 10 and 2000 $s^{-1}$. The average viscosity over the shear range was recorded.

### 5.9.4 Synthetic Methods

***triethyl(chloromethyl)silane***: A 217.5 mL (0.435 mol) portion of ethyl magnesium chloride (2M in THF) solution was added to a 1-L round bottomed flask under nitrogen atmosphere. The solution was cooled to 0°C with an ice bath. Separately, trichloro(chloromethyl)silane (25 g, 0.136 mol) was dissolved in anhydrous THF (200 mL) in an addition funnel under argon. The trichloro(chloromethyl)silane solution was added dropwise to the stirring Grignard over the course of about an hour. After complete addition, the solution was removed from the ice bath and allowed to reach room temperature. Precipitation of $MgCl_2$ was evident and the solution was allowed to stir vigorously overnight where the mixture became unable to be stirred. Saturated sodium bicarbonate solution was added slowly and the solids were then filtered under vacuum and washed with THF. The aqueous layer was separated and washed with more THF and DCM. These organics were recombined with the original organic layer. It was washed with brine, dried over $MgSO_4$, and the solvents removed at 65 torr to yield 21.44 g of the desired triethyl(chloromethyl)silane in 85% yield. $^{1}$HNMR (400 Hz, $CDCl_3$) 2.84 (s, 2H), 0.97(t, 9H), 0.65(q, 6H) $^{13}$CNMR (400 Hz, $CDCl_3$) 27.55, 7.14, 2.20 Expected: C(51.03), H(10.40) Actual: C(50.98), H(10.32)

***2-((triethylsilyl)methyl)isoindoline-1,3-dione***: Trichloro(chloromethyl)silane (20.15 g, 0.12 mol) was added to a stirring mixture of potassium phthalimide (27.83 g, 0.15 mol) and anhydrous $K_2CO_3$ (2.9 g, 0.02 mol) in anhydrous DMF (200 mL) under argon. The mixture was brought to 100°C and stirred for 20 hours. After cooling to room temperature, ice water (300 mL) was added, followed by 200 mL of diethyl ether. The ethereal layer was separated from the aqueous layer and washed with brine and dried

over MgSO4. The aqueous layer was brined with solid NaCl, washed twice more with 100 mL portions of ether, and the organic layer separated, washed with brine, dired over MgSO4 and combined with the original organic layer. The solution was rotovapped at 70°C under vacuum to yield 26.47 g of 2-((triethylsilyl)methyl)isoindoline-1,3-dione in 80% yield. $^{1}$HNMR (400 Hz, $CDCl_3$) 7.77 (m, 2H), 7.65 (m, 2H), 3.21 (s, 2H), 0.96 (t, 9H), 0.61 (q, 6H) $^{13}$CNMR (400 Hz, $CDCl_3$) 168.47, 133.54, 132.28, 122.80, 25.15, 7.07, 3.04 Expected: C(65.41), H(7.69), N(5.09) Actual: C(65.13), H(7.71), N(5.04)

***(aminomethyl)triethylsilane (TESMA)***: 2-((Triethylsilyl)methyl)isoindoline-1,3-dione (25.92 g, 0.0945 mol) was dissolved in anhydrous MeOH (315 mL) under an inert atmosphere and stirred with mechanical stirring. Anhydrous hydrazine (8.9 mL, 0.284 mol) was added in one portion to the MeOH solution and the temperature of the solution was brought to 60°C. During the course of the reaction, phthalylhydrazide formation was evidenced by a cloudy-gel like precipitate. After 5 hours of reaction, the solution was cooled and 2M HCl was added until a solid white precipitate was formed in the single aqueous phase. The solid was filtered under vacuum and washed with more 2M HCl. The collected liquid layer was then basified with 1M NaOH until a pH of 14 was reached. Diethyl ether was added to extract the amine product. The ether was then washed with brine, dried over $MgSO_4$ and removed at 45°C by distillation. The crude (aminomethyl)triethylsilane was attempted to be distilled under argon but it was noticed that as the temperature increased to 170°C a yellow sludge formed in the distillation flask. The heat was removed and the crude distilled at 25°C at 0.6 mmHg to give 3.63 g of pure (aminomethyl)triethylsilane in a 27% isolated yield. $^{1}$HNMR (400 Hz, $CDCl_3$) 2.24 (s, 2H), 1.74 (s, 2H), 0.95 (t, 9H), 0.57 (q, 6H) $^{13}$CNMR (400 Hz, $CDCl_3$) 26.68, 7.36, 2.10 Expected: C(57.86), H(13.18), N(9.64) Actual: C(56.56), H(13.28), N(9.13)

***2-(aminoethyl)triethylsilane (TESEA) via PTC reactions***:

Multiple reaction conditions were used to synthesize 2-(aminoethyl)triethylsilane through phase-transfer catalyzed reactions.

Triethyl(chloromethyl)silane (4.94 g, 0.03 mol) was added to a 100 mL RB under nitrogen atmosphere. Anhydrous THF (30 mL) was added followed by NaCN (3.04 g, 0.06 mol). The mixture was vigorously stirred and tetra-butyl ammonium chloride (0.172 g, 0.6 mmol) was added last. The mixture was brought to 66°C and reacted overnight. The reaction was then cooled and the solids filtered. The THF solvent was removed by rotovap and only starting material was recovered. No reaction occurred.

TBACl (0.054 g, 0.15 mmol) and NaCN (0.294 g, 0.006 mol) were added to a mixture of toluene and water (19 mL and 1 mL). The reactants and catalyst were stirred until conditioned (smooth suspended powder). Triethyl(chloromethyl)silane (0.525 g, 0.003 mol) was then added and the solution refluxed at 110°C for 6 days. To the mixture was added more toluene and water. The toluene layer was extracted with brine multiple times to remove PTC and dried with $MgSO_4$. After evaporation of the toluene, only starting material remained. No reaction had taken place.

Triethyl(chloromethyl)silane (0.506 g, 0.003 mol) was added to anhydrous DMSO (20 mL) along with NaCN (0.311 g, 0.006 mol). The mixture was heated to 100°C and stirredfor 48 hours under nitrogen atmosphere. The solution was then cooled to room temperature and ether and water were added. A cloudy white ether layer existed above the dark brown aqueous layer. The organic layer was then separated from the aqueous layer and washed with water, brine, and dried with $MgSO_4$. After evaporation of ether, nothing remained in the flask. It was expected that if product had formed, it was not extractable from the aqueous layer.

KCN (1.56 g, 0.024 mol) and TBACl (0.1668 g, 0.6 mmol) were stirred in 10 mL of toluene overnight at 90°C to condition the catalyst and salt. The triethyl(chloromethyl)silane (1.025 g, 0.006 mol) was added and the reaction was conducted at 90°C for 24 hours. After 24 hours, a $^{1}$HNMR showed only starting material and no product.

KCN (1.54 g, 0.024 mol) and 18-crown-6 (0.162 g, 0.6 mmol) were stirred in 10 mL of toluene overnight at 90°C to condition the catalyst and salt. 18-crown-6 is specifically used for potassium salts. The triethyl(chloromethyl)silane (0.95 g, 0.006 mol) was then added and the reaction was conducted at 90°C for 24 hours. Like the ammonium PTC reaction, the only species visible by $^{1}$HNMR was the starting material.

Triethyl(chloromethyl)silane (2.091 g, 0.012 mol) was added to a RB flask under nitrogen atmosphere followed by addition of KCN (3.915 g, 0.048 mol) and TBACl (0.353 g, 1.2 mmol). The mixture was brought to 100°C and reacted for 24 hours. After 24 hours, $^{1}$HNMR only showed starting material and no product formation.

***2-(aminoethyl)triethylsilane (TESEA) via boronation/amination:***

Two methods were designed to synthesize TESEA via boronation/amination routes. The first was boronation with $BH_3$, the second with a methylated boron derivative.

Triethylvinylsilane (10.0 g, 0.0703 mol) was added to anhydrous THF (11.2 mL) in a flame-dried RB flask. The solution was cooled with an ice bath and borane (1M in THF) (26 mL, 0.026 mol) was added dropwise over about 30 minutes. After addition, the ice bath was removed and the solution was stirred at room temperature for 1 hr. Hydroxylamine-*O*-sulfonic acid (7.90 g, 0.0703 mol) was added under an increased argon flow. The reaction was exothermic and the mixture was brought to THF reflux. After 3 hrs, the $^{1}$HNMR showed no evidence of the alkene but little formation of the triplet indicative of the desired amine. After 18 hrs, the $^{1}$HNMR looked the same. The reaction

was cooled after 18 hrs and 50 mL of 1M HCl was added. MTBE was added and 3 phases were present. The MTBE layer was separated and the aqueous layer was basified with a 10% NaOH solution. MTBE was added to extract the desired amine product, washed with brine, and dried with $MgSO_4$. The MTBE layers prior to basification and after basification were rotovapped separately. The mass spec of the second layer showed primarily remaining solvent, the first layer showed high MW species corresponding to the starting material and product boron complexes. These fractions were recombined and stirred with 2M HCl at 60°C for an hour. After the same purification procedure was done, the result had not changed. To address this, a methylated boron species was created in order to facilitate the amination step.

Triethylvinylsilane (10.0 g, 0.0703 mol) was added to 25 mL anhydrous dichloromethane in a RB flask under argon. The solution was cooled to 0°C with an ice bath. Chloroborane-dimethylsulfide complex (3.59 mL, 0.0344 mol) was added slowly over 30 minutes. The solution was then removed from the ice bath and stirred at room temperature overnight. During reaction, the solution changed from colorless to pale yellow but then became colorless again. An aspirator was used to remove the dichloromethane and the result was a colorless oily substance which was immediately added anhydrous pentane (53 mL). $Al(Me)_3$ (2M in hexane ) (11.7 mL, 0.0234 mol) was added slowly to the solution at 0°C. The addition of the aluminum species led to the precipitation of a white precipitate which became soluble and a brown precipitate then formed after reaction at room temperature for 1 hr. This has been proposed to be $AlCl_3$. The solution was then cannulated under vacuum to another flask under argon. 23 mL of a saturated ammonium chloride solution as added and a white precipitate formed. Upon separation, the di-(silyl)methylborane was redissolved in water and hexane was added. The hexane layer was then removed, washed with brine and dried over $MgSO_4$ which

was vacuum filtered and the solvent rotovapped. A clear oil remained after evaporation. The oil was added to 87 mL of anhydrous THF under argon. Hydroxylamine-*O*-sulfonic acid (17.69 g, 0.148 mol) was added via solid addition arm at RT. The reaction was stirred vigorously overnight. 3 more equivalents of hydroxylamine-*O*-sulfonic acid were added to the mixture and the mixture stirred for another 24 hours. The reaction was stopped by added 50 mL of 2M HCl, 10 mL methanol, and 20 mL $H_2O$. This solution was stirred for 0.5 hours. Diethyl ether (50 mL) was then added. The organic layer was separated from the aqueous layer. It was a deep yellow color. After basification of the aqueous layer with 1M NaOH and re-extraction with ether, the ether layer was dried and rotovapped but nothing remained. The initial organic layer showed no product by $^1$HNMR.

***3-(aminopropyl)triethylsilane (TEtSA)***: To a 3-neck 250 mL round bottomed flask fitted with a condenser under inert atmosphere was added 80 mL anhydrous toluene (0.751 mol), triethylsilane (25.5 mL, 0.160 mol), and Pt-DVDS (1.2 mL of a 2 wt% Pt-DVDS in xylenes solution, 0.32 mmol). This solution was allowed to stir at room temperature for approximately five minutes, at which point allylamine (24 mL, 0.320 mol) was added and the reaction was heated to 110°C overnight. Reaction progress was monitored via $^1$H NMR for the disappearance of the starting silane. The reaction mixture was allowed to cool to room temperature and the solvent and excess allylamine were removed via rotavap. The product 3-(aminopropyl)triethylsilane was distilled under a 2 mmHg vacuum at 80°C to yield 24.8 g of desired product in 89% yield. $^1$HNMR (400 Hz, $CDCl_3$) 2.63 (t, 2H), 1.39 (sex, 6H), 1.08 (s, 2H), 0.90 (t, 9H), 0.49 (q, 8H) $^{13}$CNMR (400 Hz, $CDCl_3$) 45.47, 27.88, 18.63, 7.90, 6.95, 2.87 Expected: C(62.35), H(13.37), N(8.08) Actual: C(62.41), H(13.42), N(7.94)

***4-(aminobutyl)triethylsilane (TESBA)***: Pt-DVDS ((2% Pt in xylenes solution) 8.01 mL, 0.7 mmol) was added to triethylsilane (12.21 g, 0.105 mol) in a 250 mL RB flask under nitrogen atmosphere. The solution became dark yellow. To it was added anhydrous toluene (40 mL) followed by 4-amino-1-butene (5.0 g, 0.0703 mol). The solution was heated to 80°C and reacted for 20 hours. The solution became dark brown after about 30 minutes of stirring. After 20 hours, the $^{1}$HNMR confirmed disappearance of the starting material and the reaction was cooled and the solvent and excess triethylsilane was rotovapped. The crude residue was distilled at a vacuum of 1.95 mmHg and the product distilled at 68°C. 8.67 g of desired 4-(aminobutyl)triethylsilane was isolated to provide a yield of 66%. $^{1}$HNMR (400 Hz, $CDCl_3$) 2.62 (t, 2H), 1.40 (p, 2H), 1.27 (s, 2H), 1.17 (s, 2H), 0.86 (t, 9H), 0.44 (q, 8H) $^{13}$CNMR (400 Hz, $CDCl_3$) 41.83, 37.95, 21.04, 11.09, 7.32, 3.16 Expected: C(64.09), H(13.45), N(7.47) Actual: C(62.34), H(13.33), N(6.92)

***N-(3-(triethylsilyl)propyl)formamide***: 3-(Aminopropyl)triethylsilane (8.69 g, 0.05 mol) was added to a RB flask under argon. Ethylformate (5.25 mL, 0.065 mol) was added dropwise over 15 minutes at 10°C. The temperature of the solution was increased to 60°C and stirred for 3 hours. The solution was then cooled and rotovapped to remove the by-product, EtOH, and excess ethylformate to provide 9.72 g of N-(3-(triethylsilyl)propyl)formamide in 97% yield. $^{1}$HNMR (400 Hz, $CDCl_3$) 8.13 (s)/8.01 (d)(1H), 5.96 (s, 1H), 3.23 (q)/3.15 (q) (2H), 1.47 (s, 2H), 0.89 (t, 9H), 0.48 (q, 8H) $^{13}$CNMR (400 Hz, $CDCl_3$) 161.19, 41.43, 24.09, 8.51, 7.37, 3.13

***N-methyl-3-(triethylsilyl)propan-1-amine***: *N*-(3-(Triethylsilyl)propyl)formamide (8.49 g, 0.042 mol) was added to 80 mL of anhydrous THF under an inert atmosphere in a RB flask. The solution temperature was brought to 60°C and 50.7 mL of a (1M in THF) $LiAlH_4$ solution was added slowly over 45 minutes. The temperature increased upon

addition. After stirring for 18 hours at 60°C, the resulting mixture was cooled and to it was added 2.5 mL $H_2O$ followed by 5 mL of a 10% NaOH solution. 10.5 mL of $H_2O$ were then added and the entire mixture was filtered through a pad of celite and washed with hexane and MeOH. The collected solution was then introduced into a separatory funnel and the organic layer was separated. The aqueous layer was washed with hexane and the organic layer was combined with the previous. They were both washed with brine and dried over $MgSO_4$. The solvents were removed via rotovap distillation. The resulting liquid was distilled under reduced pressure at 1 mmHg and 48°C to provide 5.68 g of the N-methyl-3-(triethylsilyl)propan-1-amine corresponding to a 73% isolated yield. $^1$HNMR (400 Hz, $CDCl_3$) 2.54 (t, 2H), 2.42 (s, 3H), 1.46 (s, 2H), 1.37 (s, 1H), 0.91 (t, 9H), 0.50 (q, 8H) $^{13}$CNMR (400 Hz, $CDCl_3$) 55.70, 36.37, 24.09, 8.73, 7.42, 3.23 Expected: C(64.09), H(13.45), N(7.47) Actual: C(63.12), H(13.47), N(7.47)

***N-(3-(dimethylethylsilyl)propyl)formamide***: 3-(Aminopropyl)dimethylethylsilane (7.3 g, 0.05 mol) was added to a RB flask under argon. Ethylformate (5.25 mL, 0.065 mol) was added dropwise over 15 minutes at 10°C. The temperature of the solution was increased to 60°C and stirred for 4 hours. The solution was then cooled and rotovapped to remove the by-product, EtOH, and excess ethylformate to provide 8.47 g of N-(3-(dimethylethylsilyl)propyl)formamide in 98% yield. $^1$HNMR (400 Hz, $CDCl_3$) 8.14 (s)/ 8.00 (d) (1H), 5.79 (s, 1H), 3.25 (q)/3.16(q) (2H), 1.48 (s, 2H), 0.89 (t, 3H), 0.47 (q, 4H), -0.06 (s, 6H) $^{13}$CNMR (400 Hz, $CDCl_3$) 161.11, 41.28, 24.12, 11.92, 7.25, 6.68, 4.07

***3-(dimethylethylsilyl)-N-methylpropan-1-amine***: *N*-(3-(Dimethylethylsilyl)propyl)formamide (7.83 g, 0.0452 mol) was added to 120 mL of anhydrous THF under an inert atmosphere in a RB flask. The solution temperature was brought to 60°C and solid $LiAlH_4$ (3.091 g, 0.081 mol) was added slowly via solid addition arm over 30 minutes. After stirring for 18 hours at 60°C, the resulting mixture was cooled

with a dry/ice acetone bath to keep the temperature at about 0°C. To it was added 3 mL $H_2O$ followed by 6 mL of a 10% NaOH solution. 12 mL of $H_2O$ were then added and the entire mixture was filtered through a pad of celite and washed with THF and $H_2O$. The collected solution was then introduced into a separatory funnel and heavily brined with NaCl. The organic layer was separated. The aqueous layer was washed with hexane and the organic layer was combined with the previous. They were both washed with brine and dried over $MgSO_4$. The solvents were removed via rotovap distillation. The resulting liquid was distilled under reduced pressure at 3.4 mmHg and 36°C to provide 3.54 g of the N-methyl-3-(dimethylethylsilyl)propan-1-amine corresponding to a 49% isolated yield. $^{1}$HNMR (400 Hz, $CDCl_3$) 2.47 (t, 2H), 2.35 (s, 3H), 1.40 (s, 2H), 1.00 (s, 1H), 0.84 (t, 3H), 0.40 (q, 2H), -0.12 (s, 6H) $^{13}$CNMR (400 Hz, $CDCl_3$) 55.47, 36.32, 24.10, 12.15, 7.21, 6.73, -4.10 Expected: C(60.30), H(13.28), N(8.79) Actual: C(58.97), H(13.17), N(8.42)

## 5.10 References


(1) Shirota, H.; Castner, E. W. *Journal of Physical Chemistry B* **2005**, *109*, 21576.

(2) Chuit, C.; Corriu, R. J. P.; Reye, C.; Young, J. C. *Chemical Reviews* **1993**, *94*, 1371.

(3) Gerlach, D.; Brendler, E.; Heine, T.; Wagler, J. *Organometallics* **2007**, *26*, 234.; Hagen, A. P.; Callaway, B. W. *Journal of Inorganic & Nuclear Chemistry* **1972**, *34*, 487.

(4) Sidorkin, V. E.; Belogolova, E. F.; Pestunovich, V. A. *Chemistry-a European Journal* **2006**, *12*, 2021.

(5) Blasucci, V.; Dilek, C.; Huttenhower, H.; John, E.; Llopis-Mestre, V.; Pollet, P.; Eckert, C. A.; Liotta, C. L. *Chemical Communications* **2009**, 116.; Bacsik, Z.; Atluri, R.; Garcia-Bennett, A. E.; Hedin, N. *Langmuir* **2010**, *26*, 10013.

(6) Perry, R. J.; Grocela-Rocha, T. A.; O'Brien, M. J.; Genovese, S.; Wood, B. R.; Lewis, L. N.; Lam, H.; Soloveichik, G.; Rubinsztajn, M.; Kniajanski, S.; Draper, S.; Enick, R. M.; Johnson, J. K.; Xie, H.-b.; Tapriyal, D. *ChemSusChem* **2010**, *3*, 919.

(7) Schirlin, D. G., et al. "Substituted Silyl Alkylene Amines." US Patent 5,384,312, Jan. 24, **1995**.

(8) Amundsen, L. H.; Nelson, L. S. *Journal of the American Chemical Society* **1951**, *73*, 242.

(9) Rathke, M. W.; Inoue, N.; Varma, K. R.; Brown, H. C. *Journal of the American Chemical Society* **1966**, *88*, 2870.

(10) Brown, H. C.; Kim, K. W.; Srebnik, M.; Singaram, B. *Tetrahedron* **1987**, *43*, 4071.

(11) Marzinke, et al. "Method for the Preparation of Aminopropyl or Aminoalkyl Functional Polyalkyl or Aryl Siloxanes." US Patent 6,177,583 B1, Jan. 23, **2001**.

(12) Bishnoi, S.; Rochelle, G. T. *Chemical Engineering Science* **2000**, *55*, 5531.; Glasscock, D. A.; Critchfield, J. E.; Rochelle, G. T. *Chemical Engineering Science* **1991**, *46*, 2829.

(13) Sartori, G.; Savage, D. W. *Industrial & Engineering Chemistry Fundamentals* **1983**, *22*, 239.

(14) Dai, H.; Chang, P. R.; Geng, F.; Yu, J.; Ma, X. *Journal of Polymers and the Environment* **2009**, *17*, 225.

# CHAPTER 6: BRANCHED TRIALKYLSILYLAMINES FOR $CO_2$ CAPTURE

## 6.1 Introduction

I have shown in Chapters 4 and 5 that the $CO_2$ capture properties of trialkylsilylamines can be effectively tuned by making small modifications in the molecular liquid structure. To this point alkyl functionality on the silicon atom has been modified along with the chain length between the silicon and nitrogen atoms to gain an understanding from a structure-property standpoint of the $CO_2$ capture properties. In this chapter, I am discussing the effects of introducing branching along the propyl chain in trialkylsilylpropylamines. First, it is helpful to put into context the work in this chapter in relation to branching of other amine systems as $CO_2$ capture targets.

$CO_2$ capture research has been thoroughly investigated for small molecular weight primary and secondary amines, for example MEA and DEA in Figure 6.1. These, as well as other polyamine examples have shown promising alternatives to 30% aqueous MEA solutions. However, they are all aqueous solutions. Aqueous solutions invoke a large energy penalty due to the high heat capacity and boiling point of water to reverse the system. Degradation is also a major issue with alcohol amines. This has driven my research to focus on non-aqueous amine RevILs for $CO_2$ capture and specifically within this chapter understand the role of branching on silylamine RevIL systems.

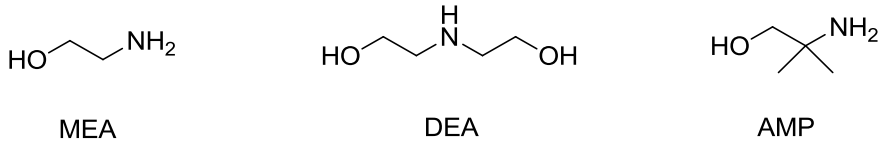


**Figure 6.1.** Examples of amine systems commonly investigated for $CO_2$ capture as well as a common "branched" amine

"Branched" amine derivatives have been investigated in aqueous systems. The term branched refers to substitution patterns along the propyl backbone of the amino-silicon chain at the α and β positions. Secondary or tertiary amines are not included in this study. Examples of aqueous branched amines for $CO_2$ capture have been reported by Sartori and Savage.[1] One example of interest outlined in their work is the molecule, 2,2-dimethylethanolamine, or AMP (Figure 6.1). This derivative was shown to have increased basicity due to the steric encumbrance of the two methyl groups $\alpha$ to the amine. In the presence of water, $CO_2$ capture equilibria lies towards formation of the ammonium cation and carbonate anion rather than the formation of ammonium carbamate ion pairs. The equilibrium pathways are outlined in Figure 6.2.

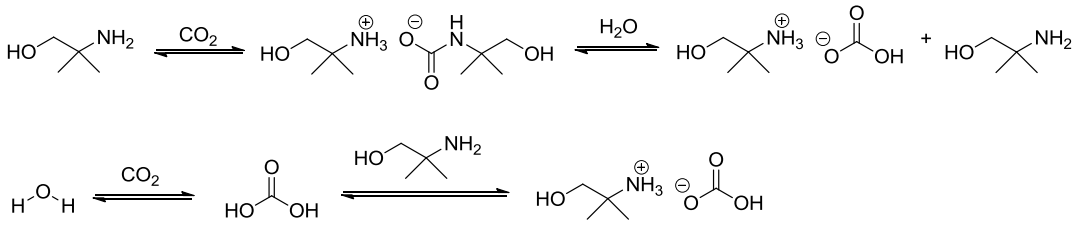


**Figure 6.2.** Equilibrium reaction of branched amines with $CO_2$ in an aqueous environment

The branched amines can be advantageous because the carbamate formed is destabilized, pushing the $CO_2$ reaction equilibrium towards protonation of the amine rather than reaction with $CO_2$. As a result, the overall $CO_2$ capacity is increased with a ratio of chemically captured $CO_2$ from 0.5 mol $CO_2$/mol amine in non-aqueous systems to 1 mol $CO_2$/mol amine.

Recently GE Energy reported series of non-aqueous poly-siloxylamines for $CO_2$ capture. Included in their study were siloxyamines which contained branching; however, no discussion was offered in terms of structure property relationships.[2]

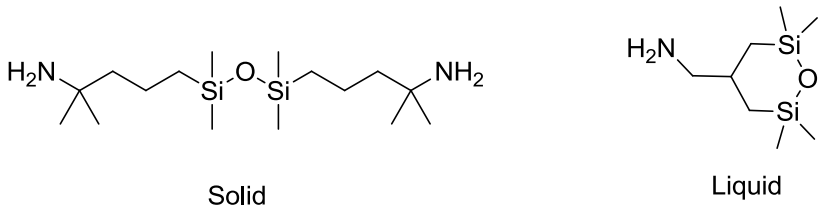


**Figure 6.3.** Siloxy-amines developed by GE for $CO_2$ capture

All but one of the siloxyamines that were investigated formed solids, hence full conversion to the theoretical amounts of $CO_2$ possible were not achieved. This did not allow a clear understanding the structural role, if any, of the branching on the $CO_2$ capabilities of these systems. Noteworthy, one of the siloxylamine systems was a liquid. This system is a cyclic amine with one reactive site and is shown in Figure 6.3. It was the only species that was found to have a higher capacity than the theoretical uptake based on the 0.5 mol$CO_2$/mol amine ratio. This was attributed to physical absorption and “adventitious” water in the system forming bicarbonate. For my research, I have been focusing on the synthesis and analysis of novel trialkylsilylamines that contain methyl or

ethyl substituent, “branching”, at the α and β positions with respect to the amine reactive site.

In Chapter 4, it was discussed that changes in the substitution patterns around the silicon atom in trialkylsilylpropylamines had significant effects on the temperature of reversal, $CO_2$ capacity and the viscosity at maximum conversion. Specifically, the viscosity decreased from 6088 cP to 2359 cP at 25°C simply upon replacement of ethyl to hexyl groups. However, the effect on the enthalpy of reaction, as expected since the reaction and reactive site remain virtually unchanged, was within experimental error.

We decided to implement structural changes close to the amine group, at the α and β positions, in order to impart steric disturbance close to the reaction site itself. By introducing steric hindrance around the amine reactive site, we aimed not only for the enthalpy of reaction to be reduced by destabilizing the carbamate formed, but the ion pair could have steric influences that promoted poor packing and coordination leading to lower initial viscosities. To first gain a qualitative understanding as to the effects of branching of trialkylsilylpropylamine derivatives, DFT calculations were run on potential molecular liquid candidates. It was expected that evaluation of the nucleophilicity and steric hindrance at the amine site would provide a measure of the stability of the carbamate formed.

### 6.2 DFT Calculations of branched silylpropylamines

A series of α and β-substituted 3-(aminopropyl)tripropylsilane derivatives were first investigated with Spartan® 2010 prior to any synthetic efforts to narrow down the candidates worth pursuing experimentally (Figure 6.4). The α and β positions were functionalized with both methyl and ethyl groups singly, and bi-functionalized with methyl groups.

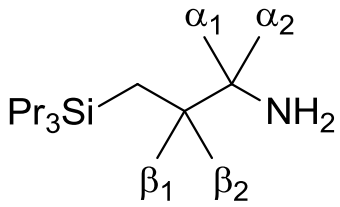


**Figure 6.4.** General diagram of the tripropylsilylpropylamine functionalized at the α and β positions

Structures were first constructed in Spartan® and optimized to their lowest energy confirmations. Density functional theory (DFT) calculations, at the B3LYP:6-31G* level of theory were then conducted on the lowest energy confirmation of each branched molecular liquid designed. The calculations included investigations into the exposed area on the nitrogen atom of each compound and the Mulliken atomic charge[3] on the nitrogen atom. These two values were chosen because they gave information pertinent to the nucleophilicity of the reactive amine site as well as steric hindrance.

The results of the calculations are shown in Table 6.1. It was found that the Mulliken charge on nitrogen had little correlation between structural modifications on the TPSA motif. Calculated values ranged from -0.715 in the βE-TPSA derivative up to -0.730 for the αE-TPSA derivative. The nitrogen exposed area did show more variation with structural changes. From the unsubstituted TPSA control to adding two methyl groups to the α-carbon of the amine, the available area on the nitrogen changed from 8.274 Å to 7.721 Å. Although this effect was expected, it was surprisingly not the largest effect. The βE-TPSA derivative had an available area of 7.102 Å. The extra degree of freedom added when extending the methyl group to an ethyl group allows for rotation that blocks the amine. Shown in Figure 6.5 are the electron potential map representations at lowest energy confirmation of the βM-TPSA and βE-TPSA

derivatives. The red circle indicates the lone pair on the nitrogen, the most electronically dense are of the entire species. The βE-TPSA derivative shows that the terminal -$CH_3$ on the ethyl group can interfere with the nitrogen lone pair by rotation towards the amine and also has limited interference in the case that the terminal -$CH_3$ group on the ethyl chain is rotated away.

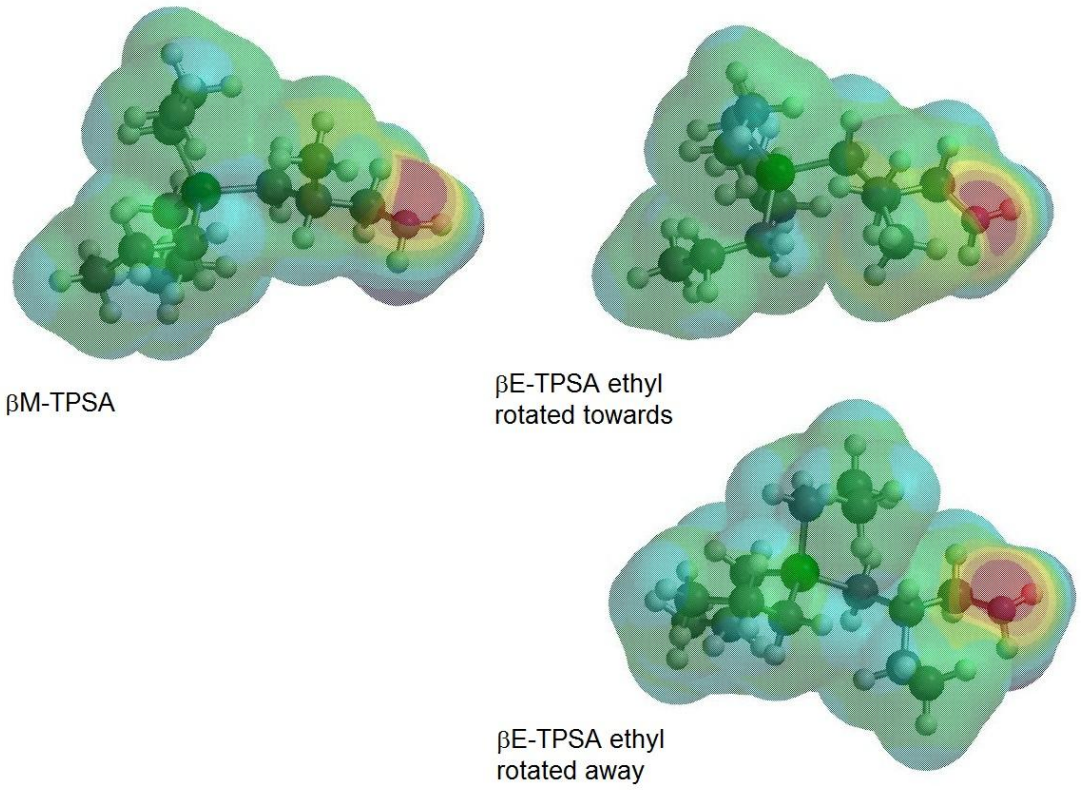


**Figure 6.5.** DFT electron potential maps of the βM-TPSA and βE-TPSA derivatives

Rotation towards the amine, although electronically disfavored would partially block the amine and cause steric hindrance resulting in a lower available area.

**Table 6.1.** DFT calculations of the exposed area and mulliken charge on branched TPSA derivatives

| **Molecular Liquid*** | **Nitrogen Exposed Area** ($Å^2$) | **Nitrogen Atomic Charge** (Mulliken charge) |
|---|---|---|
| TPSA | 8.274 | -0.717 |
| αM-TPSA | 7.919 | -0.721 |
| α,αDM-TPSA | 7.721 | -0.713 |
| αE-TPSA | 7.948 | -0.730 |
| βM-TPSA | 7.862 | -0.717 |
| β,βDM-TPSA | 7.769 | -0.721 |
| βE-TPSA | 7.102 | -0.715 |

*M=methyl, E=ethyl, DM=dimethyl

These calculations were investigated to gain insight into amine structures that may have potential in favorable $CO_2$ capture properties which include low viscosities, low enthalpies of reversal, moderate reversal temperatures and high capacities. Synthetic efforts were focused on the α-methyl, α,α-dimethyl, β-methyl and β-ethyl derivatives (Table 6.2). These structures were chosen because they represented each of the substitution positions and showed the most change with respect to the unsubstituted TPSA derivative. The selection of the specific branched derivatives to explore was a combination of results from the Spartan calculations as well as accessible synthetic pathways.

**Table 6.2.** Branched silylamine structures investigated in the capture of $CO_2$

| Structures of Branched TEtSA Analogs | | |
|---|---|---|
| TEtSA 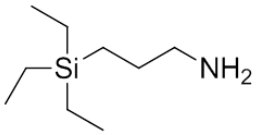 | αM-TEtSA 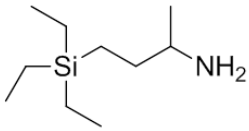 | α,αDM-TEtSA 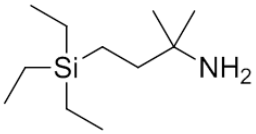 |
| βM-TEtSA 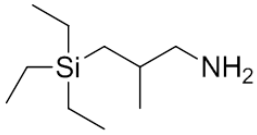 | βE-TEtSA 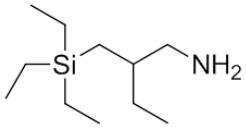 | |

Although TPSA derivatives were used in the DFT calculations, derivatives of TEtSA, it is the triethylsilyl subsitituted amines that were synthesized due to higher capacities achievable with less overall molecular weight. Another stipulation was that if the effects expected such as lower reversal temperature and lower viscosities were apparent, then TPSA derivatives would have even lower reversal and viscosities making analysis problematic.

### 6.3 Synthetic Methods for branched amine preparation

Because desired branched amines are not commercially available, nor are most of the branched allylamine precursors, synthetic schemes were custom-designed. Like the trialkysilymaines analogs, the key transformation in the synthesis of the four branched amines is the hydrosilylation reaction step.[4] This reaction has been presented in detail in Chapter 4. In all cases, I chose to react triethylsilane with the custom-made

allyl amine in the presence of Pt-DVDS as a catalyst. The reaction is shown in Figure 6.6.

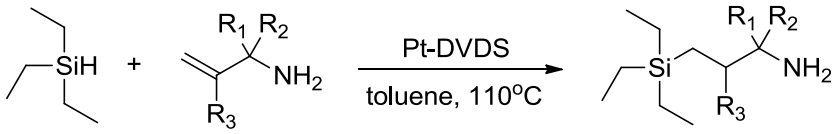


**Figure 6.6.** General hydrosilylation step in all branched reactions

Original strategies and alternative strategies, when necessary, were investigated to enable the preparation of gram quantities of branched silylamines. Each silylamine was purified via distillation and characterized by $^{1}$HNMR, $^{13}$CNMR, and EA.

I recognize that in some cases the strategies adopted to synthesize lab quantities of branched silylamines may not be economical or adequate for production scales. Yet, for screening purposes, these syntheses were suitable. Additionally, experimental conditions have not been optimized for yield or reaction time. The synthesis of TEtSA, the unsubstituted derivative was described in Chapter 4 which will be used a comparative structure through the discussion.

As many methodologies have been constructed for the successful syntheses of the branched amine derivatives shown in Table 6.2, I will highlight the attempted approaches and going into detail for the synthetic pathways that were successful. The experimental section at the end of the document will report however all the syntheses including the ones that were not successful for the formation of these amines.

### 6.3.1 Methodology for the synthesis of desired branched amine derivatives through Overman rearrangement

An initial approach to the synthesis of all of the branched amine derivatives followed a method developed by Larry Overman.[5] This method is highlighted because starting from allyl alcohols substituted with alkyl functionalities at both the terminal and internal carbon of the alkene, α and β substituted allyl amines have been synthesized.

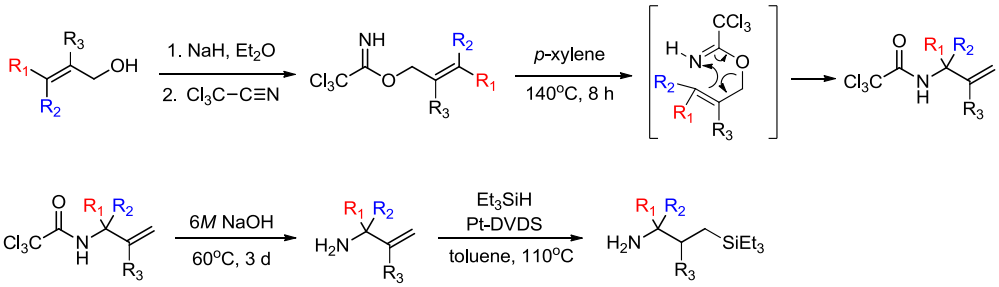


**Figure 6.7.** General Overman rearrangement scheme

From Figure 6.7, it can be seen that substitution at the terminal carbon of the alkene in allyl alcohol starting material leads to α-substituted functionalities in the final amine products. Reaction of the alcohol under basic conditions with trichloroacetonitrile forms an allylic trichloroacetimidate. Thermal (Overman) rearrangement proceeds through a 3,3-sigmatropic rearrangement yielding α-substituted trichloroacetamide protected allyl amines. Deprotection with NaOH has been reported to provide the desired substituted allyl amines.[6] This methodology was investigated in the syntheses of both the αM-TEtSA and α,αDM-TEtSA derivatives. The formation of the trichloroacetamide protected allyl amine derivatives was successful; however, the deprotection step led to the volatile, water soluble allyl amine product. The isolation of the neutral allyl amines from water was not feasible. The hydrosilylation directly from the

protected amines was also attempted prior to the deprotection step in order to form the trichloroacetamide protected products which were expected to have high boiling points and be relatively hydrophobic. Although this approach seemed promising, hydrosilylation of the trichloroacetamide protected allylamines with triethylsilane in the presence of Pt-DVDS failed to provide the desired product. Literature examples have demonstrated reduction of carbonyls in the presence of silanes and transition metal catalysts.[7] This methodology is presented in both the schemes for αM-TEtSA and α,αDM-TEtSA.

### 6.3.2 Synthetic Approaches to formation of 3-(aminobutyl)triethylsilane (αM-TEtSA)

Three separate routes were developed for the synthesis of αM-TETSA through: (1) Overman rearrangement, (2) a Gabriel synthesis, and (3) benzylhydroxylamine substitution of allylic carbonates. These three pathways are represented in Figure 6.8.

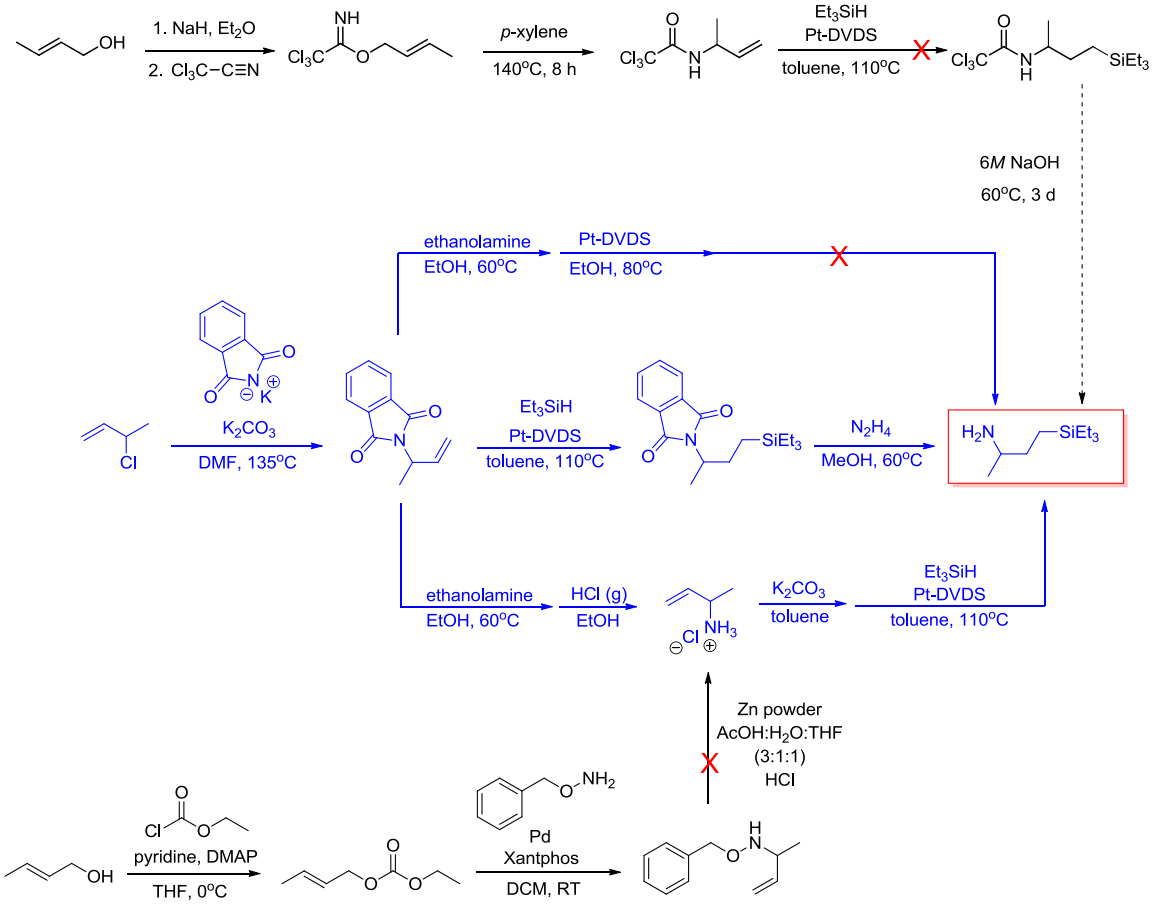


**Figure 6.8.** Synthetic pathways towards the synthesis of αM-TEtSA

## 6.3.2.1 Overman Rearrangement

The Overman rearrangement was previously described as the initial method to the formation of αM-TEtSA. Although on paper the scheme seemed promising, the hydrosilylation reaction was not successful and the deprotection step to form the allyl amine derivative led to unresolved separation and isolation issues. Therefore, another

approach to the αM-TEtSA was developed from a literature procedure for the formation of the α-methylallyl amine hydrochloride salt starting from crotyl alcohol.[8]

6.3.2.2 Benzylhydroxylamine Subsitution

Crotyl alcohol was reacted with ethylchloroformate to provide successfully the ethyl crotyl carbonate which was then reacted with benzyl hydroxylamine in the presence of palladium the ligand Xantphos. Under these conditions, the benzyl hydroxyl amine displaced the carbonate functionality in an $S_N2'$ fashion. In our hands, the $S_N2'$ pathway was favored and the benzylhydroxylamine protected α-methylallyl amine was formed. Following the literature method for the formation of the hydrochloride salt of 3-amino-1-butene, activated zinc was added to a solution of the benzylhydroxylamine protected-allyl amine in a mixed solvent of acetic acid, water, and THF. Unfortunately, the reaction did not proceed and this synthetic approach was not investigated further. This led to a relatively conventional approach to the formation of amines following a Gabriel synthesis method which is highlighted in blue in Figure 6.8.

6.3.2.3 Gabriel Synthesis

The Gabriel synthetic method was designed to yield the 3-amino-1-butene hydrochloride salt. The salt was desired because of the high volatility of allyl amine derivatives. The 3-amino-1-butene salt could under neutralization under basic conditions to provide the reactive 3-amino-1-butene precursor to the established hydrosilylation reaction. The synthesis of the 3-amino-1-butene hydrochloride salt was successful following a Gabriel synthesis pathway from 3-chloro-1-butene (Figure 6.9).

First, the 3-chloro-1-butene was reacted with potassium phthalimide and $K_2CO_3$ in DMF to form 3-phthalimido-1-butene, a procedure adapted from literature.[9,10]

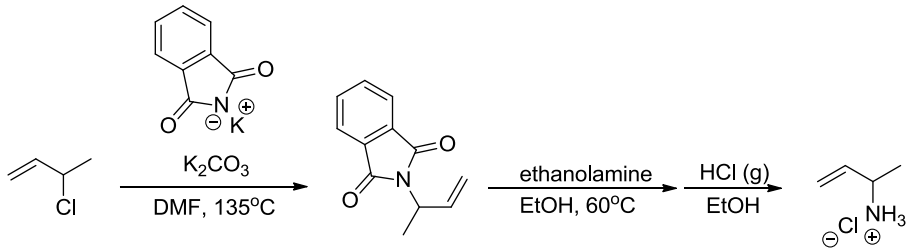


**Figure 6.9.** Formation of 3-amino-1-butene hydrochloride salt through Gabriel synthesis

To deprotect the amine, the 3-phthalimido-1-butene was reacted with ethanolamine in EtOH. Ethanolamine was used rather than hydrazine because it is a mild reagent. After 3 hrs of reaction, the deprotected 3-amino-1-butene was distilled with EtOH under argon. The boiling point of the allylamine is very close to that of EtOH and by distilling them together, acidification with HCl could be performed to yield the desired salt. HCl gas was sparged through the distilled fraction for 15 minutes and the EtOH was removed by rotary distillation under vacuum to isolate the 3-amino-1-butene hydrochloride salt in 85% yield.[9]

From the 3-amino-1-butene hydrochloride salt, two pathways were attempted to form the desired αM-TEtSA. First, the neutralization of the 3-amino-1-butene hydrochloride was necessary to perform the hydrosilylation reaction with triethylsilane in toluene, the common reaction solvent for this method. The neutralization reaction was conducted by stirring the 3-amino-1-butene hydrochloride salt with excess anhydrous $K_2CO_3$ in anhydrous toluene at room temperature for 24 hours. The mixture remained heterogeneous because of the base and starting materials low solubility in non-polar solvents. After confirming by $^1$HNMR the appearance of the neutral 3-amino-1-butene,

the resulting slurry was filtered and the paste-like material was washed repeatedly with anhydrous toluene. The collected toluene solution was then subjected to hydrosilylation with triethylsilane at 110°C in the presence of Pt-DVDS (Figure 6.10). $^{1}$HNMR showed the disappearance of vinyl peaks from the allyl amine derivative. As a result, the reaction was cooled and the toluene and excess triethylsilane were removed under vacuum. The desired αM-TEtSA was formed in 33% yield.

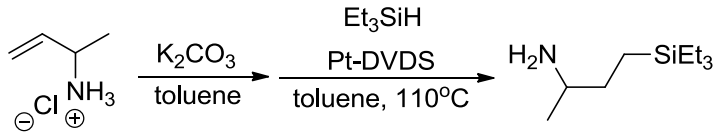


**Figure 6.10.** Hydrosilylation of the 3-amino-1-butene hydrochloride salt for the formation of αM-TEtSA

The low yield of this reaction was possibly due to incomplete neutralization of the 3-amino-1-butene hydrochloride salt prior to hydrosilylation. Therefore an attempt to perform the hydrosilylation without neutralization was attempted. The salt was not soluble in toluene and the reaction did not proceed by $^{1}$HNMR.

It was then hypothesized that the hydrochloride protection and neutralization step may be the limiting factor in the formation of αM-TEtSA and the hydrosilylation was tried immediately after deprotection of the phthalimide protecting group. The 3-amino-1-butene was distilled with EtOH, as mentioned before, after deprotection of the phthalimide with ethanolamine (Figure 6.11). This distillate containing the free amine was added to anhydrous toluene with triethylsilane and Pt-DVDS. Upon addition, the solution bubbled and after 24 hours, $^{1}$HNMR showed evidence that the reaction had not

proceeded. This was a far-reached attempt as it is known that hydrosilylations are not conducted in protic solvents because the platinum catalyst can be poisoned and deactivated.

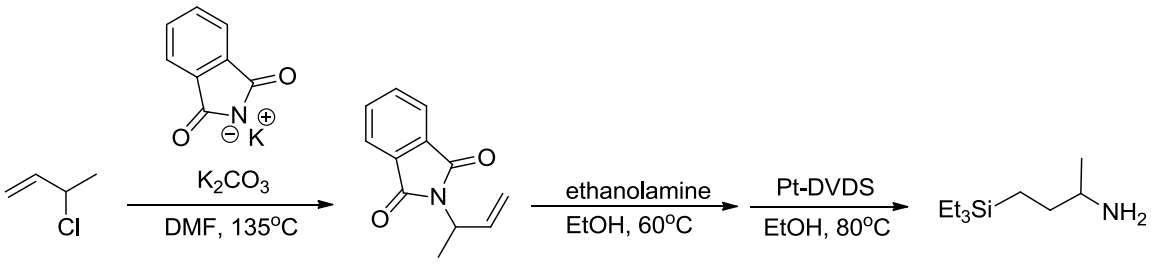


**Figure 6.11.** Attempted Gabriel synthesis and hydrosilylation in ethanol

Therefore to eliminate the acidification and neutralization step altogether, the hydrosilylation was conducted from the 3-phthalimido-1-butene (Figure 6.12). Deprotection after hydrosilylation was expected to yield the desired product with no concerns about volatility and isolation of the amine. The reaction proved to be effective in forming the 3-(phthalimido-butyl)triethylsilane with 76 % yield. Deprotection of the pthalimide protecting group with hydrazine was straightforward and afforded the desired αM-TEtSA in 62 % yield.

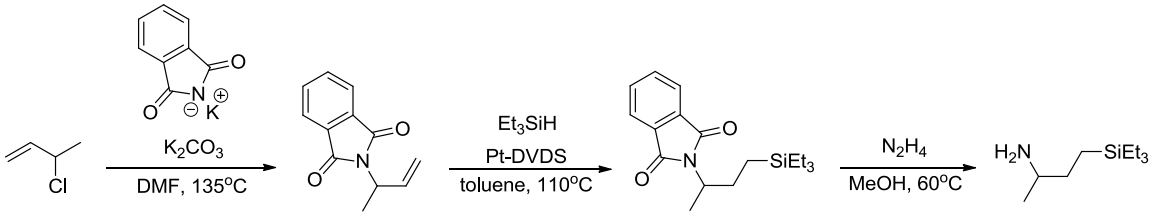


**Figure 6.12.** Successful synthesis of αM-TEtSA through Gabriel synthesis, hydrosilylation, and reduction

The α,αDM-TEtSA, presented next, was a key compound to study because the α-carbon is completed substituted. This substitution could result in lower reversal energy (enthalpy and reversal temperature) and lower viscosity from disrupted packing in the RevIL form.

### 6.3.3 Synthetic approaches towards the formation of 2-methyl-4-(triethylsilyl)butan-2-amine (α,αDM-TEtSA)

The synthesis of α,αDM-TEtSA was attempted through two main pathways, an Overman rearrangement and through hydrosilylation of a commercially available dimethylated propargylamine which are shown in Figure 6.13.

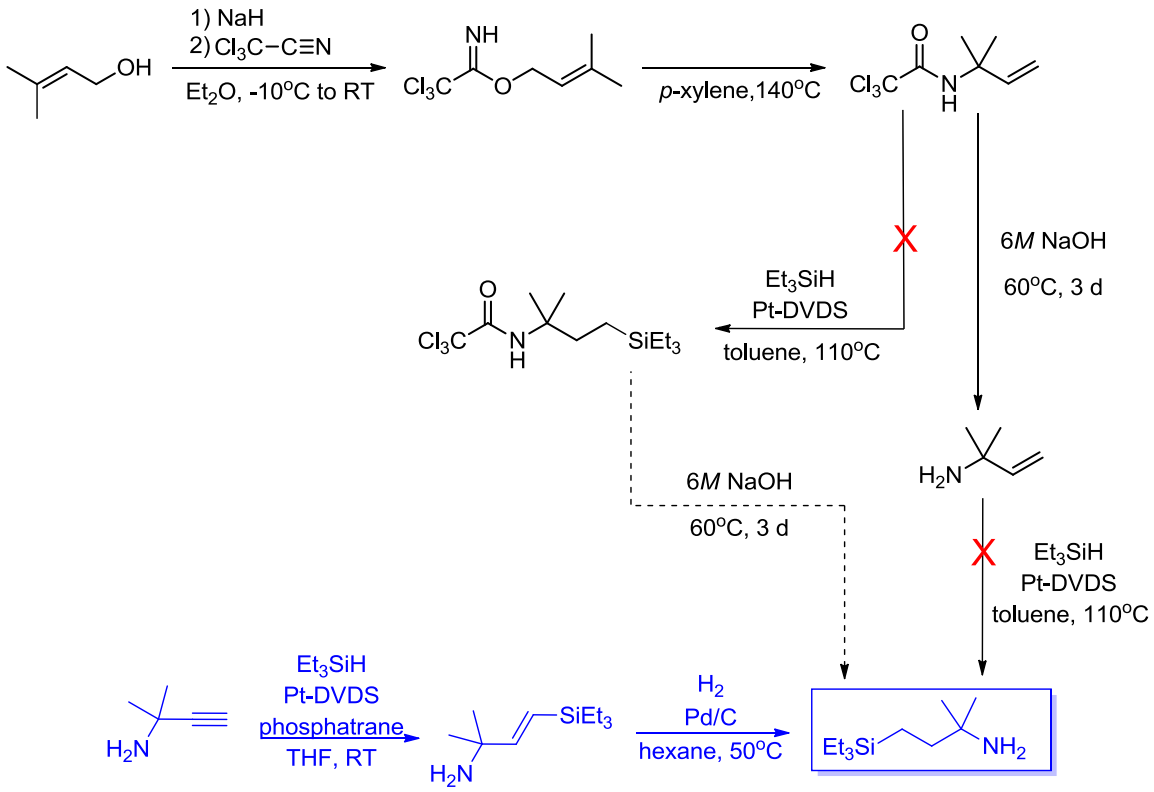


**Figure 6.13.** Synthetic pathways developed for the formation of α,αDM-TEtSA

6.3.3.1 Overman Rearrangement

The Overman rearrangement was carried out by reacting prenyl alcohol with trichloroacetonitrile to form the prenyl trichloroacetimidate. The rearrangement was successful in refluxing p-xylene with 88% yield.[6,11] Unfortunately, the next step, hydrosilylation, failed to provide the α,αDM-TEtSA. An alternative two-step method was then considered by analogy with literature precedent. Furthermore, volatile allyl amino derivatives were avoided by this synthetic approach which made this method more attractive.

6.3.3.2 Hydrosilylation and reduction of propargylamine

The first step was the hydrosilylation of α,α-dimethylpropargyl amine with triethylsilane in the presence of Pt-DVDS. A bulky phosphatrane ligand was used to form specifically a trans-unsaturation between the β and γ carbons of the desired product amine in an 80% yield.[12] In this particular reaction the trans-only derivative is not required but another colleague was involved in the investigation of unsaturated silylamines and the trans-only product was synthesized. The second step proceeded through reduction of the internal alkene by hydrogenation with palladium on carbon as a catalyst to provide an 88% yield of the desired amine (Figure 6.14).[13]

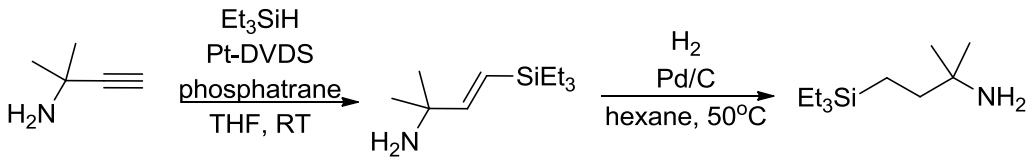


**Figure 6.14.** Hydrosilyation and reduction of α,α-dimethylpropargyl amine to form α,αDM-TEtSA

### 6.3.4 Hydrosilylation in the synthesis of 2-methyl-3-(triethylsilyl)propan-1-amine (βM-TEtSA)

The β-methyl derivative of TETSA was successfully synthesized through hydrosilylation of the commercially available 2-methylallylamine (Figure 6.15).[4] The reaction was conducted at 80°C rather than 110°C as usual because of the low boiling point of the 2-methylallylamine starting material and upon vacuum distillation, the product was yielded in 75%.

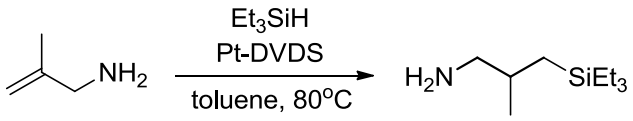


**Figure 6.15.** Hydrosilylation reaction to form βM-TEtSA

### 6.3.5 Synthetic approaches for the formation of 2-((triethylsilyl)methyl)butan-1-amine (βE-TEtSA)

The synthesis of the βE-TEtSA derivative was of particular interest because in the Spartan® calculation of the exposed nitrogen area, an indication of the steric hindrance, this derivative had the lowest value of nitrogen exposed area. Unlike the βM-TEtSA derivative, the β-ethylallyl amine was not commercially available and synthesis of this derivative was required. Four approaches were considered and are shown in Figure 6.16.

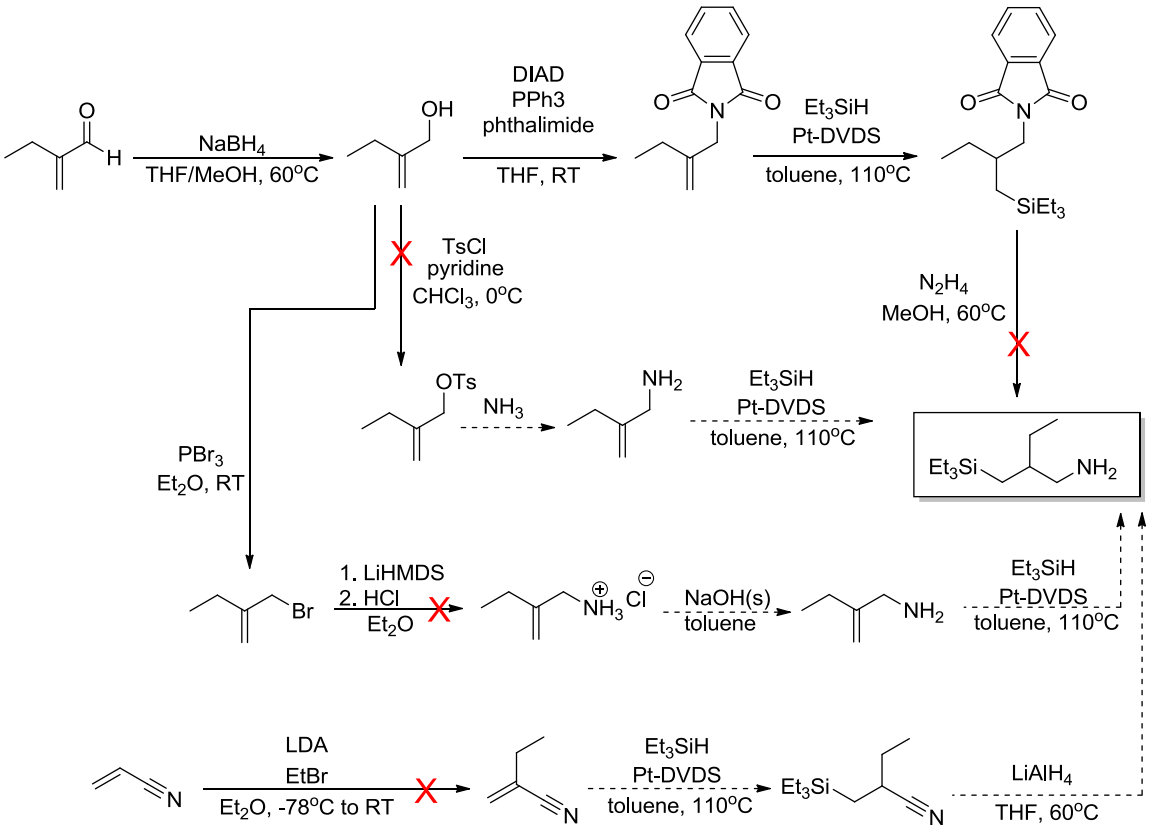


**Figure 6.16.** Synthetic pathways constructed for the formation of βE-TEtSA

6.3.5.1 Formation of the 2-ethyl allylamine hydrochloride

The synthesis of the βE-TEtSA derivative was approached through the first three routes starting from a 2-ethylallyl alcohol intermediate. This intermediate alcohol was prepared by the reduction of 2-ethylacrolein with sodium borohydride. It was reported in literature, that the desired 2-ethylallyamine hydrochloride salt was obtained in 22% overall yield with no isolation or purification following this method.[14]

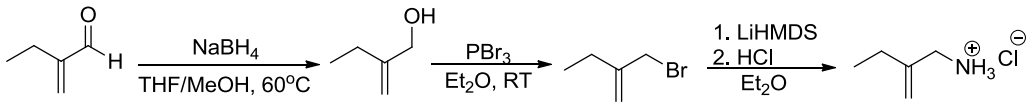


**Figure 6.17.** Formation of the 2-methylene-butylamine hydrochloride salt

It is reported in the literature that the 2-ethylallyl alcohol was converted to the 2-ethylallyl bromide through reaction with $PBr_3$, as shown in Figure 6.17. This reaction was also successful in my hands, providing the 2-ethylallyl bromide in 16% crude yield (not isolated from diethyl ether). In principle, the displacement of the bromide by bis(trimethylsilyl)amide and deprotection with HCl should yield the 2-ethylallyl amine hydrochloride salt . However, attempts at this substitution failed. This method was not further pursued.

6.3.5.2 Tosylation of 2-ethylallyl alcohol

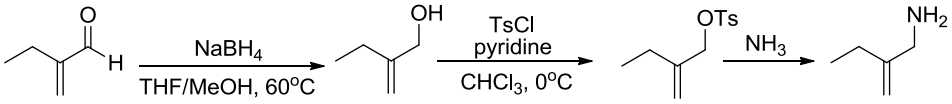


**Figure 6.18.** Modified formation of the 2-methylene-butylamine hydrochloride salt

The development of the second alternative method was essentially motivated by the avoiding the inefficient neutralization and extraction hydrochloride salt form of the 2-ethylallyl amine. The desired βE-TEtSA was projected to be formed through hydrosilylation with the 2-ethylallyl amine directly, upon substitution of a tosyl group through reaction with ammonia (Figure 6.18).[15] Although disappearance of the starting alcohol was observed in the $^1$HNMR, the desired tosylated intermediate from the

reaction of tosyl chloride with 2-ethylallyl alcohol in the presence of pyridine was not formed.[16]

6.2.5.3 Mistunobu Reaction to form allyl phthalimide

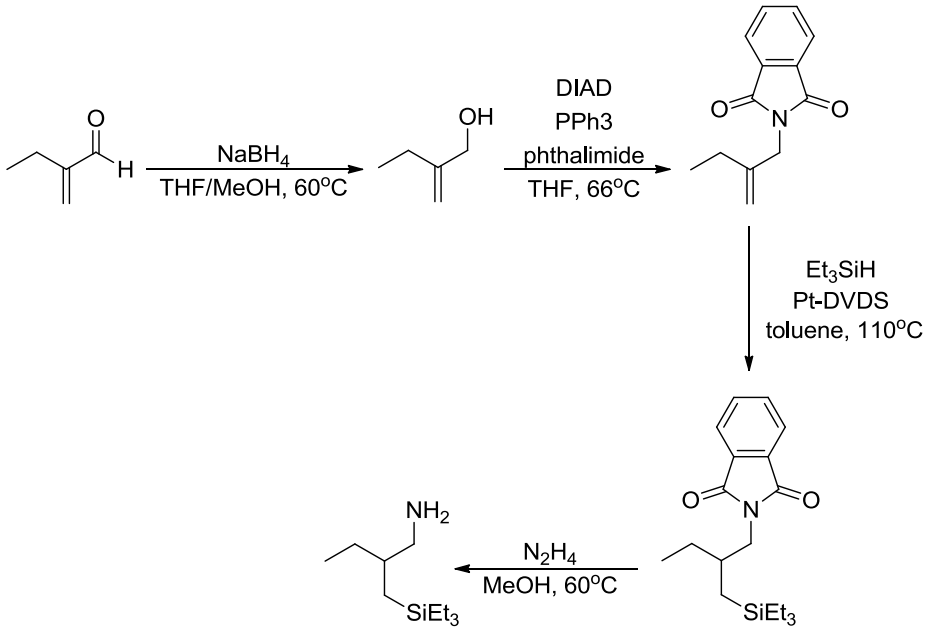


**Figure 6.19.** Mitsunobu reaction pathway for the formation of βE-TEtSA

A third method which included as a key step the Mitsunobu reaction was then investigated to form the 2-ethylallyl phthalimide (Figure 6.19).[17] This procedure was of particular interest because the phthalimide protection would avoid (1) volatile intermediates/products and (2) inefficient acidification and neutralization steps. Practically, the 2-ethylallylalcohol was added to a stirring solution of $PPh_3$ and

phthalimide in THF. Diisopropylazodicarboxylate (DIAD) was added slowly and the reaction was brought to reflux conditions. The NMR showed only partial conversion after 24 hrs. As a consequence, more $PPh_3$, DIAD, and phthalimide were added to drive the reaction to completion. After work-up and purification by column chromatography, 2-(2-methylenebutyl)isoindoline-1,3-dione was obtained in 67% isolated yield.

2-(2-methylenebutyl)isoindoline-1,3-dione was then reacted with triethylsilane in toluene at 110°C. Pt-DVDS was used as a catalyst to promote the hydrosilylation reaction and because of the steric bulk at the β position, 5 mol% eq of Pt-DVDS catalyst were used. This is 25 times more than the hydrosilylation with allyl amine. After 4 weeks the reaction was stopped. The crude residue was puridfied by column chromatography. 2-(2-((triethylsilyl)methyl)butyl)isoindoline-1,3-dione was obtained from distillation under vacuum (0.2 mmHg and 82°C) to provide crude phthalimide protected βE-TEtSA, which was carried to the next step without further purification. Phthalimide deprotection of the 2-(2-((triethylsilyl)methyl)butyl)isoindoline-1,3-dione with hydrazine was conducted but did not show progress after 24 hours. Indeed, $^1$HNMR indicated that the reaction did not proceed-only starting materials were evidenced.

6.2.5.4 Acrylonitrile Substitution

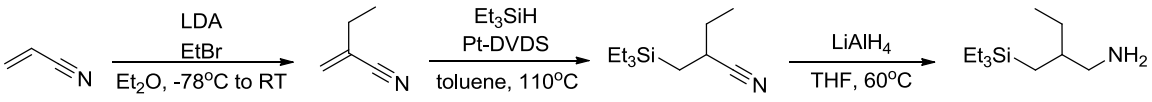


**Figure 6.20.** Acrylonitrile substitution pathway for the formation of βE-TEtSA

The fourth and final pathway, shown in Figure 6.20, was attempted through ethyl substitution at the β-carbon of acrylonitrile. It has been shown that substitution at this position is possible under basic conditions.[18] The 2-ethylacrylonitrile could then be hydrosilylated to form the desired βE-TEtSA as a nitrile protected amine. Reduction with $LiAlH_4$ was hypothesized to give the final desired βE-TEtSA. The first alkylation step was conducted with pre-formed LDA and acrylonitrile to generate an anion at the β-carbon. Upon addition of ethyl bromide and subsequent reaction quenching with saturated ammonium chloride solution, extraction of the desired product in ether was not achieved. It was expected that polymerization of the acrylonitrile may have been a competitive reaction. All experimental procedures can be found in detail in the experimental methods section at the end of the chapter. A new pathway towards the βE-TEtSA derivative is highlighted in the conclusions and recommendations chapter.

Of the four branched derivatives explored, three were successfully synthesized: αM-TEtSA, α,αDM-TEtSA, and βM-TEtSA, along with the unsubstituted TEtSA derivative described throughout Chapters 4 and 5. Table 6.3 displays the synthesis and characterization of these 3 branched amines. All three of these amines are new compositions of matter and were characterized by $^{1}$HNMR, $^{13}$CNMR, and EA. These four molecules were used as tools to investigate the role of branching on the $CO_2$ capture properties of trialkylsilylamines.

**Table 6.3.** Yield and distillation temperature of successfully formed branched silylamines

| Structure | Overall Yield from Starting Material | Distillation Temperature |
|---|---|---|
| αM-TEtSA | 32% | 73°C at 2.7 mmHg |
| α,αDM-TEtSA | 65% | Not purified by distillation |
| βM-TEtSA | 75% | 51°C at 0.65 mmHg |

## 6.3 Results and Discussion

The amines that were formed, TEtSA, αM-TEtSA, α,αDM-TEtSA, and βM-TEtSA were all reacted with $CO_2$ to form RevILs and an analyzed by viscosity, gravimetry, and DSC. The reaction of these amines is shown in Figure 6.21. The three branched amine derivatives were reacted with $CO_2$ following the same procedure outlined in Chapters 4 and 5.

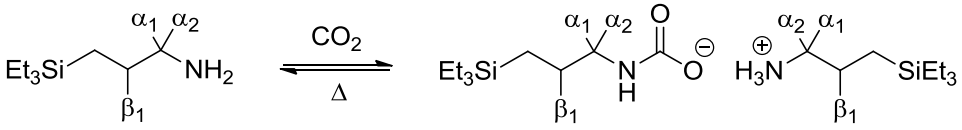


**Figure 6.21.** Reaction of branched silylamines with $CO_2$

### 6.3.1 $CO_2$ capture capacity in branched amine RevILs

The $CO_2$ uptake capacity was measured with a gravimetric technique. Each measurement was run in triplicate. As primary amine reactions, the chemisorption is

dictated by the stoichiometry of the reaction, hence 0.5 mol of $CO_2$/mol of amine. The physisorption may vary with structure and would be especially instructive from a structure-property relationship standpoint.

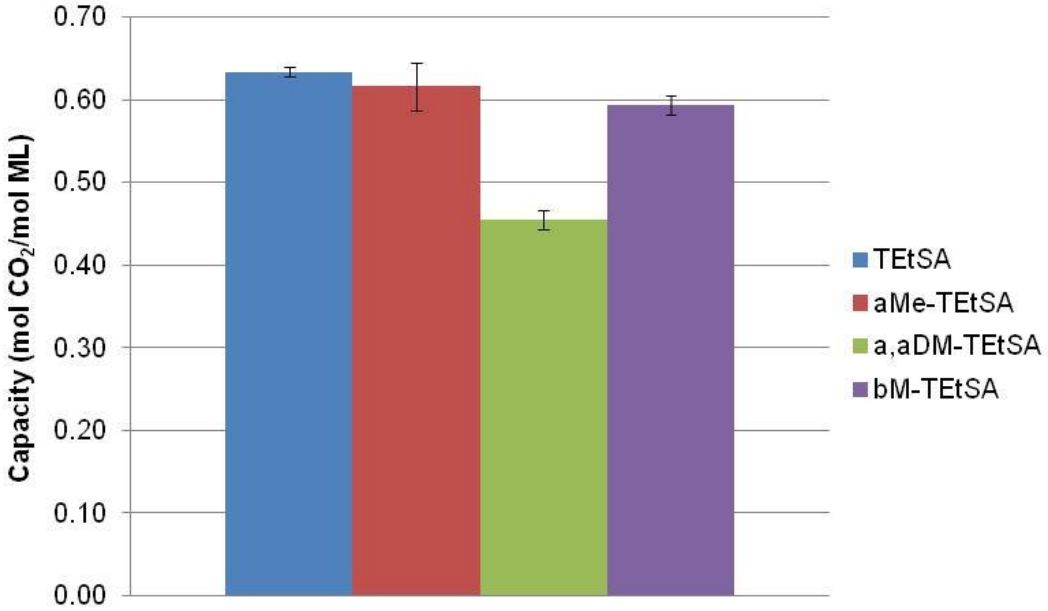


**Figure 6.22.** $CO_2$ capacity of branched silylamines

The experimentally measured gravimetric $CO_2$ capacity including chemisorption and physisorption, showed enhanced capacity compared to theoretical predictions based on 0.5 mol of $CO_2$ per mol of amine and a physisorption of 0.02 mol (based upon Henry constant predictions at 1 bar) and are displayed in Figure 6.22. The enhanced $CO_2$ capacities are on the order of 20% for the TEtSA, αM-TEtSA, and βM-TEtSA. When introducing branching at the α and β positions, it was questioned that the reaction may not go to full completion that because of carbamate destabilization. It is in fact the case for the α,αDM-TEtSA. With di-substitution in the α position, hindering the reaction, the

overall gravimetric capacity was measured at about 0.47 mol $CO_2$/mol amine. Both the αM-TEtSA and βM-TEtSA had capacities of 0.6 mol $CO_2$/mol amine. Unquestionably, enhanced capacity is obtained (consistently and within experimental errors). This is attributed to carbamic acid formation (Chapter 4). The carbamic acid formation is an added benefit of these non-aqueous silylated amine systems, enabling higher $CO_2$ capture capacities than originally predicted. This demonstrates that structural changes at the molecular level can contribute to design an optimum system with higher performance than the aqueous MEA standard.

The motivation behind investigating the branched systems were to clearly understand the effect of the structure modifications on the key properties for $CO_2$ capture such as viscosity and enthalpy of the reversal process.

### 6.3.2 Thermodynamic properties of branched amine RevILs

#### 6.3.2.1 Effect of α and β substitution of silylamine RevILs on reversal temperature

Reversal temperatures were calculated from DSC measurements of the preformed RevILs. Two endotherms were apparent in all cases, the first corresponding to the thermally driven reversal of $CO_2$ and the second corresponding to the vaporization of the molecular liquid. The first endotherm was integrated from baseline to baseline and the reported temperature of reversal is taken from the tangent line to the curve where it intersects the baseline.

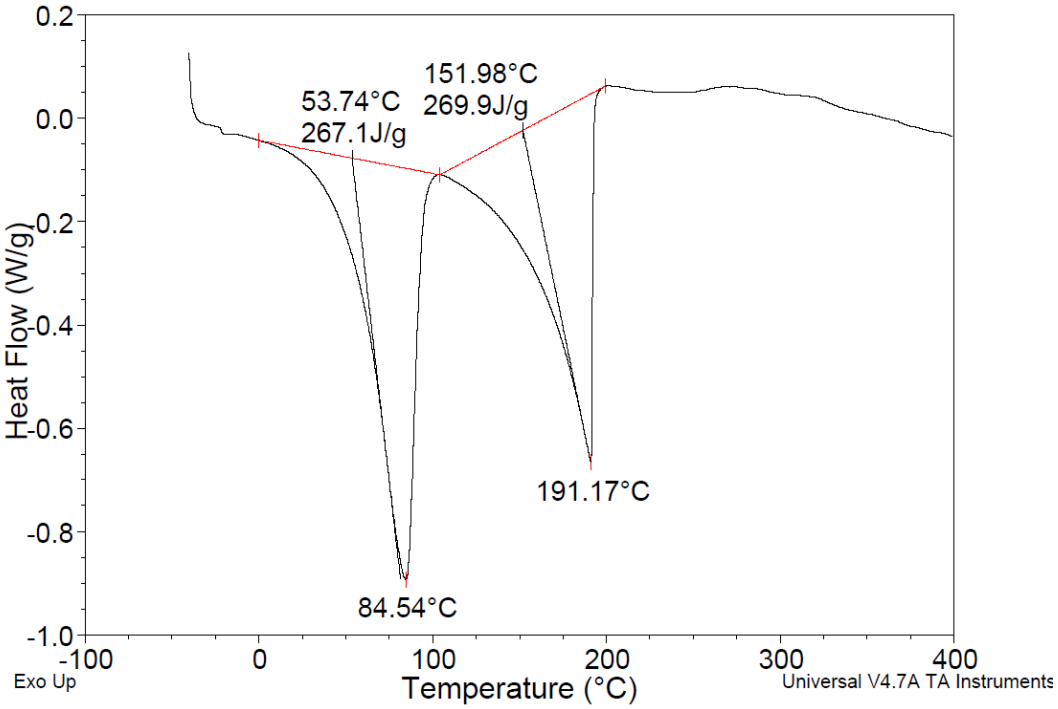


**Figure 6.23.** DSC thermogram of αM-TEtSA

An example DSC is shown in Figure 6.23 for the αM-TEtSA RevIL. The calculated reversal temperature was found to be 53.74°C and the evaporation temperature, 151.98°C. A comparison of the calculated reversal temperatures from DSC measurements of the branched amines are reported in Figure 6.24 below.

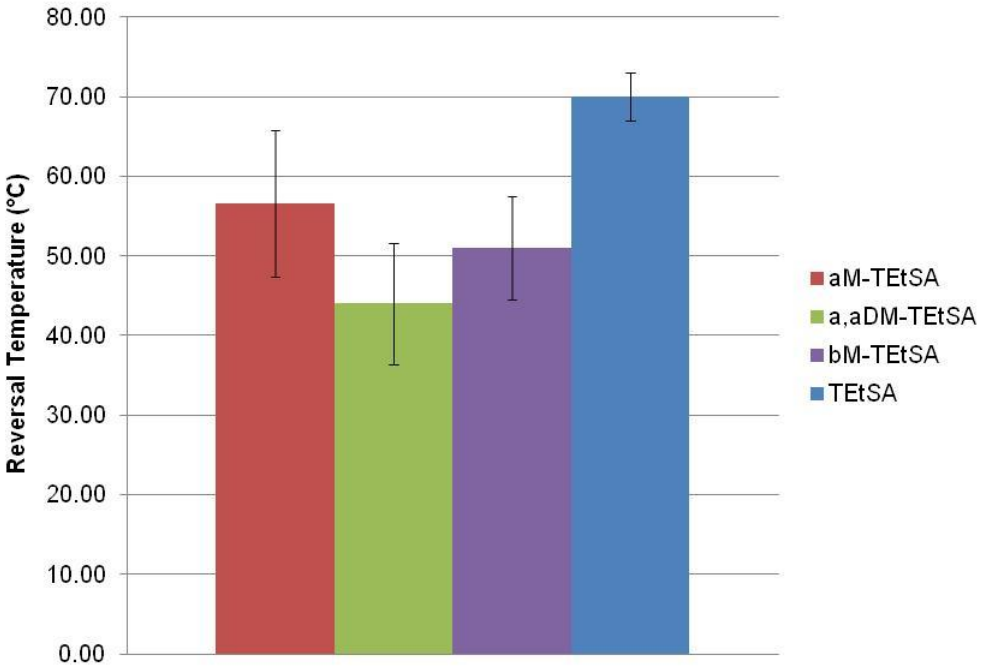


**Figure 6.24.** Reversal temperature as a function of branched silylamine Rev-IL structure

It is apparent that reversal onset in the branched amines is on average about 15°C lower than in the unsubstituted TEtSA derivative, as expected from increasing carbamate instability arguments. The α,αDM-TEtSA had the lowest reversal temperature of all of the branched structures at 44°C. Reversal temperature can now be controlled, not only by substitution around the silicon atom, shown in Chapter 4, but also by branching along the propyl backbone.

6.3.2.2 Enthalpy of reversal as a function of α and β substitution on silylamine RevILs

If destabilization of the formed carbamate is true, or rather if the formed carbamate has a higher free energy, then the enthalpy of reversal should be lower than that of the stable non-branched carbamates. Enthalpy was calculated from integration of

DSC measurements and compilation of the branched amine RevIL enthalpies are shown in the graph below (Figure 6.25).

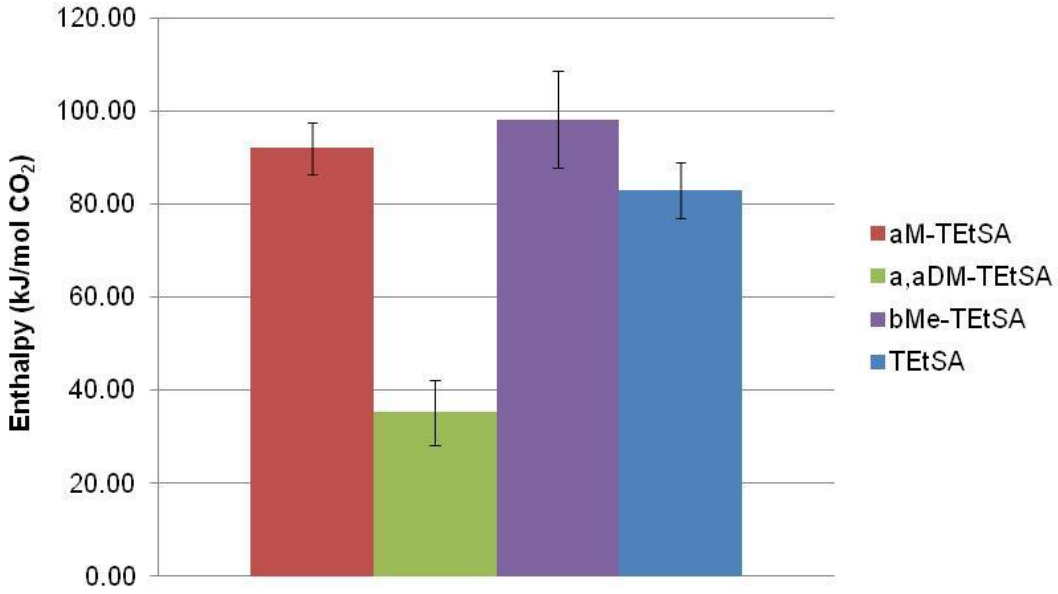


**Figure 6.25.** $CO_2$ reaction enthalpy as a function of branched silylamine Rev-IL structure

Enthalpy values fell within the range of 90 kJ/mol $CO_2$ for the mono-methyl substituted branched TEtSA derivatives. The α,αDM-TEtSA had the lowest reversal enthalpy at 36 kJ/mol $CO_2$. This was consistent with the theory of carbamate destabilization. The enthalpy value for TEtSA was reported in Chapter 4 to be on the order of 110 kJ/mol of $CO_2$ based on a 0.5 mol/amine ratio but when the actual capacity is taken into account, the resulting enthalpy is 81 kJ/mol $CO_2$.

### 6.3.3 Viscosities of silylamine RevILs substituted at the α and β positions

One of the important considerations in a $CO_2$ capture process is the viscosity of the system. One of the motives behind studying branched silylated amines structures was the role that branching would play on viscosity. It was hypothesized that introducing

steric hindrance, as well as asymmetry (although asymmetry was not investigated separately) through branching along the backbone of the silyl propylamine chain would cause disruptive interactions in the packing ability of the carbamate and ammonium ions. Viscosity measurements were conducted on the fully formed RevILs at 25°C and 40°C and are displayed in Figure 6.26.

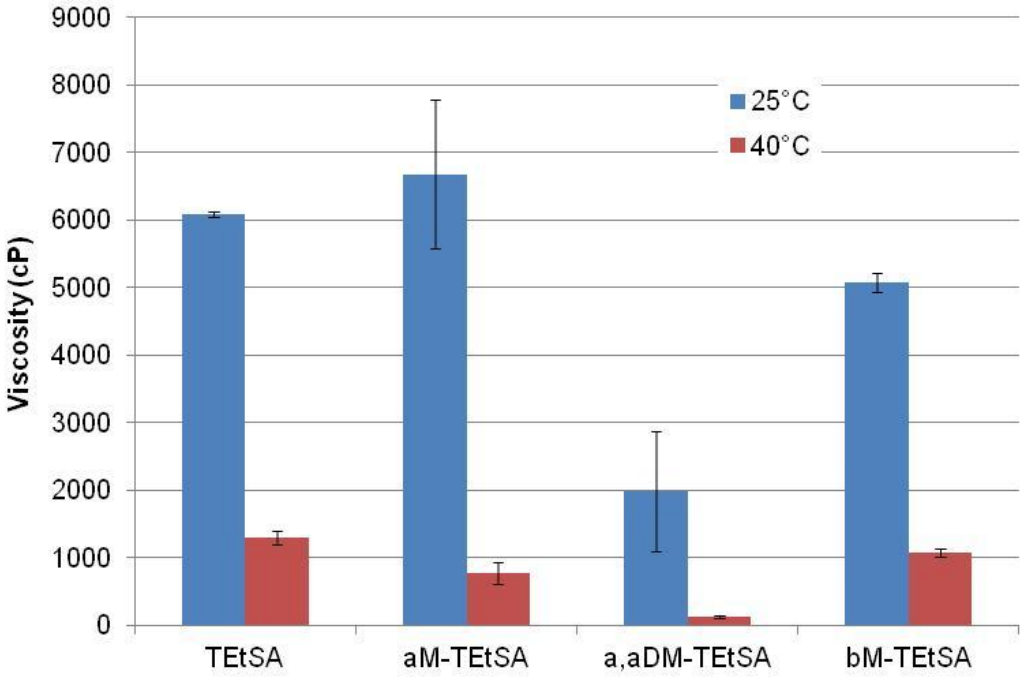


**Figure 6.26.** Viscosities of branched silylamine RevILs as a function of temperature

The addition of a methyl group on the α-carbon to the amine has no significant impact on the viscosity at 25°C. Within error, the values are equal for TEtSA and αM-TEtSA. The βM-TEtSA derivative has a viscosity of 5100 cP, about 1000 cP lower than that of TEtSA or the αM-TEtSA derivative. The α,αDM-TEtSA had the lowest viscosity, 1700 cP, at 25°C. This low viscosity compared to the other branched derivatives may be

due to the fact that the equilibrium in the α,αDM-TEtSA lies below full conversion. It was shown In Chapter 4 that the viscosity of these RevIL systems increased exponentially as complete conversion was approached. Although the αM-TEtSA had little effect on viscosity of the ionic liquid formed from reaction with $CO_2$, di-substitution at this position led to a great decrease. It was hypothesized that α-carbon substitution would have more of an impact than β-derivatization but the case for single substitution the opposite trend is observed. It may be caused by packing of ions not changing significantly by branching but packing of the propyl chain being disrupted farther away from the ion pair. This is in agreement with changing alkyl chain length around the silicon atom. This viscosity decrease could be very advantageous in $CO_2$ capture because higher conversions could be used without viscosity concerns.

At 40°C it was apparent that branching on the α-carbon to the amine did have a significant effect on $CO_2$ capture viscosities. From highest to lowest were TEtSA, βM-TEtSA, αM-TEtSA, and α,αDM-TEtSA. The reversal temperature of the α,αDM-TEtSA ionic liquid was found to be the lowest of all of the branched amines at 44°C and so it should be noted that partial reversal most likely took place during the measurement.

## 6.4 Conclusions

Through the synthesis and study of branched TEtSA derivatives it was found that branching at the α position to the amine has the most predominant effects on viscosity, reversal temperature, capacity, and enthalpy. Di-substitution at that position had the most marked effect which is suspected to be a result of carbamate destabilization. The destabilization is believed to be essentially due to steric effects, which is consistent with preliminary DFT calculations. These amines have promise in being industrially viable

capture solvents, especially if a substitution pattern that favored higher reversal temperatures such as dimethylethyl were to be implemented around the silicon atom. This has been previously shown to increase the reversal temperature, necessary in these cases to be viable at 40°C. More industrially viable syntheses would be needed to be developed for the appropriate candidates as these substitution patterns require multi-step methods.

## 6.5 Experimental Methods

### 6.5.1 $CO_2$ reaction

Reactions of molecular liquids were performed by syringing a sample of the desired molecular liquid from the glove box into a dram vial. The vial was capped with a septum and a diffuser tube attached to a $CO_2$ line was used to introduce $CO_2$. $CO_2$ was flowed through the samples at a flow rate of 200 mL/min for 150 minutes. The diffuser tube was stirred in the solution as the reaction progressed to ensure mixing. The formed RevIL was then subjected to analytical experiments to understand the role of structure on RevIL properties.

### 6.5.2 DSC Measurements

DSC measurements were performed in triplicate with a Q20 TA DSC Instrument. Sample weight was recorded in an aluminum hermetic pan crimped with an aluminum lid and measured against an empty pan. The DSC was calibrated with an Indium standard. Samples were held at -40$^{o}$C and ramped to 400°C at a ramp rate of 5°C/min. Reversal temperature was determined from the intersection of two tangents drawn at the beginning and bottom of the reversal endotherm. A similar treatment was used to determine the temperature of evaporation. Heat of regeneration was calculated by integrating the reversion endotherm with respect to time.

### 6.5.3 Viscosity

The viscosity of each ionic liquid was measured using a Rheosys Merlin II cone and plate viscometer. Samples were applied to the plate and were allowed to reach thermal stability prior to data collection. Shear rates varied between 10 and 2000 $s^{-1}$. The average viscosity over the shear range was recorded.

### 6.5.4 FT-IR for physisorption

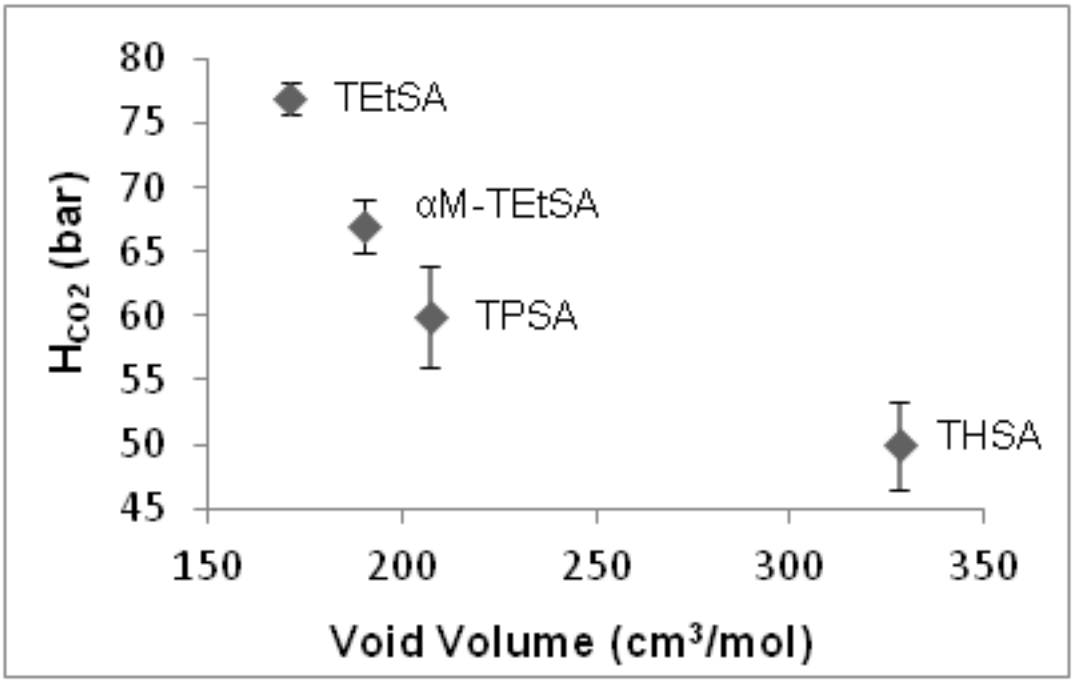


**Figure 6.27.** Henry's constant as a function of void volume

αM-TEtSA RevIL was pre-formed by reaction with $CO_2$ and submitted to increasing pressures of $CO_2$ in a pressure cell designed for the ATR-FTIR instrument. Henry's constant was calculated to be 67 bar at 35°C, consistent with void volume calculations for the prediction of $CO_2$ physisorption. At 1 bar, $CO_2$ physisorption is considered to be almost negligible (Figure 6.27).

The investigation into many synthetic pathways to form the branched silylamines was introduced within the main body of the text. The successful methods were explained more in depth but the methods that did not prove to be fruitful will de described here. I will begin with the synthetic approaches to the αM-TEtSA derivative.

### 6.5.5 Synthesis of αM-TETSA

***(E)-but-2-en-1-yl 2,2,2-trichloroacetimidate:*** A solution consisting of 8.5 mL crotonyl alcohol (99.96 mmol) in 15 mL anhydrous diethyl ether (0.1429 mol) was added to a 3-neck 250 mL round bottomed flask containing sodium hydride (60% dispersion in mineral oil; 0.492 g prior to washing with anhydrous heptane; 12.3 mmol) in 50 mL anhydrous diethyl ether (0.476 mol) at -10°C. The reaction mixture was stirred at that temperature until evolution of hydrogen gas ceased. 10.1 mL trichloroacetonitrile (101 mmol) was then added dropwise over the course of 20 minutes. The reaction mixture became first yellow, then brown. It was allowed to warm to room temperature and the solvent was removed via rotavap. Upon addition of 100 mL of 99:1 hexanes:methanol to the resulting brown oil, a brown precipitate formed. This was removed via gravity filtration and 20.518 g of the crude product trichloroacetimidate was recovered. The trichloroacetimidate was not purified further and carried on "as-is" to the next step.

$^{1}$HNMR (400 Hz, $CDCl_3$) 8.27 (s, 1H), 5.86 (m, 1H), 5.72 (m, 1H), 4.73 (d, 2H), 1.76 (d, 3H) $^{13}$CNMR (400 Hz, $CDCl_3$) 162.62, 131.86, 124.28, 111.69, 69.93, 17.87

***N-(but-3-en-2-yl)-2,2,2-trichloroacetamide:*** The crude trichloroacetimidate was dissolved in 200 mL *p*-xylene and heated at reflux overnight. 20.518 g of the crude trichloroacetamide was recovered which is 100% yield, however column chromatography gave the pure trichloroacetamide in approximately 17% yield. $^{1}$HNMR (400 Hz, $CDCl_3$) 6.55 (s, 1H), 5.86 (m, 1H), 5.25 (d of d, 1H) 5.19 (d of d, 1H), 4.53 (m, 1H), 1.35 (d, 3H) $^{13}$CNMR (400 Hz, $CDCl_3$) 160.98, 137.59, 115.56, 92.69, 49.04, 19.71 mp: 30-32°C

***(E)-but-2-en-1-yl ethyl carbonate***: Pyridine (20 mL), DMAP(0.075 g), and crotyl alcohol (5 mL) were stirred together in anhydrous THF(300 mL) at 0$^{o}$C. Ethylchloroformate (15.6 mL) was added dropwise for 15 minutes to the solution and after complete addition the solution became a cloudy white mixture. The mixture was allowed to stir for 16 hrs at room temperature. To the solution was added brine and ether. The organic layer was washed with 10% HCl and brine and then dried over MgSO4. Filtration and evaporation of the solvent led to the formation of (E)-but-2-en-1-yl ethyl carbonate (7.92 g) in 93 % yield. $^{1}$HNMR (400 Hz, $CDCl_3$) 5.82 (m, 1H), 5.61 (m, 1H), 4.54 (d, 2H), 4.18 (q, 2H), 1.72 (d, 3H), 1.30 (t, 3H) $^{13}$CNMR (400 Hz, $CDCl_3$) 155.01, 132.08, 124.58, 68.26, 63.78, 17.67, 14.20

***O-benzyl-N-(but-3-en-2-yl)hydroxylamine:*** *O*-benzylhydroxylamine hydrochloride salt (13.2 g) was stirred with 15 mL of a 2M KOH solution. DCM (60 mL) was added after stirring for 15 minutes. The organic layer was washed with brine and dried over MgSO4. The DCM layer was sparged with nitrogen for 1 hour. Xantphos (0.76 g), Allylpalladium chloride dimer (0.237 g), and (E)-but-2-en-1-yl ethyl carbonate (7.9 g) were then added at room temperature. The solution turned yellow and after 3 hrs of reaction was a dark

brown. Gas evolution indicated decarbonation. The reaction was stopped by evaporation of the DCM. Hexanes were then added and a dark brown solid precipitated. Filtration followed by evaporation of the hexane led to a mixture of regioisomers (63% crude yield). Column chromotagraphy was run on a gradient starting from pure hexane to 5% EtOAc in hexane. The column was then flushed with EtOAc and the pure branched amine structure (2.69 g) was recovered in an isolated 28% yield. $^{1}$HNMR (400 Hz, $CDCl_3$) 7.26-7.35 (m, 5H), 5.81 (m, 1H), 5.20 (d, 1H), 5.11 (d, 1H), 4.72 (s, 2H), 3.62 (p, 1H), 1.16 (d, 3H) $^{13}$CNMR (400 Hz, $CDCl_3$) 139.76, 137.82, 128.38, 128.34, 127.77, 116.00, 76.73, 59.04, 17.95

***but-3-en-2-aminium chloride***: Zinc powder was activated following a literature procedure*. Zinc powder was washed with a 5% HCl solution, ethanol, acetone, diethyl ether and then dried in high vacuum overnight at room temperature. A solution of *O*-benzyl-N-(but-3-en-2-yl)hydroxylamine (0.5 g, 0.003 mol) was prepared in AcOH:THF:water (3:1:1) (25 mL, 8.5 mL, 8.5 mL). Activated zinc powder (2.62 mol) was added in two portions and was stirred vigorously at 60°C. After 4 hours, water was added as well as ether. The ether layer was removed and the aqueous layer was basified with NaOH. Ether was added again and the organics extracted into it. HCl (neat) was then added to the ether layer but not precipitation of salt occurred.

***2-(but-3-en-2-yl)isoindoline-1,3-dione:*** Potassium phthalimide (24.26 g, 0.13 mol) and anhydrous $K_2CO_3$ (4.32 g, 0.03 mol) were added to a dried 3-neck RB flask fitted with a reflux condenser under nitrogen atmosphere. Anhydrous DMF (75 mL) was added and the mixture was heated to 135$^{o}$C. 3-chloro-1-butene (9.05g, 0.1 mol) was then added dropwise over 15 minutes at 135$^{o}$C. The reaction mixture was allowed to stir for 18hrs. The mixture was then cooled and ice water(500 mL) was added. A white precipitate formed which was filtered under vacuum and washed with aliquots of 1M HCl (100 mL),

water (100 mL), 1M NaOH (100 mL), and water (100 mL). The solid was then dried under vacuum to provide pure 2-(but-3-en-2-yl)isoindoline-1,3-dione (13.38 g) in 67% yield. $^{1}$HNMR (400 Hz, $CDCl_3$) 7.82 (m, 2H), 7.70 (m, 2H), 6.19 (m, 1H), 5.23 (d, 1H), 5.15 (d, 1H), 4.93 (p, 1H), 1.58 (d, 3H) $^{13}$CNMR (400 Hz, $CDCl_3$) 167.92, 136.80, 133.84, 133.02, 123.11, 116.33, 48.93, 18.21 Melting point: 76-79°C.

***but-3-en-2-aminium chloride:*** 2-(But-3-en-2-yl)isoindoline-1,3-dione (13.38 g) was deprotected by addition to ethanolamine (7.3 mL) in EtOH (40 mL), a milder nucleophile than conventional hydrazine. Upon stirring at 45°C overnight, a mixture of 3-amino-1-butene product and EtOH were distilled together at 78oC under nitrogen atmosphere. An HCl gas line was introduced into the solution and was then sparged through the distillate for 15 minutes. The EtOH was evaporated to provide 5.85 g of the 3-amino-1-butene HCl salt as a white solid (hygroscopic) (85% yield). $^{1}$HNMR (400 Hz, $CDCl_3$) 8.46 (s, 3H), 5.96 (m, 1H), 5.42 (d, 1H), 5.31 (d, 1H), 3.90 (m, 1H), 1.49 (d, 3H) $^{13}$CNMR (400 Hz, $CDCl_3$) 134.62, 119.30, 49.94, 19.01

***2-(4-(triethylsilyl)butan-2-yl)isoindoline-1,3-dione:*** Triethylsilane(23.2 g, 0.2 mol) and Pt-DVDS(3.2 mL of 2% Pt solution in xylenes, 0.3 mmol) were added to a 3-neck RB flask under nitrogen atmosphere. Anhydrous toluene(80 mL) was added followed by 2-(but-3-en-2-yl)isoindoline-1,3-dione(30.0 g, 0.15 mol) in a single addition. The mixture was brought to 110°C and was stirred for 20 hrs. The solution was cooled and the toluene and excess triethylsilane removed by vacuum evaporation. The resulting crude was distilled under vacuum to provide 2-(4-(triethylsilyl)butan-2-yl)isoindoline-1,3-dione (36.0 g) in 76% yield. Distillation temperature: 108°C at 0.7 mmHg. $^{1}$HNMR (400 Hz, $CDCl_3$) 7.82 (m, 2H), 7.70 (m, 2H), 4.23 (s, 1H), 2.01 (m,1H), 1.72 (m,1H), 1.46 (d, 3H), 0.88 (trip, 9H), 0.48 (q,7H), 0.37 (t of d, 1H) $^{13}$CNMR (400 Hz, $CDCl_3$) 168.61, 133.73, 132.01, 123.01, 50.58, 28.14, 18.30, 8.42, 7.37, 3.10

***3-(aminobutyl)triethylsilane:*** 2-(4-(Triethylsilyl)butan-2-yl)isoindoline-1,3-dione(16.9 g, 0.053 mol) was added to anhydrous methanol (250 mL) in a 3-neck RB flask under nitrogen. The solution was brought to 60$^{o}$C and to it was added hydrazine (5.11 g, 0.16 mol) in one aliquot. The reaction solution was stirred for 3.5 hrs until stirring was hindered by formation of a cloudy gel-like white precipitate. The reaction was cooled and 2M HCl (250 mL) was added slowly. The precipitate was filtered and washed with 2M HCl and water. The collected solution was then basified with 10% NaOH until the pH was above 9. The aqueous layer was extracted with diethyl ether (3x 100 mL.) The organic layer was washed with brine, dried with $MgSO_4$ and concentrated with vacuum evaporation. Vacuum distillation provided pure 3-(aminobutyl)triethylsilane (6.1 g) in 62% yield.Distillation temperature: 73$^{o}$C at 2.7 mmHg. $^{1}$HNMR (400 Hz, $CDCl_3$) 2.74 (s, 1H), 1.26 (m, 2H), 1.16 (s, 2H), 1.03 (d, 3H), 0.90 (t, 9H), 0.49 (q and m overlapping, 8H) $^{13}$CNMR (400 Hz, $CDCl_3$) 49.71, 34.18, 23.25, 7.48, 7.37, 3.14 Expected: C(64.09), H(13.45), N(7.47) Actual: C(63.03), H(13.47), N(7.39)

### 6.5.6 βM-TEtSA

***2-methyl-3-(triethylsilyl)propan-1-amine:*** Triethylsilane (17.44 g) and Pt-DVDS (6.37 mL of a 2% Pt in xylenes) were added to a dry RB flask under nitrogen atmosphere. Anhydrous toluene (40 mL) was added followed by β-methylallyl amine (10.0 g). The solution was brought to 80oC and reacted for 48 hrs. The reaction was allowed to cool and the solvent and remaining triethylsilane was evaporated. The remaining mixture was distilled under a vacuum of 0.65 torr at 51°C. 19.6 g of 2-methyl-3-(triethylsilyl)propan-1-amine was isolated to give a 75% yield. $^{1}$HNMR (400 Hz, $CDCl_3$) 2.51 (m, 1H), 2.43 (m, 1H), 1.54 (m, 1H), 1.11 (s, 2H), 0.91 (t, 9H), 0.90 (d, 3H), 0.51 (q, 6H), 0.61 (d of d, 1H), 0.32 (d of d, 1H) $^{13}$CNMR (400 Hz, $CDCl_3$) 51.75, 32.79, 20.39, 16.69, 7.46, 4.01 Expected: C(64.09), H(13.45), N(7.47) Actual: C(63.31), H(13.54), N(7.33)

### 6.5.7 α,αDM-TEtSA

***3-methylbut-2-en-1-yl 2,2,2-trichloroacetimidate***: Prenyl alcohol(15.5 mL in 25mL ether) was reacted with NaH(0.699 g 60% dispersion in mineral oil) in anhydrous ether (80 mL) at -10°C. Trichloroacetonitrile (14.8 mL) was added dropwise over 15 minutes. The reaction was allowed to warm to room temperature. The ether was removed and the remaining material was washed with a 99:1 hexane:MeOH solution. Upon washing, a precipitate formed and was filtered from the solution. The solution was concentrated to provide prenyltrichloroacetimidate in 91% yield as an oil. $^{1}$HNMR (400 Hz, $CDCl_3$) 8.25 (s, 1H), 5.47 (t, 1H), 4.78 (d, 2H), 1.76 (d, 6H) 13CNMR (400 Hz, $CDCl_3$) 162.82, 139.96, 117.90, 66.31, 25.81, 18.21

***2,2,2-trichloro-N-(2-methylbut-3-en-2-yl)acetamide:*** Thermal rearrangement of 3-methylbut-2-en-1-yl 2,2,2-trichloroacetimidate was done in refluxing p-xylene. 3-methylbut-2-en-1-yl 2,2,2-trichloroacetimidate (0.035 mol) was added to 100 mL of anhydrous p-xylene and the solution was stirred at 138°C for 20 hours. P-xylene was then removed under vacuum to provide the to provide 2,2,2-trichloro-N-(2-methylbut-3-en-2-yl)acetamide in88% yield. Purification through a Celite plug gave pale yellow crystals. $^{1}$HNMR (400 Hz, $CDCl_3$) 6.60 (s, 1H), 6.00 (d of d, 1H), 5.20 (d, 1H), 5.15 (d, 1H), 1.52 (s, 6H) $^{13}$CNMR (400 Hz, $CDCl_3$) 160.20, 141.86, 113.15, 93.14, 55.82, 26.34

***2-methylbut-3-en-2-amine:*** 2,2,2-Trichloro-N-(2-methylbut-3-en-2-yl)acetamide (25 g, mol) was dissolved in 300 mL of 6M NaOH. The solution was stirred at 60°C for 3 days. After 3 days, 3 portions of diethylether(100 mL) were added. Brine was added and the organic layers collected and dried over $MgSO_4$. Ether was distilled at 35°C and the amine was distilled at 69oC under atmospheric conditions but contained ether and xylenes which was a contaminant of the starting materials. The solution was primarily

ether. It was expected that the amine had appreciable solubility in the water phase as well as potential losses from reaction at 60°C.

***(E)-2-methyl-4-(triethylsilyl)but-3-en-2-amine:*** A 3-neck 100 mL round bottomed flask was fitted with a condenser and stirbar and placed under argon. To this was added 6 mL 2 wt% Pt-DVDS in xylenes (3.04 x $10^{-4}$ mol Pt) and 1.10 mL 0.5 *M* 2,8,9-triisobutyl-2,5,8,9-tetraaza-1-phosphabicyclo[3.3.3]undecane solution (2.75 x $10^{-4}$ mol) in diethyl ether. The reaction mixture was heated at 60°C for 10 minutes. After cooling to room temperature, 30 mL of anhydrous inhibitor-free THF (0.370 mol) and 5.4 mL triethylsilane (0.0340 mol) was added to the flask and allowed to stir for several minutes. 3.2 mL 2-methyl-3-butyn-2-amine (0.0304 mol) was then added to the solution, which then turned a pale yellow. The reaction was allowed to stir at room temperature; reaction progress was measured by the disappearance of the terminal alkyne peak in the $^{13}C$ NMR spectrum. After 72 h reaction time, the solvent was removed via rotavap. Distillation under reduced pressure (60°C at 5 mmHg) yielded 4.78 g of (E)-2-methyl-4-(triethylsilyl)but-3-en-2-amine as a clear oil in 80% yield. $^{1}$HNMR (400 Hz, $CDCl_3$) 6.10 (d, 1H), 5.55 (d, 1H), 1.17 (s, 2H), 1.14/1.13 (s overlapping, (6H)), 0.88 (t of d, 9H), 0.52 (q of d, 6H) $^{13}$CNMR (400 Hz, $CDCl_3$) 157.50, 118.58, 52.24, 30.20, 7.28, 3.47

***2-methyl-4-(triethylsilyl)butan-2-amine:*** Hydrogenation of (E)-2-methyl-4-(triethylsilyl)but-3-en-2-amine was carried out in a Parr reactor. The reactor was first loaded with 0.0545 g 5 wt% Pd/C (2.56 x $10^{-5}$ mol Pd; 0.11% catalyst loading wt alkene) and then purged several times with dry nitrogen. 35 mL anhydrous hexane (0.268 mol) and 4.78 mL of the (E)-2-methyl-4-(triethylsilyl)but-3-en-2-amine (0.0240 mol) were added to the reactor, which was then pressurized with hydrogen (80 psi) and heated at 50°C for 12 hours. Upon cooling, the excess $H_2$ was vented, and the catalyst was

removed from the reaction mixture via filtration with Celite. $^{1}$HNMR of the product mixture revealed the total absence of any alkene peaks, indicating that the reaction had gone to completion. Removal of the solvent via rotavap yielded 4.25 g of the desired saturated product (88% isolated yield). $^{1}$HNMR (400 Hz, $CDCl_3$) 1.24 (m 2H), 1.09 (s, 2H), 0.99 (s, 6H), 0.86 (t, 9H), 0.42 (q, 8H) $^{13}$CNMR (400 Hz, $CDCl_3$) 50.20, 39.02, 29.81, 7.59, 5.22, 3.30 Expected: C(65.59), H(13.51), N(6.95) Actual: C(64.03), H(13.51), N(6.67)

### 6.5.8 βE-TEtSA

Initially, to avoid volatile allylamine derivatives, a tosylation procedure was attempted.

***2-ethylallyl alcohol***: 2-Ethylacrolein (16.8 g) was dissolved in a solution of MeOH/THF (1:4) and cooled to 0$^{o}$C. The $NaBH_4$(7.66 g) was added slowly with a solid addition arm and reacted for 1 hr. The reaction was allowed to come to RT and reacted for another 1.5 hrs. After workup, ether was removed slowly through distillation with slight vacuum. The product was obtained as a 73% solution in ether which is 92% yield. $^{1}$HNMR (400 Hz, $CDCl_3$) 4.99 (s, 1H), 4.85 (s, 1H), 4.07 (s, 2H), 2.06 (q, 2H), 1.69 (s, 1H), 1.05 (t, 3H) $^{13}$CNMR (400 Hz, $CDCl_3$) 150.66, 107.92, 104.99, 25.63, 12.09

***2-methylenebutyl 4-methylbenzenesulfonate***: 2-Ethylallyl alcohol (0.184 mol) was added to a stirring solution of tosylchloride (35.07 g, 0.184 mol) in anhydrous diethylether (150 mL). The solution was stirred at RT where pyridine (19.25 mL, 0.24 mol) was added and the solution became a cloudy mixture. After 4 hours of reaction at room temperature, a precipitate formed. Water (100 mL) was then added and the ether layer was separated. It was washed with water, brine, and dried with $MgSO_4$. The 1HNMR of the crude showed a complex mixture. EtOAc was then added to the crude mixture and a white insoluble solid formed. The solid was filtered to give clean white crystals. After washing with more EtOAc, another precipitate formed. Both of these were

attributed to tosyl chloride starting material and pyridinium tosylate salts. NMR of the remaining material had no vinyl peaks indicative of the product or starting material.

***2-ethylallyl bromide***: The 2-ethylallylalcohol(0.19 mol) was dissolved in anhydrous ether (200 mL). The reaction was kept at $0^{o}$C while $PBr_3$(40.6 g) was added dropwise. The reaction was stirred at RT overnight. The solution was then cooled and ice water added. The 2-ethylallylbromide was extracted with ether, washed with brine, dried with $MgSO_4$ and concentrated to give 34.34g of a 16% solution of product in ether. $^{1}$HNMR (400 Hz, $CDCl_3$) 5.13 (s, 1H), 4.94 (s, 1H), 3.96 (s, 2H), 2.22 (q, 2H), 1.05 (t, 3H). This was consistent with literature and the next step was carried out with the crude product.

***2-methylenebutan-1-aminium chloride:*** LiHMDS (72 mL of a 1M solution in hexanes) was added to a RB flask under nitrogen atmosphere. A dry ice/acetone bath was used to keep the reaction at -40°C and 2-ethylallyl bromide (0.06 mol in ether) was added slowly. The mixture was a light yellow suspension which was brought to room temperature and then heated at 65°C overnight where everything had dissolved. After 48 hrs of stirring it was noted that a milky yellow precipitate was formed. The reaction was stopped after 72 hrs of stirring and filtered through a pad of celite treated with hexane. The hexane was rotovapped from the collected solution to provide a yellow oil. Upon adding more hexane, a milky yellow precipitate kept forming which was not found to be the desired silylprotected allyl amine.

***2-(2-methylenebutyl)isoindoline-1,3-dione:*** 2-Ethylallyl alcohol (0.184 mol,15.82g), $PPh_3$( 48.32 g,0.184 mol), and phthalimide(27.07 g, 0.184 mol) was added to 60mL of anhydrous THF. The cloudy white mixture was stirred vigorously at 0°C under inert atmosphere. DIAD (0.184 mol, 36.23 mL) was added dropwise, keeping the temperature at $0^{o}$C and the mixture became yellow with a white solid suspension. After complete addition, the mixture was stirred at RT for 20 hrs. After 20 hours, the reaction was

incomplete. More equivalents of phthalimide (2.23 g), $PPh_3$ (4.10 g), and DIAD (3 mL) were added as well as 20 mL of anhydrous THF. After another 18 hrs, DIAD (6.1 mL), $PPh_3$ (8.19 g), and phthalimide (4.56 g) were added. 24 hrs later DIAD (3.05 mL), $PPh_3$ (4.06 g), and phthalimide (2.26 g) were added again. After 24 more hours the reaction was stopped by washing the mixture with water and diluted with EtOAc and hexanes. The organic layer was washed with saturated $NaHCO_3$ solution, brine, and dried over $MgSO_4$. The solvent was rotovapped and a light yellow sludge was recovered. Hexane was added to the crude residue and a white solid precipitated out and was filtered. The hexane soluble material was washed with 10% NaOH, extracted with EtOAc and the organics were rotovapped. Column chromatography was used to separate the mixture of materials. A gradient was used from pure hexane to 10% EtOAc in hexane. The fractions containing product were subjected to solvent evaporation, affording white needles (26.47 g) in 67% yield. $^1$HNMR (400 Hz, $CDCl_3$) 7.84 (m 2H), 7.72 (m, 2H), 4.88 (s, 1H), 4.83 (s, 1H), 4.24 (s, 2H), 2.07 (q, 2H), 1.08 (t, 3H) $^{13}$CNMR (400 Hz, $CDCl_3$) 168.08, 144.89, 133.96, 132.03, 123.30, 109.71, 42.39, 26.68, 11.83 EI-MS: expected: 215.0946, actual: 215.0947

***2-(2-((triethylsilyl)methyl)butyl)isoindoline-1,3-dione:*** 2-(2-Methylenebutyl)isoindoline-1,3-dione (15.0 g, 0.07 mol) was dissolved in 40 mL of anhydrous toluene at RT. Triethylsilane (16.28 g, 0.14 mol) was added followed by Pt-DVDS (15.96 mL of a 2% Pt in xylenes solution). The reaction was brought to 110oC and refluxed. The $^1$HNMR after 48 hrs showed 32% conversion. More Pt-DVDS (12.5 mL) was added and the reaction was stirred at reflux for 11 days. $^1$HNMR still showed incomplete conversion so 12.5 mL of Pt-DVDS was added. The reaction was stopped after 26 days of reaction. It was found that the alkene proton peaks used to monitor the reaction by $^1$HNMR were still apparent. TLC showed that the starting material had

disappeared. This indicates that the amount of platinum and the reaction time was far more than necessary and possibly led to side reactions. The solvent was rotovapped from the solution. Column chromatography was used to purify the mixture. A silica gel column was loaded with hexane and the material then added. A solvent gradient starting from pure hexane was used. It was found that platinum residues flowed through the column and component separation was very difficult. Collected fractions which indicated product by $^{1}$HNMR were combined and concentrated. This material was distilled under high vacuum (0.2 torr) and the product collected at 82°C. The product was expected to be in the crude mixture and used for the next step, however no reaction with hydrazine led to the hypothesis that what seemed like product was only decomposed material. The 'product' was still crude and was used in the next step impure. GC-MS confirmed no product.

***2-((triethylsilyl)methyl)butan-1-amine (βE-TEtSA)***: 2-(2-((Triethylsilyl)methyl)butyl)isoindoline-1,3-dione (12.8 g, 0.039 mol assuming 100% pure) was added to anhydrous MeOH (32 mL) under argon. To the solution was added hydrazine (3.2 mL, 0.116 mol) and the reaction was brought to 60°C and allowed to react for 24 hours. Normally, this reaction produces a cloudy-gel like phthalylhydrazide by-product but that product was not evidenced. The reaction was quenched with 2M HCl and no precipitate formed indicating no reaction had taken place. The solution was then basified with 10% NaOH and the organics were extracted with ether, washed with brine, and dried with $MgSO_4$. Once the ether was removed, the crude solution was the same prior to the addition of hydrazine.

***2-methylenebutanenitrile:*** The formation of LDA was achieved by adding nBuLi (19.2 mL of a 2.5 M in hexanes solution, 48 mmol) dropwise to a stirring solution of diisopropylamine (4.85 g, 47.9 mmol) in anhydrous THF (80 mL) at 0°C. The solution

was cooled to -78°C and reacted for 15 minutes. A solution of acrylonitrile (2.12 g, 40 mmol in 15 mL THF) was added slowly over 30 minutes. The solution turned dark yellow and bubbled. EtBr (4.8 g, 44 mmol in 15 mL THF) was then added over 5 minutes and the solution was stirred for 2 hrs at -78°C. It was then warmed to room temperature and was very dark brown. Saturated ammonium chloride was added and a yellow precipitate formed as well as a red precipitate in separate layers. Ether and brine were added and three phases were present. Water was added to break the emulsion in between the organic and aqueous layers but was unsuccessful. The solid emulsion was filtered and the organic layer was dried with $MgSO_4$ and rotovapped. Nothing was recovered. It was expected that polymerization of the acrylonitrile or side reactions occurred to give the precipitates and emulsion.

## 6.6 References


(1) Sartori, G.; Savage, D. W. *Industrial & Engineering Chemistry Fundamentals* **1983**, *22*, 239.

(2) Perry, R. J.; Grocela-Rocha, T. A.; O'Brien, M. J.; Genovese, S.; Wood, B. R.; Lewis, L. N.; Lam, H.; Soloveichik, G.; Rubinsztajn, M.; Kniajanski, S.; Draper, S.; Enick, R. M.; Johnson, J. K.; Xie, H.-b.; Tapriyal, D. *ChemSusChem* **2010**, *3*, 919.

(3) Mulliken, R. S. *Journal of Chemical Physics* **1955**, *23*, 1833,; Mulliken, R. S. *Journal of Chemical Physics* **1955**, *23*, 1841.; Mulliken, R. S. *Journal of Chemical Physics* **1955**, *23*, 2338.

(4) Marzinke, et al. "Method for the Preparation of Aminopropyl or Aminoalkyl Functional Polyalkyl or Aryl Siloxanes." US Patent 6,177,583 B1, Jan. 23, **2001**.

(5) Overman, L. E. *Journal of the American Chemical Society* **1976**, *98*, 2901.

(6) Fletcher, A. J.; Bax, M. N.; Willis, M. C. *Chemical Communications* **2007**, 4764.

(7) Addis, D.; Das, S.; Junge, K.; Beller, M. *Angewandte Chemie-International Edition* **2011**, *50*, 6004,; Kuwano, R.; Takahashi, M.; Ito, Y. *Tetrahedron Letters* **1998**, *39*, 1017.

(8) Faller, J. W.; Wilt, J. C. *Organometallics* **2005**, *24*, 5076.; Johns, A. M.; Liu, Z. J.; Hartwig, J. F. *Angewandte Chemie-International Edition* **2007**, *46*, 7259.

(9) Wang, H.; Matsuhashi, H.; Doan, B. D.; Goodman, S. N.; Ouyang, X.; Clark, W. M. *Tetrahedron* **2009**, *65*, 6291.

(10) Semenow, D.; Shih, C. H.; Young, W. G. *Journal of the American Chemical Society* **1958**, *80*, 5472.

(11) Nagashima, H.; Wakamatsu, H.; Ozaki, N.; Ishii, T.; Watanabe, M.; Tajima, T.; Itoh, K. *J. Org. Chem.* **1992**, *57*, 1682.

(12) Aneetha, H.; Wu, W.; Verkade, J. G. *Organometallics* **2005**, *24*, 2590.

(13) Schilling Jr., C. L., "Preparation of Sterically Hindered Aminohydrocarbylsilanes as Coupling Agents." US Patent 5,030,746 A, Jul. 9, **1991**.

(14) Cheng, B.; Sunderhaus, J. D.; Martin, S. F. *Organic Letters* **2010**, *12*, 3622.

(15) Kabalka, G. W.; Varma, M.; Varma, R. S.; Srivastava, P. C.; Knapp, F. F. *Journal of Organic Chemistry* **1986**, *51*, 2386.

(16) Ding, R.; He, Y.; Wang, X.; Xu, J.; Chen, Y.; Feng, M.; Qi, C. *Molecules* **2011**, *16*, 5665.

(17) Sen, S. E.; Roach, S. L. *Synthesis-Stuttgart* **1995**, 756.

(18) Verdegem, P. J. E.; Monnee, M. C. F.; Lugtenburg, J. *Journal of Organic Chemistry* **2001**, *66*, 1269.; Hill, J. S.; Isaacs, N. S. *Tetrahedron Letters* **1986**, *27*, 5007.

# CHAPTER 7: CONCLUSIONS AND RECOMMENDATIONS

## 7.1 Conclusions

MPV reductions of three relevant pharmaceutical model compounds were enhanced through the development of a highly active catalyst. Rather than using the conventional $Al(OiPr)_3$ catalyst in iPrOH that is used on an industrial scale for the reduction of (*S*)-CMK, $Al(OtBu)_3$ was found to be superior in both rate and catalyst loading needed. This was attributed to the lower state of aggregation of the $Al(OtBu)_3$ as compared to $Al(OiPr)_3$. In fact, the reduction rate of benzaldehyde to benzyl alcohol was increased 20-fold using $Al(OtBu)_3$ in iPrOH! It was found that catalyst loading could be reduced from 50 mol% to 20 mol% with faster rates than the current industrial reduction of (*S*)-CMK. This is a significant advantage (i.e., sustainable) because the overall cost is reduced by using less catalyst and the amount of waste generated is also decreased with less catalyst. Furthermore, $Al(OtBu)_3$ is a cheap, commercially available alternative to $Al(OiPr)_3$. It was found that rate enhancements were observed when using a mixed solvent system which allowed for the first successful implementation of an MPV reduction in continuous flow! Benzaldehyde was reduced in continuous flow with only 20 mol% $Al(OtBu)_3$ at 80°C and in only 11 minutes, the reduction was complete. Acetophenone was also applied to continuous flow successfully. Continuous flow is extremely advantageous in the scaling out of processes, limiting the time between patent filing and industrial production. I considered the implementation of $Al(OtBu)_3$ to be a breakthrough catalyst for MPV reductions and allowed for not only improvements in batch reductions but also in continuous flow.

The second project saw the successful design of trialkylsilylamines as novel $CO_2$ capture solvents. These systems were found to have superior $CO_2$ capacities to 30% aqueous MEA solutions. This enhanced capacity was not only from complete chemical reaction with the silylamine but also physical capture due to sorption into the formed ionic liquid, a unique characteristic of these systems. Furthermore, carbamic acid stability was found to contribute to even higher $CO_2$ capacities than initially predicted for all liquid forming systems! Four different modifications to the basic trialkylsilylamine structure were made and results of these modifications led to valuable information to the optimization of these one-component RevILs towards promising $CO_2$ capture solvents. An optimum candidate that I feel could be a definite step in the right direction towards replacement of aqueous amines is the 2-(aminoethyl)triethylsilane or TESEA that I have provided a synthesis pathway for in the recommendations. The capacity is expected to remain high, the enthalpy, based on trends established should be below MEA and the reversal temperature is expected to be between 70 and 80°C, well below that of the 120°C reversal temperatures required of aqueous amines. Another key structure that I feel would be very promising would be the α,αDM-DMESA because I have shown that decreasing silylsubstitution raises the reversal temperature so that it could be functional at 40°C while having low viscosity, low enthalpy, and high capacity.

It was found that the structure-property relationships studied in this thesis are vital to making the appropriate modifications to trialkylsilylamine systems for $CO_2$ capture. As an important realization, the placement of methyl groups on this basic trialkylsilylpropylamine structure makes a significant difference and a comparison of the viscosities is shown in Figure 7.1. Methyl substitution around the silicon atom was found to lead to solid formation as was methyl group substitution in the propylaminochain to form the butyl linker. However, methyl groups on the actual backbone of the propyl chain

remained liquid upon reaction with $CO_2$. In fact, viscosity decreased when moving the methyl group from the α to the β position. Adding the methyl group onto the amine, forming a secondary amine actual reduced the viscosity of the formed liquid to below 200 cP primarily due to the extremely low reversal temperature of the secondary amine systems. It was also found in all liquid forming RevILs that viscosity could be controlled by conversion and low viscosities (on the order of a few hundred) could be achieved with conversions as high as 65-70%.

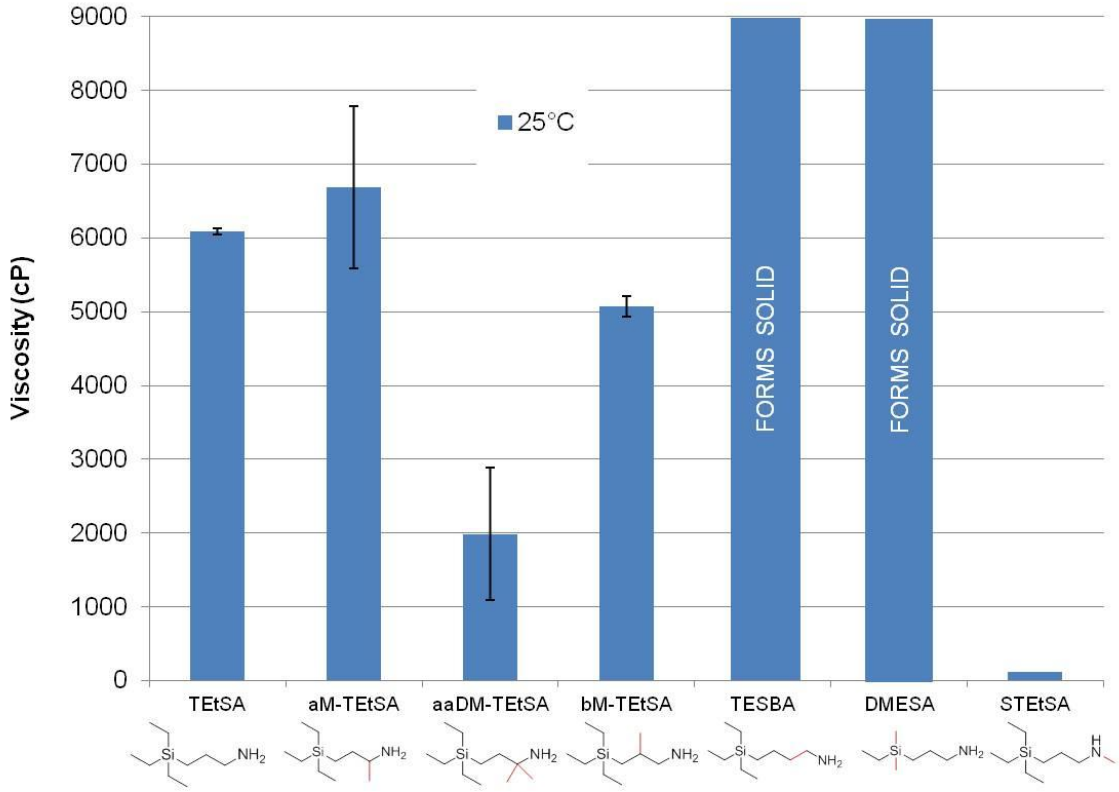


**Figure 7.1.** Viscosities of varying methyl placement in silylamines

Reversal temperature was also affected drastically with methyl group placement. The secondary amine of TEtSA had a reversal temperature of 25°C as it was the most unstable carbamate, followed by di-methyl substitution at the α-carbon of the silylpropylamine, mono-α and mono-β substitutions, and then the unsubstituted silylpropylamine.

Enthalpy was found to be relatively unchanged in most modifications. The largest effects on enthalpy were making the primary amine secondary, resulting in an enthalpy drop of almost 11 kJ/mol $CO_2$ and substitution of the α-position with two methyl groups which dropped the enthalpy as low as 36 kJ/mol $CO_2$!

Overall, it was realized that judicious modifications of the molecular liquid silylamine structure had major effects on the capture and reversal properties of these systems.

## 7.2 Recommendations

1) In the MPV reduction project, aluminum alkoxides were used in attempt to alter the diastereoselectivity of the alcohol products formed. It was found that $Al(OtBu)_3$ did not affect the ratio of (*R,S*)-CMA to (*S,S*)-CMA but increased the rate dramatically. One of the reasons the (*S*)-CMK was hypohesized to be so fast is that the product alcohols precipitate from solution in iPrOH. A mixed solvent system was also used (toluene and iPrOH) and the alcohol products still precipitated. This was the limiting factor in the conversion of this reduction to a continuous flow process, a definite advantage for AMPAC, who uses this reduction on an industrial scale in batch.[1] I recommend that a mixed solvent system be investigated that solubilizes the (*S*)-CMK products. Another method that could be investigated is to change the protecting group to one that is tertiary as it has been shown with phthalimide to increase the ratio of (*R,S*)-CMA to (*S,S*)-CMA.

If a tertiary protecting group could be used to change the *dr* as well as change the solubility of the product in iPrOH or the mixed solvent system. This would allow for the conversion from batch to continuous flow. AMPAC could then convert from batch to continuous flow using a lower aluminum alkoxide catalyst loading for the reduction of (*S*)-CMK, a true advantage in time and cost. Because the products would not precipitate it may be expected that the reaction would be much slower, however amine interactions and hydrogen bonding of the substrate with the aluminum alkoxide may be the cause of the fast reduction of (*S*)-CMK compared to other ketones like acetophenone. Furthermore, the chlorine atom on the α-carbon to the carbonyl should assist in the rate due to enhanced electrophilicity of the carbonyl through inductive effects.

2) It was established in Chapter 6 that the βE-TEtSA derivative was difficult to synthesize based on the methods attempted. This particular derivative showed the most change in nitrogen exposed area in the Spartan® calculations and therefore would be an interesting candidate for testing. I propose a new synthetic method from commercially available acrylonitrile and an inexpensive base, DABCO, to promote the α-ethyl substitution of acrylonitrile.[2] Hydrosilylation,[3] followed by nitrile reduction with $LiAlH_4$ should provide the desired compound (Figure 7.2).[4]

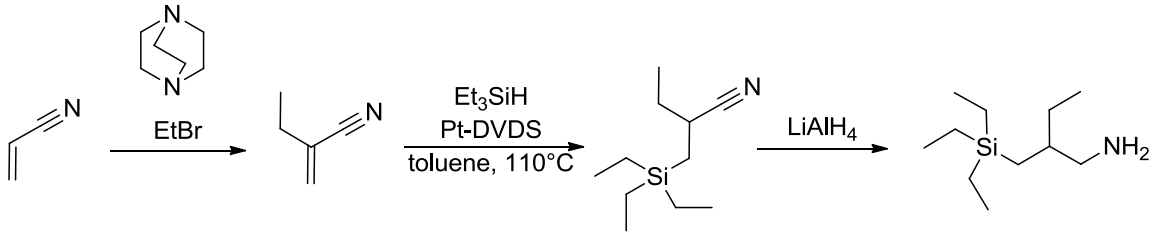


**Figure 7.2.** Synthesis of βE-TEtSA through a nitrile intermediate

3) As a candidate that I feel would be very promising for $CO_2$ capture, I propose a synthesis from the commercially available vinylphthalimide with triethylsilane followed by hydrazine reduction in the formation of TESEA (Figure 7.3).

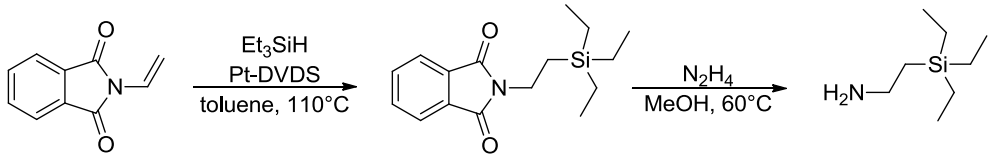


**Figure 7.3.** Synthetic method for the formation of TESEA from vinylphthalimide

4) As mentioned in the conclusions, the dimethylethylsilyl derivative of α,αDM-TEtSA could prove very effective in capturing $CO_2$ in a more sustainable manner than current aqueous amine systems. I propose the synthesis reported in Chapter 6 using dimethylethylsilane as opposed to triethylsilane (Figure 7.4).

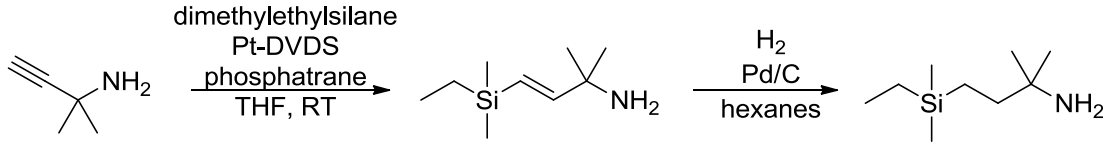


**Figure 7.4.** Synthesis of α,αDM-DMESA

5) One particular area of interested that has not been addressed with these silylated amine systems that may contribute extensively to increased viscosity is the role of intermolecular interaction between the amines, forming the ammonium and carbamate ions versus intramolecular interactions. It is speculated that if intramolecular interactions were more prevalent, the viscosity of the overall ionic liquid may be altered, and possibly lowered. To study this, I propose to investigate models like diaminocyclopropanes (Figure 7.5).

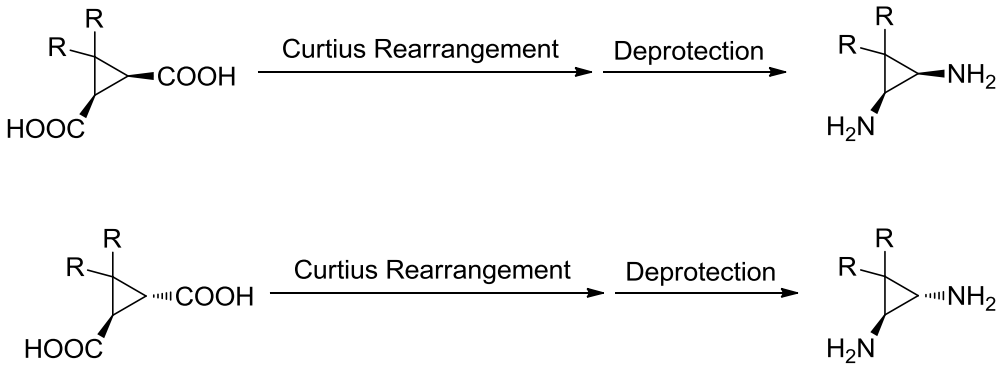


**Figure 7.5.** Cyclopropyldiamines for study of intra and intermolecular interactions

The cyclopropane rings effectively lock the amine chirality into place. One structure is the cis-amino cyclopropane, the other is the trans. It is hypothesized that the cis confirmation would have primarily intramolecular bonding whereas the trans would have intermolecular bonding. The synthesis of these amines is possible from chirally pure commercially available cyclopropyl carboxylic acids. The acids could be reacted with DPPA and triethylamine in tert-butanol to form the desired boc-protected diamines which could then be protected.[5] The Curtius rearrangement does not affect the chiral center, therefore chiral integrity would remain.

## 7.3 References


(1) Marzinke, et al. "Method for the Preparation of Aminopropyl or Aminoalkyl Functional Polyalkyl or Aryl Siloxanes." US Patent 6,177,583 B1, Jan. 23, **2001**.

(2) Hill, J. S.; Isaacs, N. S., *Tetrahedron Letters* **1986**, *27*, 5007-5010.

(3) Belyakova, Z. V.; Pomerantseva, M. G.; Chekrii, E. N.; Chernyshev, E. A.; Storozhenko, P. A., *Russian Journal of General Chemistry* **2010**, *80*, 927-929.

(4) Amundsen, L. H.; Nelson, L. S., *Journal of the American Chemical Society* **1951**, *73*, 242-244.

(5) Scriven, E. F. V.; Turnbull, K., *Chemical Reviews* **1988**, *88*, 297-368.

# APPENDIX A: ACCEPTED PROPOSAL FOR ACS-GCI PHARMACEUTICAL ROUNDTABLE AWARD 2012

I have been instrumental in developing collaboration between our sustainable, green chemistry group (Eckert/Liotta) and Dr. Stefan France's synthetic organic chemistry group. This collaboration led to the idea of integrating Dr. France's groups work in Homo-Nazarov based approaches for the synthesis of functionalized heterocycles to continuous flow. Because this work is particularly of interest to the pharmaceutical community, we envisioned optimization and conversion of batch multi-step reactions to continuous flow operations, of which the advantages have been described in Chapter 3. The accepted grant proposal is shown below. The ACS-GCI award was received by our collaborative group and will continue through 2014.

## A.1 Green and Effective Continuous Flow Multi-Step Synthesis of Heteroaromatic Ring-Fused Cyclohexanones

### A.1.1 Abstract

Green chemistry and engineering are creating a culture change for the future directions of industry. As the needs of industry change, innovation becomes a necessity. Continuous process technologies have already been identified as vehicles for its environmental and economic advantages by enabling superior mixing, heat transfer and notably lower cost through the "scaling-out" strategies as opposed to the traditional "scaling-up". Also central to pharmaceutical-oriented synthetic strategies are heteroaromatic-fused ring systems since they are present in biologically active molecules and are building blocks for complex pharmaceutical synthesis. Recently, the synthesis of heteroaromatic fused cyclohexyl compounds was reported via the catalytic homo-Nazarov cyclization. Unfortunately this ground-breaking strategy utilizes 1) a

reactive diazoketone intermediate, 2) a relatively high loading (up to 30 mol %) of an expensive Lewis acid catalyst for high yield, and 3) a chlorinated solvent.

We propose to develop continuous and sustainable Lewis acid-catalyzed homo-Nazarov cyclization processes involving reactive donor-acceptor cyclopropanes for the production of biologically active molecules. In these instances, transfer of critical technology variables from batch to continuous flow can maximize performances in term of reaction yield and product selectivity while minimizing solvent and catalyst needs. The goal is to ultimately eliminate chlorinated solvents. By taking advantage of the high mixing and heat transfer performances of our glass continuous flow reactor, we propose to establish the benefits of continuous process technology for pharmaceutical industry to conduct multistep synthesis, namely (1) the Lewis-acid catalyzed homo-Nazarov to yield heteroaromatic-fused cyclohexyl rings and (2) the synthesis of the diazoester and cyclopropane precursors. We propose to concretely assess the benefits of continuous process technology for the homo-Nazarov cyclization using Aspen for process optimization and cost analysis. Finally, we propose to deliver a realistic roadmap for technology transfer from batch to continuous mode.

The Eckert-Liotta group is a combination of chemical engineers, physical and synthetic chemists with extensive experience in working with industrial partners to develop processes that are both environmentally benign and economically viable. The research group has expertise in demonstrating the superiority of a continuous process in terms of reaction control and efficiency (higher atom economy). The France group is a well-recognized synthetic chemistry group with expertise in synthetic methodology development. They have established $In(OTf)_3$ as a batch process catalyst for homo-Nazarov cyclizations in maximizing product yield, activity and selectivity—opening a

new, unexplored synthetic avenue for the key pharmaceutical heteroaromatic-fused cyclohexanone motifs.

### A.1.2 Background

#### A.1.2.1 Homo-Nazarov Cyclization

Six-membered rings are extremely important structural subunits for the vast majority of natural products and pharmaceuticals. Given this prevalence, synthetic chemists have continuously been interested in the development of stereoselective methodologies for their preparation. Some of the most efficient protocols include the Diels-Alder reaction (which remains the standard bearer for the formation of six-membered rings), polyene cyclizations,[1] intramolecular ene-reactions,[2] Robinson annulations,[3] and other transition-metal mediated annulations.[4] Yet, a viable, but underexplored approach to six-membered carbo- and heterocycles has been exemplified by the homo-Nazarov cyclization (Figure A.1). In this reaction, cyclopropyl vinyl ketones are converted into $\alpha,\beta$-unsaturated cyclohexenones. The proposed mechanistic steps involve acid-promoted ring opening of the cyclopropane ring to afford a 1,3-dipole. This species then undergoes intramolecular attack by the adjacent vinyl $\pi$-electrons to afford a cyclic oxylallyl cation. Elimination to quench the cation followed by tautomerization of the enol affords the cyclohexenone product.

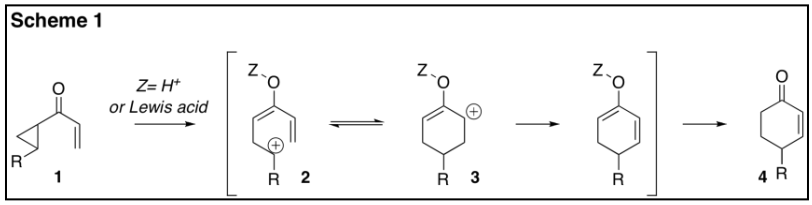


**Figure A.1.** Homo-Nazarov Cyclization

The France lab has recently pioneered several novel homo-Nazarov technologies catalyzed by Lewis acids using donor-acceptor cyclopropanes containing a secondary acceptor group that “polarizes” the resulting cyclic oxyallyl cation by localizing charge density. We first demonstrated that $In(OTf)_3$ effectively catalyzes the homo-Nazarov cyclizations of alkenyl cyclopropyl ketones to afford methylene cyclohexenols and/or cyclohexenones in good to high yields (Figure A.2).[5] This general method also works for cyclopropyl heteroaryl ketones where treatment with $In(OTf)_3$ similarly provides 2,3- and 3,4-heteroaryl-fused cyclohexanones in good to high yields (56-91%) with modest diastereo selectivities (1:1 to >20:1 dr, Figure A.2).[6] This method is amenable to a variety of heteroaromatics, including furan, thiophene, pyrrole, indole and benzofuran. Furthermore, the method tolerates a wide range of functional groups and substituents.

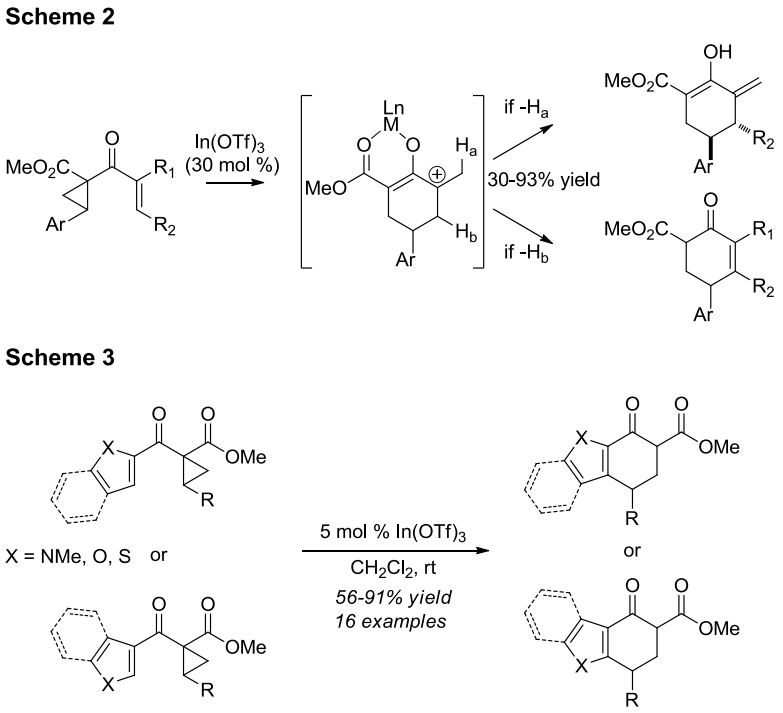


**Figure A.2.** Catalytic Homo-Nazarov and fused heteroaromatics

A.1.2.2 Continuous flow Technology

Although the pharmaceutical industry has long favored batch processing, the advantages of continuous flow processing technology are now being documented, due to mounting economic competition and commercial production benefits.[7, 8] When *scaling- up* batch processes, pilot scale units must be built and operated to ascertain accurate heat and mass transfer mechanisms; this is hardly sustainable and subtracts substantially from the marketable patent life of the product. In contrast, continuous flow processing allows for the advantages of *scale-out*, eliminating the pilot plant and engineering associated with production scale—a clear financial incentive. Continuous flow technology also enables greener processes in terms of energy, solvent consumption, atom efficiencies and as a result waste generation. For instance, enhanced mixing improves the mass transfer of biphasic systems, which leads to better yields, catalyst recovery and subsequent recycling schemes. The ability to accurately control the reaction temperature leads to exact control of reaction kinetics and product formation. This increases product quality and reproducibility by eliminating unfavorable selectivity (by-product formation), which is impactful both from an environmental and a financial stand-point.

We have experience in converting pharmaceutically-relevant, batch processes to continuous flow processes. We successfully designed, built and used a continuous flow reactor to carry out a two-step reaction sequence for the preparation of the key HIV protease inhibitor intermediate, 1-benzyl-3-diazo-2-oxopropylcarbamic acid *tert*-butyl ester (Figure A.3).[9]

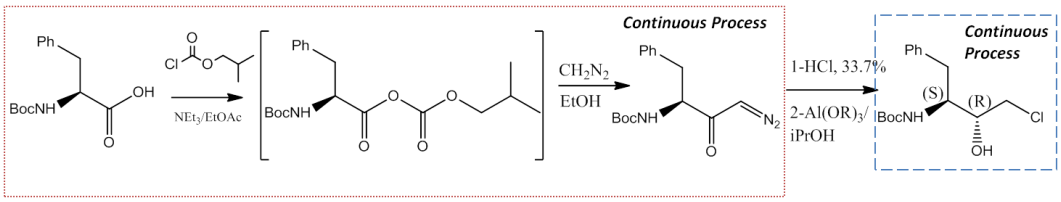


**Figure A.3.** Continuous formation of (S)-CMK through a diazoketone

Indeed, continuous technology was regarded—and demonstrated—as beneficial in this particular synthesis since it involves the formation of a temperature sensitive mixed anhydride intermediate and its subsequent reaction with trimethylsilyldiazomethane (a highly reactive reagent) to yield the diazoketone isolable intermediate. By modifying the chemistry and maximizing the mixing and heat transfer, the continuous flow process enabled superior (in fact quantitative) yields at milder reaction temperature (4$^{o}$C instead of -20$^{o}$C). Subsequently, we aimed at developing Meerwein-Ponndorf-Verley (MPV) reductions of model compounds in the Corning® glass reactor. As a result, we pioneered continuous MPV reductions of the model compounds acetaldehyde and acetophenone (a simple analogue for *N*-Boc-(*R*)-benzyl-2-oxo-3-chloropropylamine) by (1) establishing Al(O*t*Bu)$_3$ as an highly active, efficient and cost-effective catalyst for MPV reductions of aldehydes and ketones and (2) implementing Al(O*t*Bu)$_3$ as catalyst for continuous reductions processes of ketones and aldehydes to their corresponding alcohols (upon optimization of solvent, temperature, catalyst loading for example).

Continuous flow processing technology has been used in industry for large-scale synthesis for almost 30 years. Within the past 10 years, the technology has become more widespread due to the commercial-availability of microreactors and bench-top

continuous flow systems. Despite this growth, only a handful of multi-step flow syntheses have been reported.

### A.1.3 Objectives

(1) Design and optimize experimental protocols to conduct the Lewis-acid catalyzed homo-Nazarov cyclizations in continuous mode

As a batch, the homo-Nazarov reaction was demonstrated with two different solvents (dichloromethane and acetonitrile) and Lewis-acid catalysts at loading up to 30 mol %. Unquestionably, continuous flow strategy can contribute to the optimization of the process to maximize performances in term of reaction yield and product selectivity while minimizing solvent (ultimately eliminating chlorinated solvents) and catalyst needs.

(2) Establish an experimental protocol to prepare the diazoester and cyclopropane precursors in continuous mode

It is not sufficient to perform one step in continuous mode. In reality, enabling multi-step synthesis will be essential for the continuous technology to meet its promises and be truly innovative. We will investigate the synthesis of the homo-Nazarov precursors as shown in Figure A.4. Each of these steps will be first optimized individually in the reactor as they can benefit from a continuous process design (they involve highly reactive intermediate and reagent).

(3) Develop a multistep strategy that enables the complete process to be conducted continuously

We will integrate each of the steps into one, continuous process. The optimization of the process will be performed and provide the basis for economic and environmental assessment.

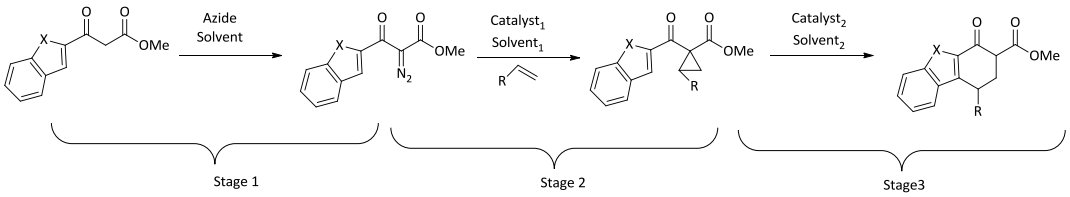


**Figure A.4.** General heteroaromatic homo-Nazarov multistep synthesis

(4) Definite economic and environmental assessment of the benefits and viability of the continuous approach

Through the use of the Aspen software suite, a detailed process model will be shaped, allowing for an accurate economic and environmental analysis and process optimization.

### A.1.4 Project Approach

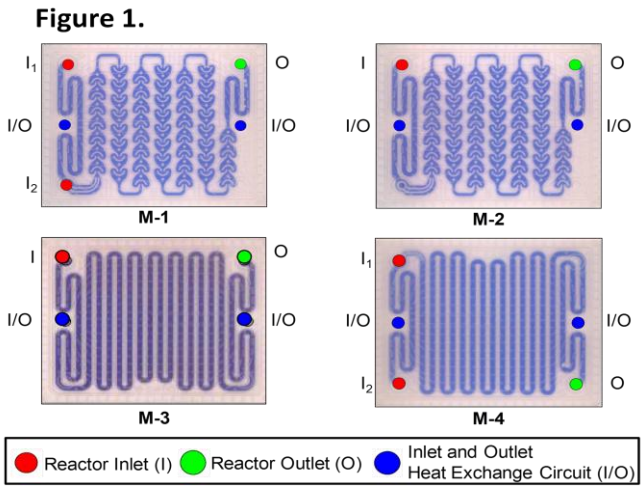


**Figure A.5.** Corning® Glass Flow Reactor plates

We propose to utilize the glass Corning® continuous flow reactor for the proposed research (Figure A.5). The assembly of microstructures (161mm x 131mm x 8mm) made of glass is compatible with a wide range of chemicals and solvents and corrosion-resistant over a wide range of temperatures (-25$^{o}$C to 200$^{o}$C) and pressures (up to 18 bar). The Corning microstructures was designed for our needs and optimized for specific operations including, but not limited to: multi-injection, mixing, residence time, and heat transfer. All of the microstructures are equipped with two fluidic layers (-25$^{o}$C to 200$^{o}$C, up to 3 bar) for heat exchange on either side of the reaction layer. Heat transfer rates are proportional to heat transfer surface area and inversely proportional to volume. These microstructures facilitate an optimum surface-to-volume ratio for improved heat transfer.

Aim 1: Technologic transfers from Batch to Continuous to conduct the Lewis-acid catalyzed homo-Nazarov cyclizations and Optimization (solvent, catalysts loading, temperature etc…)

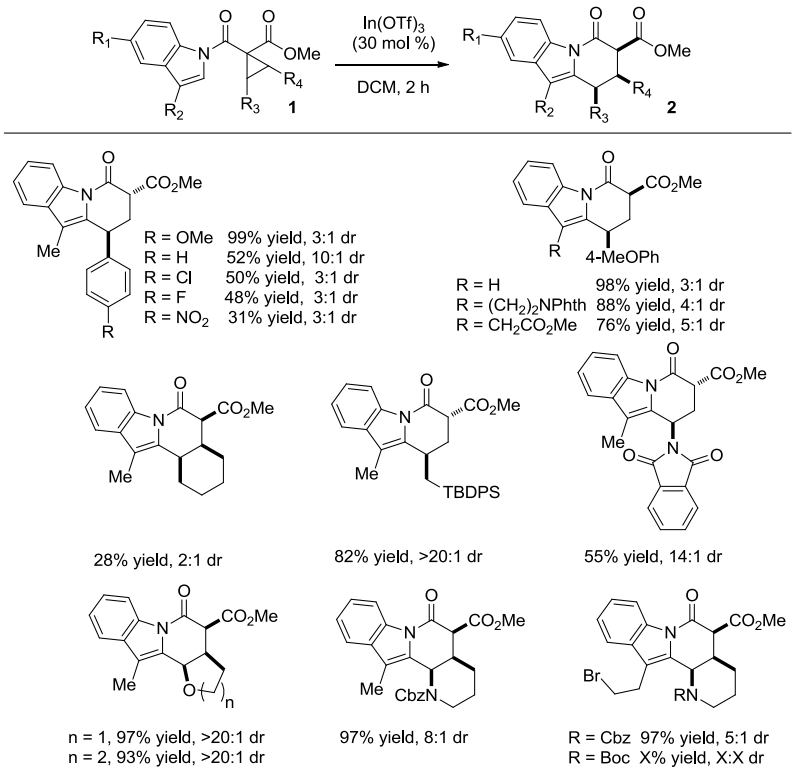


**Figure 2.** Homo-Nazarov Cyclization of *N*-Acyl Indolyl Cyclopropanes

**Figure A.6.** Breadth of the homo-Nazarov cyclization for pharmaceutically relevant heterocycles

We recently disclosed an efficient and modular approach to hydropyrido[1,2-*a*]indole-6(7*H*)-ones via the $In(OTf)_3$-catalyzed homo-Nazarov cyclizations of methyl 1-(1*H*-indole-carbonyl)-1-cyclopropane carboxylates (Figure A.6). Mechanistically, the protocol involves cyclopropane ring-opening in the presence of a Lewis acid catalyst, followed by an intramolecular Friedel-Crafts alkylation of the indole. This transformation specifically generates the lactam ring portion of the hydropyrido[1,2-*a*]indole-6(7*H*)-ones. The hydropyrido[1,2-*a*]indole skeleton is a key structural motif that appears in the core structures of an impressive number of naturally-occurring indole alkaloids and

pharmaceutically-relevant compounds. When cyclopropanes **1** were subjected to 30 mol% $In(OTf)_3$ in $CH_2Cl_2$ at 25˚C, the anticipated homo-Nazarov cyclizations readily occurred and afforded dihydropyrido[1,2-*a*]indole-6(7*H*)-ones **2** in good to excellent yields (55-99% yield) with some diastereoselection (from 2:1 *trans*:*cis dr* to >20:1 *dr*). To date we have applied this method to a diverse set of *N*-acyl indolyl substrates to determine the scope and limitation of the reaction (Figure A.6).[10] The method is amenable to a variety of functionalities including alkyl and aryl halides, protected alkyl amines, ethers, silyl groups, and nitro groups. This method is highly modular and can be easily carried out on a multi-gram scale.

Although this represents a ground-breaking strategy, this multi-step synthesis utilizes reactive diazo species, a rather high catalyst loading (up to 30 mol %) of an expensive Lewis acid catalyst and chlorinated solvents in enable high yield. As a consequence, we propose to first investigate the $In(OTf)_3$-catalyzed homo-Nazarov cyclization methyl 1-(1H-indole-carbonyl)-1-cyclopropanecarboxylates (Figure A.7) in the continuous flow reactor as a function of (1) catalyst loading, (2) temperature, (3) solvent and (4) concentration. Although dichloromethane will be first investigated in a preliminary phase (to compare performances with the batch results), our aim is to move toward non-chlorinated solvents such as toluene and THF. Extension to other Lewis acid catalysts, such as $Al^{3+}$, $Sc^{3+}$ and $Zn^{2+}$ salts, will also be considered.

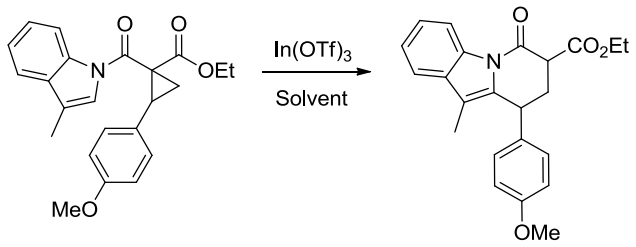


**Figure A.7.** Homo-Nazarov of methyl 1-(1H-indole-carbonyl)-1-cyclopropanecarboxylates

Aim 2: Technologic transfers from Batch to Continuous to prepare the diazoester and cyclopropane precursors

The preparations of the precursors to the homo-Nazarov are deemed to benefit from being run in continuous mode as they involve heterogeneous catalysis and/or energetic reagents and intermediates. Indeed, the 1-(1H-indole-carbonyl)-1-cyclopropanecarboxylate is synthesized using the following four-step sequence starting with the requisite indole: (1) *N*-acylation with commercially-available methyl malonyl chloride to give the 1,3-dicarbonyl intermediate; (2) diazo transfer to provide the $\alpha$-diazoester; (3) rhodium-catalyzed cyclopropanation in the presence of an alkene to afford the desired cyclopropyl *N*-acyl indole; and (4) $In(OTf)_3$-catalyzed homo-Nazarov cyclization (Figure A.8). The preparation of the diazoester and cyclopropane intermediates will be investigated in the continuous reactor as a function of (1) temperature, (2) solvent, (3) catalyst loading and (4) concentration.

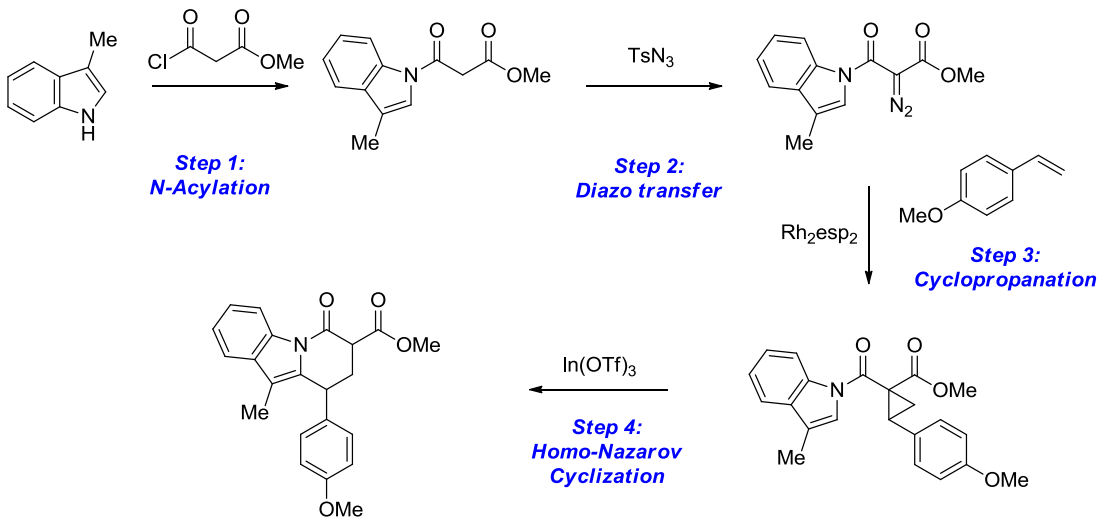


**Figure A.8.** Multi-step synthesis to ethyl 9-(4-methoxyphenyl)-10-methyl-6-oxo-6,7,8,9-tetrahydropyrido[1,2-a]indole-7-carboxylate

Aim 3: Develop a multistep strategy that enables the multi-step process to be conducted continuous mode.

Combining the previous steps into a multi-step continuous synthesis will finally be demonstrated, providing a roadmap to the pharmaceutical industry for the synthesis of heteroaromatic ring-fused cyclohexanones. The configuration shown in Figure A.9 will be used for multistep synthesis. M-3 and M-1 will be used as heating and cooling units where as M-2 will be used for residence time and both M-4's will be used for sequential reagent introduction and mixing.

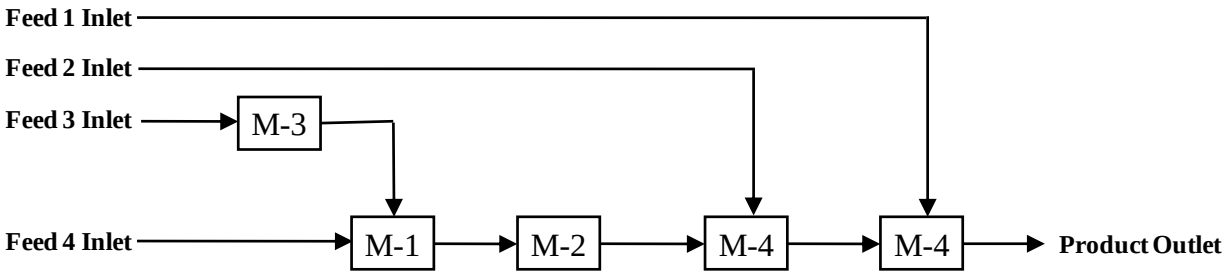


**Figure A.9.** Proposed microstructure assemblies that will be used for the multistep synthesis reaction

Aim 4: Process Assessment

Through the use of the Aspen software suite, a detailed process model can be created that will allow for an accurate economic analysis and process optimization to be performed. The Aspen software suite is an extremely powerful tool that makes use of high order thermodynamic calculations in order to design various process operation units (e.g., reactors, distillation columns, strippers, etc.). The thermodynamic calculations are performed based on a user-defined equation of state (e.g., Peng-Robinson, Soave-Redlick-Kwong, NRTL, UNIFAC, UNIQUAC, etc.) that is best able to predict the specific material species at the potential operating conditions. Once a process model has been developed and optimized, using up-to-date economic information (e.g., raw material costs, capital/equipment costs, and operating costs) Aspen is capable of providing a life-cycle analysis of the designed process model. The ability to perform this level of process design and economic analysis is absolutely crucial to the development of new technology and intellectual property.

### A.1.4 Conclusions/Impact

We propose to design and optimize a far-reaching, unexplored approach to the synthesis of fused heterocyclic rings, a pharmaceutical prevalent motif, for continuous flow processes. By integrating flow technology *early on* in the development of the synthetic strategy, we propose to contribute in establishing the continuous multistep synthesis as a transformative technology. Unquestionably, this research will be a milestone from which we can build-upon to develop flow-processes; for example, stereoselective, green synthetic schemes toward pharmaceutical applications.[11]

## A.2 References


(1) Zhao, Y. J.; Li, B.; Tan, L. J. S.; Shen, Z. L.; Loh, T. P., *Journal of the American Chemical Society* **2010**, *132*, 10242-10244.

(2) Arai, N.; Ohkuma, T., *Tetrahedron* **2011**, *67*, 1617-1622.

(3) Massicot, F.; Iriarte, A. M.; Brigaud, T.; Lebrun, A.; Portella, C., *Organic & Biomolecular Chemistry* **2011**, *9*, 600-603.

(4) Constable, E. C.; Drew, M. G. B.; Ward, M. D., *Journal of the Chemical Society-Chemical Communications* **1987**, 20, 1600-1601.

(5) Patil, D. V.; Phun, L. H.; France, S., *Organic Letters* **2010**, *12*, 5684-5687.

(6) Phun, L. H.; Patil, D. V.; Cavitt, M. A.; France, S., *Organic Letters* **2011**, *13*, 1952-1955.

(7) Jimenez-Gonzalez, C.; Poechlauer, P.; Broxterman, Q. B.; Yang, B. S.; Ende, D. A.; Baird, J.; Bertsch, C.; Hannah, R. E.; Dell'Orco, P.; Noorrnan, H.; Yee, S.; Reintjens, R.; Wells, A.; Massonneau, V.; Manley, J., *Organic Process Research & Development* **2011**, *15*, 900-911.

(8) Andrews, I.; Dunn, P.; Hayler, J.; Hinkley, B.; Hughes, D.; Kaptein, B.; Lorenz, K.; Mathew, S.; Rammeloo, T.; Wang, L.; Wells, A.; White, T. D., *Organic Process Research & Development* **2011**, *15*, 748-756.

(9) Pollet, P.; Cope, E. D.; Kassner, M. K.; Charney, R.; Terett, S. H.; Richman, K. W.; Dubay, W.; Stringer, J.; Eckert, C. A.; Liotta, C. L., *Industrial & Engineering Chemistry Research* **2009**, *48*, 7032-7036.

(10) Patil, D. V.; Cavitt, M. A.; Grzybowski, P.; France, S., *Chemical Communications* **2011**, *47*, 10278-10280.

(11) Patil, D. V.; Cavitt, M. A.; France, S., *Heterocycles* **2012**, *84*, 1363-1373.

## APPENDIX B: POLYAMINES FOR USE AS HIGH CAPACITY $CO_2$ CAPTORS

### B.1 Introduction

Chapters 4, 5, and 6 in the main body of this thesis document the structure-property relationship associated with silylated amines for use as non-aqueous $CO_2$ captors. Even though the silylated amines showed an increased capacity over theoretical predictions, higher capacities may be achieved through multiple reactive sites on one molecule. Compounds containing multiple amines reactive sites, including secondary amines as well as ethylene oxide units, were investigated (Table B.1). Ethylene oxide motifs were used because it was hypothesized that the oxygen, ammonium interaction may have a marked effect on reversal properties and the interactions are shown in Figure B.1.

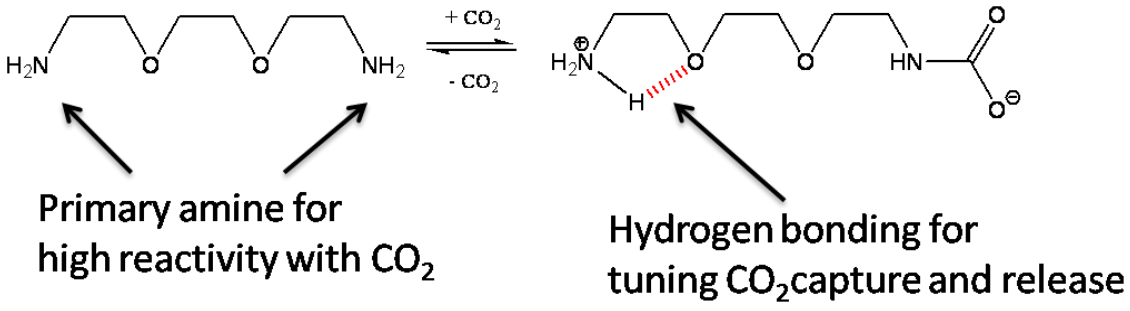


**Figure B.1.** Ammonium and other oxygen intramolecular interaction

Polyols have also been shown to reduce viscosity in amine blends for $CO_2$ capture.[1] Of the amines studied, 3 were not commercially available and their synthesis is outlined

here within. Namely, pentaerithrtiyl tetramine (2), tetra-(2-amino-ethoxymethyl)methane (7), and tetra-(3-amino-propoxymethyl)methane (8).

**Table B.1.** Polyamine structures investigated for $CO_2$ capture

| Molecular Liquid Structure | Molecular Liquid Structure |
|---|---|
| (1) 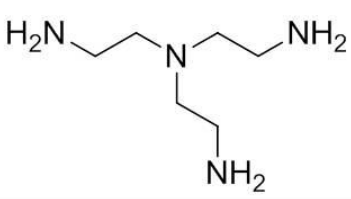 | (2) 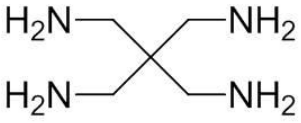 |
| (3) 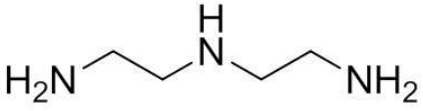 | (4) 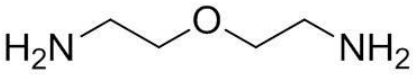 |
| (5) 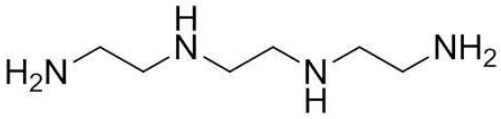 | (6) 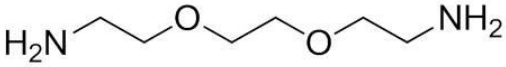 |
| (7) 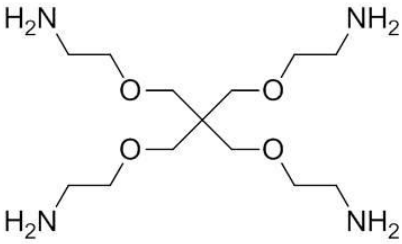 | (8) 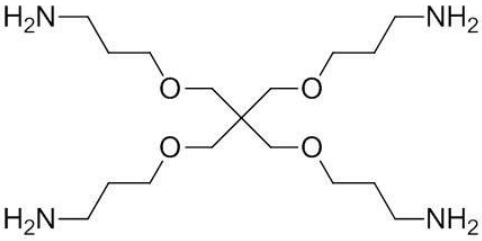 |

## B.2 Synthesis of Polyamines

### B.2.1 Synthesis of tetra-amine (2)

Tetra-amine (2) has a high nitrogen to carbon ratio making it an excellent candidate for enhanced $CO_2$ capacity. The synthetic method was derived from a literature procedure and is shown in Figure B.2.[2]

Pentaerythritol tetrabromide was reacted successfully with sodium azide which afforded the pentaerithrityl tetraazide. The tetraazide was then carried forward to the amine hydrochloride salt by way of amination with ammonia in the presence of $PPh_3$. The use of Amberlite® IRA-400 resin to neutralize the salt to form the free amine was not successful and the synthesis was not continued because other polyamine derivatives with high symmetry did not perform as anticipated and will be discussed after the synthesis section.

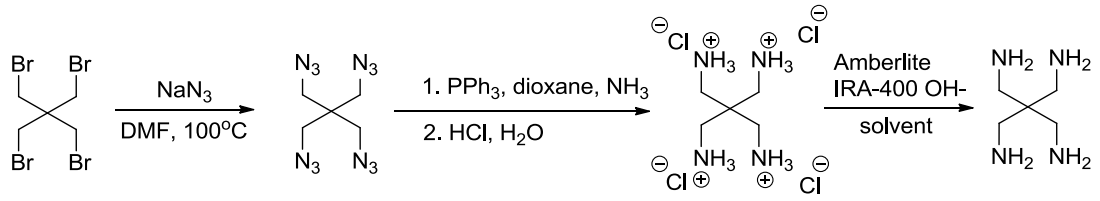


**Figure B.2.** Synthetic pathway towards polyamine (2)

### B.2.2 Synthesis of tetra-amine (7)

The formation of amine (7) was attempted by reaction through Michael reaction of pentaerythritol with acrylonitrile under basic conditions to form the tetranitrile in accordance with the literature. The tetranitrile intermediate was then converted to the

tetra-carboxylic acid which was isolated by continuous extraction. It was envisioned that a Curtius rearrangement in t-BuOH could provide the desired tert-butyl carbamate or Boc protected-tetraamine product with ethylene linkage between the nitrogen atom and the ethereal oxygen on each “branch”. Deprotection with TFA could then provide the desired tetra-amine (7). A scheme was based on a literature report for the formation of the tetra-acid (Figure B.3).[3] The formation was stopped at the tetra-acid step based on other polyamine reactivities with $CO_2$.

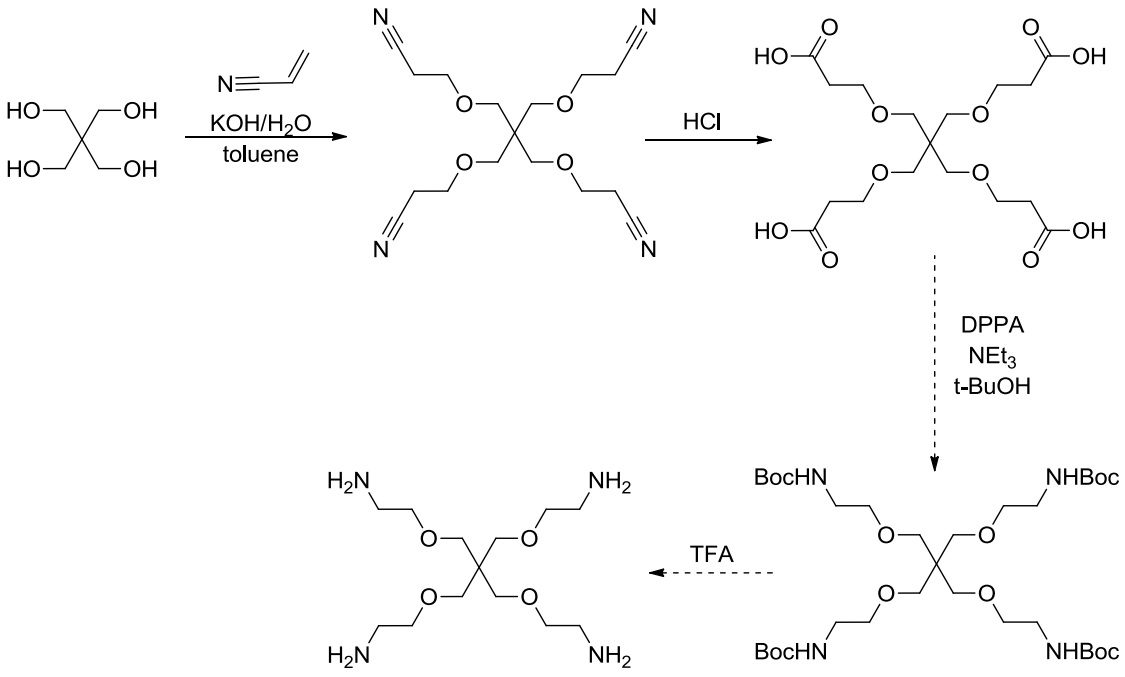


**Figure B.3.** Synthetic approach to the formation of polyamine (7)

### B.2.3 Synthesis of tetra-amine (8)

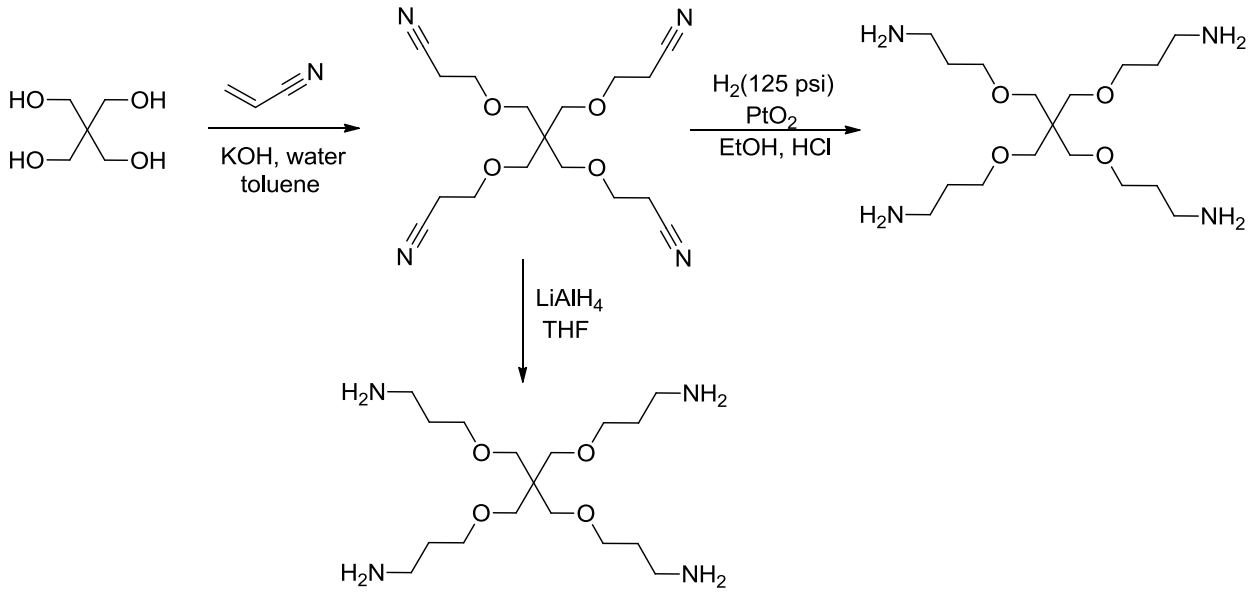


**Figure B.4.** Synthetic approach to polyamine (8)

Formation of polyamine 8 was envisioned through a two-step synthesis.[4] The tetranitrile was synthesized following the same procedure as the previous polyamine. Two attempts were made to reduce the nitrile groups to amines. The first attempt was carried out using $LiAlH_4$ in THF (Figure B.4). The reaction was run for 30 days and upon workup, no tetra-amine was isolated. Mass spec analysis led to the identification of partially reduced tetranitrile in this case. Hydrogenation was also attempted with $PtO_2$ and 125 psi of $H_2$ in EtOH. The NMR showed reaction of the tetranitrile after 3 days to other species but upon neutralization and workup, no tetra-amine was recovered. Previous reports showed that the tetra-amine, commonly used as a dendrimer scaffold

was a viscous oil[5] therefore efforts to continue the synthesis were discontinued as this would not be favorable for our application.

## B.3 Polyamines as $CO_2$ captors

Commercially available amines, in particular, amines (3) and (6) were studied for their $CO_2$ capture properties. These compounds were reacted with $CO_2$ as described in Chapter 4 and analyzed by viscosity and capacity measurements. Viscosities will be addressed first as they are pertinent to understand why these systems are not suitable for anhydrous $CO_2$ capture applications.

### B.3.1 Viscosities of polyamine upon $CO_2$ exposure

The reaction of (3) with $CO_2$ in anhydrous conditions produced an extremely viscous gel. Likewise the reaction of (6) in anhydrous conditions also led to a very viscous gel. The viscosity measurements were taken of the “complete” reaction where maximum gravimetric uptake was observed.

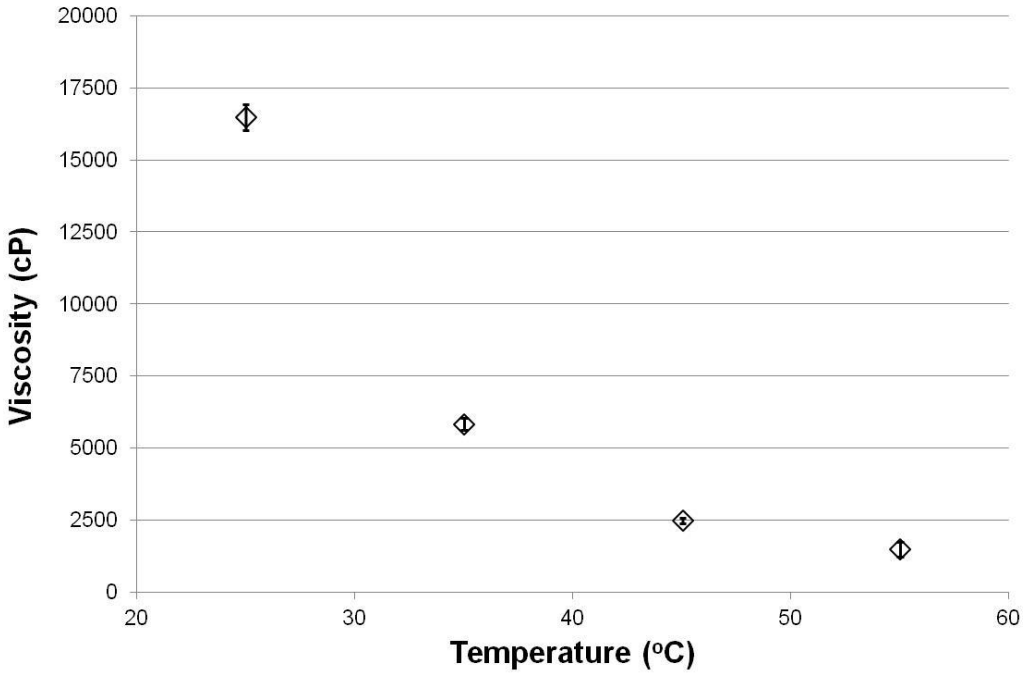


**Figure B.5.** Viscosity as a function of temperature in the ionic species of polyamine (3)

Figure B.5 shows the viscosity of the reaction of amine (3)-IL with $CO_2$ as a function of temperature. Viscosities at 25°C reached over 16000 cP. The same trend was seen with amine (6)-IL. Viscosity versus temperature is shown for the ionic species formed upon reaction with $CO_2$ in Figure B.6. Viscosity reached over 16000 cP at 25°C as well.

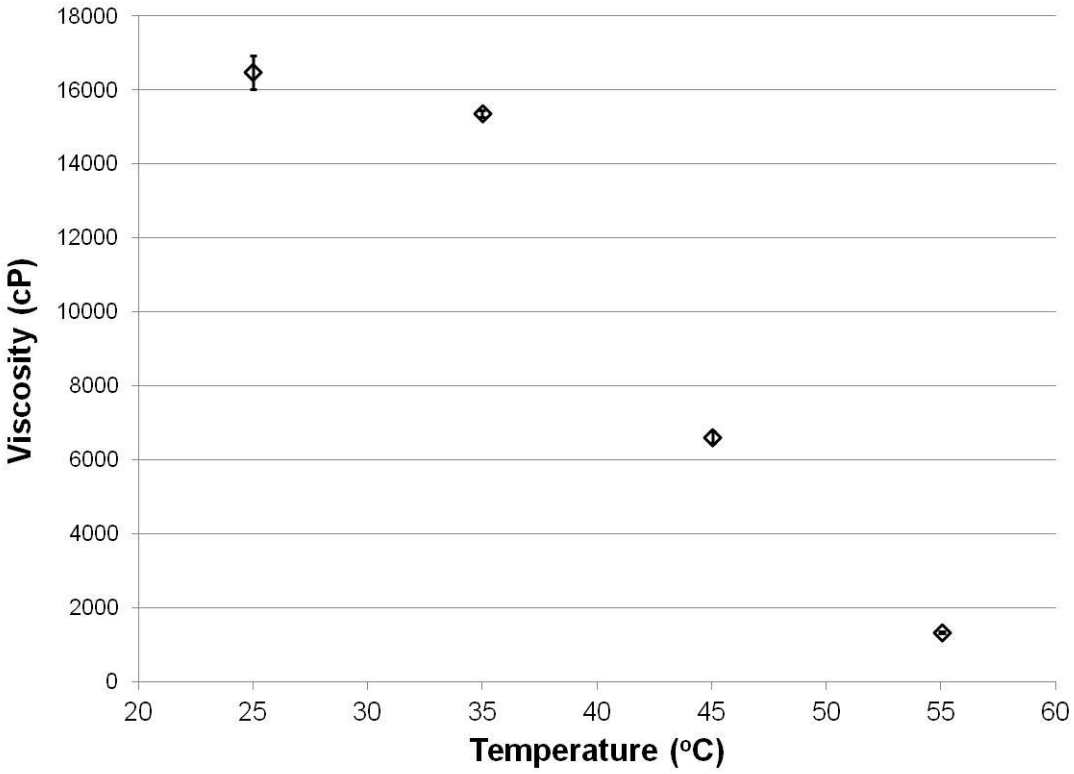


**Figure B.6.** Viscosity as a function of temperature of the ionic species of polyamine (6)

This viscosity of these systems is linked to the internal interactions between the amine chains. Shown in Figure B.7 below, diethylenetriamine (3) when reacted with $CO_2$ can form an extensive intermolecular and intramolecular hydrogen and ionic bonding network. In the green box is intermolecular hydrogen bonding, in red is intermolecular ion pairing, and in blue is intramolecular ion pairing.

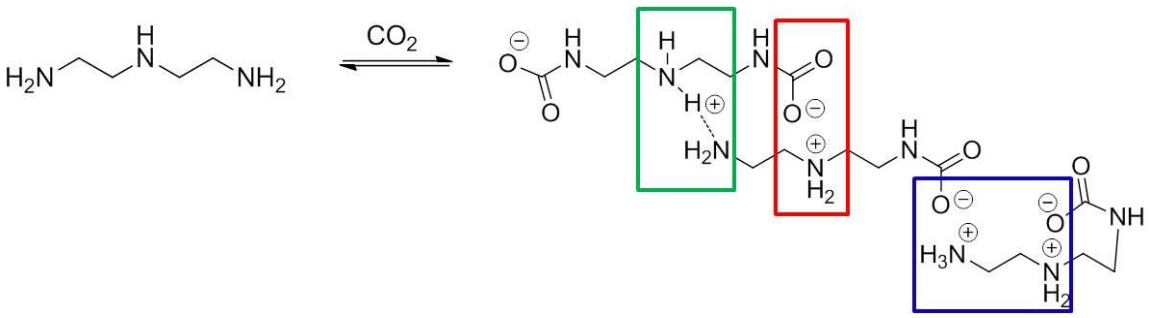

**Figure B.7.** Inter and intramolecular interactions leading to high viscosities in polyamines

Because of this extensive network of interactions, viscosities are very high. It is also interesting to note that (6) although expected to have lower viscosities than the amino analog (3) because of the unreactive ether linkages, resulted in very high viscosity ionic materials. This may be due to the hydrogen bonding ability of the oxygen atoms along the backbone with the formed ion pairs as well as intermolecular interactions between reacted and unreacted amines. Because the viscosities are high and the “free amines” for enhanced capture are engaged in these internal interactions, theoretical capacities are not achieved.

### B.3.2 Capacity as a function of tetra-amine structure with reaction of $CO_2$

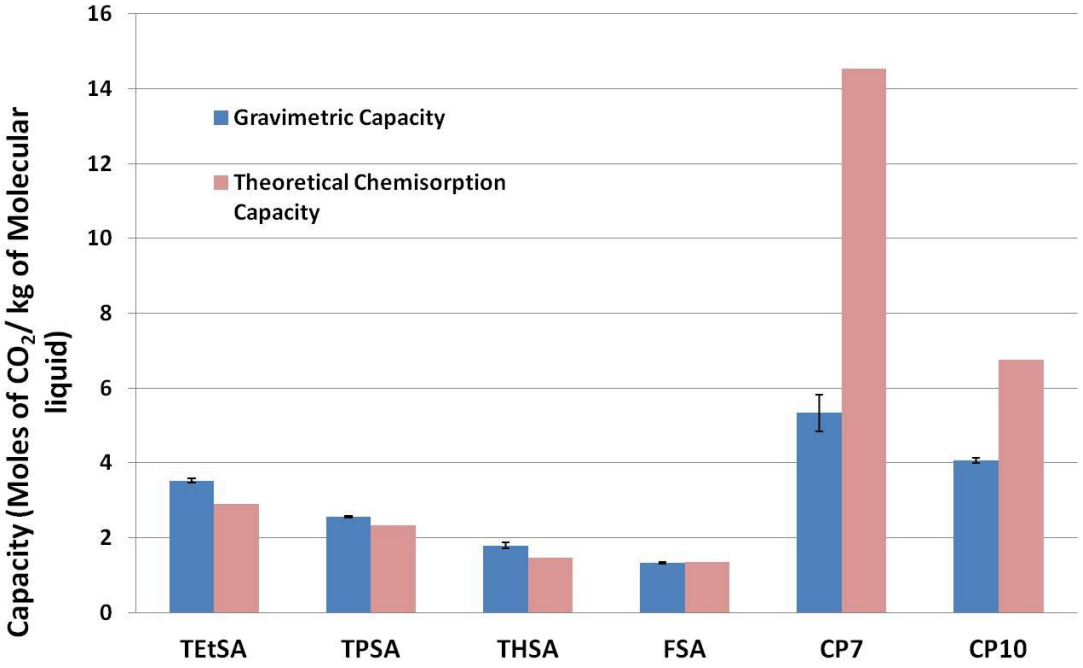


**Figure B.8.** Gravimetric capacities of polyamines compared to the silylamine counterparts

Upon complete reaction of $CO_2$, mass transfer limitations as well as internal interactions limit the complete conversion expected from theoretical calculations. In Figure B.8 it is noted that (3)-IL and (6)-IL both had capacities that only reached 50-60% completion with no more weight gain upon extended reaction times. One can see the potential benefit of using polyamines in that the theoretical capacities are 3 times higher for (6) than TEtSA and (3) is 7 times as high based on molecular weight.

### B.3.3 Reversal Temperatures

DSC measurements were conducted on the formed ionic species through reaction of $CO_2$ with the two polyamines (3) and (6). Each of their DSC thermograms are highlighted in Figures B.9 and B.10, respectively. In both cases, two endothermic events are evidenced, the first corresponding to the reversal of $CO_2$ and the second corresponding to the vaporization of the initial polyamine molecular liquid.

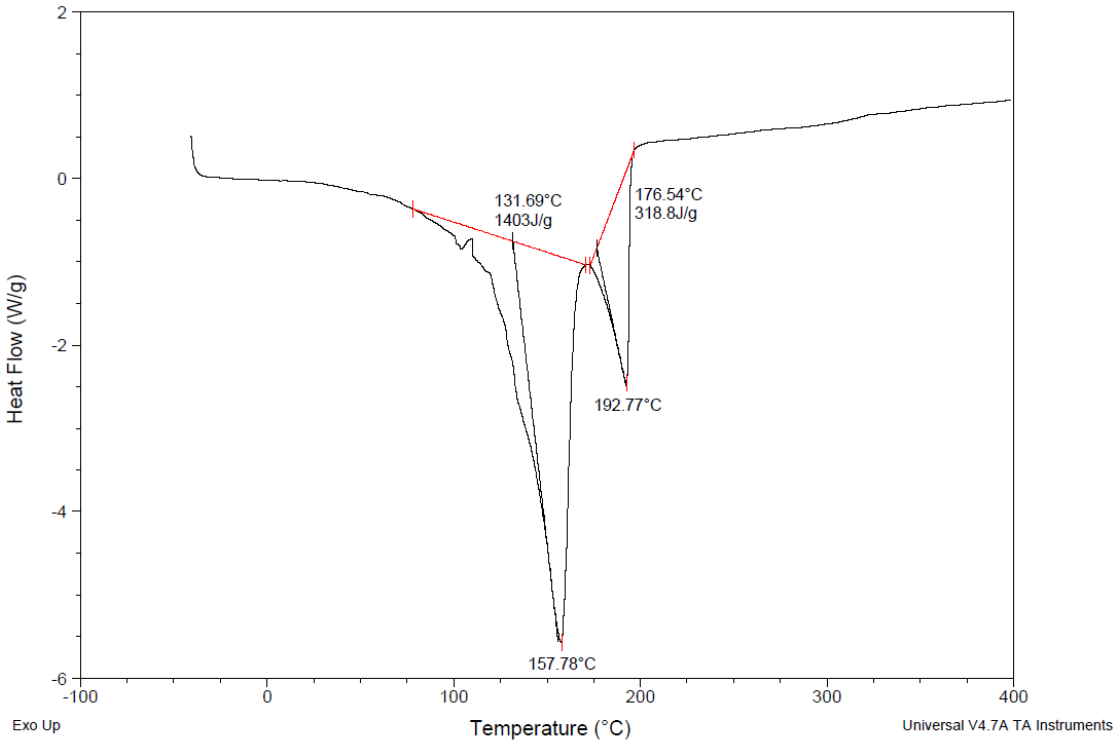


**Figure B.9.** DSC thermogram of polyamine (3) ionic species

Figure B.9 shows the DSC thermogram of (3)-IL as a function temperature. From the tangent to the $CO_2$ reversal endotherm, the reversal temperature is 131.69°C, much higher than the reversal temperatures of the silylated amines in Chapters 4-6. This is actually even higher than the reversal temperature required to reverse 30% aqueous MEA solutions.

Figure B.10 shows the DSC thermogram of (6)-IL with both endotherms. The reversal temperature calculated from the tangent to the reversal endotherm was found to be 91.25°C. This molecule, with ether linkages rather than secondary amine linkages has a reversal temperature that is 40°C lower than the polyamine (3). This is conjectured to be a function of the amount of inter and intramolecular interactions between formed ionic species.

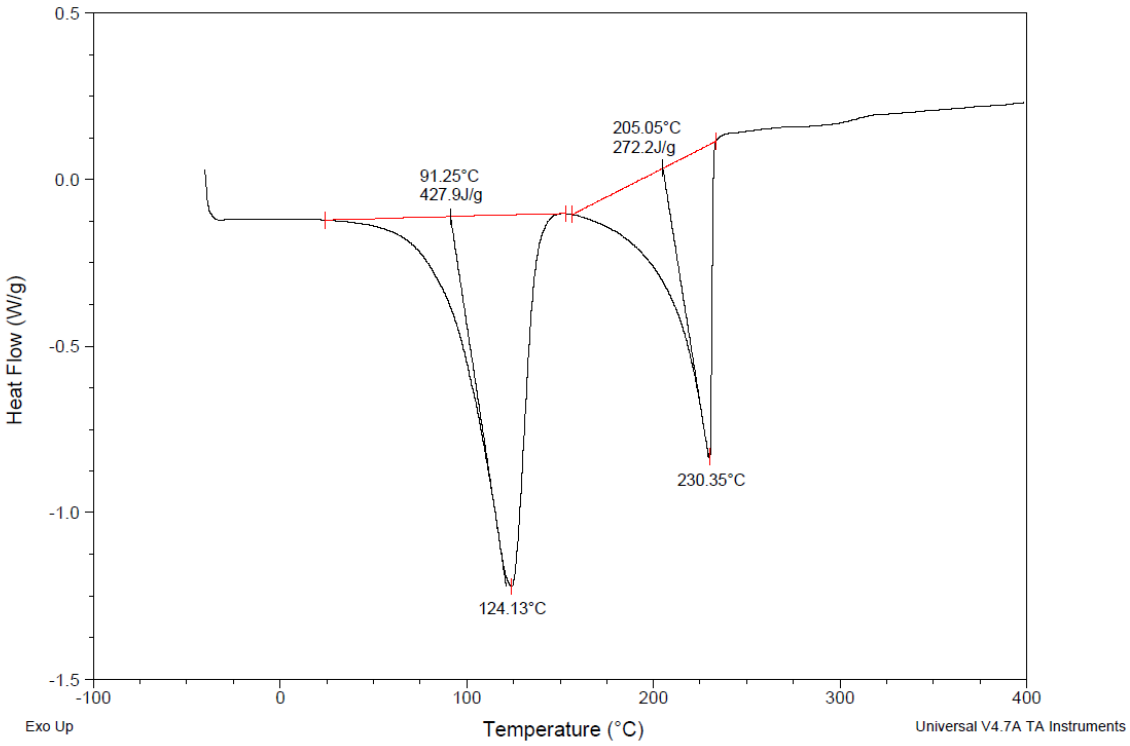


**Figure B.10.** DSC thermogram of polyamine (6) ionic species

Although a more favorable reversal temperature, the viscosity and capacity are definite limitations to the application of this polyamine for $CO_2$ capture.

## B.4 Conclusions

Although polyamines have multiple reactive sites and their $CO_2$ capacities are expected to be very high, in reality, capacities were never shown to reach their maximum loading. Limited by internal hydrogen bonding and ionic interactions, viscous gel-like materials were formed upon reaction of polyamines with strictly amines (3) as well as ethereal linkages (6). These species exhibit high reversal temperatures above 100°C and high viscosities making their application under anhydrous conditions unsuitable for $CO_2$

capture. Possible uses could however include using these polyamines as additives to other amine blends to increase capacity.

## B.5 Experimental Methods

### B.5.1 $CO_2$ reactions

Reactions of molecular liquids were performed by syringing a sample of the desired molecular liquid from the glove box into a dram vial. The vial was capped with a septum and a diffuser tube attached to a $CO_2$ line was used to introduce $CO_2$. $CO_2$ was flowed through the samples at a flow rate of 200 mL/min for 75 minutes. The diffuser tube was stirred in the solution as the reaction progressed to ensure mixing. The formed RevIL was then subjected to analytical experiments to understand the role of structure on RevIL properties.

### B.5.2 DSC/TGA

DSC measurements were performed in triplicate with a Q20 TA DSC Instrument. Sample weight was recorded in an aluminum hermetic pan crimped with an aluminum lid and measured against an empty pan. The DSC was calibrated with an Indium standard. Samples were held at -40$^{o}$C and ramped to 400°C at a ramp rate of 5°C/min. Reversal temperature was determined from the intersection of two tangents drawn at the beginning and bottom of the reversal endotherm. A similar treatment was used to determine the temperature of evaporation. Heat of regeneration was calculated by integrating the reversion endotherm with respect to time.

### B.5.3 Viscometry

The viscosity of each ionic liquid was measured using a Rheosys Merlin II cone and plate viscometer. Samples were applied to the plate and were allowed to reach thermal

stability prior to data collection. Shear rates varied between 10 and 2000 $s^{-1}$. The average viscosity over the shear range was recorded.

### B.5.4 Synthesis of Amines

**Pentaerithrityl tetraazide:** Pentaerythritol tetrabromide (0.54 g) was added to a stirring solution of $NaN_3$ (1.12 g) in DMF (10 mL). The solution was stirred at 80$^oC$ for 24 hrs. Upon cooling and addition of water, ether was added and the organics were extracted, washed with brine and dried over $MgSO_4$. The solution was concentrated in ether to yield 0.296 g of tetra-azide (90%). MS showed a peak at 237 corresponding to the desired product.

**Pentaerithrityl tetraamine hydrochloride salt**: The tetraazide (0.296 g) was then reacted with $PPh_3$(1.8 g) in dioxane (5.4 mL) and 20% ammonia (8.8 mL). After 24 hours of reaction, the solvents were evaporated. Chloroform was added to dissolve the components, followed by addition of 2M HCl (50 mL). The aqueous layer was then evaporated leaving a crude solid which was washed with more cold concentrated HCl and EtOH and filtered to give a 30% yield of the desired hydrochloride salt (0.187 g). NMR data matched literature reports.[2]

**Pentaerithrityl tetraamine:** Pentaerithrityl tetraamine hydrochloride salt (0.187 g) was added to anhydrous THF with Amberlite IRA-400 OH resin. The mixture was stirred for 48 hours but no product was recovered upon evaporation of THF.

**Tetrakis[(cyanoethoxy)methyl]methane*:*** Pentaerythritol (5.1 g) was added to a mixture of toluene (30 mL) and 4.1 mL of a 40% KOH solution in water. The mixture was stirred vigorously. Acrylonitrile (35 mL) was added dropwise keeping the temperature below 25$^oC$. The reaction was stirred at RT for 3 hrs and then 2M HCl was added slowly. The toluene layer was washed with brine, dried over $MgSO_4$, and the solution concentrated via rotovap. The crude oil was distilled to remove the bis-cyanoethylether

(110°C at 0.5 mmHg) and the remaining oil was pure tetranitrile (11.6 g, 81% yield). $^{1}$HNMR (400 Hz, CDCl3) 3.65 (t, 8H), 3.48 (s, 8H), 2.60 (t, 8H) $^{13}$CNMR (400 Hz, CDCl3) 118.17, 68.66, 65.57, 45.55, 18.75

**tetrakis[(carboxyethoxy)methyl]methane**: Tetrakis[(cyanoethoxy)methyl]methane (15 mmol) was added to concentrated aqueous HCl (25 mL) and heated at 75°C for two hours. The reaction mixture was diluted with water and continuously extracted with ethyl ether for four days. The ether layer was separated, dried with $MgSO_4$ and concentrated *in vacuo* to yield 40% of solid tetrakis[(carboxyethoxy)methyl]methane (2.5 g). mp: 95-98°C $^{1}$HNMR (400 Hz, d6-DMSO) 3.50 (t, 8H), 3.21 (s, 8H), 2.38 (t, 8H) this was consistent with literature reports.[3]

**Tetrakis-[3-(aminopropoxy)methyl]methane**: Tetrakis[(cyanoethoxy)methyl]methane (0.599 g, 1.4 mmol) was added to 15 mL of anhydrous THF under argon. $LiAlH_4$ (1M in THF) (8.6 mL, 8.6 mmol) was added and the reaction was stirred at 50°C. After 19 days, a 2 mL aliquot was removed and water and NaOH were added. $^{1}$HNMR did not show desired reaction. The reaction was let stir for 30 days total. The reaction was quenched with 20 mL $H_2O$, 30 mL 20% NaOH, and 20 mL $H_2O$. 30 mL of brine were added. There were no bubbles indiciative of $LiAlH_4$ quenching and the reaction was found to have only the singly and doubly reduced nitriles by LC-MS.

**Tetrakis-[3-(aminopropoxy)methyl]methane:** Tetrakis[(cyanoethoxy)methyl]methane (0.702 g, 2 mmol) was added to a solution of EtOH (25 mL) and 1M HCl (1 mL). To a 250 mL parr reactor was added $PtO_2$ (100 mg) and the Parr was flushed with nitrogen and vacuum was pulled. The starting material solution in EtOH was then syringed in. Hydrogen gas was pressurized to 125 psi in the Parr reactor and the mixture was stirred vigorously with mechanical stirring. The temperature was brought to 50°C and the reaction was carried out for 3 days under hydrogen. The reaction was then cooled and

depressurized. A 1 mL aliquot was taken and the solvents rotovapped. EtOAc was used to dissolve the crude and the solution was washed with saturated $NaHCO_3$ solution and rinsed with water and brine and dried over $MgSO_4$. The solvent was removed and a $^1$HNMR did not show indicative peaks of the desired product.[5]

## B.6 References


(1) Seo, J. B.; Jeon, S. B.; Lee, S. S.; Kim, J. Y.; Oh, K. J. *Korean Journal of Chemical Engineering* **2011**, *28*, 1698.; Tan, J.; Shao, H. W.; Xu, J. H.; Du, L.; Luo, G. S. *Industrial & Engineering Chemistry Research* **2011**, *50*, 3966.

(2) Adil, K.; Goreskhnik, E.; Courant, S.; Dujardin, G.; Leblanc, M.; Maisonneuve, V. *Solid State Sciences* **2004**, *6*, 1229.

(3) Newkome, G. R.; Weis, C. D. *Organic Preparations and Procedures International* **1996**, *28*, 242.

(4) Newkome, G. R.; Lin, X. F. *Macromolecules* **1991**, *24*, 1443.

(5) Hukkamaki, J.; Pakkanen, T. T. *Journal of Molecular Catalysis A-Chemical* **2001**, *174*, 205

## VITA

Kyle Flack was born on December 3rd, 1986 in Wilmington, NC to Mike and Beth Flack. He was actively involved in St. Paul's Lutheran Church, the Boy Scouts of America, and the E.A. Laney High School marching band. After graduating from E.A. Laney High School in 2004, Kyle chose to attend N.C. State University in 2004 to pursue a BS in Chemistry. While at NC State he participated in the Power Sound of the South Marching Band, Jazz Band, Alpha Chi Sigma Chemistry fraternity, and did undergraduate research with Dr. Jonathan Lindsey. He was awarded the National Starch and Chemical Foundation Award in 2007 and graduated Summa Cum Laude in May 2008. He continued his chemistry career by enrolling in graduate school at Georgia Tech in August of 2008. He joined the Eckert/Liotta Research group and chose a focus in organic chemistry. While working for the Eckert/Liotta group, he was awarded both the Presidential Fellowship and was a ConocoPhillips fellow from 2009-2012. He will continue his career in chemistry at BASF Chemical Co. in the Professional Development Program, starting his first rotation in July 2012 in Iselin, NJ.